PHOSPHAZIDES AS ANCILLARY LIGANDS IN URANIUM AND THORIUM COORDINATION CHEMISTRY

TARA KATHLEEN KARN DICKIE
Bachelor of Science (Honours), McMaster University, 2014

A thesis submitted
in partial fulfilment of the requirements for the degree of

DOCTOR OF PHILOSOPHY

in

EARTH, SPACE, AND PHYSICAL SCIENCE

Department of Chemistry and Biochemistry
University of Lethbridge
LETHBRIDGE, ALBERTA, CANADA

PHOSPHAZIDES AS ANCILLARY LIGANDS IN URANIUM AND THORIUM COORDINATION CHEMISTRY

TARA DICKIE

Date of defence: May 12th, 2022

Dr. P. Hayes Thesis Supervisor	Professor	Ph.D.
Dr. M. Gerken Thesis Examination Committee Member	Professor	Ph.D.
Dr. R. Boeré Thesis Examination Committee Member	Professor	Ph.D.
Dr. S. Patitsas Internal Examiner	Associate Professor	Ph.D.
Dr. S. Bart External Examiner Purdue University	Professor	Ph.D.
Dr. B. Demeler Chair, Thesis Examination Committee	Professor	Ph.D.

Abstract

The synthesis of uranium(IV) and thorium(IV) phosphazide complexes is described herein. Two new series of ancillary ligands featuring phosphazide groups are presented, leveraging potassium ion stabilization of the phosphazides to facilitate salt metathesis transfer of the ligands to uranium and thorium. These complexes and their precursors were prepared and characterized by multi-nuclear (^{1}H, ^{13}C and ^{31}P) NMR spectroscopy, single crystal X-ray diffraction experiments and elemental analysis.

Step wise N_2 elimination from the diphosphazide ligands was observed and, in some cases, the asymmetric mixed phosphazide/phosphinimine system was isolated and characterized. The complexes bearing diphosphazide ligands were compared to the analogous complexes containing phosphinimines, and, in the pyrrole-based system, the phosphazides were shown to allow for reactivity that is not available to their phosphinimine counterparts.

Contributions of Authors

The following thesis chapters containing original research are based on the following publications, the contents of which are reproduced with permissions from the corresponding publishers:

Chapter 1 –MacNeil, C.S.; Dickie, T. K. K.; Hayes, P. G. Actinide Pincer Chemistry: A New Frontier, in: *Pincer Compounds: Chemistry and Applications*; Morales-Morales, D., Ed.; Elsevier, 2018; pp. 133–172.

Chapter 2 – Dickie, T. K. K.; MacNeil, C. S.; Hayes, P. G. Consecutive N_2 loss from a uranium diphosphazide complex. *Dalton Trans.*, **2020**, *49*, 578–582.

Chapter 3 – Dickie, T. K. K.; Aborawi, A. A.; Hayes, P. G. Diphosphazide-Supported Trialkyl Thorium(IV) Complex. *Organometallics* **2020**, *39*, 2047–2052.

Chapter 4 –Dickie, T. K. K.; Hayes, P. G. Thorium(IV) Diphosphazide Complexes: CO_2 Insertion Into Th–C and Th–N Bonds. *Organometallics* **2022**, *41*, 278–283.

I am responsible for the experimental research reported in this thesis. In Chapter 1, Dr. C.S. MacNeil and I shared responsibility for the writing of the review, including writing and editing all subsections. In Chapter 2, Dr. C.S. MacNeil synthesized 1,2-diazidobenzene and initially developed the procedure to isolate K_2L", which I reproduced. I am solely responsible for all of the resulting uranium chemistry, including synthesis and characterization. In Chapter 3, I am responsible for the initiation and development of the project. A. A. Aborawi initially synthesized $L_{PN3}Th(CH_2SiMe_3)_3$ under my supervision, and I reproduced the procedure to characterize the complex. A. A. Aborawi aided with $^{13}C\{^1H\}$ NMR characterization of the complexes in Chapter 3. In Chapter 5, Dr. Dylan J.

Webb synthesized the phosphines $^{i}Pr_2P[(2\text{-}OH)(3,5\text{-}^{t}Bu)C_6H_2]$ and $Ph_2P[(2\text{-}OH)(3,5\text{-}^{t}Bu)C_6H_2]$ and Chris P. Forfar synthesized $TiCl_3(THF)_3$. A. A. Aborawi initially performed the $B(C_6F_5)_3$ reaction with $L_{PN3}Th(CH_2SiMe_3)_3$, which I reproduced. Prof. René T. Boeré aided with the X-ray crystallography in Chapters 2, 3, 4 and 5 and Dr. Dylan J. Webb and Jackson P. Knott performed all combustion measurements.

Acknowledgements

First, to my supervisor Paul: in my ups and downs in grad school, I always knew that I could count on you to bring me up. It's rare in any job to have a supervisor who always leaves you in a better mood after a meeting. I am so grateful to have such an understanding and empathetic supervisor, in addition to someone who holds me to a high standard in quality of work. If more professors were like you, academia would certainly be a more accessible and accepting place. I thank you especially for your support in the final years of my degree; where my own self-confidence fell, your support was unwavering.

The Hayes group will always hold a special place in my heart. To the old school, Brooke and Jackson, thank you for welcoming me so quickly into the group. To the new group – Desmond, Dylan, Ed, Sam and Daisy: some of us are leaving and some are just starting your adventures in grad school, but I wish you all the best. To Ash, it was a pleasure mentoring you. Good luck in all your endeavours–I know that you will be successful. To Connor: it's hard to articulate how much your friendship means to me. You make me want to be a better chemist and you push me to see the potential in myself. I would not be half the chemist I am today without you. To Kayla, my dearest friend, no matter how crazy life gets, we will get through it together. Love you always.

The Hardly-Know-Its, our amazing trivia team that is comprised of my good friends Amanda, Jalyce, David, Ashley, Mike, and Rob that has been going strong for 7 years, I love you all.

Music plays a valuable role in my life, and my nights in the choir are what kept me sane throughout all the chemistry. Thank you to the U of L Singers and especially to Dr. Janet Youngdahl for helping me keep in mind the importance of balance and recreation.

Justin–you were my biggest supporter and constant for 5 years. I wish you nothing but happiness and success in your future endeavours.

To my family: Mom, Dad, Steve, Ange, Lincoln and little niece or nephew-to-be. I couldn't have done this without your constant support.

I would also like to thank the many professors and teaching assistants at the U of L that have made a lasting impact on my career and my life. Special thanks to Dr. Greg Patenaude for listening to my crazy ideas and for helping me discover my passion for pedagogy.

Thank you to my committee members Prof. René Boeré and Prof. Michael Gerken, as well as Prof. Steve Patitsas, Prof. Borries Demeler and Prof. Suzanne Bart for attending my Ph.D. defence. Thank you all for your contributions.

To Brady: thank you for sticking it through with me. You have been there for me through everything. I couldn't have done this without you. I look forward to the future with you, wherever it may take us.

Finally, to anyone that is reading this and finds themselves in a dark place: it is ok to not be ok. Just take a breath and do the next right thing.

Table of Contents

ABSTRACT iii
CONTRIBUTIONS OF AUTHORS iv
ACKNOWLEDGEMENTS vi
TABLE OF CONTENTS viii
LIST OF COMPOUNDS xi
LIST OF TABLES xvi
LIST OF FIGURES xvii
LIST OF SCHEMES xix
LIST OF ABBREVIATIONS AND SYMBOLS xx

1. INTRODUCTION 1

1.1. ACTINIDES 1
1.1.1. Properties of the Actinides *1*
1.1.2. General Synthetic Strategies for Preparing Actinide Complexes *4*
1.2. PHOSPHAZIDES 6
1.2.1. Introduction to Phosphazides and the Staudinger Reaction *6*
1.2.2 Characterization of Phosphazides *8*
1.2.3 Methods of Phosphazide Stabilization *9*
1.2.4 Phosphazides as Ligands in Coordination Chemistry *11*
1.3. THESIS GOALS AND OUTCOMES 21
1.4. REFERENCES FOR CHAPTER 1 23

2. CONSECUTIVE N_2 LOSS FROM A URANIUM DIPHOSPHAZIDE COMPLEX 29

2.1. ABSTRACT 29
2.2. INTRODUCTION 29
2.3. SYNTHESIS AND CHARACTERIZATION OF URANIUM PHOSPHAZIDOSALEN AND PHOSPHASALEN COMPLEXES 33
2.4. CONCLUSIONS 38
2.5. EXPERIMENTAL DETAILS FOR CHAPTER 2 39
2.5.2. Laboratory Equipment and Apparatus *39*
2.5.3. Solvents *39*
2.5.4. Instrumentation and Details for NMR Experiments *40*
2.5.5. Additional Instrumentation *40*
2.5.6. Additional Safety Considerations *41*
2.5.7. Synthetic Methods *41*
2.5.8. Crystallographic Details *47*
2.6. REFERENCES FOR CHAPTER 2 51

3. DIPHOSPHAZIDE-SUPPORTED TRIALKYL THORIUM(IV) COMPLEX 53

3.1. ABSTRACT 53
3.2. INTRODUCTION 53
3.3. SYNTHESIS OF THORIUM PHOSPHAZIDE AND PHOSPHINIMINE COMPLEXES 55
3.4. CONCLUSIONS 62
3.5. EXPERIMENTAL DETAILS FOR CHAPTER 3 62
3.5.1. Laboratory Equipment and Apparatus *62*
3.5.2. Solvents *63*
3.5.3. Instrumentation and Details for NMR Experiments *63*
3.5.4. Additional Instrumentation *64*

3.5.5. Additional Safety Considerations *64*
3.5.6. Synthetic Methods *64*
3.5.7. Crystallographic Details *71*
3.6. REFERENCES FOR CHAPTER 3 ..... *75*

4. THORIUM(IV) DIPHOSPHAZIDE COMPLEXES: CO_2 INSERTION INTO TH–C AND TH–N BONDS 80

4.1. ABSTRACT 80
4.2. INTRODUCTION 81
4.3. CO_2 INSERTION INTO TH–C AND TH–N BONDS 83
4.4. N_2 LOSS FROM PHOSPHAZIDE LIGANDS 88
4.5. REACTION CHEMISTRY OF COMPLEX 1 92
4.6. CONCLUSIONS 93
4.7. EXPERIMENTAL DETAILS FOR CHAPTER 4 94
4.7.1. Laboratory Equipment and Apparatus *94*
4.7.2. Solvents *94*
4.7.3. Instrumentation and Details for NMR Experiments *95*
4.7.4. Additional Instrumentation *95*
4.7.5. Additional Safety Considerations *96*
4.7.6. Synthetic Methods *96*
4.7.7. Crystallographic Details *102*
4.8. REFERENCES FOR CHAPTER 4 106

5. PRELIMINARY RESULTS AND FUTURE WORK 109

5.1. U(VI) OXO COMPLEXES 109
5.1.1. Background *109*
5.1.2. U(VI) Oxo Phosphasalen and Phosphazidosalen Complexes *109*
5.1.3. Future Work – Towards U(VI) Oxo Chloride Complexes *115*
5.2. CATIONIC THORIUM ALKYL COMPLEXES 116
5.2.1. Background *116*
5.2.2. Synthesis of Alkylthorium Cations and Evidence for a Thorium Dication *117*
5.2.3. CO_2 Insertion into a Thorium Alkyl Cation *119*
5.2.4. Future Work – Towards Cationic Thorium Polymerization Catalysts *119*
5.3. TH(IV) AND U(IV) PINCER COMPLEXES WITH A BISPHOSPHINIMINE PYRROLE LIGAND 120
5.3.1. Background *120*
5.3.2. Synthesis of Th(IV) and U(IV) Pincer Complexes *121*
5.3.3. X-Ray Crystal Structure Comparisons *122*
5.3.4. Cationic Pincer Complexes *124*
5.3.5. Future Work – Towards Base-free Cationic Actinide Complexes *126*
5.4. TITANIUM(III) COORDINATION COMPLEXES WITH PHOSPHAZIDE LIGANDS 128
5.4.1. Background *128*
5.4.2. Titanium(III) and U(IV) Diphosphazide Complexes *128*
5.4.3. N_2 loss from Titanium(III) Diphosphazide Complex *131*
5.4.4. Future Work – Towards N_2 Capture from a Coordinated Phosphazide *132*
5.5. GROUP 1 PHOSPHAZIDE COMPLEXES AND OTHER PHOSPHAZIDES 133
5.5.1. Background *133*
5.5.2. Cis and Trans Aryl Phosphazides *133*
5.5.3. Group 1 Phosphazides *135*
5.5.4. Cyclopyrrolazide Ligand *136*
5.5.5. Future Work – Towards A Systematic Comparison of Stabilized Phosphazides *138*
5.6. EXPERIMENTAL DETAILS FOR CHAPTER 5 139
5.6.1. Laboratory Equipment and Apparatus *139*
5.6.2. Solvents *139*
5.6.3. Instrumentation and Details for NMR Experiments *140*
5.6.4. Additional Instrumentation *140*
5.6.5. Additional Safety Considerations *141*

5.6.6. Synthetic Procedures *141*
5.6.7. Crystallographic Details *152*
5.7. REFERENCES FOR CHAPTER 5 160

List of Compounds

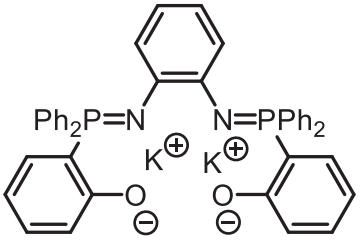

K_2L

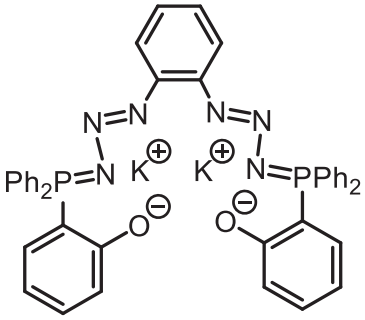

K_2L''

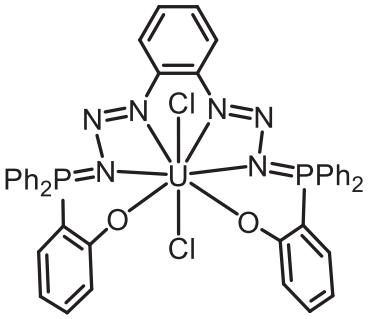

2-1

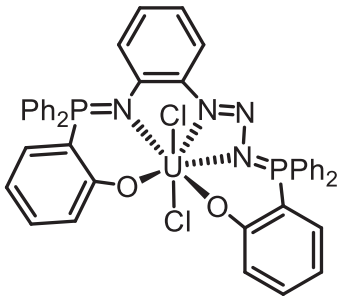

2-2

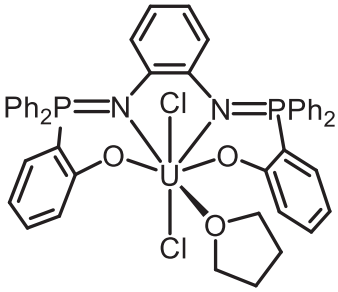

2-3

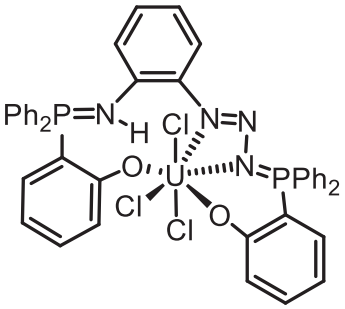

2-4

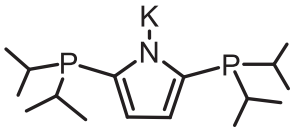

3-1

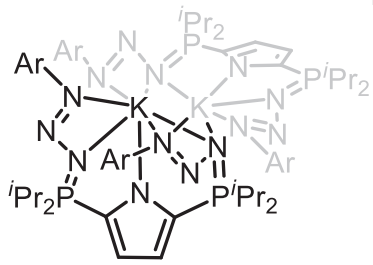

3-2

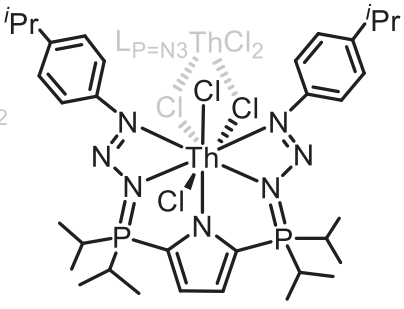

3-3

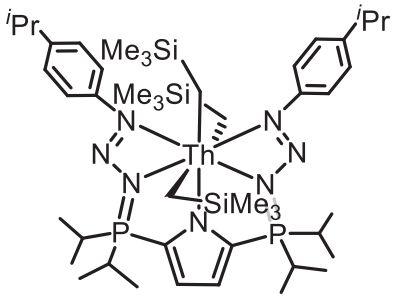

3-4

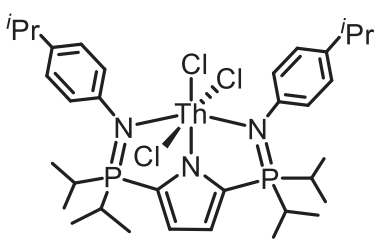

3-5

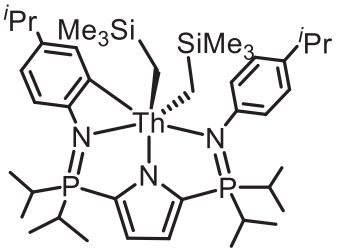

3-6

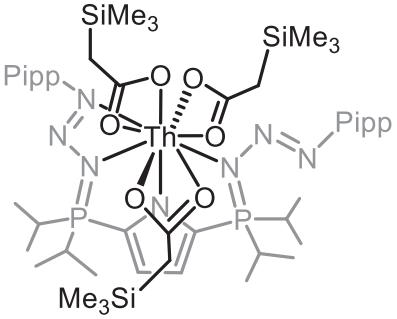

4-1

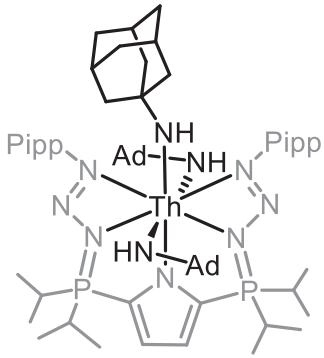

4-2

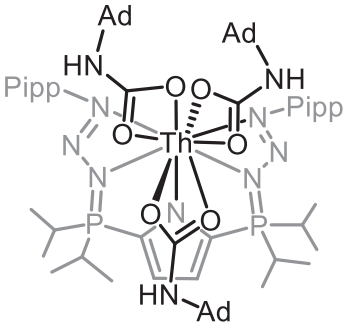

4-3

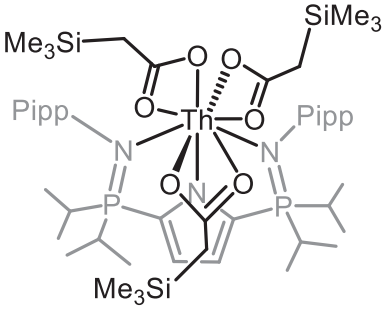

4-4

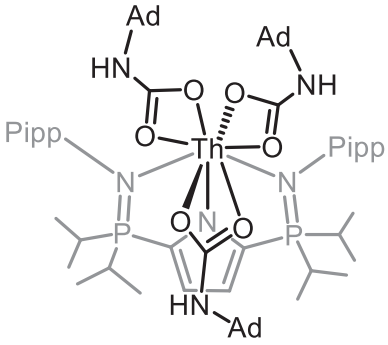

4-5

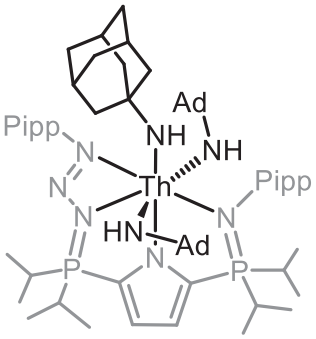

4-6

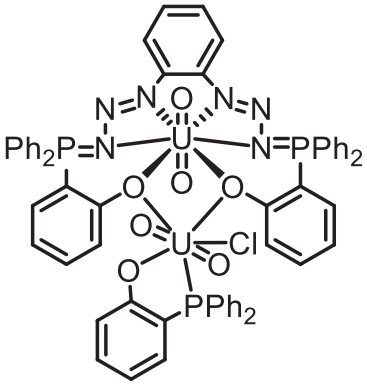

L''U(O)$_2$U(O)$_2$Cl[Ph$_2$P[(2-O)C$_6$H$_4$]

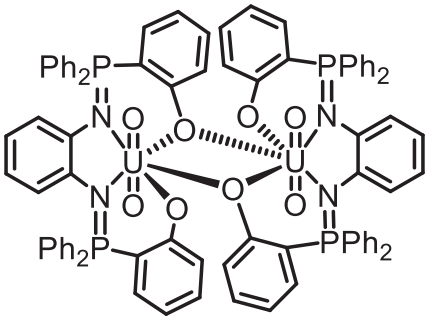

[LU(O)$_2$]$_2$

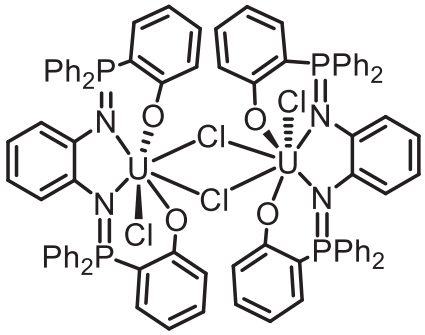

[LUCl(μ-Cl)]$_2$

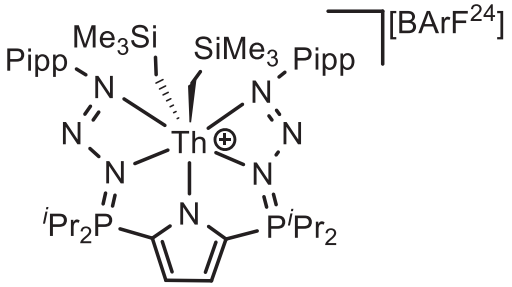

[L$_{PN3}$Th(CH$_2$SiMe$_3$)$_2$][BArF^{24}]

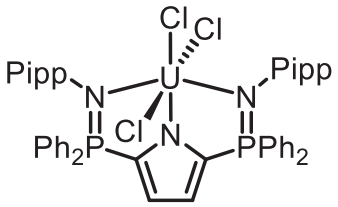

$_{Ph}L^{Pipp}UCl_3$

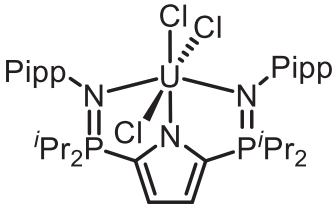

$_{i\text{Pr}}L^{Pipp}UCl_3$

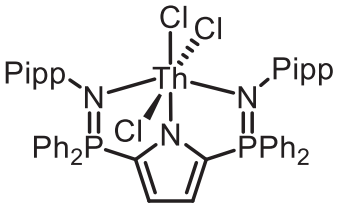

$_{Ph}L^{Pipp}ThCl_3$

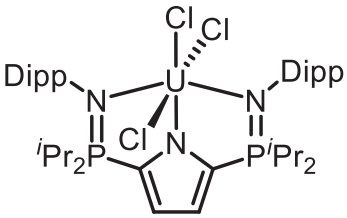

$_{i\text{Pr}}L^{Dipp}UCl_3$

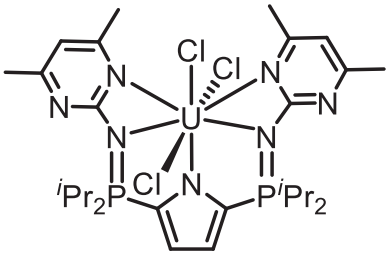

$_{i\text{Pr}}L^{Pyr}UCl_3$

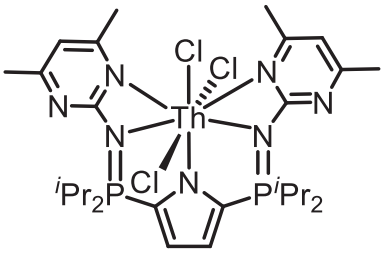

$_{i\text{Pr}}L^{Pyr}ThCl_3$

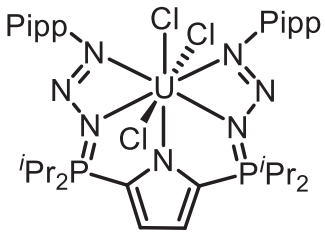

$L_{PN3}UCl_3$

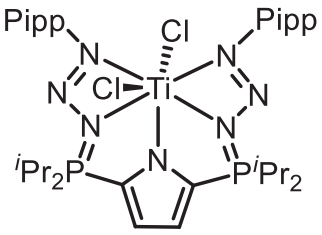

$L_{PN3}TiCl_2$

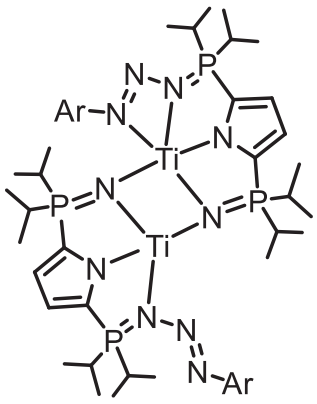

$[L_{PN3/PN\text{-}}TiCl_2]_2$

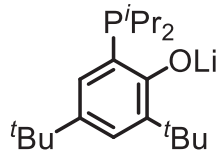

$Ph_2P[(2\text{-}OLi)(3,5\text{-}^tBu)C_6H_2]$

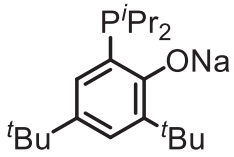

$Ph_2P[(2\text{-}ONa)(3,5\text{-}^tBu)C_6H_2]$

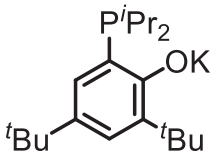

$Ph_2P[(2\text{-}OK)(3,5\text{-}^tBu)C_6H_2]$

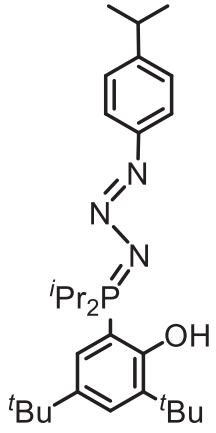

$[(2\text{-}OH)(3,5\text{-}^tBu)C_6H_2]^iPr_2P{=}N_3$ (Pipp)

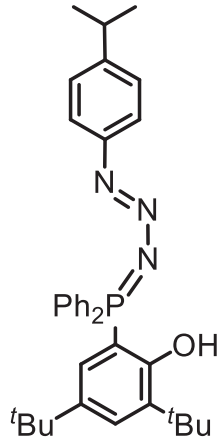

$[(2\text{-}OH)(3,5\text{-}^tBu)C_6H_2]Ph_2P{=}N_3$ (Pipp)

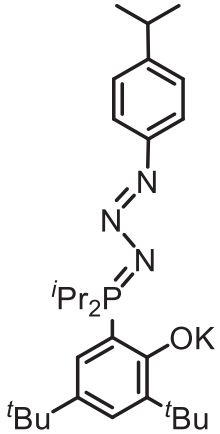

$[(2\text{-}OK)(3,5\text{-}^tBu)C_6H_2]^iPr_2P{=}N_3$ (Pipp)

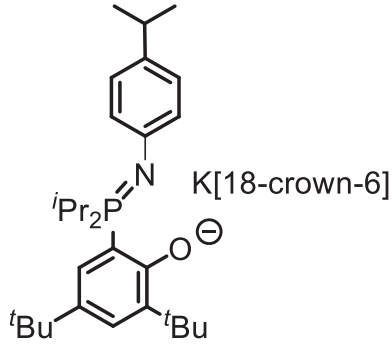

$[(2\text{-}OK)(3,5\text{-}^tBu)C_6H_2]^iPr_2P{=}N(Pipp)$ [18-crown-6]

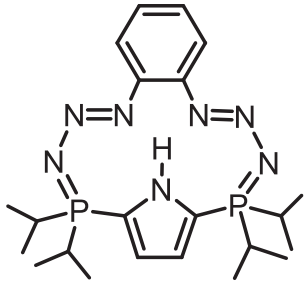

Cyclopyrrolazide

List of Tables

Table 2.1. Crystallographic details for complexes discussed in Chapter 2. 49
Table 3.1. X-ray crystallographic data and structure refinement for complexes **3-2**, **3-3**, **3-4**, **3-5** and **3-6**. 73
Table 4.1. X-ray crystallographic data and structure refinement for complexes **4-1, 4-2, 4-3** and **4-6**. 104
Table 5.1. Selected bond distances (Å) and angles (º) for L"$U(O)_2U(O)_2Cl[Ph_2P[(2\text{-}O)C_6H_4]$. 111
Table 5.2. Selected bond distances (Å) and angles (º) for $[LU^{VI}(O)_2]_2$ and $[LU^{IV}Cl(\mu\text{–}Cl)]_2$ 114
Table 5.3. Selected bond distances (Å) and angles (º) for $[_{iPr}L^{Pipp}]UCl_3$, $[_{Ph}L^{Pipp}]UCl_3$, $[_{iPr}L^{Dipp}]UCl_3$, $[_{Ph}L^{Pipp}]ThCl_3$ and $[_{iPr}L^{Pipp}]ThCl_3$ 123
Table 5.4. Selected bond distances (Å) and angles (º) for $[(_{iPr}L^{Pipp})ThCl_2(dme)][BArF^{24}]$ and $[_{iPr}L^{Pipp}]ThCl_3$ 125
Table 5.5. Selected bond distances (Å) and angles (º) for $[_{iPr}L^{Pyr}]ThCl_3$ and $[_{iPr}L^{Pyr}]UCl_3$. 127
Table 5.6. Selected bond distances (Å) and angles (º) for $L_{PN3}TiCl_2$ and $L_{PN3}UCl_3$. 130
Table 5.7. Selected bond distances (Å) and angles (º) for $^{i}Pr_2P[(2\text{-}OH)(3,5\text{-}^{t}Bu)C_6H_2]$ and cyclopyrrolazide. 135
Table 5.8. X-ray crystallographic data and structure refinement for the complexes in Chapter 5. 154

List of Figures

Figure 1.1. Examples of organoactinide complexes supported by carbocyclic ligands.....3
Figure 1.2. Methods of phosphazide stabilization 9
Figure 1.3. Coordination modes of coordinated phosphazides. 12

Figure 2.1. X-ray crystal structures of **2-1**, **2-2** and **2-3** with thermal ellipsoids drawn at 30% probability. Hydrogen atoms, P-phenyl groups, except for the ipso carbons, coordinated THF C atoms and solvent molecules of recrystallization (benzene, THF) are omitted for clarity; **2-3**: connectivity structure of **2-3.** 34
Figure 2.2. Solid-state structure of complex **2-4** with thermal ellipsoids shown at 30% probability. Hydrogen atoms except for H1, P(C5H5)2 groups excluding *ipso-C*, and solvent molecules of recrystallization (benzene) are omitted for clarity. The position of H1 was located directly in the difference map.....37

Figure 3.1. Left: X-Ray crystal structure of complex **3-4**. Thermal ellipsoids are represented at 50% probability. Hydrogen atoms have been omitted for clarity. Right: X-ray crystal structure of **3-6**. Thermal ellipsoids are represented at 50% probability. Hydrogen atoms have been omitted for clarity. 59

Figure 4.1. Ligand systems that support actinide-stabilized phosphazides. 82
Figure 4.2. Left: X-ray crystal structure of complex **4-1** with thermal ellipsoids drawn at 30% probability. Hydrogens have been removed for clarity. Only the major component of the disorder model is shown.. Right: Connectivity structure of complex **4-3**. Non-NH hydrogen atoms have been omitted for clarity. 85
Figure 4.3. X-ray crystal structure of complex **4-2** with thermal ellipsoids drawn at 30% probability. Non-NH hydrogens have been removed for clarity. Only the major component of the disorder model is shown. Only one of the two independent molecules in the asymmetric unit is depicted. 86
Figure 4.4. Stacked $^{31}P\{^{1}H\}$ NMR spectra of a sample of complex **4-3** in benzene-d_6 heated in a J. Young NMR tube. 90
Figure 4.5. X-ray crystal structure of **4-6** with thermal ellipsoids drawn at 30% probability. Non-NH hydrogens have been removed for clarity. Only the major component of the disorder model is shown.. 92

Figure 5.1. X-ray crystal structure of L"$U(O)_2U(O)_2Cl[Ph_2P[(2\text{-}O)C_6H_4]$. Thermal ellipsoids are drawn at 30% probability. Hydrogens have been removed for clarity. 111
Figure 5.2. X-ray crystal structures of L"UCl_2 (left) and L"$U(O)_2U(O)_2Cl[Ph_2P[(2\text{-}O)C_6H_4]$ fragment (right). Thermal ellipsoids are drawn at 30% probability. Hydrogens have been removed for clarity. Only the L"$U(O)_2$ fragment of L"$U(O)_2U(O)_2Cl[Ph_2P[(2\text{-}O)C_6H_4]$ is shown for comparison purposes. 112

Figure 5.3. X-ray crystal structures of $[LUCl(\mu\text{–}Cl)]_2$, $[LU(O)_2]_2$ and $LUCl_2(THF)$. The $LUCl_2(THF)$ structure is not of sufficient quality to discuss metrical parameters and is only used to determine atom connectivity. Thermal ellipsoids are drawn at 30% probability. Hydrogens have been removed for clarity.....114
Figure 5.4. X-ray crystal structures of uranium(IV) and thorium(IV) pincer complexes. Thermal ellipsoids are drawn at 50% probability. Hydrogens have been removed for clarity. 122
Figure 5.5. X-ray crystal structures of $[(_{iPr}L^{Pipp})UCl_2(THF)][BArF^{24}]$ and $[(_{iPr}L^{Pipp})ThCl_2(dme)][BArF^{24}]$. Thermal ellipsoids are drawn at 50% probability. Hydrogens have been removed for clarity. 125
Figure 5.6. X-ray crystal structures of $[_{iPr}L^{Pyr}]ThCl_3$ and $[_{iPr}L^{Pyr}]UCl_3$. Thermal ellipsoids are drawn at 50% probability. Hydrogens have been removed for clarity. 127
Figure 5.7. X-ray crystal structures of $L_{PN3}TiCl_2$ and $L_{PN3}UCl_3$. Thermal ellipsoids are drawn at 50% probability. Hydrogens have been removed for clarity. 130
Figure 5.8. X-ray crystal structure of $[L_{PN3/PN}\text{-}TiCl_2]_2$. Thermal ellipsoids are drawn at 50% probability. Hydrogens have been removed for clarity. 131
Figure 5.9. X-ray crystal structures of $Ph_2P[(2\text{-}OH)(3,5\text{-}^tBu)C_6H_2]$ and $^iPr_2P[(2\text{-}OH)(3,5\text{-}^tBu)C_6H_2]$. Thermal ellipsoids are drawn at 50% probability. Hydrogens have been removed for clarity.....135
Figure 5.10. X-ray crystal structure of cyclopyrrolazide. Thermal ellipsoids are drawn at 50% probability. Hydrogens have been removed for clarity. 137

List of Schemes

Scheme 1.1. Synthesis of tetrabenzyluranium derivatives. 6
Scheme 1.2. Reaction mechanism of the Staudinger reaction..... 7
Scheme 1.3. An H-bonding stabilized phosphazide and it's decomposition *via* intramolecular aza-Wittig reaction [46]. 10
Scheme 1.4. Synthesis of *cis*- and *trans*-phosphazides featuring a bulky dicarbadodecaborane [47]. 11
Scheme 1.5. Some examples of phosphazides stabilized by group 1 metals [48,49]..... 13
Scheme 1.6. Coordination of a pre-formed, metal-free phosphazide to a molybdenum centre [54]. 15
Scheme 1.7. Isomerization of a borane-stabilized phosphazide using UV irradiation [71]. 16
Scheme 1.8. Three different coordination modes of phosphazides stabilized by nearby boranes [72]. 17
Scheme 1.9. Isolation of the first scandium phosphazide, and the reaction chemistry of lutetium phosphazides [75]. 18
Scheme 1.10. Thermal decomposition of a cerium(IV) diphosphazide complex [76]. 19
Scheme 1.11. The only reported example of a metal phosphazide with three phosphazide units [77]. 20

Scheme 2.1. Some examples of stabilized phosphazides.[4h,5,10] 30
Scheme 2.2. Comparison of phosphasalen ligand synthesis by the Kirsanov reaction (a)[9a] and by the Staudinger reaction (this work) (b). 32
Scheme 2.3. Synthesis of uranium complexes **2-1** and **2-3.** 35
Scheme 2.4. Reaction of phosphazidosalen ligand **K_2L''** with 18-crown-6. 36

Scheme 3.1. Phosphinimine formation and methods of phosphazide stabilization..... 54
Scheme 3.2. Synthesis of compound **3-2**..... 56
Scheme 3.3. Synthesis of compounds **3-3** to **3-6**..... 58

Scheme 4.1. Synthesis of complexes **4-1**, **4-2** and **4-3**. 84
Scheme 4.2. Synthesis of complexes **4-4**, **4-5** and **4-6**. 89

Scheme 5.1. Synthesis of U(VI) phosphazidosalen and phosphasalen complexes. 110
Scheme 5.2. Proposed synthesis of a U(V) diphosphazide complex..... 115
Scheme 5.3. Synthesis of a thorium diphosphazide cation..... 117
Scheme 5.4. Synthesis of a series of uranium(IV) and thorium (IV) pincer complexes. 121
Scheme 5.5. Synthesis of a uranium(IV) and thorium(IV) pincer cation..... 124
Scheme 5.6. Synthesis of a uranium(IV) and thorium(IV) complex with internal lewis-bases..... 126
Scheme 5.7. Synthesis of a titanium(III) diphosphazide complex and its decomposition 129
Scheme 5.8. Synthesis of *cis* and *trans* aryl phosphazides..... 134
Scheme 5.9. Synthesis of a cyclic *cis*-diphosphazide..... 136

List of Abbreviations and Symbols

Å	Angstrom
Ad	1-adamantyl
Anal	Calcd calculated (elemental analysis)
Ar	aryl
$BArF^{24}$	$[B(C_6H_3(CF_3)_2)_4]$
br	broad
BCF	tris(pentafluorophenyl)borane
C	Celsius
Cp	cyclopentadienyl
Cp*	pentamethylcyclopentadienyl
d	doublet
dme	1,2-dimethoxyethane
equiv	equivalents
η	eta (coordination)
FLP	frustrated Lewis pair
g	gram(s)
h	hour(s)
Hz	hertz
I	nuclear spin quantum number
^{i}Pr	isopropyl
J	symbol for coupling constant

K	Kelvin
κ	kappa (coordination)
m	multiplet
Me	methyl
mg	milligram
MHz	megahertz
mL	millilitre(s)
min	minute(s)
mmol	millimol(s)
NMR	nuclear magnetic resonance
ov	overlapping
Ph	phenyl
ppm	parts per million
q	quartet
R	alkyl or aryl group
s	singlet
Sol	solvent
sp	septet
t	triplet
^{t}Bu	*tert*-butyl
THF	tetrahydrofuran
tol	toluene
δ	chemical shift (parts per million)

°	degree
$^{n}J_{XY}$	n-bond coupling constant between X and Y
1D	one dimensional
$\{^{1}H\}$	proton decoupled
2D	two dimensional
λ	wavelength

1. Introduction[a,b,c]

1.1. Actinides

1.1.1. Properties of the Actinides

Chemistry with actinide metals has historically been underdeveloped due to the inherent difficulties in handling molecular actinide complexes. Actinide chemistry is generally only practiced with thorium and uranium for reasons of cost and availability, as well as radioactivity. While all the actinide elements are radioactive, thorium and uranium have extremely long half-lives compared to most other metals in the actinide series. Thorium-232 is an α-emitter with $t_{1/2}$ > 14 billion years. Depleted uranium is primarily U-238, which also emits an α-particle when it decays and has a half-life of more than 4 billion years. For these reasons, uranium and thorium are generally considered weakly radioactive [1,2]. Despite the associated complications, actinide chemistry is of great fundamental interest, and has thus blossomed into a rapidly emerging subfield of both inorganic and organometallic chemistry.

The actinide metals are similar to the lanthanides in size but have access to a greater number of oxidation states, a trait more commonly shared with transition metals. The actinide elements are also recognized for their ability to form complexes with high coordination numbers (>6) which can lead to unique chemical transformations. Such reactivity is also often attributed to the large, diffuse *f*-orbitals which participate much more

---

[a] *Coord. Chem. Rev.* reference style used throughout this chapter

[b] Adapted with permission from C. S. MacNeil, T. K. K. Dickie, P. G. Hayes, Actinide Pincer Chemistry: A New Frontier, in: D. Morales-Morales (Ed.), Pincer Compounds: Chemistry and Applications, Elsevier, Amsterdam, Netherlands, 2018, pp. 133–172.

[c] Adapted from T. K. K. Dickie, P. G. Hayes. Phosphazides as Ligands in Coordination Chemistry. In preparation.

in covalent bonding than their lanthanide counterparts [3,4]. Notably, computational investigations have shown that the actinide 5*f* orbitals provide access to chemical transformations which are not possible with transition metals because of their ability to hybridize and stabilize transition states that would normally be inaccessible [5,6]. In June of 2017, a 60-year-old debate sparked by Glenn Seaborg on the covalent nature of the actinide–chlorine bond [7] may have been resolved experimentally [8]. Compelling evidence for 5*f*–3*p* orbital mixing in $AmCl_6^{3-}$ was obtained using X-ray absorption spectroscopy (XAS). Covalency in actinide–ligand bonding is also relevant to nuclear waste management, where the topic is hotly debated.

Although uranium and thorium are both actinide metals, each display markedly different reactivity. Thorium can generally only access the 4+ oxidation state, while uranium complexes in the 3+ to 6+ oxidation states are commonly reported [1]. The enhanced reactivity of An(III) ions comes at a cost; the negative reduction potential (E^{Θ} – 0.6 V (U), –3.7 V (Th) for the $M^{IV/III}$ redox couple in MX_6 ions) [9] discourages redox cycles needed in certain catalytic reactions. Nevertheless, the greater range of readily available oxidation states avails a wide realm of potential chemistry, but it can also lead to additional decomposition pathways, particularly for species in solution. Tetravalent uranium, the most common oxidation state for that metal, is also paramagnetic, which can present challenges regarding characterization *via* NMR (nuclear magnetic resonance) spectroscopy, such as line broadening, loss of coupling, and huge chemical shift ranges [10].

Organoactinide chemistry traces its roots to heteroleptic π-complexes (e.g., $(Cp^*/Cp)_2AnX$, $Cp^* = C_5Me_5^-$; $Cp = C_5H_5^-$; X = I, Cl), much in the same way organotransition metal chemistry became popularized by discrete single-metal

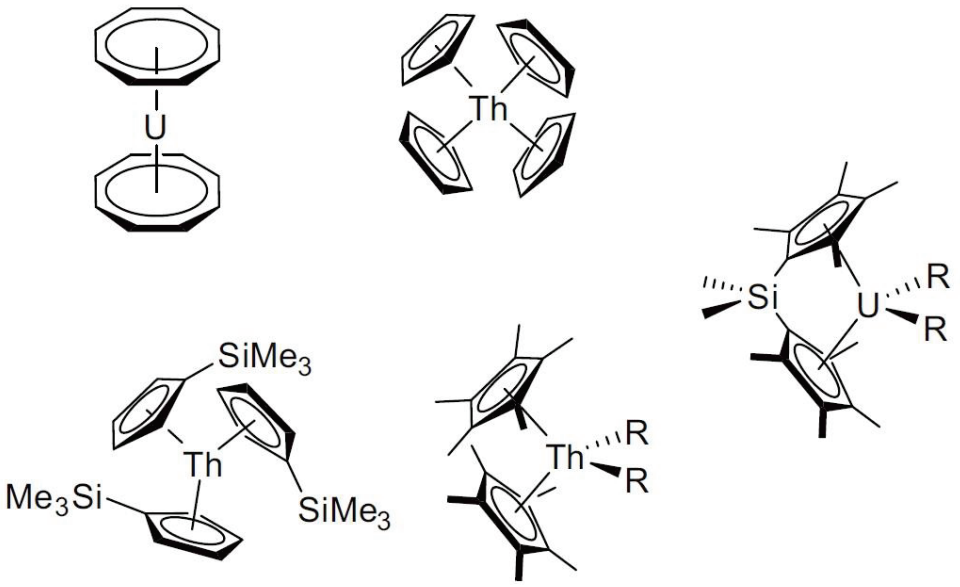

Figure 1.1. Examples of organoactinide complexes supported by carbocyclic ligands.

π-complexes and the metallocene class, Cp_2M (M = transition metal) [11]. Early publications highlighted the successful pairing of carbocyclic ligands and actinide metals; Marks [12–14], Evans [8,15–17], Ephritikhine [18–21], and others have contributed pioneering work in this respect (Figure 1.1). Notably, as the structural diversity of available ancillary ligands has increased considerably over the past several decades, exciting and unprecedented reaction chemistry and catalysis involving *d*-block, lanthanide, and actinide metals has been reported at a continuously accelerating rate. In a 2015 annual survey of the organometallic chemistry of lanthanides and actinides, Edelmann remarks that "approximately 20% of the papers published in 2015 were in the area of organoactinide chemistry" [4].

Hybrid ligands that incorporate both soft and hard donors can engender reactivity not available to the metallocenes. The development of meridionally coordinating pincer ligands has been a watershed moment in this respect and has contributed to the advancement of knowledge insofar that entirely new fields have evolved. For example,

David Milstein has published a substantial body of work that enhances our understanding of how pincer ligands and metals cooperate in chemical transformations, particularly with respect to the lofty goal of catalytically functionalizing unactivated hydrocarbons and simple diatomics (N_2, CO, CH_4) [22]. Redox-active pincer ligands capable of multielectron transformations have conferred noble metal reactivity to first-row *d*-block elements (Fe, Co, Ni, Mn). As a whole, actinide chemistry continues to be dominated by sterically demanding carbocyclic ligand sets, a consequence of large ionic radii and preference for high coordination numbers. Herein lies the main challenge of actinide chemistry, the delicate balance between stabilizing the reactive metals without rendering them inert. To this end, rational ligand design has been a huge boon to the area of actinide chemistry.

1.1.2. General Synthetic Strategies for Preparing Actinide Complexes

The comparatively slow progression of actinide chemistry is due in part to the geopolitical and logistical constraints placed on the acquisition and transport of radiotoxic metals. A compounding effect of this reality is that viable actinide starting materials are less common than for rare earth and transition metals, which are not typically under such strict regulations. Despite these challenges, actinide halide complexes have become available by operationally simple protocols, and a handful of reports outlining the preparation of valuable uranium and thorium halide solvento adducts ($UBr_3(THF)_4$ [23], $UI_3(THF)_4$ [23], $UI_3(DME)_2$ [23], $UI_3(py)_4$ [23], $UI_4(OEt_2)_2$ [24], $UI_4(NCMe)_4$ [25], $UI_4(NCPh)_4$ [26], $ThCl_4(THF)_{3.5}$ [27], $ThBr_4(THF)_4$ [28], $ThBr_4(py)_4$ [28], $ThBr_4(NCMe)_4$ [28], $ThI_4(THF)_4$ [29], $ThCl_4$(1,4-dioxane)$_2$ [27], $ThCl_4(DME)_2$ [27], $ThI_4(DME)_2$ [29]; DME = 1,2-dimethoxyethane, py = pyridine) have been disclosed. The stability of these

starting materials allows for reliable preparation and handling, which is crucial for any synthetic campaign. Given that actinide complexes often suffer from thermal instability, it should come as no surprise that cases of decomposition have been observed in solvated actinide species, and thus, such reactivity must be kept in mind. For example, $ThI_4(DME)_2$ is robust whereas $ThI_4(THF)_4$ undergoes ring-opening of THF to afford $ThI_3[O(CH_2)_4I](THF)_3$ [29]. Furthermore, UI_3(1,4-dioxane) demonstrates substantial thermal stability and is resistant to deleterious pathways that plague the analogous THF adducts. While uranium and thorium are the primary metals for which actinide complexes have been reported, neptunium and plutonium starting materials are available as solvated trivalent iodide complexes $NpI_3(THF)_4$ [23], $PuI_3(THF)_4$ [23], $PuI_3(py)_4$ [23], $PuI_3(Et_2O)_x$ [30] and, and more recently, as tetravalent chloride species, $NpCl_4(DME)_2$ and $PuCl_4(DME)_2$ [31]. From the availability of these complexes, significant potential for coordination chemistry with transuranic elements exists. Given that salt metathesis protocols represent the predominant entry point for ancillary ligand-supported actinide chemistry, any improvement upon the synthesis of actinide halides is noteworthy.

Alkane elimination has been used to generate coordination complexes from proteo ligands and solvated trialkyl rare earth compounds [32,33]. In contrast, examples where favorable alkane elimination has resulted in complex formation are not as common for the actinides. A glaring absence in the availability of stable organoactinide reagents capable of alkane elimination pathways has undoubtedly slowed progress in this area. A 2015 report on the improved and new syntheses of various homoleptic U(IV) benzyl derivatives by Bart and co-workers could represent a turning point in the practicality of using alkane elimination strategies to generate well-defined organoactinide complexes (Scheme 1.1) [12,34]. Arnold and co-workers [35] recently added to this discussion by providing details

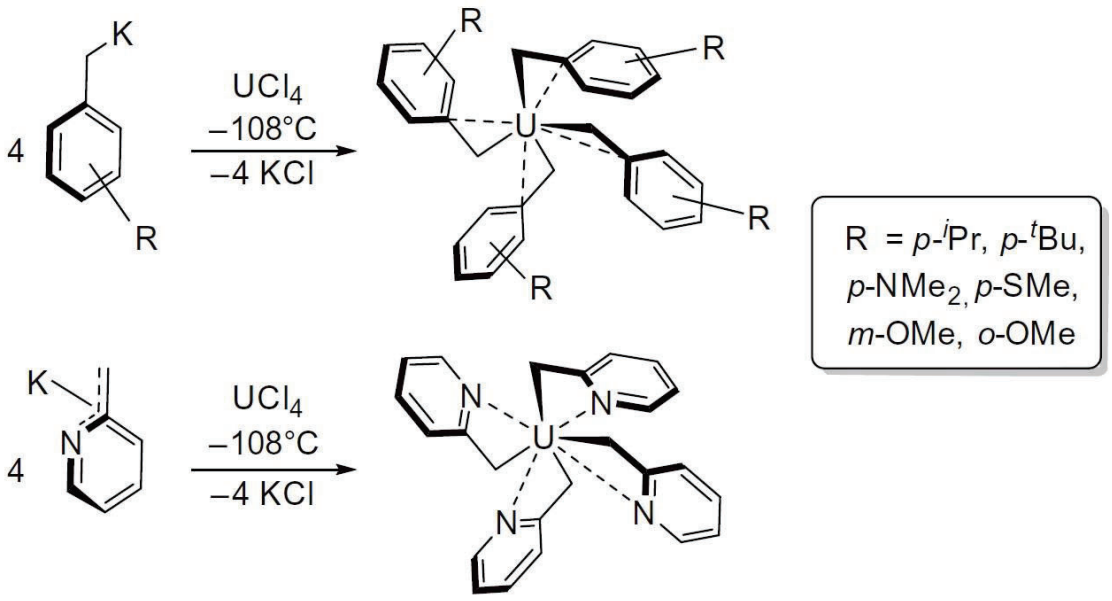

Scheme 1.1. Synthesis of tetrabenzyluranium derivatives.

on the formation of the homoleptic U(III) aryl complex U[2,6-(4-^{t}BuC$_6$H$_4$)$_2$C$_6$H$_3$]$_3$, which contains reactive U–C bonds and facilitates the double insertion of ^{i}PrN=C=N^{i}Pr. Thus, there is clearly growing potential for alkane elimination routes as diverse avenues into actinide coordination chemistry. Finally, amine elimination methods, though even less common, have been explored using U(NEt$_2$)$_4$ [36]. The availability of An(N(SiMe$_3$))$_3$ (An = U, Np, Pu) [25,32] will likely also prove useful for generating An(III) complexes bearing amido functionalities.

1.2. Phosphazides

1.2.1. Introduction to Phosphazides and the Staudinger Reaction

The Staudinger reaction, introduced in 1919, has been utilized across the chemical sciences for the formation of phosphinimines (or "iminophosphoranes") from tertiary phosphines (PR$_3$) and organic azides (R'–N$_3$) [37]. The phosphinimine (R$_3$P=N–R')

functional group has found utility in coordination chemistry due to the ease by which the steric and electronic properties can be fine-tuned at both the P and N heteroatoms, allowing for diverse coordination behaviour that renders them valuable ligands in inorganic and organometallic chemistry [38]. Despite the ubiquity of the Staudinger reaction, the phosphazide intermediate is rarely addressed. Phosphazides are often considered fleeting, unstable to the elimination of dinitrogen, and their infrequent isolation is often unintended. The

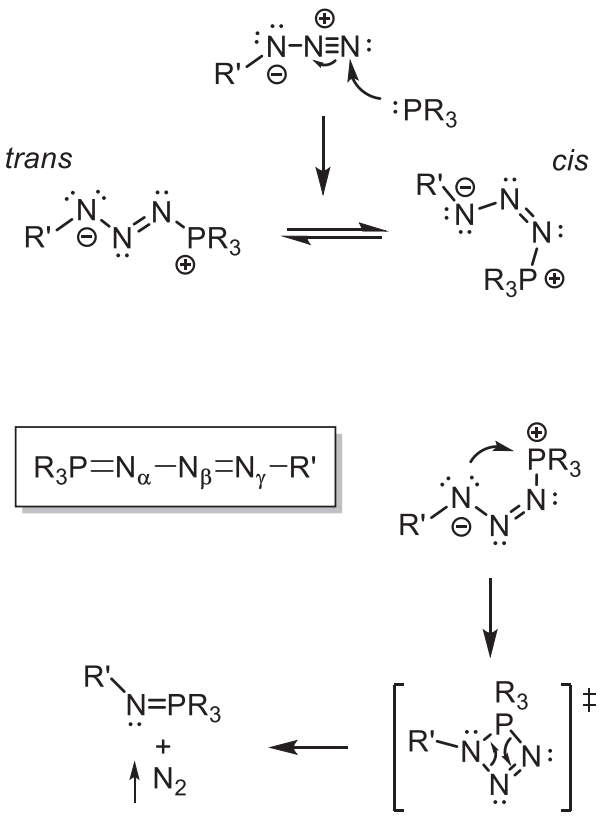

Scheme 1.2. Reaction mechanism of the Staudinger reaction

mechanism of the Staudinger reaction has been thoroughly examined computationally (Scheme 1.2) [39-42]. These studies have revealed that of the two phosphazide isomers, *cis* and *trans*, the *cis* arrangement is generally the more stable due to electrostatic interactions between phosphorus and the gamma (γ) nitrogen [42]. The *cis* phosphazide can cyclize to form the four-membered transition state which readily releases dinitrogen, a process that is highly favoured. Accordingly, the vast majority of isolated phosphazides have been characterized in the solid state as the *trans* isomer, as the barrier to isomerization can prevent dinitrogen loss.

1.2.2. Characterization of Phosphazides

Phosphazides can be characterized in many ways, but simple ^{1}H NMR spectroscopy is rarely helpful in distinguishing phosphinimines from phosphazides. Conversely, ^{31}P NMR spectroscopy is immensely valuable for identifying phosphazides, and the $P{=}N_3$ resonance is almost always found 10-20 ppm downfield of the corresponding P=N signal. Elemental analysis is also useful for confirming phosphazide complexes, as they often contain very high nitrogen content. Infrared spectroscopy was often used before the advent of modern-day X-ray crystallography; however, the requisite P=N and N=N stretches can overlap with other signals, making them difficult to locate. When identifiable, a phosphazide $P{=}N_3$ stretch is often found at a higher wavenumber than the corresponding P=N stretch in a phosphinimine. For example, the simple cobalt phosphazide complex $CoBr_2[furN_3{=}P(C_6H_{11})_3]{\bullet}Et_2O$ displayed a $P{=}N_3$ stretch of 1223 cm^{-1} and an N–N stretch of 970 cm^{-1}, and can be compared to the P=N stretch in $CoBr_2[furN{=}P(C_6H_{11})_3]_2$ at 1096 cm^{-1} [43]. Finally, X-ray crystallography is invaluable for identifying phosphazides, and the recent increase in reported azides is undoubtedly due to the rapid advancement of this technology. Phosphazides in the solid state often display bond lengths that support a somewhat delocalized bonding representation. The mean N–N distances, in all crystallographically-characterized coordinated phosphazides is 1.355 Å (N_α–N_β), and 1.267 Å for N_β–N_γ[d], which can be compared to standardized N–N single bonds 1.454 (Å) and N=N double bonds 1.245 (Å) [44].

[d] The N_α–N_β and N_β–N_γ distances for all metal- and boron-phosphazides with reported X-ray crystal structures from 1978-2022 was collected and the mean was calculated (52 in total).

1.2.3. Methods of Phosphazide Stabilization

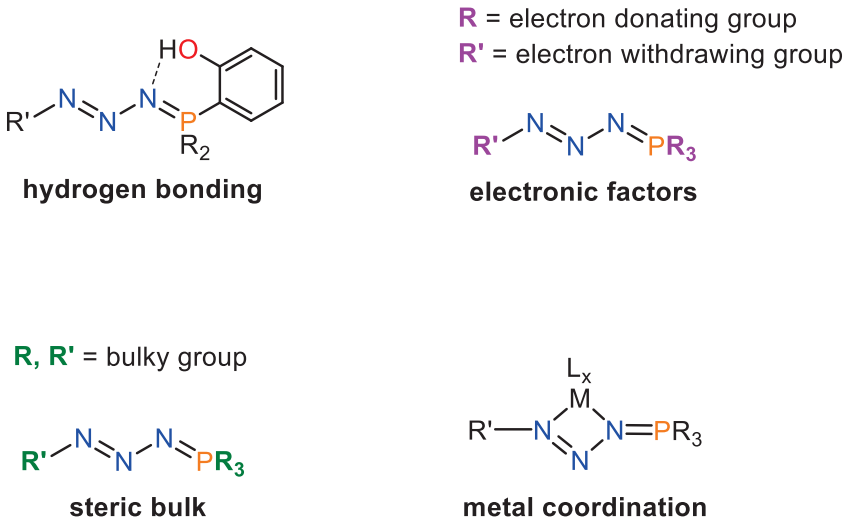

Figure 1.2. Methods of phosphazide stabilization

Phosphazides can be stabilized by one or more different factors [45]. Figure 1.2 depicts a general overview of these methods. Most systems involve disfavouring the *trans* to *cis* isomerization by lowering the ground state energy of the *trans* isomer. For example, strong electron donors on phosphorus, as well as electron withdrawing groups on nitrogen, have been shown to stabilize the *trans* isomer [5]. Interaction of a lone pair on one of the nitrogen atoms in an H-bonding interaction can also result in an isolated phosphazide. Valasco *et al.* isolated the phosphazide *o*-(Ph_3PN_3)C_6H_4[(CO)NH(CO)-*p*-tolyl)] (**1**) upon reaction of *N*-(4-Methylbenzoyl)-*o*-azidobenzamide with triphenylphosphine at 0 °C in diethylether (Scheme 1.3) [46]. An intermolecular H-bonding interaction from a neighbouring N*H* is the likely source of the stability of phosphazide **1**. A solid-state structure of **1** was not obtained; however, the significant downfield shift of the N*H* signal in the ^{1}H NMR spectrum (from 10.54 ppm to 13.98 ppm) suggests an interaction between the N*H* and the phosphazide. Upon heating **1** to reflux in toluene for 6 hours, 2-(4-

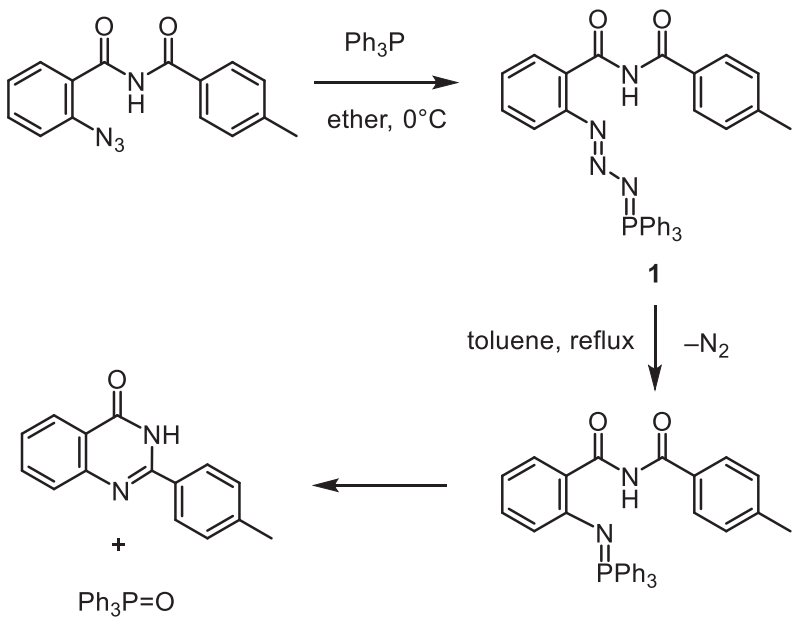

Scheme 1.3. An H-bonding stabilized phosphazide and its decomposition *via* intramolecular aza-Wittig reaction [46].

methylphenyl)-3H-quinazoline-4-one was isolated. This product is the result of initial N_2 loss to produce a phosphinimine, followed by an immediate intramolecular aza-Wittig reaction, along with concomitant production of $Ph_3P{=}O$.

Sterically demanding groups on either the N or P atoms can hinder the formation of the cyclic transition state and prevent liberation of dinitrogen gas. A report by R. D. Kennedy describes two phosphazides with large dicarbadodecaboranes 1-(N_3PPh_3)-2-Me-*closo*-1,2-$C_2B_{10}H_{10}$ (**2**) and 1-(N_3PPh=)-2-Ph-*closo*-1,2-$C_2B_{10}H_{10}$ (**3**) (Scheme 1.4) [47]. Intriguingly, in the solid state, compound **2** contains a phosphazide in the *cis*-form, whereas **3** contains a *trans*-phosphazide. The phenyl group on the borane cluster in **3** likely prevents *cis*-isomerization, and the borane cluster itself provides sufficient steric bulk to disfavour the four-membered transition state required for N_2 extrusion.

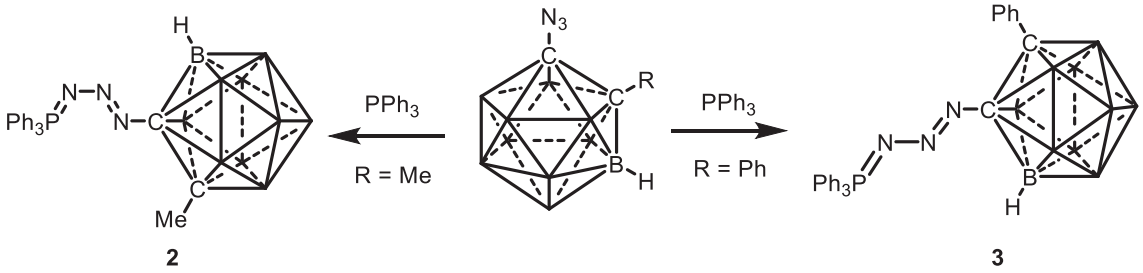

Scheme 1.4. Synthesis of *cis*- and *trans*-phosphazides featuring a bulky dicarbadodecaborane. Unlabelled vertices are B–Cl. [47] .

1.2.4. Phosphazides as Ligands in Coordination Chemistry

Coordination of the phosphazide unit to a metal or metalloid centre has been shown in many instances; however, it is rarely intentional, and very few examples of reaction chemistry have been reported. A summary of the crystallographically confirmed coordination and bonding modes of phosphazides is given in Figure 1.3 and will be referred to throughout the chapter. It should be noted that these coordination modes are established by X-ray crystallography, and the solution-state structure could differ. What constitutes an interaction between the metal and the phosphazide donor can be ambiguous, depending on the metal-nitrogen distance. The significance of these interactions is not always clear-cut, and can only be implied using coordination geometry, reaction chemistry and van der Waals radii. Phosphazides are generally considered neutral, L-type ligands, regardless of the bonding mode. I have depicted all examples of phosphazides with localized multiple bonding; however, it could be argued that the bonding in the phosphazide is delocalized, and the reality is likely somewhere in-between.

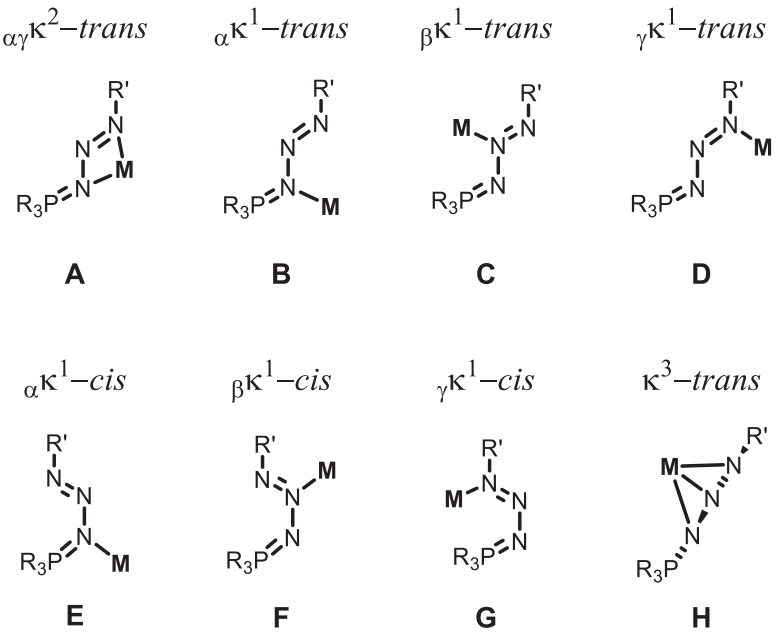

Figure 1.3. Bonding modes of coordinated phosphazides.

Phosphazide complexes have been reported for metals from across the periodic table. They can be separated into group 1 [48-50], groups 3-7 [51-57] , groups 8-12 [58-64], groups 13-14 [65-74], and actinides and lanthanides [75-78].

The first transition metal phosphazide, $CoBr_2[furN_3P(C_6H_{11})_3]\bullet Et_2O$ (**4**; fur = 2-COC_4H_3O), was described by Kirmaier and colleagues in 1977 [43]. Complex **4** was prepared by reaction of $CoBr_2[P(C_6H_{11})_3]_2$ with $FurN_3$, as well as preformed phosphazide $FurN_3P(C_6H_{11})_3$ with $CoBr_2$ at low temperature (>0 °C). Unfortunately, no solid-state structure was obtained; however, IR and EA analysis substantiated the presence of a phosphazide moiety.

Another early example of transition metal phosphazides was published by Haymore *et al.* in 1978, wherein they explored the reaction of Ph–N_3 and *p*-tol–N_3 (*p*-tol = 4-MeC_6H_5) with various phosphine complexes of tungsten and molybdenum [51,52]. In 1982, they were able to obtain the first X-ray crystal structure of a metal phosphazide,

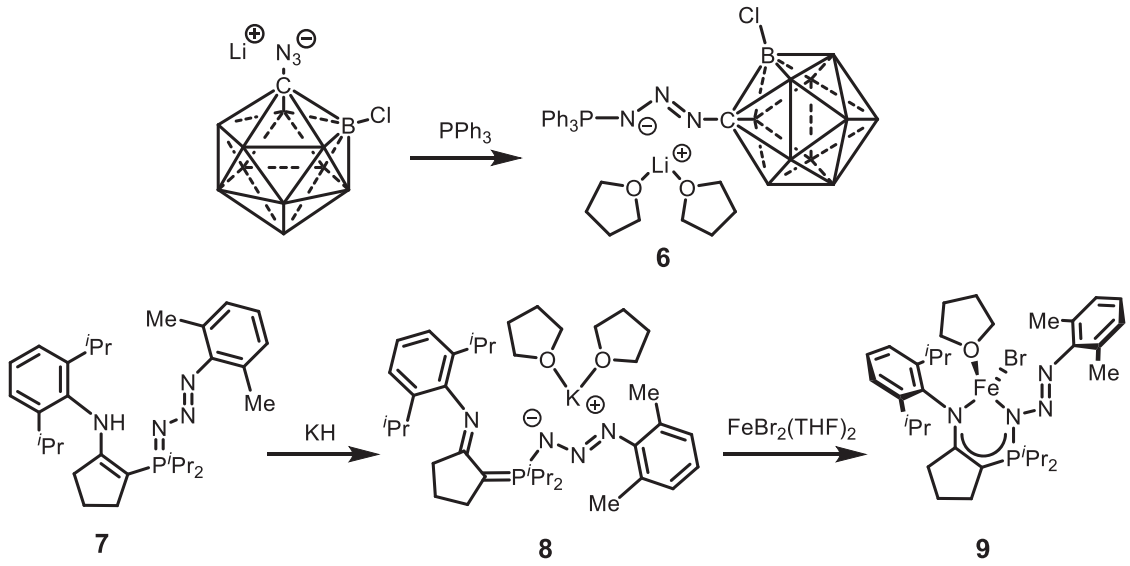

Scheme 1.5. Some examples of phosphazides stabilized by group 1 metals [48,49].

$WBr_2(CO)_3$(*p*-tolN_3PPh_3) (coordination mode A) (**5**) [52]. Complex **5**, as well as one equivalent of free *p*-tol$N{=}PPh_3$, was formed upon combination of $WBr_2(CO)_3(PPh_3)_2$ with two equivalents of *p*-tolN_3. This reaction was unfortunately complicated by the fact that $WBr_2(CO)_3(PPh_3)_2$ and $RN{=}PPh_3$ exist in equilibrium with $WBr_2(CO)_2(RN{=}PPh_3)_2$ and free PPh_3. Notably, compound **5** is stable in refluxing benzene for 2 hours. Intriguingly, the analogous reaction between dicarbonyl $WBr_2(CO)_2(PPh_3)_2$ and two equivalents of *p*-tolN_3 was accompanied by rapid loss of N_2, giving $WBr_2(CO)_2$(tol$N{=}PPh_3)_2$. Finally, reaction of Re(III) phosphine complexes with azides only resulted in oxidation of the metal to Re(IV), with no evidence of rhenium phosphazides.

The first example of a group 1 stabilized phosphazide was reported by Lavallo and co-workers [48]. A lithium salt of an azido carboranyl cluster was reacted with PPh_3 to produce the lithium stabilized phosphazide $[Ph_3P{=}N_3CB_{11}Cl_{11}]Li(THF)_2$ (**6**). X-ray crystallography revealed that the lithium cation is bound to both N_α and N_γ of the phosphazide (coordination mode A, Scheme 1.5, top), as well as two THF molecules, in the solid state. This phosphazide was determined to be surprisingly thermally robust, with

no loss of N_2 even upon heating for 24 hours at 150 °C in FC_6H_5. However, in THF an equilibrium exists between PPh_3 and the free azide vs. compound **6**. At 60 °C, only PPh_3 is visible in the $^{31}P\{^1H\}$ NMR spectrum, suggesting complete dissociation from the phosphazide. Conversely, when the sample was cooled to −35 °C the equilibrium shifted completely to **6**. This is likely due to THF solvation of the Li ion, disrupting the formation of the phosphazide. In CH_2Cl_2 this equilibrium does not exist; a single ^{31}P NMR resonance for compound **6** was observed at 25 °C.

Unlike the aforementioned examples where the phosphazide was generated in the presence of a metal, the Fryzuk group reported the synthesis of a metal-free phosphazide, which was subsequently coordinated to potassium [49]. The metal-free phosphazide was prepared by reaction of the cyclopentylidene-based phosphine-imine (2,6-^{i}Pr$_2$C$_6$H$_3$)N=C$_5$H$_7$(2-P^{i}Pr$_2$) with one equivalent of xylyl azide (2,6-Me$_2$C$_6$H$_3$-N$_3$) in THF. (Scheme 1.5, bottom). The N–H interaction (2.046(16) Å), along with the steric bulk imparted by the xylyl group, are likely reasons for the stability of the resultant enamine-phosphazide $HEpN_3^{iPr,Me}$ (**7**, $EpN_3^{iPr,Me}$ = (2,6-^{i}Pr$_2$C$_6$H$_3$)N=C$_5$H$_6$[2-P^{i}Pr$_2$N$_3$(2,6-Me$_2$C$_6$H$_3$)]). Upon addition of KH, the amine was deprotonated, leading to a slight upfield shift in the $^{31}P\{^1H\}$ NMR resonance (δ 50.9 to δ 49.0). Solid-state experiments revealed a K^+ ion bound in coordination mode A, the first example of a potassium-bound phosphazide [$K(EpN_3^{iPr,Me})(THF)$] (**8**). Notably, the phosphazide was transferred intact from potassium to iron upon reaction with $FeBr_2(THF)_2$, affording the unusual iron complex [$FeBr(EpN_3^{iPr,Me})(THF)$] (**9**) (coordination mode B; Fe–Nα = 2.039(7) Å, Fe–Nγ = 2.710(8) Å). Given the utility of salt metathesis reactions as a common route to prepare metal complexes, such chemistry is particularly intriguing.

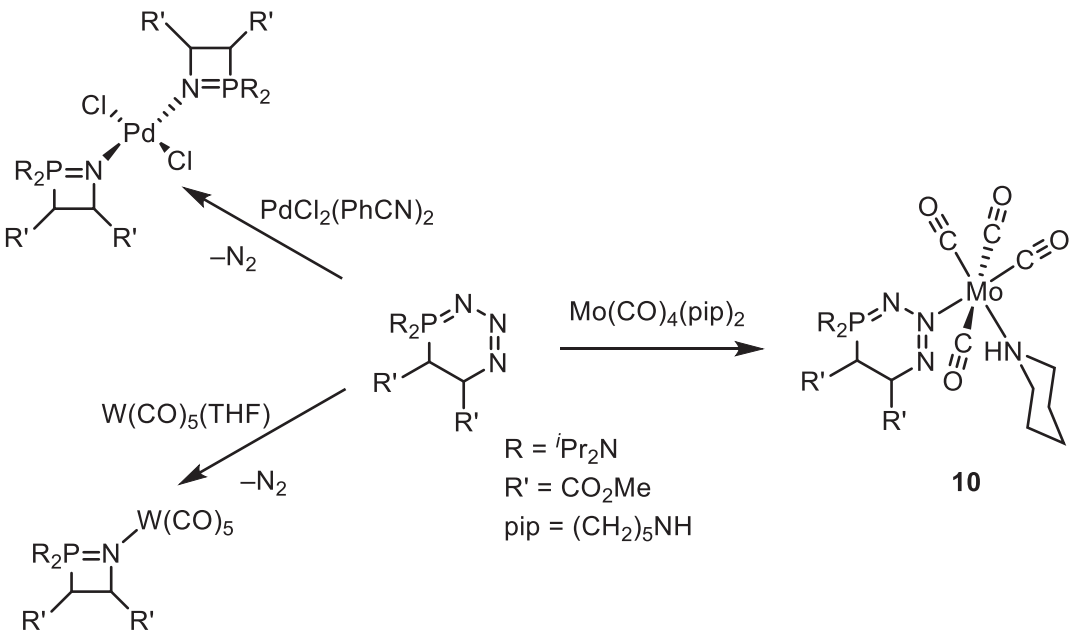

Scheme 1.6. Coordination of a pre-formed, metal-free phosphazide to a molybdenum centre [54].

Bertrand *et al.* successfully characterized the metal-free cyclic *cis*-phosphazide ($^{i}Pr_2N)_2PN_3[CH(CO_2Me)]_2$ and attempted to coordinate the pre-formed phosphazide to several metal centres (Scheme 1.6) [54]. Surprisingly, only the molybdenum phosphazide $[(^{i}Pr_2N)_2PN_3\{CH(CO_2Me)\}_2]Mo(CO)_4(pip)$ (**10**) was isolable. Addition of either $PdCl_2(PhCN)_2$ or $W(CO)_5(THF)$ to $(^{i}Pr_2N)_2PN_3[CH(CO_2Me)]_2$ prompted the loss of N_2 and formation of a four-membered, heterocyclic phosphinimine which coordinates to both Pd and W (Scheme 1.6). Meanwhile, the analogous reaction with $Mo(CO)_4(pip)_2$ (pip = $(CH_2)_5NH$) afforded complex **10**, wherein molybdenum is bound by the N_β nitrogen of the *cis*-phosphazide. To our knowledge, this is the only known example of coordination mode F. The large N_α–N_β–N_γ angle of 124.2(3)° is enforced by the cyclical nature of the phosphazide and is unchanged from the free molecule (124.0(3)°) [78]. As expected, the phosphazide ring maintains its planarity, and the geometry about molybdenum approaches ideal octahedral.

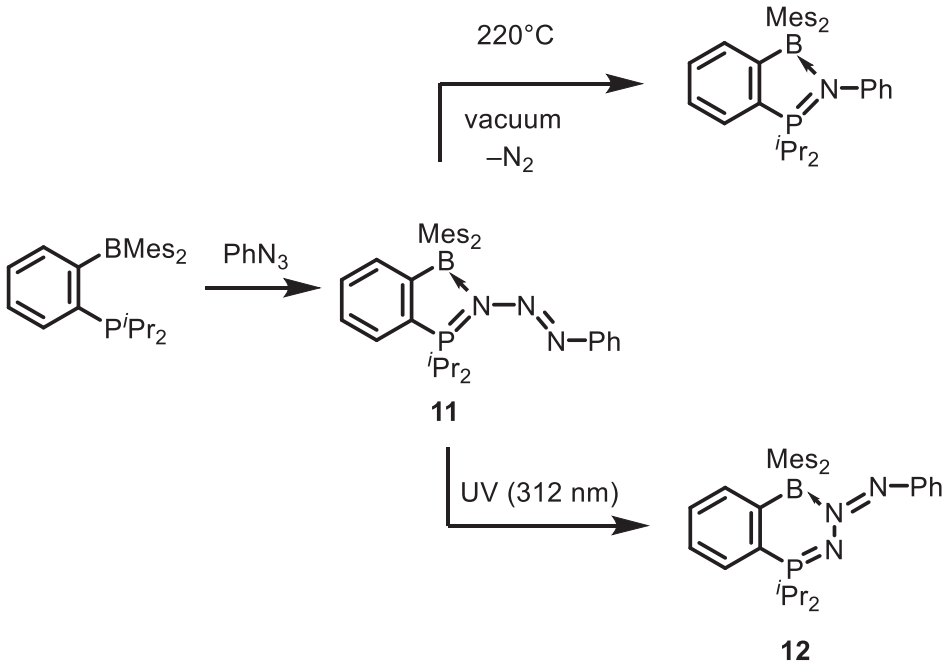

Scheme 1.7. Isomerization of a borane-stabilized phosphazide using UV irradiation [71].

In a groundbreaking report from Bourissou in 2007, a borane-stabilized phosphazide *cis*-*ortho*-(^{i}Pr$_2$P=N$_3$Ph)C$_6$H$_4$(BMes$_2$) (**11**) was found to change coordination mode upon irradiation with UV light [71]. Compound **11** is extremely thermally stable and exhibits only 10% conversion to the phosphinimine when heated to reflux in toluene for 18 hours; as a consequence, photolysis experiments were pursued. When a THF solution of **11** was irradiated for 4 hours (λ=312 nm), the *cis*-N$_\alpha$-coordinated phosphazide (coordination mode E) undergoes photo-isomerization to a *trans*-phosphazide coordinated through the β-nitrogen (*trans*-*ortho*-(^{i}Pr$_2$P=N$_3$Ph)C$_6$H$_4$(BMes$_2$), **12**, Scheme 1.7). This represents yet another new phosphazide coordination mode, G. The previously planar **11** changes to a boat conformation; however, the B–N distance is not altered drastically (*c.f.* **11**: 1.649(2) Å vs. **12**: 1.684(7) Å). At 120.4(2)° the N$_\alpha$–N$_\beta$–N$_\gamma$ angle in **11** is markedly larger and sits between the average values for non-cyclic coordinated phosphazides (110.6°) and the cyclic phosphazide **10** (124.2(3)°). Similarly, Slootweg *et al.* were able to completely

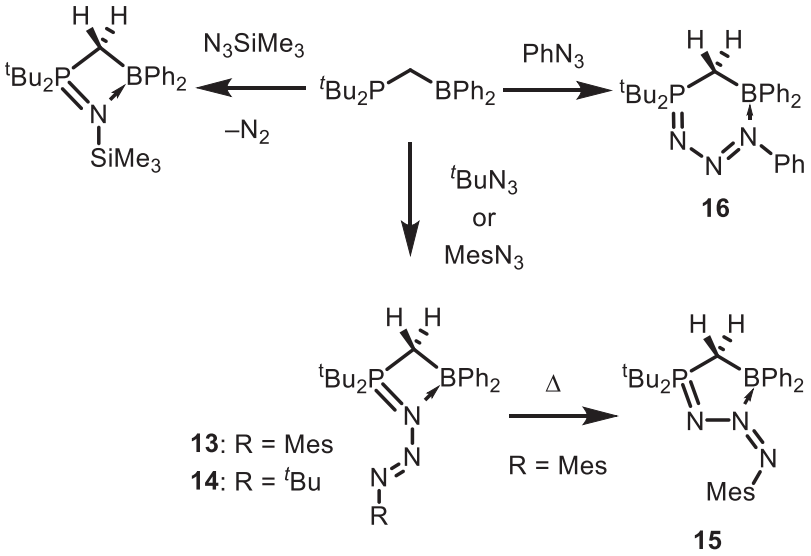

Scheme 1.8. Three different coordination modes of phosphazides stabilized by nearby boranes [72].

isomerise *cis*-(^{t}Bu$_2$P=N$_3$Mes)CH$_2$(BPh$_2$) (**13**) to *trans*-(^{t}Bu$_2$P=N$_3$Mes)CH$_2$(BPh$_2$) (**15**) by heating at 75 °C in toluene for 3 days (Scheme 1.8) [72]. Alternately, when PhN$_3$ was used instead of ^{t}BuN$_3$ or MesN$_3$, γ-nitrogen coordinated phosphazide *trans*-(^{t}Bu$_2$P=N$_3$Ph)CH$_2$(BPh$_2$) (**16**) (coordination mode G) was isolated.

The chemistry of the lanthanides is far less developed than that of the transition metals, but the field is quickly growing, and that trend is also evident in the number of recently published lanthanide phosphazide complexes. Cui and co-workers isolated the first rare-earth phosphazide complexes upon the addition of three equivalents of MesN$_3$ to Sc and Lu phosphine dialkyl complexes LM(CH$_2$SiMe$_3$)$_2$(THF) (M = Sc, Lu; L = (2,6-C$_6$H$_3$Me$_2$)NCH$_2$C$_6$H$_4$PPh$_2$) [75]. Complexes [L^{N3Mes}]M[($\kappa^{\alpha\beta}$-MesN$_3$CH$_2$SiMe$_3$)]$_2$ (M = Sc (**14**), Lu (**15**); L^{N3Mes} = (2,6-C$_6$H$_3$Me$_2$)NCH$_2$C$_6$H$_4$PPh$_2$N$_3$Mes) are the result of azide insertion into the metal–P and two metal–C bonds (Scheme 1.9). The two complexes are isostructural and display coordination mode A; the metal–N$_\alpha$ distances are shorter than the metal–-N$_\gamma$ distances (Sc–N$_\alpha$ = 2.276(2) Å, Sc–N$_\gamma$ = 2.528(2) Å; Lu–N$_\alpha$ = 2.367(7) Å, Lu–

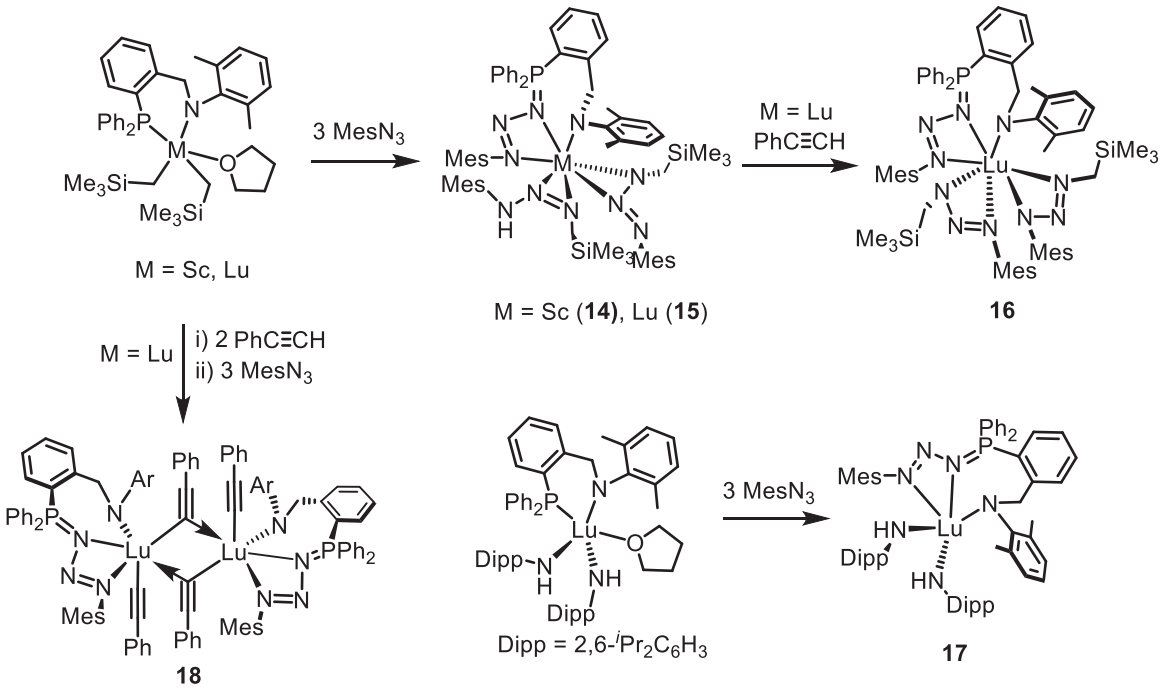

Scheme 1.9. Isolation of the first scandium phosphazide, and the reaction chemistry of lutetium phosphazides [75].

N_γ = 2.566(6) Å). Lutetium phosphazide **15**, in the presence of phenylacetylene, undergoes isomerization of the triazenide ligand to form $[L^{N3Mes}]Lu[(\kappa^{\alpha\gamma}\text{-}MesN_3CH_2SiMe_3)]_2$ (**16**) (Scheme 1.9) [75]. The phosphazide P–N and N–N bond lengths in **16** are essentially unchanged relative to **15**. Since compound **15** is the result of inserting one equivalent of azide into each of the two Lu–C bonds, the Cui and colleagues replaced the $–CH_2SiMe_3$ groups with NHDipp moieties, as the azide is unlikely to insert into a Lu–N bond. As anticipated, when 3 equivalents of $MesN_3$ were added to $LLu(NHDipp)_2(THF)$, only one azide insertion occurred, generating a single phosphazide functionality in $L^{N3Mes}Lu(NHDipp)_2$ (complex **17**, coordination mode A). Finally, when phenylacetylene was added *before* the azide, the dimeric lutetium phosphazide, $(L^{N3Mes}Lu(C{\equiv}CPh)_2)_2$, (**18**, coordination mode A), that bears bridging acetylide ligands, formed. Presumably the first step in this transformation is the generation of $LLu(C{\equiv}CPh)_2$ and $SiMe_4$, *via* a σ-bond

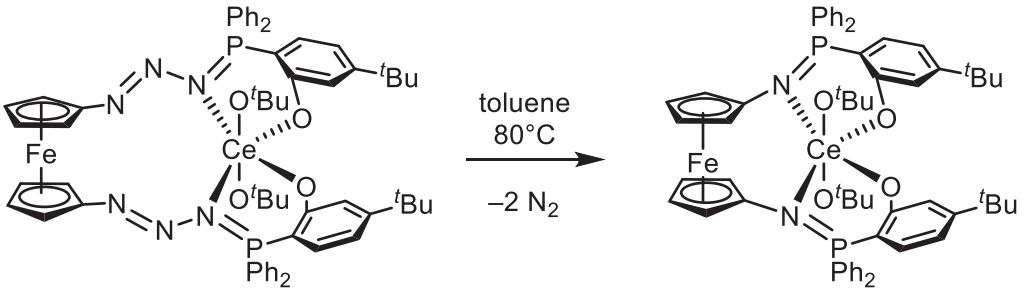

19

Scheme 1.10. Thermal decomposition of a cerium(IV) diphosphazide complex [76].

metathesis process. This compound must then react with mesityl azide, creating the phophazide groups.

The cerium diphosphazide complex $[Fc(N_6O_2)]Ce(O^tBu)_2$ (Fc = 1,1′-ferrocenylene; $Fc(N_6O=)$ = κ^4-1,1′-$[(N_3)PPh_2(2\text{-}O\text{-}3\text{-}^tBuC_6H_4)]_2Fc$) (**19**, Scheme 1.10), that features a ferrocene backbone, was isolated by Diaconescu and co-workers [76]. The ferrocenium group precludes the possibility of a κ^2-coordinated phosphazide due to the constricted ligand binding pocket. Correspondingly, complex **19** exhibits coordination mode B, wherein only the α-nitrogens of the ligand are coordinated to cerium, at distances of 2.5523(36) Å and 2.5355(37) Å. The 6-coordinate cerium centre is best described as distorted square pyramidal. Heating complex **19** at 85 °C in toluene afforded the corresponding phosphinimine complex, along with concomitant liberation of 2 equivalents of dinitrogen.

$CeN[CH_2CH_2N(AdN_3{=}P^iPr_2)]_3$ (**20**), synthesized by Zhu and colleagues, is not only one of the few lanthanide phosphazide complexes, it is also the only example of a triphosphazide metal complex [77]. Complex **20**, which was prepared by reaction of three equivalents of adamantyl azide with the cerium complex $[CeN\{CH_2CH_2N(P^iPr_2)\}_3]_2$ (Scheme 1.11), exhibits a single resonance (δ 29.5 in benzene-d_6) in its $^{31}P\{^1H\}$ NMR spectrum, and surprisingly, does not decompose when heated in toluene at 80 °C for 12

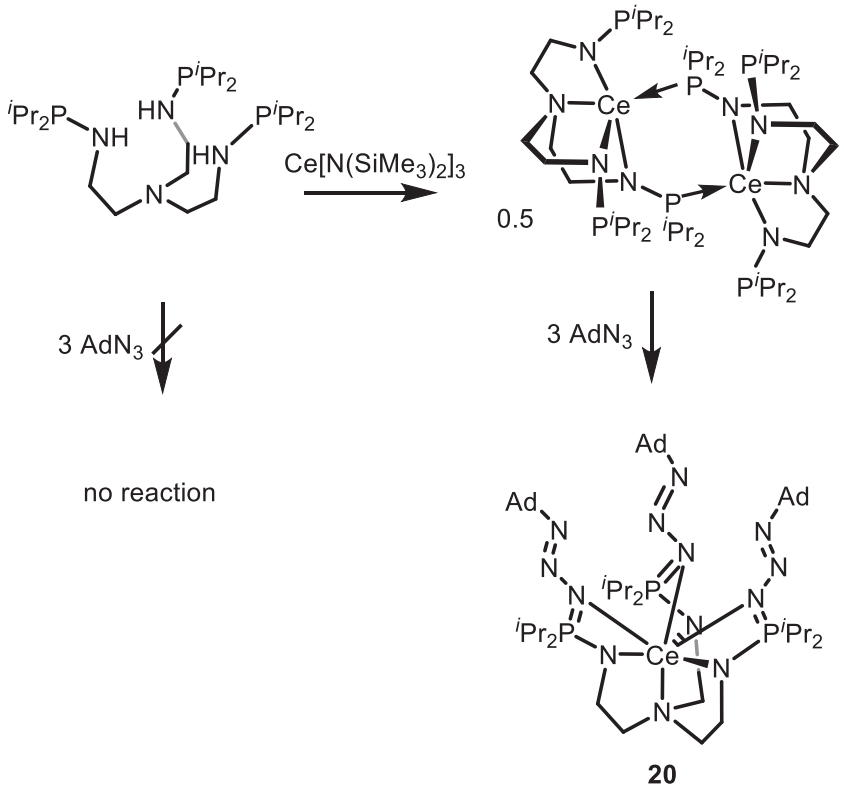

Scheme 1.11. The only reported example of a metal phosphazide with three phosphazide units [77].

hours. When three equivalents of Me_3SiN_3 was added to $[CeN\{CH_2CH_2N(P^iPr_2)\}_3]_2$ instead of AdN_3, immediate N_2 loss occurred, suggesting that the steric bulk of the adamantyl group is essential for phosphazide stabilization. Intriguingly, the neutral triphosphine ligand $N[CH_2CH_2NH]_3$ is completely unreactive toward azides, indicating that the cerium centre is necessary for facilitating phosphine attack on the azide. Solid-state analysis reveals that the heptacoordinate cerium is bound only by the α-nitrogens of the three *trans* phosphazides (coordination mode B), and the crowded metal centre cannot accommodate a κ^2-phosphazide.

1.3. Thesis Goals and Outcomes

The interest in phosphazides is rapidly growing. Of the 72 metal-coordinated phosphazides that have been reported, 60 have been published after 2006, and approximately half were reported in the past 5 years. While phosphazides can vary incredibly in thermal stability, their ability to access 8 different coordination modes provides a niche in the maturing fields of coordination and organometallic chemistry, especially since the discovery of new functional groups is uncommon. Before the publications featured in this dissertation, there were no reported phosphazide complexes of actinides. Actinide complexes are particularly suited to achieve the potential of phosphazides as ligands, as their high coordination numbers and affinity for hard nitrogen donors is ideal for accommodating multiple phosphazide units. Recognizing this, it was the goal of this thesis to synthesize ligands containing stabilized phosphazides, coordinate these ligands to uranium and thorium, and investigate the stability and reactivity of the resulting actinide complexes.

First, a derivative of the phosphasalen ligand featuring two phosphazides is described in Chapter 2. This phosphazidosalen ligand was coordinated to uranium and step-wise N_2 elimination was observed from the resulting uranium complex L"UCl_2 (**2-1**).

Using the knowledge obtained from Chapter 2, a related diphosphazide ligand, L_{PN3}, was made, taking inspiration from the pyrrole-based phosphinimine ligand $L_{P=N}$. This system allowed for the isolation of a rare trialkyl thorium complex $L_{PN3}Th(CH_2SiMe_3)_3$ (**3-4**) as described in Chapter 3.

Chapter 4 showcases the reaction chemistry of the thorium diphosphazide trialkyl species $L_{PN3}Th(CH_2SiMe_3)_3$ and its derivatives with CO_2 to make carbamates and carboxylates.

Finally, Chapter 5 provides preliminary results for other related projects. These include the exploration of U(VI) chemistry with phosphasalen and phosphazidosalen ligands, titanium(III) and (IV) chloride complexes with the L_{PN3} ligand, uranium and thorium cations and metal-free phosphazide compounds. I endeavoured to provide all of the necessary information so that the projects could be continued by future students.

1.4. References for Chapter 1

[1] S.A. Cotton, The actinides, Annu. Rep. Prog. Chem., Sect. A: Inorg. Chem.106 (2010) 286–294.

[2] S. Cotton, Lanthanide and Actinide Chemistry, John Wiley & Sons, Chichester, 2006, p. 145–153.

[3] F.T. Edelmann, Lanthanides and actinides: Annual survey of their organometallic chemistry covering the year 2011, Coord. Chem. Rev. 257 (2013) 1122–1231.

[4] F.T. Edelmann, Lanthanides and actinides: Annual survey of their organometallic chemistry covering the year 2015, Coord. Chem. Rev. 318 (2016) 29–130.

[5] A. Yahia, L. Maron, Is Thorium a d Transition Metal or an Actinide? An Answer from a DFT Study of the Reaction between Pyridine N-Oxide and $Cp_2M(CH_3)_2$ with M = Zr, Th, and U, Organometallics 28 (2009) 672–679.

[6] L. Castro, A. Yahia, L. Maron, Are 5*f* Electrons Really Active in Organoactinide Reactivity? Some Insights from DFT Studies, Chem. Phys. Chem. 11 (2010) 990–994.

[7] R.M. Diamond, K. Street, G.T. Seaborg, An Ion-exchange Study of Possible Hybridized 5f Bonding in the Actinides, J. Am. Chem. Soc. 76 (1954) 1461–1469.

[8] J.N. Cross, J. Su, E.R. Batista, S.K. Cary, W.J. Evans, S.A. Kozimor, *et al.*, Covalency in americium (III) hexachloride, J. Am. Chem. Soc. 139 (2017) 8667–8677.

[9] L.J. Nugent, R.D. Baybarz, J.L. Burnett, Electron-transfer spectra and the II-III oxidation potentials of some lanthanide and actinide halides in solution, J. Phys. Chem. 73 (1969) 1177–1178.

[10] D.B. Leznoff, C.E. Hayes, G. Mund, Paramagnetic Organometallic Complexes, in: R. A. Scott (Ed.), Encyclopedia of Inorganic and Bioinorganic Chemistry, John Wiley & Sons Ltd, 2011.

[11] C.E. Hayes, D.B. Leznoff, Actinide coordination and organometallic complexes with multidentate polyamido ligands, Coord. Chem. Rev. 266–267 (2014) 155–170.

[12] P.J. Fagan, J.M. Manriquez, T.J. Marks, Organometallics of the f-Elements, In: T.J. Marks, R.D. Fischer (Eds.), Proceedings of the NATO Advanced Study Institute held at Sogesta, Urbino, Italy, September 11–22, 1978, Springer, Dordrecht, The Netherlands, 1979, p. 113–148.

[13] T.J. Marks, J.R. Kolb, Covalent transition metal, lanthanide, and actinide tetrahydroborate complexes, Chem. Rev. 77 (1977) 263–293.

[14] T.J. Marks, Chemistry and Spectroscopy of f-Element Organometallics Part II: the Actinides, In: S. J. Lippard (Ed.), Progress in Inorganic Chemistry, John Wiley & Sons, Hoboken, NJ, 2007, p. 223–333.

[15] W.J. Evans, S.A. Kozimor, J.W. Ziller, $[(C_5Me_5)_2U][(\mu\text{-}Ph)_2BPh_2]$ as a four electron reductant, Chem. Commun. (2005) 4681–4683.

[16] W.J. Evans, S.A. Kozimor, J.W. Ziller, A.A. Fagin, M.N. Bochkarev, Facile Syntheses of Unsolvated UI3 and Tetramethylcyclopentadienyl Uranium Halides, Inorg. Chem. 44 (2005) 3993–4000.

[17] W.J. Evans, D.J. Wink, D.R. Stanley, Reinvestigation of the reaction of tert-butyllithium with uranium tetrachloride: formation of catalytically active uranium (III) hydride complexes, Inorg. Chem. 21 (1982) 2565–2573.

[18] J.-C. Berthet, J. Maynadié, P. Thuéry, M. Ephritikhine, Linear uranium metallocenes with polydentate aromatic nitrogen ligands, Dalton Trans. 39 (2010) 6801–6807.

[19] J.-C. Berthet, Y. Miquel, P.B. Iveson, M. Nierlich, P. Thuéry, C. Madic, *et al.*, The affinity and selectivity of terdentate nitrogen ligands towards trivalent lanthanide and uranium ions viewed from the crystal structures of the 1∶3 complexes, J. Chem. Soc., Dalton Trans. (2002) 3265–3272.

[20] J.-C. Berthet, M. Nierlich, Y. Miquel, C. Madic, M. Ephritikhine, Selective complexation of uranium(III) over lanthanide(III) triflates by 2,2′:6′,2″-terpyridine. X-Ray crystal structures of $[M(OTf)_3(terpy)_2]$ and $[M(OTf)_2(terpy)_2(py)][OTf]$ (M = Nd, Ce, U) and of polynuclear μ-oxo uranium(IV) complexes resulting from hydrolysis, Dalton Trans. (2005) 369–379.

[21] J.-C. Berthet, C. Rivière, Y. Miquel, M. Nierlich, C. Madic, M. Ephritikhine, Selective Complexation of Uranium(III) over Cerium(III) and Neodymium(III) by 2,2′:6′,2″-Terpyridine − X-ray Crystallographic Evidence for Uranium-to-Ligand π Back-Bonding, Eur. J. Inorg. Chem. 2002 (2002) 1439–1446.

[22] J.R. Khusnutdinova, D. Milstein, Metal–Ligand Cooperation, Angew. Chem. Int. Ed. 54 (2015) 12236–12273.

[23] L.R. Avens, S.G. Bott, D.L. Clark, A.P. Sattelberger, J.G. Watkin, B.D. Zwick, A Convenient Entry into Trivalent Actinide Chemistry: Synthesis and Characterization of $AnI_3(THF)_4$ and $An[N(SiMe_3)_2]_3$ (An = U, Np, Pu), Inorg. Chem. 33 (1994) 2248–2256.

[24] C.D. Carmichael, N.A. Jones, P.L. Arnold, Low-Valent Uranium Iodides: Straightforward Solution Syntheses of UI_3 and UI_4 Etherates, Inorg. Chem. 47 (2008) 8577–8579.

[25] J.-C. Berthet, P. Thuéry, M. Ephritikhine, New Efficient Synthesis of [UI4(MeCN)4]. X-ray Crystal Structures of $[UI_2(MeCN)_7][UI_6]$, $[UI_4(py)_3]$, and $[U(dmf)_9]I_4$, Inorg. Chem. 44 (2005) 1142–1146.

[26] A.E. Enriquez, B.L. Scott, M.P. Neu, Uranium(III)/(IV) Nitrile Adducts Including $UI_4(N{:}CPh)_4$, a Synthetically Useful Uranium(IV) Complex, Inorg. Chem. 44 (2005) 7403–7413.

[27] T. Cantat, B.L. Scott, J.L. Kiplinger, Convenient access to the anhydrous thorium tetrachloride complexes $ThCl_4(DME)_2$, $ThCl_4(1,4\text{-dioxane})_2$ and $ThCl_4(THF)_{3.5}$ using commercially available and inexpensive starting materials, Chem. Commun. 46 (2010) 919–921.

[28] D.L. Clark, T.M. Frankcom, M.M. Miller, J.G. Watkin, Facile solution routes to hydrocarbon-soluble Lewis base adducts of thorium tetrahalides. Synthesis, characterization, and x-ray structure of $ThBr_4(THF)_4$, Inorg. Chem. 31 (1992) 1628–1633.

[29] N.E. Travia, M.J. Monreal, B.L. Scott, J.L. Kiplinger, Thorium-mediated ring-opening of tetrahydrofuran and the development of a new thorium starting material: preparation and chemistry of $ThI_4(DME)_2$, Dalton Trans. 41 (2012) 14514–14523.

[30] A.J. Gaunt, A.E. Enriquez, S.D. Reilly, B.L. Scott, M.P. Neu, Structural Characterization of $Pu[N(SiMe_3)_2]_3$, a Synthetically Useful Nonaqueous Plutonium(III) Precursor, Inorg. Chem. 47 (2008) 26–28.

[31] S.D. Reilly, J.L. Brown, B.L. Scott, A.J. Gaunt, Synthesis and characterization of $NpCl_4(DME)_2$ and $PuCl_4(DME)_2$ neutral transuranic An(IV) starting materials, Dalton Trans. 43 (2014) 1498–1501.

[32] A. Pindwal, K. Yan, S. Patnaik, B. M. Schmidt, A. Ellern, I. I. Slowing, C. Bae, A. D. Sadow, Homoleptic trivalent tris (alkyl) rare earth compounds, J. Am. Chem. Soc. 139 (2017), 16862–16874.

[33] M.M. Hänninen, M.T. Zamora, P.G. Hayes, in: G. van Koten, R.A. Gossage (Eds.), The Privileged Pincer-Metal Platform: Coordination Chemistry & Applications, Springer International Publishing, Cham, Switzerland, 2016, pp. 93–178.

[34] S.A. Johnson, J.J. Kiernicki, P.E. Fanwick, S.C. Bart, New benzylpotassium reagents and their utility for the synthesis of homoleptic uranium (IV) benzyl derivatives, Organometallics 34 (2015) 2889–2895.

[35] M.A. Boreen, B.F. Parker, T.D. Lohrey, J. Arnold, A homoleptic uranium (III) tris (aryl) complex, J. Am. Chem. Soc. 138 (2016) 15865–15868.

[36] J.-C. Tourneux, J.-C. Berthet, T. Cantat, P. Thuéry, N. Mézailles, P. Le Floch, *et al.*, Uranium (IV) nucleophilic carbene complexes, Organometallics 30 (2011) 2957–2971.

[37] H. Staudinger, J. Meyer, Über neue organische phosphorverbindungen III. Phosphinmethylenderivate und phosphinimine, Helv. Chim. Acta, 2 (1919) 635-646.

[38]D.J.H. Webb, P.G. Hayes, Coordination Chemistry of Phosphinimine Containing Ligands, in: C. Edwin, G. Parkin, L. Que (Eds.), Comprehensive Coordination Chemistry III, Elsevier, 2021, pp. 131-157.

[39] W.Q. Tian, Y.A. Wang, Mechanisms of Staudinger reactions within density functional theory, J. Org. Chem., 69 (2004) 4299-4308.

[40] M. Fianchini, F. Maseras, DFT characterization of the mechanism for Staudinger/aza-Wittig tandem organocatalysis, Tetrahedron, 75 (2019) 1852-1859.

[41] M. Alajarin, C. Conesa, H.S. Rzepa, *Ab initio* SCF-MO study of the Staudinger phosphorylation reaction between a phosphane and an azide to form a phosphazene, J. Chem. Soc., Perkin Trans. 2, (1999) 1811-1814.

[42] C. Widauer, H. Grützmacher, I. Shevchenko, V. Gramlich, Insights into the Staudinger Reaction: Experimental and Theoretical Studies on the Stabilization of *cis*-Phosphazides, Eur. J. Inorg. Chem., 1999 (1999) 1659-1664.

[43] W. Beck, W. Rieber, H. Kirmaier, Reaktionen von Halogeno-Phosphin-Metall(II)-Komplexen mit organischen Aziden. Phosphatriazen-Kobalt(II) -Komplexe / Reactions of Halogeno Phosphine Metal(II) Complexes with Organic Azides. Phosphatriazene Cobalt(II) Complexes, Z. Naturforsch. B, 32 (1977) 528-532.

[44] Bond Lengths in Crystalline Organic Compounds, In: David R. Lide, ed., CRC Handbook of Chemistry and Physics, Internet Version 2005, CRC Press, Boca Raton, FL, 2005.

[45] M.W.P. Bebbington, D. Bourissou, Stabilised phosphazides, Coord. Chem. Rev., 253 (2009) 1248-1261.

[46] M.D. Velasco, P. Molina, P.M. Fresneda, M.A. Sanz, Isolation, Reactivity and Intramolecular Trapping of Phosphazide Intermediates in the Staudinger Reaction of Tertiary Phosphines with Azides, Tetrahedron 56 (2000) 4079–4084.

[47] R. D. Kennedy, Stabilization of acyclic phosphazides using the ortho-closo-dicarbadodecaboranyl residue, Chem. Commun. 46 (2010) 4782-4784.

[48] A.L. Chan, J. Fajardo, Jr., J.H. Wright, 2nd, M. Asay, V. Lavallo, Observation of Room Temperature B–Cl Activation of the $HCB_{11}Cl_{11}^-$ Anion and Isolation of a Stable Anionic Carboranyl Phosphazide, Inorg. Chem., 52 (2013) 12308-12310.

[49] T. Ogawa, T. Suzuki, N.M. Hein, F.S. Pick, M.D. Fryzuk, Cleavage of an aryl carbon–nitrogen bond of a phosphazido iron (II) complex promoted by hydride metathesis, Dalton Trans., 44 (2015) 54-57.

[50] A.L. Hawley, A. Stasch, Structural Diversity in Sterically Demanding Diiminophosphinato Alkali Metal Complexes, Eur. J. Inorg. Chem., 2015 (2015) 258-270.

[51] G.L. Hillhouse, B.L. Haymore, Interaction of aryl azides with tungsten complexes. Three new types of reactions yielding coordinated RN_3PR_3, RN_3H, and RN, J. Organomet. Chem., 162 (1978) C23-C26.

[52] G.L. Hillhouse, G.V. Goeden, B.L. Haymore, Stabilization of $RN{:}NN{:}PR_3$. Preparation and structural characterization of stable tetraarylphosphazide complexes containing molybdenum and tungsten, Inorg. Chem., 21 (1982) 2064-2071.

[53] G.C. Fortman, B. Captain, C.D. Hoff, Stoichiometric and Catalytic Conversion of 1-Adamantyl Azide to 1-Adamantyl Isocyanate by $[Cr(CO)_3Cp]_2$ and Reaction with $Mo(CO)_3(P^iPr_3)_2$ To Form $Mo(\kappa^2\text{-}^iPr_3P{=}NN{=}NAd)(CO)_3(P^iPr_3)$, Organometallics, 28 (2009) 3587-3590.

[54] K. Bieger, G. Bouhadir, R. Réau, F. Dahan, G. Bertrand, Ligand Behavior of a (*Z*)-Phosphazide (a 1,2,3,4λ^5-Triazaphosphinine) and of the Corresponding Phosphazene (a 1,2λ^5-Azaphosphete), J. Am. Chem. Soc., 118 (1996) 1038-1044.

[55] V. Cadierno, M. Zablocka, B. Donnadieu, A. Igau, J.-P. Majoral, A. Skowronska, Unexpected Formal [1+3] Cycloadditions between Azides and α-Zirconated

Phosphanes: A Route to Unprecedented Phosphazide and Iminophosphorane Complexes, Chem. Eur J., 6 (2000) 345-352.

[56] X. Xu, G. Kehr, C.G. Daniliuc, G. Erker, Reactions of a Cationic Geminal Zr^{+}/P Pair with Small Molecules, J. Am. Chem. Soc., 135 (2013) 6465-6476.

[57] I.G. Albuerne, M.A. Alvarez, M.E. Garcia, D. Garcia-Vivo, M.A. Ruiz, P. Vega, P–N and N–Mo Bond Formation Processes in the Reactions of a Pyramidal Phosphinidene-Bridged Dimolybdenum Complex with Diazoalkanes and Organic Azides, Inorg. Chem., 59 (2020) 7869-7883.

[58] A.A. Danopoulos, R.S. Hay-Motherwell, G. Wilkinson, S.M. Cafferkey, T.K.N. Sweet, M.B. Hursthouse, Reactions of iridium and ruthenium complexes with organic azides, J. Chem. Soc., Dalton Trans., (1997) 3177-3184.

[59] L. LePichon, D.W. Stephan, Contrasting Formation of a (Phenylthio)phosphinimine and (Phenylthio)phosphazide. Synthesis of Metal Complexes, Inorg. Chem., 40 (2001) 3827-3829.

[60] A.N. Walstrom, B.C. Fullmer, H. Fan, M. Pink, D.T. Buschhorn, K.G. Caulton, Influence of the Metal Orbital Occupancy and Principal Quantum Number on Organoazide (RN_3) Conversion to Transition-Metal Imide Complexes, Inorg. Chem., 47 (2008) 9002-9009.

[61] M.A. Alvarez, M.E. García, R. González, M.A. Ruiz, Nucleophilic and Electrophilic Behavior of the Phosphinidene-Bridged Complex $[Fe_2(\eta^5\text{-}C_5H_5)_2(\mu\text{-}PCy)(\mu\text{-}CO)(CO)_2]$, Organometallics, 27 (2008) 1037-1040.

[62] M.A. Alvarez, M.E. Garcia, R. Gonzalez, M.A. Ruiz, Reactions of the phosphinidene-bridged complexes $[Fe_2(\eta^5\text{-}C_5H_5)_2(\mu\text{-}PR)(\mu\text{-}CO)(CO)_2]$ (R = Cy, Ph) with electrophiles based on *p*-block elements, Dalton Trans., 41 (2012) 14498-14513.

[63] M. Lamberti, G.C. Fortman, A. Poater, J. Broggi, A.M.Z. Slawin, L. Cavallo, S.P. Nolan, Coordinatively unsaturated ruthenium complexes as efficient alkyne–azide cycloaddition catalysts, Organometallics, 31 (2012) 756-767.

[64] N. Ehrlich, D. Baabe, M. Freytag, P.G. Jones, M.D. Walter, Pyrrolyl-based pincer complexes of iron–Synthesis and electronic structure, Polyhedron, 143 (2018) 83-93.

[65] J. Backs, M. Lange, J. Possart, A. Wollschlager, C. Muck-Lichtenfeld, W. Uhl, Facile Modulation of FLP Properties: A Phosphinylvinyl Grignard Reagent and Ga/P- and In/P_2-Based Frustrated Lewis Pairs, Angew. Chem., Int. Ed., 56 (2017) 3094-3097.

[66] W. Uhl, J. Backs, A. Hepp, L. Keweloh, M. Layh, D. Pleschka, J. Possart, A. Wollschläger, Reactions of Al/P, Ga/P and P–H functionalized frustrated Lewis pairs with azides and a diazomethane – formation of adducts and capture of nitrenes, Z. Naturforsch. B, 72 (2017) 821-838.

[67] C.M. Momming, G. Kehr, B. Wibbeling, R. Frohlich, G. Erker, Addition reactions to the intramolecular mesityl2P–CH2–CH2–B(C6F5)2 frustrated Lewis pair, Dalton Trans., 39 (2010) 7556-7564.

[68] A. Stute, L. Heletta, R. Frohlich, C.G. Daniliuc, G. Kehr, G. Erker, Anomalous Staudinger reaction at intramolecular frustrated P–B Lewis pair frameworks, Chem. Commun., 48 (2012) 11739-11741.

[69] A. Stute, G. Kehr, R. Frohlich, G. Erker, Chemistry of a geminal frustrated Lewis pair featuring electron withdrawing C6F5 substituents at both phosphorus and boron, Chem. Commun., 47 (2011) 4288-4290.

[70] L.M. Elmer, G. Kehr, C.G. Daniliuc, M. Siedow, H. Eckert, M. Tesch, A. Studer, K. Williams, T.H. Warren, G. Erker, The Chemistry of a Non-Interacting Vicinal Frustrated Phosphane/Borane Lewis Pair, Chem. Eur J., 23 (2017) 6056-6068.

[71] M.W. Bebbington, S. Bontemps, G. Bouhadir, D. Bourissou, Photoisomerizable heterodienes derived from a phosphine borane, Angew. Chem., Int. Ed., 46 (2007) 3333-3336.

[72] D.H.A. Boom, A.R. Jupp, M. Nieger, A.W. Ehlers, J.C. Slootweg, New Insights in Frustrated Lewis Pair Chemistry with Azides, Chem. Eur J., 25 (2019) 13299-13308.

[73] A.S. Ionkin, W.J. Marshall, B.M. Fish, Divalent Germanium and Tin Compounds Stabilized by Sterically Bulky P^O, P=O^O, P=S^O, and P=N^O Ligands: Synthesis and First Insights into Catalytic Application to Polyurethane Systems, Organometallics, 25 (2006) 4170-4178.

[74] J. Schneider, K.M. Krebs, S. Freitag, K. Eichele, H. Schubert, L. Wesemann, Intramolecular Tetrylene Lewis Adducts: Synthesis and Reactivity, Chem. Eur J., 22 (2016) 9812-9826.

[75] B. Liu, D. Cui, Rare-earth metal complexes stabilized by amino-phosphine ligand. Reaction with mesityl azide and catalysis of the cycloaddition of organic azides and aromatic alkynes, Dalton Trans., (2009) 550-556.

[76] E.M. Broderick, P.S. Thuy-Boun, N. Guo, C.S. Vogel, J. Sutter, J.T. Miller, K. Meyer, P.L. Diaconescu, Synthesis and Characterization of Cerium and Yttrium Alkoxide Complexes Supported by Ferrocene-Based Chelating Ligands, Inorg. Chem., 50 (2011) 2870-2877.

[77] X. Sun, W. Su, K. Shi, Z. Xie, C. Zhu, Triple Frustrated Lewis Pair-Type Reactivity on a Single Rare-Earth Metal Center, Chem. Eur J., 26 (2020) 5354-5359.

[78] K. Bieger, J. Tejeda, R. Reau, F. Dahan, G. Bertrand, Synthesis and Reactivity of Cyclic 6-Membered Six-.pi.- and Four-Membered Four-.pi. Electron Ylides, J. Am. Chem. Soc., 116 (1994) 8087-8094.

2. Consecutive N_2 Loss from a Uranium Diphosphazide Complex[e,f]

2.1. Abstract

A new 'diphosphazidosalen' ligand was synthesized and successfully transferred to uranium using salt metathesis strategies. The resultant 8-coordinate uranium(IV) diphosphazide complex [κ^6-1,2-{$(N_3)PPh_2(2\text{-}O\text{-}C_6H_4)$}$_2C_6H_4$]$UCl_2$ (**2-1**) is unstable to consecutive N_2 loss, affording the asymmetric species [κ^5-1-{$(N_3)PPh_2(2\text{-}O\text{-}C_6H_4)$}-2-{$N{=}PPh_2(2\text{-}O\text{-}C_6H_4)$}$C_6H_4$)]$UCl_2$ (**2-2**), defined by a phosphazide-phosphinimine mixed-ligand framework, and ultimately, the uranium(IV) phosphasalen complex [κ^4-1,2-{$N{=}PPh_2(2\text{-}O\text{-}C_6H_4)$}$_2C_6H_4$]$UCl_2$(THF) (**2-3**).

2.2. Introduction

In forming 'aza-ylides' (iminophosphoranes or phosphinimines) from organic azides and tertiary phosphines, the phosphazide intermediate, a neutral analogue of the triazenide ($R–(N_3)^-–R$) moiety, has the potential for rich coordination chemistry as a κ^2-*N,N* or η^3-*N,N,N* chelate, but is rarely isolated. Mechanistic studies have shown that the Staudinger reaction ($PR_3 + R–N_3 \rightarrow R_3P{=}N–R + N_2$) proceeds through a *cis*-phosphazide ($R_3P–(N_3)–R$) intermediate, which readily eliminates dinitrogen gas and phosphinimine ($R_3P{=}N–R$).[1] However, the *trans*-isomer, which is resistant to N_2 loss, can be stabilized by H-bonding,[2] as well as coordination to main group Lewis acids[3] and transition metals.[1,4]

---

[e] *Dalton Transactions* reference style used throughout this chapter

[f] Reprinted with permission from Dickie, T. K. K., MacNeil, C. S. and Hayes, P. G., *Dalton Trans.*, 2020, **49**, 578.

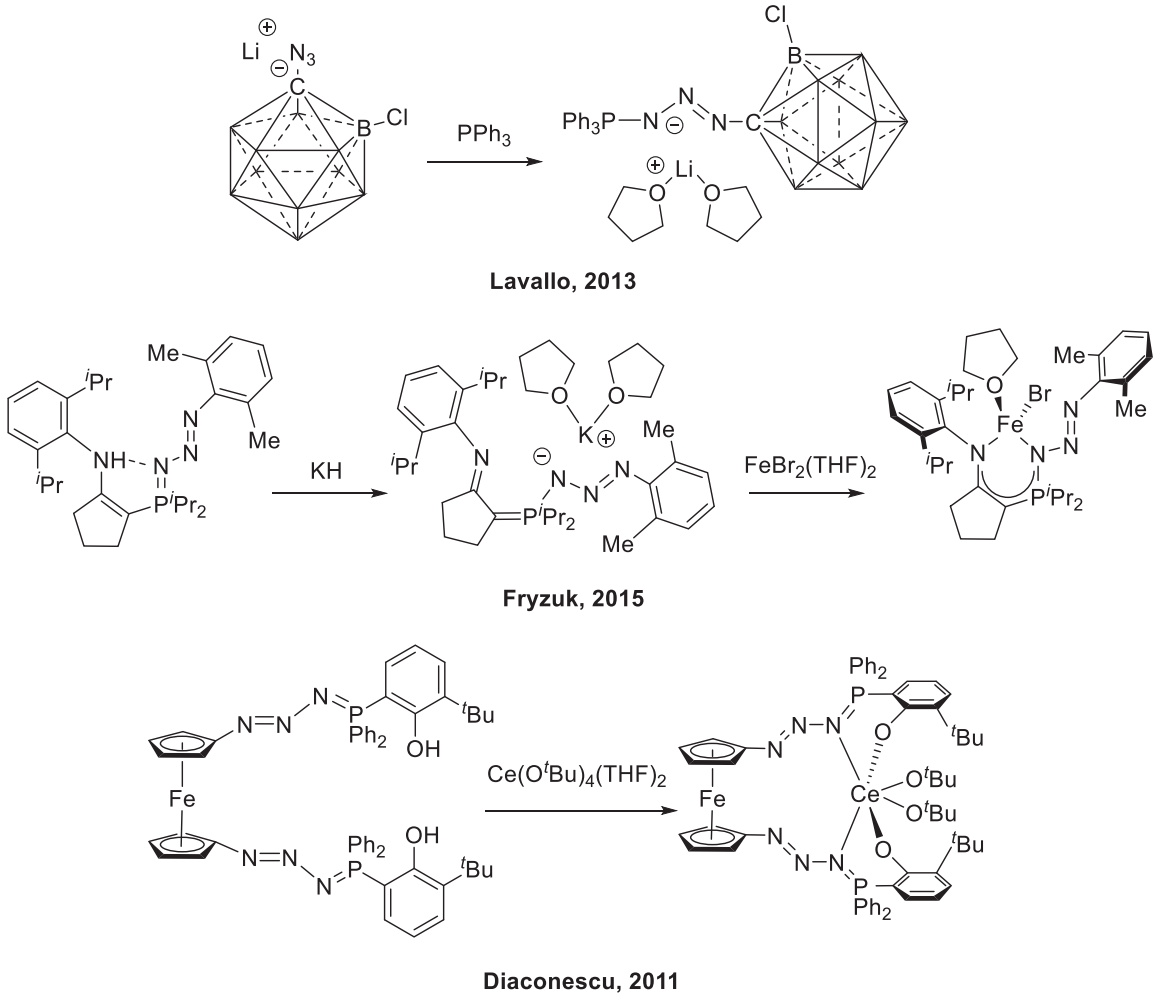

Scheme 2.1. Some examples of stabilized phosphazides.[4h,5,10]

To date, there have only been two examples of phosphazides coordinated to group 1 metals: Lavallo and co-workers reported an anionic azido carboranyl cluster with a lithium counterion which, when reacted with PPh_3, produced a lithium stabilized phosphazide (Scheme 2.1, top).[5] In the solid state, the lithium cation is bound by N_α and N_γ of the phosphazide and two THF molecules. Intriguingly, this species does not release N_2, even upon heating at 150 °C in C_6H_5F. In addition, Fryzuk prepared a sterically encumbered organic azide supported by hydrogen bonding with a nearby NH group.[4h] Upon NH deprotonation with KH, a potassium stabilized phosphazide can participate in a salt

metathesis reaction with $FeBr_2(THF)_2$ to produce an iron(II) phosphazide (Scheme 2.1, middle). Interestingly, this species undergoes an unusual radical process when exposed to the hydride $KBEt_3H$ wherein nitrogen gas is liberated and an anionic phosphinimide generated. Notably, this is the only previously published example of intentional transfer of a stabilized phosphazide.

As potential chelating ligands, phosphazides provide an opportunity to introduce functionality and coordinative-flexibility to a variety of metals, yet are seldom discussed or targeted in coordination chemistry.[1,6] Phosphinimines, in contrast, are established components in ligand design.[7] Isostructural variants of the ubiquitous 'salen' ligand have recently been developed that feature phosphinimine donors in place of the conventional Schiff base (R_2C=N–R).[8] These phosphasalen ligands, reported by Auffrant and Williams, have demonstrated exceptional stability when supporting reactive metals, notably serving as an ancillary scaffold for a highly active ring-opening polymerization yttrium catalyst.[9] The synthesis of such phosphasalen ligands has thus far been largely limited to the Kirsanov reaction,[9a] which generates the phosphinimine fragment from triarylphosphine, Br_2, and diamine over a number of steps and days (Scheme 2.2a). Although diamine starting materials are attractive from a practical standpoint, diazides provide access to diphosphazides, species which are not accessible *via* the Kirsanov reaction.

To our knowledge, the Staudinger reaction has not been utilized for the preparation of entirely organic phosphasalen ligands. However, a ferrocene-based variant reported by Diaconescu and co-workers has been disclosed, whereby 1,1′-diazidoferrocene $Fc(N_3)_2$ was reacted with a bulky phosphinophenol.[10] Notably, the cerium complex $[Fc(N_6O_2)]Ce(O^tBu)_2$ (Fc =1,1′-ferrocenylene; $Fc(N_6O_2)$ = κ^4-1,1′-[$(N_3)PPh_2$(2-O-3-

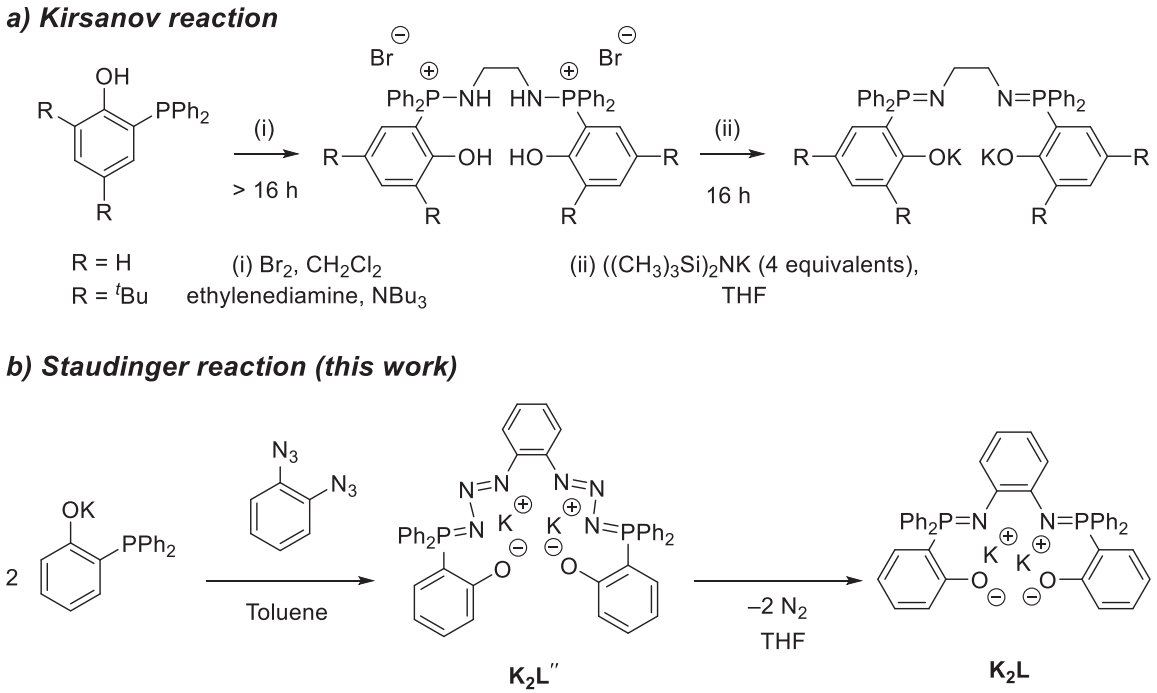

Scheme 2.2. Comparison of phosphasalen ligand synthesis by the Kirsanov reaction (a)[9a] and by the Staudinger reaction (this work) (b).

^{t}BuC$_6$H$_4$)]$_2$Fc) was isolated in the reaction, wherein the distal N atoms of a phosphazide ligand were bound to the cerium center (Scheme 2.1, bottom). Thus far, [Fc(N$_6$O$_2$)]Ce(O^{t}Bu)$_2$ appears to be the only example of a ligand featuring two phosphazide subunits coordinated to a metal, and aside from thermally promoted N$_2$ loss, its reaction/coordination chemistry has not been studied.

Herein, we provide details on the one-step synthesis and characterization of new phosphasalen and phosphazidosalen ligands and describe the conversion of phosphazide to phosphinimine at a single uranium center.

2.3. Synthesis and Characterization of Uranium Phosphazidosalen and Phosphasalen Complexes

A phosphasalen ligand featuring a rigid benzene backbone was targeted wherein 1,2-diazidobenzene would be reacted with an appropriate phosphine (Scheme 2.2b). Although the requisite 1,2-$(N_3)_2$-C_6H_4 was previously reported,[11] it had been generated *in situ* and used without characterization. In an effort to isolate this diazide, it was prepared by stepwise diazotization of 2-nitroaniline. Low-temperature analysis by an X-ray diffraction study revealed a near linear arrangement of the azide functional groups with extended conjugation in the aromatic bridge [N1–N2–N3 = 173.6(2)°, N4–N5–N6 = 171.7(2)°].

Initial attempts at reacting 1,2-diazidobenzene with $Ph_2P[(2\text{-}OH)C_6H_4]$ produced insoluble byproducts, presumed to be the result of acidic –OH protons interfering with phosphazide cyclization and subsequent N_2 loss. Therefore, to mitigate this issue, and to directly prepare phosphasalen salts suitable for subsequent salt metathesis reactions, the OH group of $Ph_2P[(2\text{-}OH)C_6H_4]$ was deprotonated with KH prior to reaction with 1,2-diazidobenzene.

Dropwise addition of 0.5 equivalents of 1,2-$(N_3)_2$-C_6H_4 to a stirring solution of $Ph_2P[(2\text{-}OK)C_6H_4]$ in toluene resulted in immediate precipitation of a bright yellow solid that exhibits a ^{31}P NMR resonance at δ 28.4 in [D_8]THF. When combined with UCl_4, a rapid change from yellow to orange was observed, along with a new signal in the ^{31}P NMR spectrum at δ 49.6. An X-ray crystallographic study confirmed the reaction product to be $L''UCl_2$, ($L'' = \kappa^6$-1,2-$[(N_3)PPh_2(2\text{-}O\text{-}C_6H_4)]_2C_6H_4$) (**2-1**), a uranium dichloride complex supported by a symmetric diphosphazide ligand. Both of the phosphazide P(N_3) units coordinate to the metal center *via* a κ^2-*N*,*N* bonding mode, with anionic phenoxide-O and

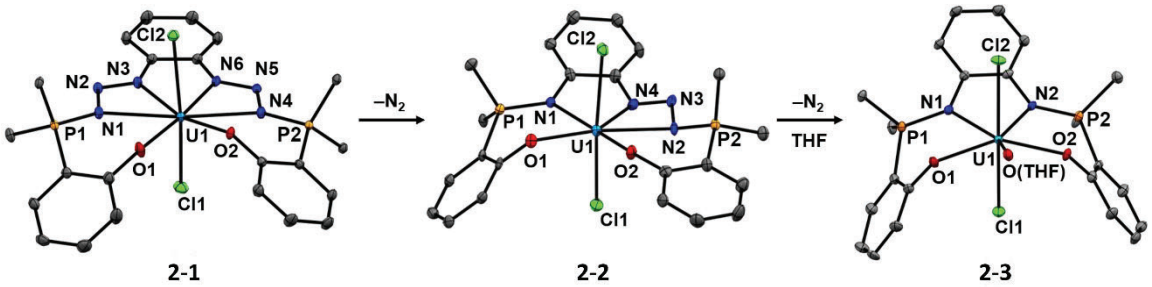

Figure 2.1. X-ray crystal structures of **2-1**, **2-2** and **2-3** with thermal ellipsoids drawn at 30% probability. Hydrogen atoms, P-phenyl groups, except for the ipso carbons, coordinated THF C atoms and solvent molecules of recrystallization (benzene, THF) are omitted for clarity. Selected bond distances (Å) and angles (°), **2-1**: U–N1 = 2.589(3), U–N3 = 2.586(2), U–N4 = 2.641(2), U–N6 = 2.613(2), U–O1 = 2.203(2), U–O2 = 2.221(2), U–Cl1 = 2.6424(8); Cl1–U–Cl2 = 163.08(3), O1–U–O2 = 79.68(8), N1–N2–N3 = 103.7(2), N4–N5–N6 = 104.1(2); P1–N1–N2–N3 = 175.1(2), P2–N4–N5–N6 = –173.8(2); **2-2**: U–N1 = 2.55(1), U–N2 = 2.52(1), U–N4 = 2.44(1), U–O1 = 2.18(1), U–O2 = 2.185(9), U–Cl1 = 2.640(3), U–Cl2 = 2.603(5), P1–N1 = 1.61(1); Cl1–U–Cl2 = 168.1(1), O1–U–O2 = 99.1(4), N2–N3–N4 = 104(1); P2–N2–N3–N4 = 165(1); **2-3**: connectivity structure of **2-3.**

Cl ligands completing the coordination sphere of the paramagnetic uranium(IV) center (Figure 2.1). Notably, the N–N–N angles in the phosphazide subunits [103.7(2) and 104.1(2)°] are substantially smaller than those observed in a previously reported metal-free phosphazide [116.55(14)°].[4d] The geometry about the eight-coordinate uranium center is best described as distorted hexagonal bipyramidal with a Cl1–U–Cl2 angle of 163.08(3)°. The diphosphazide ligand is remarkably planar, with only the O2 atom sitting out of the plane defined by U1–O1–N1–N3–N6–N4 (by 0.545 Å). In addition, the phosphazides coordinate in a markedly different manner (κ^2-*N*,*N*) than those in the cerium diphosphazide complex [Fc(N_6O_2)]Ce(O^{t}Bu)$_2$, wherein each phosphazide unit adopts an η^1-*N* bonding mode.[10] When heated, two equivalents of N_2 were liberated from [Fc(N_6O_2)]Ce(O^{t}Bu)$_2$, along with quantitative conversion to the analogous phosphinimine-bound complex. Similar to [Fc(N_6O_2)]Ce(O^{t}Bu)$_2$, both phosphazide donors in **2-1** display a *trans*-configuration with varying N–N bond lengths [N1–N2 =1.356(4), N2–N3 = 1.266(3), N5–

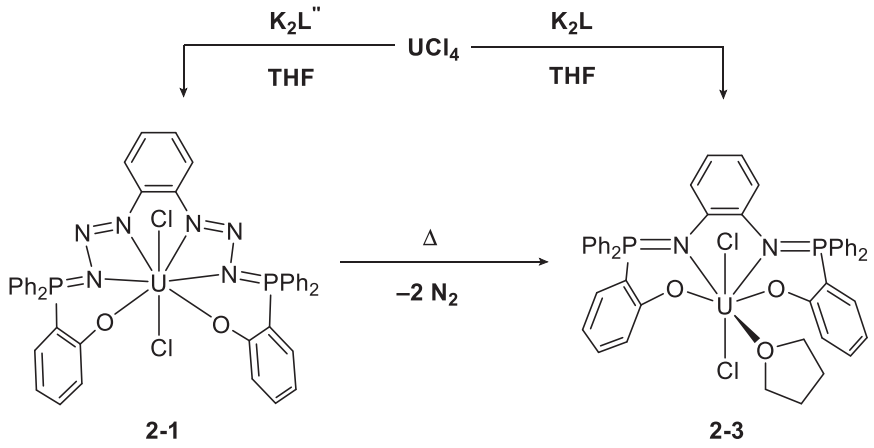

Scheme 2.3. Synthesis of uranium complexes **2-1** and **2-3.**

N6 = 1.273(3), N4–N5 = 1.358(3) Å]. Complex **2-1** is the first example of the phosphazide functionality bound to an actinide metal; as uranium can accommodate high coordination numbers, it is an ideal candidate for supporting multiple phosphazide groups.

Complex **2-1** is unstable to slow elimination of 1 equivalent of N_2 at ambient temperature in THF. After 12 hours, two new ^{31}P NMR resonances of equal intensity (δ 104.1 and 71.2) had completely supplanted the resonance attributed to complex **2-1** (δ 49.6). X-ray quality crystals grown from a concentrated benzene solution at ambient temperature permitted a study that identified the asymmetric decomposition product as $L'UCl_2$, ($L' = \kappa^5$-1-[$(N_3)PPh_2$(2-O-C_6H_4)]-2-[N=PPh_2(2-O-C_6H_4)]C_6H_4) (**2-2**), the result of singular N_2 loss from the diphosphazide ligand in **2-1** (Figure 2.1). Intriguingly, one P(N_3) phosphazide unit, which remains κ^2 bound to uranium, was conserved. The new phosphinimine donor is also coordinated to the metal, resulting in distorted pentagonal bipyramidal geometry at the seven-coordinate uranium(IV) center. Upon monitoring by ^{31}P NMR spectroscopy, a [D_8]THF solution of **2-2**, heated at 135 °C for 5 days, was observed to gradually convert into a single product (**2-3,** δ –56.4).

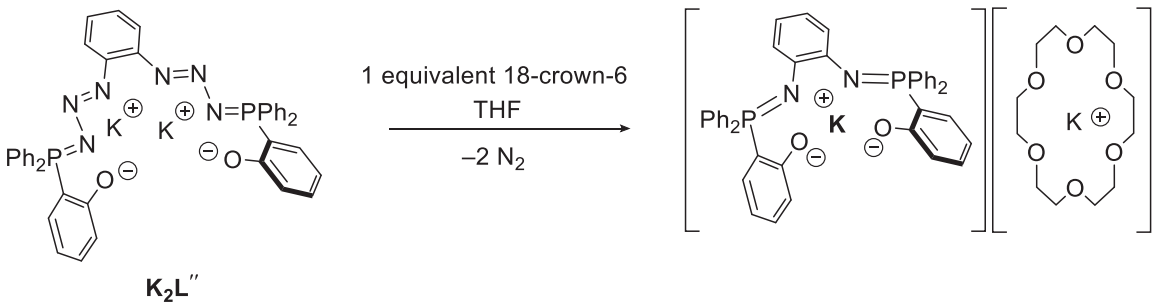

Scheme 2.4. Reaction of phosphazidosalen ligand **K_2L''** with 18-crown-6.

To confirm the identity of complex **2-3** as the product of a second consecutive N_2 elimination from **2-1**, the putative phosphasalen complex was targeted for independent synthesis by reaction of **K_2L** (L = κ^4-1,2-[N=PPh$_2$(2-OK-C$_6$H$_4$)]'$]_2$C$_6$H$_4$) with UCl$_4$. To generate **K_2L**, 1,2-(N$_3$)$_2$-C$_6$H$_4$ was added to an *in situ* generated THF solution of (2-OK-C$_6$H$_4$)PPh$_2$ (2 equiv.). Immediate yellow colouration occurred, followed by formation of a fine suspension, and ultimately, after one hour, a clear yellow solution. The $^{31}P\{^1H\}$ NMR spectrum of **K_2L** in [D$_8$]THF exhibits a broad peak at δ 11.4, a considerable upfield shift compared to the phosphazidosalen ligand (δ 28.4), thus suggesting formation of the desired phosphasalen ligand (Scheme 2.2). When **K_2L** was combined with UCl$_4$, a resonance was observed at δ –56.4 in the ^{31}P NMR spectrum, which is consistent with that obtained when complex **2-1** was heated (Scheme 2.3, right). Crystals grown from THF provided a low-quality X-ray structure that served to establish atom connectivity within the THF-coordinated uranium phosphasalen complex LUCl$_2$(THF), (L = κ^4-1,2-[N=PPh$_2$(2-O-C$_6$H$_4$)]$_2$C$_6$H$_4$) (**2-3**) (Figure 2.1). To the best of our knowledge, the only other phosphasalen-supported actinide complexes were reported by the Auffrant group,[12] rounding out diverse coordination chemistry involving transition, rare earth, and actinide metals.[8a,9,13] Notably, in the work by Auffrant, the phosphasalen ligand possessed a pyridine backbone and sterically demanding tert-butyl groups.

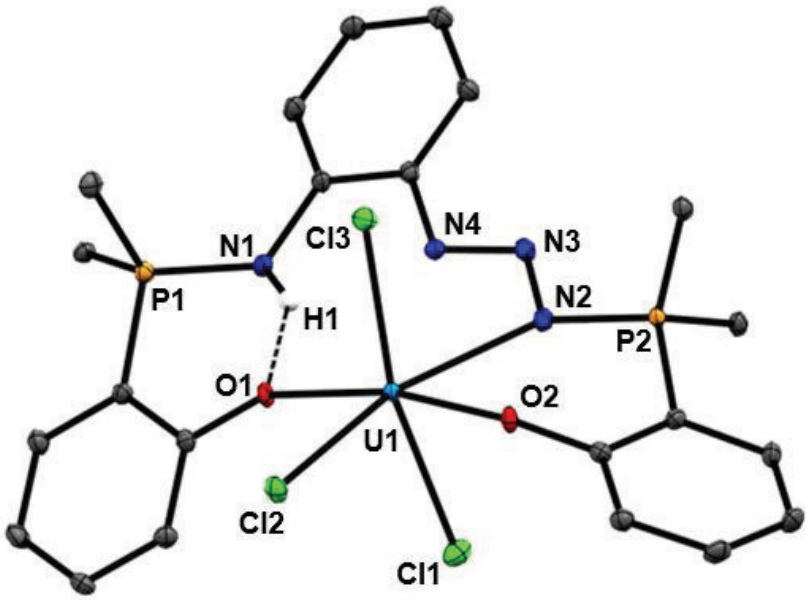

Figure 2.2. Solid-state structure of complex **2-4** with thermal ellipsoids shown at 30% probability. Hydrogen atoms, except for H1, $P(C_5H_5)_2$ groups excluding *ipso-C*, and solvent molecules of recrystallization (benzene) are omitted for clarity. The position of H1 was located directly in the difference map. Selected bond distances (Å) and angles (°) are given: U–N2 = 2.479(3), U–O1 = 2.214(2), U–O2 = 2.214(2), U–Cl1 = 2.6465(9), U–Cl2 = 2.6547(9), U–Cl3 = 2.6517(9), P1–N1 = 1.641(3), H1···O1 = 2.18(6); N2–N3–N4 = 109.9(3).

The potassiated diphosphazide ligand $\mathbf{K_2L''}$ was postulated to contain N···K interactions that prevent *trans-cis* isomerization. To confirm this formulation, 1 equivalent of 18-crown-6 was added to sequester K^+ ions, resulting in immediate dissolution of the yellow solid along with concomitant production of a clear yellow solution and gas evolution (Scheme 2.4). The appearance of a new resonance at δ 4.25 in the $^{31}P\{^1H\}$ NMR spectrum accompanied this visible change; an asymmetric intermediate with two peaks at δ 12.79 and δ –13.45 (1:1) was also observed. Rapid N_2 loss upon addition of 18-crown-6 suggests that the phosphazide subunits in $\mathbf{K_2L''}$ are indeed stabilized by coordination to the large K ions.

When complex **2-1** was heated in THF during the preparation of **2-3**, and the product extracted into benzene, a small amount of highly crystalline impurity (**2-4**) was

obtained. A uranium(IV) complex (H)L′UCl_3 (**2-4**) bearing three chloride ligands and a protonated phosphinimine, which presumably formed *via* reaction of **K_2L′′** with THF solvent or trace quantities of adventitious moisture, was identified by X-ray diffraction studies. The presence of a $R_3P{=}NH^+$ was supported by the elongated P–N distance of 1.641(3) Å which is in agreement with similar species in the literature (Figure 2.2).[14] Solution-state NMR spectroscopy identified an asymmetric complex with ^{31}P chemical shifts of δ 88.9 and δ –38.2, and 17 paramagnetically shifted ^1H resonances ranging from δ 61.6 to δ –21.3. In the solid state, the protonated phosphinimine nitrogen sits 4.319(3) Å from the uranium(IV) center. The phosphazide unit, in contrast to 7-coordinate complex **2-2**, is κ^1 bound. Complex **2-4**, while only isolable in small amounts, demonstrates the variable coordination of the phosphazide group in this system. The remaining phosphazide unit is coordinated through only the *α*-N of the phosphazide, similar to the η^1-*N* bonding mode in Diaconescu's cerium diphosphazide.[10]

2.4. Conclusions

As demonstrated, the Staudinger reaction, in combination with appropriate choice of solvent, provides convenient and selective routes to phosphazidosalen and phosphasalen ligands. The corresponding group 1 phosphazidosalen species affords a unique opportunity to explore phosphazides as a ligand in coordination chemistry using simple and versatile salt metathesis strategies. The ease with which pendant groups can be fine-tuned, the observed coordinative versatility, and the ability for intentional conversion into phosphinimines, suggest that phosphazides offer great potential as ligands in inorganic chemistry and homogeneous catalysis.

2.5. Experimental Details for Chapter 2

2.5.1. Laboratory Equipment and Apparatus

An argon filled MBraun glove box was employed for manipulation and storage of all oxygen and moisture sensitive compounds. All thermally unstable compounds were stored in a –35 °C freezer within the glove box. All reactions were performed on a double manifold high vacuum line using standard techniques or in a glove box under an atmosphere of argon.[15] Commonly utilized specialty glassware includes the swivel frit assembly, needle valves, and thick walled (5 mm) glass bombs equipped with Kontes Teflon stopcocks.[15] All glassware was stored in a 110 °C oven for a minimum of 12 hours, or flame-dried before immediate transfer to the glove box antechamber or assembled on the vacuum line and evacuated while hot.

2.5.2. Solvents

Toluene, pentane, and tetrahydrofuran (THF) solvents were dried and purified using the Grubbs/Dow purification system and stored in evacuated 500 mL bombs over titanocene[16] (toluene and hexanes) or sodium/benzophenone ketal (THF).[17] Diethyl ether, pentane, heptane, benzene, benzene-d_6, toluene-d_8, and THF-d_8 were dried and stored over sodium/benzophenone ketal in glass bombs under vacuum. Unless otherwise noted, solvents were introduced *via* vacuum transfer with condensation at –78 °C. Liquid nitrogen (–196 °C), liquid nitrogen/pentane (–130 °C), dry ice/acetone (–78 °C), dry ice/acetonitrile (–45 °C) and water/ice (0 °C) baths were used for cooling receiving flasks and to maintain low temperature conditions.

2.5.3. Instrumentation and Details for NMR Experiments

All NMR spectra were recorded at ambient temperature, except where noted, with a Bruker Avance II NMR spectrometer (300.13 MHz for ^{1}H, 75.47 MHz for ^{13}C and 121.48 MHz for ^{31}P) or Avance III NMR spectrometer (700.13 MHz for ^{1}H, 176.05 MHz for ^{13}C, and 283.54 MHz for ^{31}P) NMR spectrometer. All ^{1}H NMR spectra were referenced to $SiMe_4$ through the residual ^{1}H resonance(s) of the employed solvent; benzene-d_6 (7.16 ppm), toluene-d_8 (2.09, 6.98, 7.02 and 7.09 ppm), chloroform-d_1 (7.26 ppm) or THF-d_8 (1.73 and 3.58 ppm). ^{13}C NMR spectra were referenced relative to $SiMe_4$ through the resonance(s) of the employed solvent; benzene-d_6 (128.0 ppm), toluene-d_8 (20.4, 125.2, 128.0, 128.9, 137.5 ppm), chloroform-d_1 (77.16 ppm) or THF-d_8 (25.4, 67.6 ppm). ^{1}H NMR data for diamagnetic compounds are reported as follows: chemical shift, multiplicity (s = singlet, d = doublet, t = triplet, q = quartet, quint = quintet, sp = septet, br = broad, m = multiplet, app = apparent, obsc = obscured, ov = overlapping), coupling constants (Hz), integration, assignment. ^{13}C NMR data for diamagnetic compounds are reported as follows: chemical shift, assignment. Assignment of resonances were supported by ^{1}H–^{1}H COSY, ^{13}C{^{1}H} APT, ^{1}H–^{13}C{^{1}H} and HSQC/HMBC experiments. All uranium compounds in this paper are paramagnetic. For paramagnetic compounds, $w_{1/2}$ denotes width at half height in hertz.

2.5.4. Additional Instrumentation

Elemental analyses (%CHN) were conducted at the University of Lethbridge by Jackson Knott or Dylan Webb on an Elementar Americas Vario MicroCube Analyzer (C, H, N, O, S capabilities).

2.5.5. Additional Safety Considerations

Organic azides are both toxic and explosive. Care should be taken while handling azides, particularly if they are solvent free and/or at elevated temperatures. Phosphines are toxic and care should be taken while handling. ^{238}U is a weak α-emitter with a half-life of 4.47×10^9 years.

2.5.6. Synthetic Methods

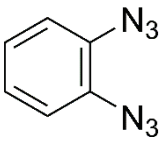

1,2-diazidobenzene: A solution comprised of 35 mL of 1M HCl and 30 mL of distilled H_2O was added to 2-azidoaniline[2] (0.510 g, 3.80 mmol) in a 250 mL round-bottomed flask equipped with a Teflon® coated stir bar. The solution was stirred at ambient temperature until the solid dissolved, after which the mixture was cooled to –5 °C using an ice/salt water bath. Solid $NaNO_2$ (0.500 g, 7.25 mmol) was added to the flask and the reaction mixture was stirred at –5° C for 1 hour. The solution was treated with a 5 mL of aqueous solution of NaN_3 (470 mg, 7.23 mmol) and stirred for 2 hours, after which a light orange solid was isolated by cold filtration. The resulting product was a red oil at ambient temperature. Yield: 0.523 g (85.9%). Single crystals suitable for X-ray diffraction were obtained from a solution of petroleum ether at –35 °C. ^1H NMR (chloroform–d_1, 300.13 MHz): δ 7.07 (ov m, 4H, Ph C*H*). $^{13}C\{^1H\}$ NMR (chloroform–d_1, 75.47 MHz): δ 131.22 (s, *C*N_3), 126.02 (s, Ph *C*H), 120.30 (s, Ph *C*H). IR (neat): ν_{max} (cm^{-1}) 2089 (vw), 1589 (s), 1488 (s), 1448 (s), 1297 (w), 1273 (w), 1154 (s), 1145(s), 1085 (s), 744 (s), 697 (s), 647 (s), 527 (s).

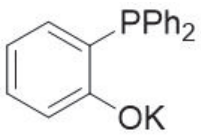

(2–OK–C_6H_4)PPh_2: In an inert atmosphere glove box, 2-(diphenylphosphino)phenol (0.118 g, 0.426 mmol) and KH (0.0188 g, 0.468 mmol) were combined in a 20 mL scintillation vial equipped with a Teflon® coated stir bar. The solids were dissolved in 8 mL of THF and gas evolution was observed from the cloudy solution. The reaction mixture was stirred for 15 minutes at ambient temperature until gas evolution ceased and the solution became clear and colourless. The reaction was stirred for another 18 hours and the solvent was removed *in vacuo* to produce a white solid (0.130 g, 96.2% yield) ^{1}H NMR (THF–d_8, 300.13 MHz): δ 7.25-7.16 (m, 10H, Ar C*H*), 6.87 (td, 1H, $^3J_{HH}$ = 7.5 Hz, $^4J_{HH}$ = 1.9 Hz, Ar C*H*), 6.41 (ddd, 1H, $^3J_{HP}$ = 6.3 Hz, $^3J_{HH}$ = 7.5 Hz, $^4J_{HH}$ = 1.9 Hz, Ar C*H*), 6.03 (m, 2H, Ar C*H*). ^{13}C{^{1}H} NMR (THF–d_8, 75.47 MHz): δ 174.63 (d, $^1J_{CP}$ = 19.2 Hz), 140.63 (d, $^1J_{CP}$ = 10.3 Hz), 134.77 (d, $^2J_{CP}$ = 18.8 Hz), 134.39 (s), 131.69 (s), 129.11 (d, $^3J_{CP}$ = 6.7 Hz), 128.80 (s), 123.39 (d, $^2J_{CP}$ = 7.7 Hz), 118.32 (s), 111.33 (s). ^{31}P{^{1}H} (THF–d_8, 121.49 MHz) δ –19.14 (s). Anal. Calcd. (%) for $C_{18}H_{14}KOP$: C: 68.33; H: 4.46. Found C: 68.09; H: 4.61.

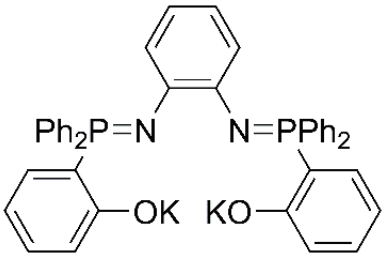

K_2L: In an inert atmosphere glove box, 1,2-diazidobenzene (0.0544 g, 0.339 mmol) was dissolved in 1 mL of THF in a 20 mL scintillation vial. The 1,2-diazidobenzene solution was added to a stirring THF (8 mL) solution of (2–OK–C_6H_4)PPh_2 (0.215 g, 0.678 mmol). The reaction mixture was stirred at 50 °C for 8 hours to ensure full conversion to K_2L resulting in a clear, orange solution. The THF was removed *in vacuo* to give a bright yellow solid (0.250 g, 99.8% yield). ^{1}H NMR (THF–d_8, 300.13 MHz): δ 7.86–7.78 (ov m, 8H, Ar C*H*), 7.42–7.33 (ov m, 14H, Ar C*H*), 7.00–6.85 (m, 4H, Ar C*H*), 6.58 (br s, 2H, Ar C*H*), 6.15–6.07 (m, 4H, Ar

C*H*). $^{13}C\{^{1}H\}$ NMR (THF–d_8, 75.47 MHz): δ 176.19 (d, $^{1}J_{CP}$ = 4.8 Hz), 147.6 (d, $^{1}J_{CP}$ = 23.0 Hz), 136.66 (s), 136.08 (d, $^{2}J_{CP}$ = 9.0 Hz), 135.24 (s), 134.43 (s), 132.43 (d, $^{2}J_{CP}$ = 9.4 Hz), 130.94 (s), 128.78 (d, $^{3}J_{CP}$ = 11.6 Hz), 121.16 (s), 119.34 (s), 119.19(s), 116.54 (s), 109.77 (s), 109.61 (s). $^{31}P\{^{1}H\}$ (THF–d_8, 121.49 MHz) δ 11.42 (s). Anal. Calcd. (%) for $C_{42}H_{32}K_2N_2O_2P_2$: C: 68.46; H: 4.38; N: 3.80. Found C: 67.83; H: 5.12; N: 3.90.

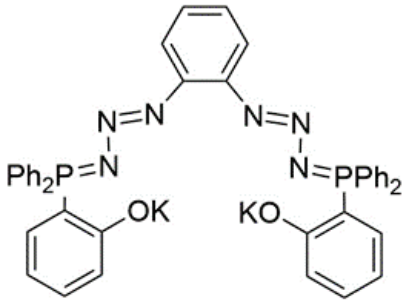

K_2L'': In an inert atmosphere glove box, 1,2-diazidobenzene (0.0579 g, 0.362 mmol) was dissolved in 2 mL of toluene and added to a stirring toluene (8 mL) solution of (2–OK–C_6H_4)PPh_2 (0.229 g, 0.723 mmol). A bright yellow precipitate formed immediately upon addition of the diazide. The reaction mixture was stirred at ambient temperature for 15 minutes. The solution was decanted from the precipitate and the remaining solvent removed *in vacuo* to afford a bright yellow solid. The resulting product was washed with pentane (3 × 1 mL) (0.214 g, 75% yield). ^{1}H NMR (THF–d_8, 300.13 MHz): δ 7.77-7.71 (ov m, 6H, Ar C*H*), 7.60–7.54 (m, 2H, Ar C*H*), 7.36–7.34 (m, 4H, Ar C*H*), 7.24-7.07 (ov m, 10H, Ar C*H*), 7.02–6.94 (m, 2H, Ar C*H*), 6.87–6.84 (m, 2H, Ar C*H*), 6.60–6.49 (m, 2H, Ar C*H*), 6.20–6.15 (m, 2H, Ar C*H*), 5.94–5.92 (m, 2H, Ar C*H*). $^{31}P\{^{1}H\}$ (THF–d_8, 121.49 MHz) δ 28.34 (br s). ^{13}C data is unavailable due to decomposition in solution and low solubility in common organic solvents. Anal. Calcd. (%) for $C_{42}H_{32}K_2N_6O_2P_2$: C: 63.62; H: 4.07; N: 10.60. Found C: 62.73; H: 4.41; N: 10.73.

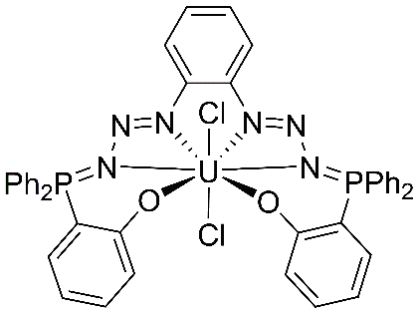

Complex 2-1: In an inert atmosphere glove box, solid **K_2L''** (0.0443g, 0.0559 mmol) and UCl_4 (0.0212g, 0.0558 mmol) were added to a 20 mL scintillation vial containing 3 mL of THF. The mixture was agitated for 30 seconds until the all **K_2L''** had been consumed and a dark orange solution prevailed. Toluene (3 mL) was added to the solution to precipitate KCl and the THF/toluene solution was filtered quickly through Celite®. The solvent was removed *in vacuo* to afford an orange-brown solid (0.0377g, 66.0% yield). Suitable crystals for X-ray diffraction were obtained in benzene–d_6 by leaving the solution at ambient temperature for 6 hours. Due to decomposition of **2-1** to **2-2** in solution, NMR spectra of compound **2-1** contain an impurity of **2-2**. ^{1}H NMR (THF–d_8, 300.13 MHz): δ 24.55 ($w_{1/2}$ = 16.2 Hz), 19.88 ($w_{1/2}$ = 11.6 Hz), 16.89 ($w_{1/2}$ = 27.0 Hz), 14.07 ($w_{1/2}$ = 16.1 Hz), 12.81 ($w_{1/2}$ = 11.4 Hz), 12.52 ($w_{1/2}$ = 15.7 Hz), 12.02 ($w_{1/2}$ = 24.1 Hz), 7.55 ($w_{1/2}$ = 10.8 Hz), 7.31 ($w_{1/2}$ = 16.8 Hz). ^{31}P{^{1}H} NMR (THF-d_8, 121.49 MHz): δ 49.61 (s, 2P, *P*N$_3$). Anal. Calcd. (%) for $C_{42}H_{32}N_6O_2P_2U$: C: 49.28; H: 3.15; N: 8.21. Found C: 49.17; H: 3.39; N: 8.22.

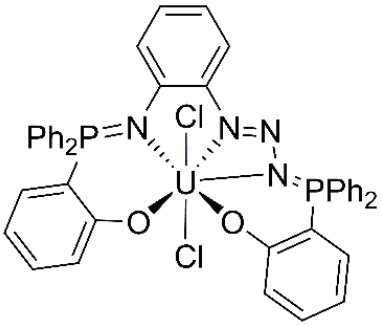

Complex 2-2: Synthesis 1- In an inert atmosphere glove box, solid **K_2L''** (0.010 g, 0.013 mmol) and $UCl_4(dme)_2$ (0.0073 g, 0.013 mmol) were added to a J. Young NMR tube containing 0.5 mL of THF-d_8. The mixture was agitated for 2 minutes during which all **K_2L''** had been consumed and a dark orange solution prevailed. The solution was heated for 12 hours at 45 °C to ensure full conversion of **2-1** to **2-2**. Crystals suitable for X-ray diffraction were obtained at ambient temperature from benzene after 24 hours. An isolated yield could not

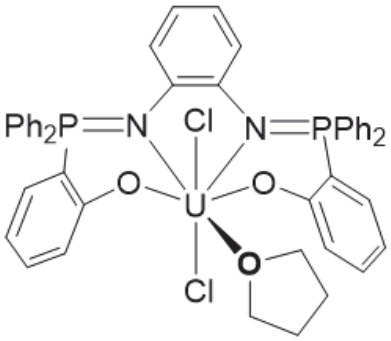

be determined due to persistent impurities (complex **2-4**). Synthesis 2- In an inert atmosphere glove box, solid Complex **2-1** (0.0377g, 0.0369 mmol) was added to a 20 mL scintillation vial containing 3 mL of THF and a Teflon® coated stir bar. The dark orange solution was stirred at 80 °C for 2 hours to ensure full conversion of **2-1** to **2-2**. The solvent was removed *in vacuo* to afford a brown solid and the product was washed with heptane (3 × 1 mL) (0.0299 g, 81.5% crude yield). An isolated yield could not be obtained due to impurities of **2-4**. ^{1}H NMR (THF–d_8, 300.13 MHz): δ 29.29 ($w_{1/2}$ = 29 Hz), 26.62 ($w_{1/2}$ = 29 Hz), 23.45 ($w_{1/2}$ = 26 Hz), 23.19 ($w_{1/2}$ = 20 Hz), 21.08 ($w_{1/2}$ = 25 Hz), 18.75 ($w_{1/2}$ = 17 Hz), 17.21 ($w_{1/2}$ = 13 Hz), 14.53 ($w_{1/2}$ = 19 Hz), 11.26 ($w_{1/2}$ = 18 Hz), 11.07 ($w_{1/2}$ = 16 Hz), 9.81 ($w_{1/2}$ = 18 Hz), 9.46 ($w_{1/2}$ = 17 Hz), –3.06 ($w_{1/2}$ = 14 Hz). ^{31}P{^{1}H} NMR (THF-d_8, 121.49 MHz): 104.07 (s, 1P), 71.15 (s, 1P). Anal. Calcd. (%) for $C_{42}H_{32}Cl_2N_4O_2P_2U$: C: 50.67; H: 3.24; N: 5.63. Found C: 50.21; H: 3.41; N: 5.71. While this compound could not be separated from small impurities of complex **2-4**, the obtained elemental analysis data is within acceptable standards, likely due to the similarity of the chemical composition of complexes **2-4** and **2-2**.

Complex 2-3: In an inert atmosphere glove box, solid K_2L (0.0200 g, 0.0271 mmol) was added to a 20 mL scintillation vial containing $UCl_4(dme)_2$ (0.0152 g, 0.0272 mmol) and a Teflon® coated stir bar. To this mixture, 6 mL of THF was added and the cloudy green solution was stirred for 4 hours. The solution was then filtered through Celite® and the solvent was removed *in vacuo* to afford a pale green solid (0.0164 g yield, 62.4%). Crystals

suitable for X-ray diffraction were obtained from a saturated solution of THF at ambient temperature after 12 hours. ^{1}H NMR (THF–d_8, 300.13 MHz): δ 32.27 ($w_{1/2}$ = 121 Hz), 25.86 ($w_{1/2}$ = 146 Hz), 20.64 ($w_{1/2}$ = 93 Hz), 17.99 ($w_{1/2}$ = 113 Hz), 13.48 ($w_{1/2}$ = 1123 Hz), 10.34 ($w_{1/2}$ = 255 Hz), 9.59 ($w_{1/2}$ = 239 Hz), 8.02 ($w_{1/2}$ = 78 Hz), 7.82 ($w_{1/2}$ = 31 Hz), 5.37 ($w_{1/2}$ = 67 Hz), 5.20 ($w_{1/2}$ = 57 Hz), –1.41 ($w_{1/2}$ = 165 Hz), –5.84 ($w_{1/2}$ = 69 Hz) ^{31}P{^{1}H} NMR (THF–d_8, 121.49 MHz): δ –56.40 (br s, 2P, *P*=N). Anal. Calcd. (%) $C_{84}H_{64}Cl_4N_4O_4P_4U_2$: C: 53.14; H: 3.88; N: 2.69. Found C: 53.53; H: 3.98; N: 3.19.

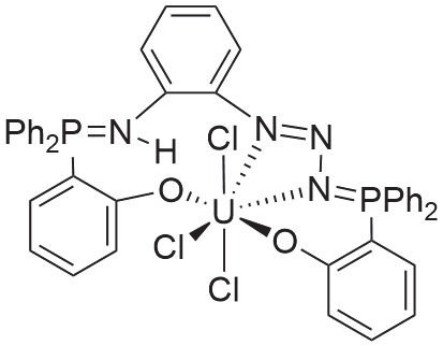

Complex 2-4: In an inert atmosphere glove box, solid **K_2L''** (0.0114 g, 0.0144 mmol) was added to a vial containing UCl_4 (0.0053 g, 0.014 mmol). To this mixture, 6 mL of THF was added and the dark orange solution was agitated until the **K_2L''** had been completely consumed, about 2 minutes. The THF solution was heated at 50 °C for 10 minutes. The solvent was removed *in vacuo* and the compound was extracted with 2 mL of benzene and filtered through Celite®. Crystals suitable for X-ray diffraction were obtained from benzene at ambient temperature after 24 hours (Yield 0.0019 g, 12% yield). ^{1}H NMR (THF–d_8, 300.13 MHz): δ 61.57 ($w_{1/2}$ = 26 Hz), 50.28 ($w_{1/2}$ = 98 Hz), 38.75 ($w_{1/2}$ = 48 Hz), 34.15 ($w_{1/2}$ = 30 Hz), 33.62 ($w_{1/2}$ = 18 Hz), 28.65 ($w_{1/2}$ = 29 Hz), 26.67 ($w_{1/2}$ = 16 Hz), 25.71 ($w_{1/2}$ = 21 Hz), 25.14 ($w_{1/2}$ = 21 Hz), 15.35 ($w_{1/2}$ = 15 Hz), 8.60 ($w_{1/2}$ = 19 Hz), 7.68 ($w_{1/2}$ = 18 Hz), 6.37 ($w_{1/2}$ = 16 Hz), 6.17 ($w_{1/2}$ = 26 Hz), 5.41 ($w_{1/2}$ = 17 Hz), –1.72 ($w_{1/2}$ = 16 Hz), –21.33 ($w_{1/2}$ = 13 Hz). ^{31}P{^{1}H} NMR (THF-d_8, 121.49 MHz): 88.93 (d, $^{3}J_{PH}$ = 13.4 Hz, 1P, doublet is due to incomplete ^{1}H decoupling), –38.16 (s, 1P). This product is a minor impurity and has eluded preparation on a large scale. As a consequence, only small

quantities of non-analytically pure material were available for combustion analysis, and repeated attempts failed to provide acceptable data.

2.5.7. Crystallographic Details

All structures were collected on a Rigaku SuperNova diffractometer equipped with a Dectris Pilatus 3R 200K-A hybrid-pixel-array detector, a four-circle goniometer, sealed graphite-monochromated Mo Kα (λ = 0.71073 Å) and Cu Kα (λ = 1.54178 Å) X-ray sources, and an Oxford cryostream-cooling device fixed at 100 K. Single crystals suitable for X-ray diffraction studies were mounted on a MiTiGen cryo-loop using desiccated Paratone–*N* oil stored in a glove box. Data reduction was accomplished by the CrysAlis^{Pro} (version 1.171.38.43) software package. Absorption corrections were applied by multi-scan techniques and empirical absorption correction using spherical harmonics, implemented in SCALE3 ABSPACK scaling algorithm. Structures were solved in the Olex2[18] environment using intrinsic phasing and refined by full-matrix least squares method on F^2 using the SHELX software suite.[19-20] All non-hydrogen (except N–H) atoms were refined anisotropically, C–H hydrogens were calculated and refined isotropically as a riding model. N–H hydrogens were located by the Fourier difference maps and refined isotropically. All measurements were performed at the University of Lethbridge. The data for 1,2-diazidobenzene was collected by C. S. MacNeil. A summary of the crystallographic data can be found below in **Table 2.1.**

Single crystals of 1,2-diazidobenzene were grown in a –35 °C freezer from petroleum ether and were kept cold while mounting using a steel trough with a cold nitrogen stream. Compounds **2-1**, **2-2**, and **2-4** were grown from a saturated solution of benzene. Unfortunately, single crystals of **2-3** grown from THF succumb to rapid decomposition upon removal from the mother liquor, resulting in the crystals becoming covered with amorphic material. However, inner portions of the crystals remain intact, allowing for modest diffraction of X-ray radiation, despite interference from the polycrystalline material. The data is not ideal and therefore discussions of the metrical parameters are not included. The data set does, however, allow for qualitative discussions associated with the connectivity of atoms, and thus, the geometry of complex **2-3**. Therefore, these structures will be referred to within this thesis as “connectivity structures”.

Table 2.1. Crystallographic details for complexes discussed in Chapter 2.

	1,2-diazidobenzene	**2-1 ·(C_6H_6)**	**2-2**
CCDC #	1533034	1533036	1942135
Empirical formula	$C_6H_4N_6$	$C_{48}H_{38}Cl_2N_6O_2P_2U$	$C_{42}H_{32}Cl_2N_4O_2P_2U$
Formula weight/g mol^{-1}	160.15	1101.71	995.58
Temperature/K	100	100	100
Crystal system	monoclinic	triclinic	orthorhombic
Space group	$P2_1/c$	P-1	$Pca2_1$
a/Å	6.7390(4)	10.72961(8)	20.8270(3)
b/Å	20.3245(11)	11.58355(6)	11.8420(2)
c/Å	5.2307(3)	19.45445(11)	15.7786(3)
α/°	90	103.8451(5)	90
β/°	95.700(5)	95.7658(6)	90
γ/°	90	102.8388(6)	90
Volume/$Å^3$	712.88(7)	2258.65(2)	3891.53(11)
Z	4	2	4
$\rho_{calc}g/cm^3$	1.492	1.620	1.699
μ/mm^{-1}	0.887	12.240	14.116
F(000)	328.0	1080.0	1936.0
Crystal size/mm^3	0.2 x 0.2 x 0.15	0.5 x 0.1 x 0.1	0.1 x 0.05 x 0.01
Radiation (Å)	CuKα (λ = 1.54184)	CuKα (λ = 1.54184)	CuKα (λ = 1.54184)
2Θ range for data collection/°	13.204 to 160.6	8.13 to 160.384	7.466 to 133.99
Index ranges	$-6 \le h \le 8$ $-25 \le k \le 25$ $-6 \le l \le 6$	$-13 \le h \le 13$ $-13 \le k \le 14$ $-24 \le l \le 24$	$-24 \le h \le 24$, $-13 \le k \le 14$, $-17 \le l \le 18$
Reflections collected	7702	87431	20838
Independent reflections	1543 $R_{int} = 0.0679$ $R_{sigma} = 0.0336$	9778 $R_{int} = 0.0408$ $R_{sigma} = 0.0188$	6585 $R_{int} = 0.0596$, $R_{sigma} = 0.0573$
Data/restraints/parameters	1543/0/109	9778/0/551	6585/19/478
Goodness-of-fit on F^2	1.044	1.122	1.001
Final R indexes [I>=2σ (I)]	$R_1 = 0.0552$ $wR_2 = 0.1445$	$R_1 = 0.0234$ $wR_2 = 0.0574$	$R_1 = 0.0336$, $wR_2 = 0.0802$
Final R indexes [all data]	$R_1 = 0.0644$ $wR_2 = 0.1537$	$R_1 = 0.0242$ $wR_2 = 0.0577$	$R_1 = 0.0373$, $wR_2 = 0.0817$
Largest diff. peak/hole / e $Å^{-3}$	0.27/-0.26	1.24/-1.54	1.76/-1.63

Programs for diffractometer operation, data collection, data reduction, and absorption correction were those supplied by Rigaku.

	2-3	**2-4 · 2(C_6H_6)**
CCDC #	N/A	1533037
Empirical formula	$C_{46}H_{40}Cl_2N_2O_3P_2U$	$C_{54}H_{45}Cl_3N_4O_2P_2U$
Formula weight/g mol^{-1}	1039.67	1188.26
Temperature/K	112.1(7)	100
Crystal system	triclinic	monoclinic
Space group	P-1	$P2_1/c$
a/Å	10.5372(2)	13.79440(10)
b/Å	10.7422(2)	17.44271(12)
c/Å	21.1847(5)	20.42070(16)
α/°	101.388(2)	90
β/°	94.545(2)	94.9425(7)
γ/°	115.774(2)	90
Volume/Å^3	2079.53(8)	4895.19(6)
Z	2	4
ρ_{calc}g/cm^3	1.660	1.611
μ/mm^{-1}	13.239	11.821
F(000)	1020.0	2340.0
Crystal size/mm^3	0.3 x 0.2 x 0.05	0.3 x 0.3 x 0.3
Radiation (Å)	CuKα (λ = 1.54184)	CuKα (λ = 1.54184)
2Θ range for data collection/°	8.668 to 160.642	6.674 to 159.382
Index ranges	$-10 \le h \le 13$ $-12 \le k \le 13$ $-27 \le l \le 26$	$-17 \le h \le 17$ $-13 \le k \le 22$ $-24 \le l \le 26$
Reflections collected	46261	55054
Independent reflections	9068 R_{int} = 0.0645 R_{sigma} = 0.0435	10594 R_{int} = 0.0315 R_{sigma} = 0.0217
Data/restraints/parameters	9068/0/500	10594/0/596
Goodness-of-fit on F^2	1.158	1.119
Final R indexes [I>=2σ (I)]	R_1 = 0.1064, wR_2 = 0.2949	R_1 = 0.0290, wR_2 = 0.0804
Final R indexes [all data]	R_1 = 0.1076, wR_2 = 0.2952	R_1 = 0.0300, wR_2 = 0.0812
Largest diff. peak/hole / e Å^{-3}	11.78/-8.77	1.30/-1.24

Programs for diffractometer operation, data collection, data reduction, and absorption correction were those supplied by Rigaku.

2.6. References for Chapter 2

1. M. W. P. Bebbington and D. Bourissou, *Coord. Chem. Rev*. **2009**, *253*, 1248.

2. (a) C.G. Chidester, J. Szmuszkovicz, D.J. Duchamp, L.G. Laurian and J.P. Freeman, Acta Cryst. **1988**, C44, 1080; (b) M. D. Velasco, P. Molina, P. M. Fresneda and M. A. Sanz, *Tetrahedron* **2000**, *56*, 4079.

3. (a) M. W. P. Bebbington, S. Bontemps, G. Bouhadir and D. Bourissou, Angew. Chem., Int. Ed., **2007**, 46, 3333; (b) A. Stute, L. Heletta, R. Frohlich, C. G. Daniliuc, G. Kehr and G. Erker, *Chem. Commun.* **2012**, *48*, 11739.

4. (a) W. Beck, W. Rieber and H. Kirmaier, *Z. Naturforsch.* **1977**, *32*, 528; (b) A. N. Walstrom, B. C. Fullmer, H. Fan, M. Pink, D. T. Buschhorn, and K. G. Caulton, *Inorg. Chem.* **2008**, *47*, 9002; (c) B. Liu and D. Cui, *Dalton Trans*. **2009**, 550; (d) G. C. Fortman, B. Captain and C. D. Hoff, *Organometallics* **2009**, *28*, 3587; (e) E. M. Broderick, P. S. Thuy-Boun, N. Guo, C. S. Vogel, J. Sutter, J. T. Miller, K. Meyer and P. L. Diaconescu, *Inorg. Chem*. **2011**, *50*, 2870; (f) M. Lamberti, G. C. Fortman, A. Poater, J. Broggi, A. M. Z. Slawin, L. Cavallo and S. P. Nolan, *Organometallics* **2012**, *31*, 756; (g) X. Xu, G. Kehr, C. G. Daniliuc and G. Erker, *J. Am. Chem. Soc*. **2013**, *135*, 6465; (h) T. Ogawa, T. Suzuki, N. M. Hein, F. S. Pick and M. D. Fryzuk, *Dalton Trans*. **2015**, *44*, 54; (i) N. Ehrlich, D. Baabe, M. Freytag, P. G. Jones and M. D. Walter, *Polyhedron* **2018**, *143*, 83.

5. A. L. Chan, J. Fajardo, J. H. Wright, M. Asay and V. Lavallo, *Inorg. Chem*. **2013**, *52*, 12308.

6. (a) A. S. Ionkin, W. J. Marshall and B. M. Fish, *Organometallics* **2006**, *25*, 4170; (b) J. Schneider, K. M. Krebs, S. Freitag, K. Eichele, H. Schubert and L. Wesemann, *Chem. Eur. J.* **2016**, *22*, 9812; (c) W. Uhl, J. Backs, A. Hepp, L. Keweloh, M. Layh, D. Pleschka, J. Possart and A. Wollschläger, *Z. Naturforsch*. **2017**, *72*, 821.

7. a) K. R. D. Johnson, M. A. Hannon, J. S. Ritch and P. G. Hayes, *Dalton Trans.* **2012**, *41*, 7873; b) K. R. D. Johnson and P. G. Hayes, *Organometallics* **2009**, *28*, 6352; c) C. A. Wheaton and P. G. Hayes, *Comments Inorg. Chem.* **2011**, *32*, 127. d) G. C. Welch, W. E. Piers, M. Parvez and R. McDonald, *Organometallics* **2004**, *23*, 1811; (e) N. M. Hein, T. Suzuki, T. Ogawa and M. D. Fryzuk, *Dalton Trans*. **2016**, *45*, 14697; (f) P. Wei, K. T. K. Chan and D. W. Stephan, *Dalton Trans.* **2003**, *0*, 3804.

8. (a) T.-P.-A. Cao, S. Labouille, A. Auffrant, Y. Jean, X. F. Le Goff and P. Le Floch, *Dalton Trans*. **2011**, *40*, 10029; (b) J. L. Brosmer and P. L. Diaconescu, *Organometallics* **2015**, *34*, 2567.

9. a) T.-P.-A. Cao, A. Buchard, X. F. Le Goff, A. Auffrant and C. K. Williams, *Inorg. Chem*. **2012**, *51*, 2157; b) C. Bakewell, T.-P.-A. Cao, N. Long, X. F. Le Goff, A. Auffrant and C. K. Williams, *J. Am. Chem. Soc*. **2012**, *134*, 20577; (c) C. Bakewell, T.-P.-A. Cao, X. F. Le Goff, N. J. Long, A. Auffrant and C. K. Williams, *Organometallics* **2013**, *32*, 1475.

10. E. M. Broderick, P. S. Thuy-Boun, N. Guo, C. S. Vogel, J. Sutter, J. T. Miller, K. Meyer and P. L. Diaconescu, *Inorg. Chem*. **2011**, *50*, 2870.

11. J. H. Hall and E. Patterson, *J. Am. Chem. Soc.* **1967**, *89*, 5856.

12. T. Cheisson, PhD Thesis, École Polytechnique 2015.

13. D. Myers, A. J. P. White, C. M. Forsyth, M. Bown and C. K. Williams, *Angew.Chem.Int. Ed*., **2017**, *56*, 5277.

14. (a) M. M. Hänninen, M. T. Zamora, C. S. MacNeil, J. P. Knott and P. G. Hayes, *Chem. Commun.* **2016**, *52*, 586. Note: Protonated phosphinimine unit has a P–N distance of 1.654(3) Å; (b) B. J. Ireland, C. A. Wheaton and P. G. Hayes, *Organometallics* **2010**, *29*, 1079. Note: Protonated phosphinimine unit has a P–N distance of 1.6393(18) Å.

15. B. J. Burger and J. E. Bercaw, Experimental Organometallic Chemistry; American Chemical Society: Washington, D.C., 1987.

16. R. H. Marvich and H. H. Brintzinger*, J. Am. Chem. Soc.* **1971**, *93*, 2046.

17. A. B. Pangborn, M. A. Giardello, R. H. Grubbs, R. K. Rosen and F. J. Timmers, *Organometallics* **1996**, *15*, 1518.

18. O. V. Dolomanov, L. J. Bourhis, R. J. Gildea, J. A. K. Howard and H. Puschmann, *J. Appl. Crystallogr*. **2009**, *42*, 339.

19. G. M. Sheldrick, *Acta Crystallogr. Sect. A* **2015**, *71*, 3.

20. G. M. Sheldrick, *Acta Crystallogr. Sect. C* **2015**, *71*, 3.

3. Diphosphazide-Supported Trialkyl Thorium(IV) Complex[g,h]

3.1. Abstract

The potassium salt of a new ligand, $KL_{P=N3}$ (**3-2**, $L_{P=N3}$ = κ^5-2,5-[(4-^{i}PrC$_6$H$_4$)N$_3$=P^{i}Pr$_2$]$_2$N(C$_4$H$_2$)$^-$), that features two units of the rare phosphazide (RN_3=PR_3) functionality, was synthesized *via* an incomplete Staudinger reaction between K[2,5-(^{i}Pr$_2$P)$_2$N(C$_4$H$_2$)] (**3-1**) and 4-^{i}PrC$_6$H$_4$N$_3$. The diphosphazide ligand was transferred to a thorium(IV) metal center using salt metathesis strategies, yielding $L_{P=N3}ThCl_3$ (**3-3**), which contains two intact and coordinated phosphazides. Reaction of complex **3-3** with 3 equiv of $LiCH_2SiMe_3$ resulted in formation of the trialkyl thorium species $L_{P=N3}Th(CH_2SiMe_3)_3$ (**3-4**). In contrast, attempts to synthesize an organothorium complex supported by the previously reported bisphosphinimine ligand $L_{P=N}$ ($L_{P=N}$ = κ^3-2,5-[(4-^{i}PrC$_6$H$_4$)N=P^{i}Pr$_2$]$_2$N(C$_4$H$_2$)$^-$) afforded the cyclometalated dialkyl complex $L^*_{P=N}Th(CH_2SiMe_3)_2$ (**3-6**, $L^*_{P=N}$ = κ^4-2-[(4-^{i}PrC$_6$H$_3$)N=P^{i}Pr$_2$]-5-[(4-^{i}PrC$_6$H$_4$)N=P^{i}Pr$_2$]N(C$_4$H$_2$)$^{2-}$) and 1 equiv of free tetramethylsilane.

3.2. Introduction

The Staudinger reaction, discovered in 1919,[1] introduced the formation of a phosphinimine group (R_3P=NR′) *via* the reaction of a tertiary phosphine (R_3P) with an organic azide (N_3R'), resulting in concomitant loss of N_2. Since its discovery, the phosphinimine functionality has been extensively utilized in coordination chemistry,

---

[g] *Organometallics* reference style used throughout this chapter

[h] Reprinted with permission from Dickie, T. K. K.; Aborawi, A. A.; Hayes, P. G. Diphosphazide-Supported Trialkyl Thorium(IV) Complex, *Organometallics* **2020**, *39*, 2047–2052.

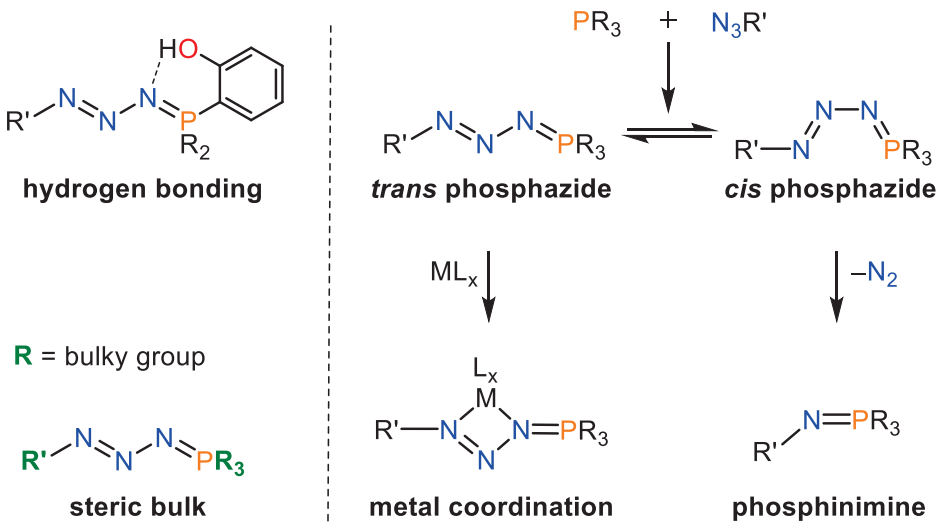

Scheme 3.1. Phosphinimine formation and methods of phosphazide stabilization.

largely due to the ease by which the steric and electronic properties can be fine-tuned by varying the phosphine[2] and/or azide[3] reactants. Notably, phosphinimines have been useful for supporting early transition metal olefin polymerization[4] and rare earth metal ring-opening polymerization catalysts.[5]

The Staudinger reaction proceeds *via* an intermediate phosphazide (R_3PNNNR') (Scheme 3.1).[6] Until recently, such phosphazides were largely considered transient species, due to the facile loss of N_2, and accordingly, were overlooked as viable functional groups in ligand design. Since Staudinger's original work, multiple methods have been developed to stabilize phosphazides and inhibit N_2 loss, including the use of tertiary phosphines and azides with bulky R groups,[7] H-bonding[8] and the coordination of phosphazides to rare-earth[9a] and transition metals.[6, 9b-c, 10]

It was recently demonstrated that phosphazide coordination to an alkali metal permits isolation of a "phosphazidosalen" ligand system.[11] Such alkali metal-stabilized phosphazides proved sufficiently stable for transfer to uranium *via* a simple salt metathesis

protocol. More specifically, the dipotassium salt of the phosphazidosalen ligand K_2L'' [L'' = κ^6-1,2-{$(N_3)PPh_2(2\text{-}O\text{–}C_6H_4)$}$_2C_6H_4$] reacted with UCl_4 to afford the first example of an actinide-stabilized phosphazide, $L''UCl_2$. In the solid-state structure of $L''UCl_2$, both phosphazide functionalities were coordinated to uranium; consecutive N_2 loss from the ligand phosphazides was documented.

Organothorium chemistry has been largely dominated by complexes stabilized by carbocyclic ligands.[12] The development of noncarbocyclic scaffolds has contributed to the diversification of thorium chemistry,[13-16] though, most ancillary ligands employed with actinide metals are either di- or trianionic. As a consequence, thorium (IV) trialkyl species, which necessarily require a single monoanionic supporting ligand, are rare. To the best of our knowledge, aside from tribenzyl variants of cyclopentadienyl Cp^RThBn_3,[17,18] the only trialkyl thorium complexes have been reported by Cheng and colleagues.[19] Cheng's complexes, $[PhC(NDipp)_2]Th(CH_2SiMe_3)_3$ (Dipp = 2,6-^{i}Pr$_2C_6H_3$)), $[Ph_2P(NDipp)_2]Th(CH_2SiMe_3)_3$, $[Ph_2P(NDipp)]Th(p\text{-}CH_2C_6H_4Me)_3$ and $^{Me2}TpTh(CH_2SiMe_3)_3$ (^{Me2}Tp = $B((CH_3)_2C_3N_2H)_3^-$), when combined with 2 equiv of $[CPh_3][B(C_6F_5)_4]$, catalyze the polymerization of isoprene. In general, thorium species bearing non-carbocyclic monoanionic ancillary ligands are uncommon, and they typically contain more than one such ligand.[20-24]

3.3. Synthesis of Thorium Phosphazide and Phosphinimine Complexes

It was hypothesized that the previously reported *NNN*-scaffold, $L_{P=N}$ ($L_{P=N}$ = κ^3-2,5-[(4-^{i}PrC_6H_4)N=P^{i}Pr$_2$]$_2$N$(C_4H_2)^-$), which features two phosphinimine groups, could be modified to generate a monoanionic diphosphazide ligand. This ligand framework was targeted because it was anticipated to provide access to a wide array of metal phosphazide

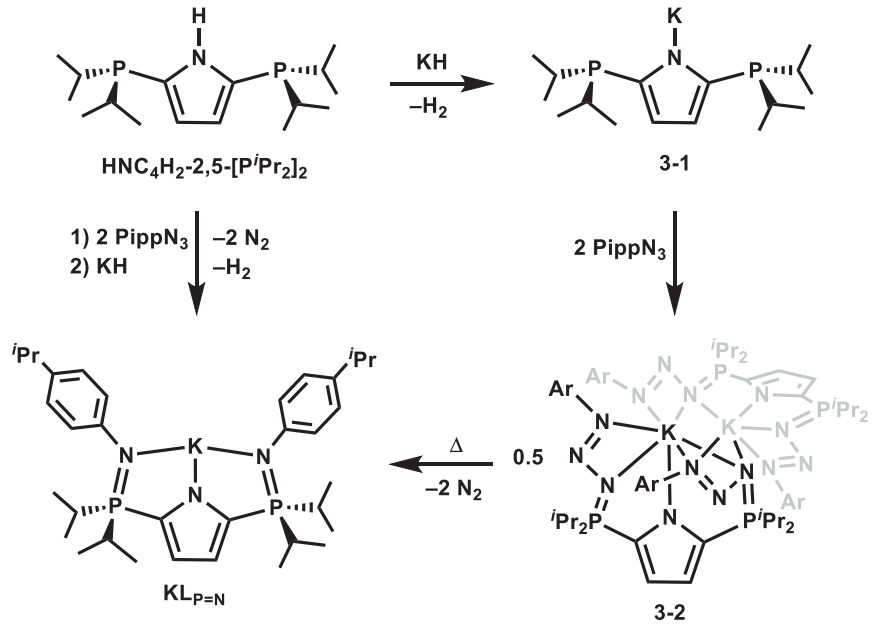

Scheme 3.2. Synthesis of compound **3-2**.

complexes, thereby shedding light upon the viability of phosphazides to serve as useful donors in coordination and organometallic chemistry.

Alkali salts of $HL_{P=N}$ have been previously prepared by reaction of the requisite group I metal hydride with the product of 2 equiv of *para*-isopropylphenyl azide ($PippN_3$) and 2,5-($^{i}Pr_2P)_2NH(C_4H_2$) (Scheme 3.2, left).[25] In this work, however, the pyrrole nitrogen was deprotonated to give K[2,5-($^{i}Pr_2P)_2N(C_4H_2$)] (**3-1**) prior to introduction of the azide, as the presence of potassium was deemed necessary to stabilize the resultant phosphazides in $KL_{P=N3}$ (**3-2**, $L_{P=N3}$ = κ^5-2,5-[(4-$^{i}PrC_6H_4)N_3$=P$^{i}Pr_2]_2N(C_4H_2)^-$, Scheme 3.2).

Diphosphazide **3-2** exhibits a diagnostic downfield singlet at δ 44.7 in the $^{31}P\{^{1}H\}$ NMR spectrum (*c.f.* δ –4.9 for compound **3-1**). A low-quality solid-state structure obtained *via* X-ray diffraction studies served to establish the atom connectivity within compound **3-2**, confirming two intact phosphazide units. Upon heating a sample of **3-2** at 55 ^{o}C for 24 hours in benzene-d_6, the $^{31}P\{^{1}H\}$ NMR spectrum revealed the signal at δ 44.7 had been

completely supplanted by an upfield-shifted resonance at δ 22.7, which closely matches that observed for $NaL_{P=N}$.[25] This information suggests the loss of 2 equiv of N_2 from diphosphazide **3-2** to afford $KL_{P=N}$ (Scheme 3.2, bottom).

Due to the success of stabilizing two phosphazides in a phosphazidosalen complex of uranium,[11] thorium was selected as an appropriate candidate for this system considering their similar ionic radii (1.05 Å for Th(IV) vs. 1.00 Å for U(IV), C.N. 8).[26] Additionally, the pentadentate, monoanionic ligand L_{PN3} was anticipated to sufficiently sterically saturate the thorium centre so as to provide access to unusual trialkyl species.

Reaction of $ThCl_4(dme)_2$ with 1 equiv of compound **3-2** in THF at –35 °C yielded an off-white solid which gave rise to a $^{31}P\{^1H\}$ NMR signal at δ 63.0 (Scheme 3.3, top). The atom connectivity of thorium diphosphazide $L_{P=N3}ThCl_3$ (**3-3**) was revealed by a low-quality solid-state structure. Complex **3-3** contains three chloride ligands, as well as two phosphazide groups that are bound to the thorium centers in a κ^2 fashion *via* the α- and γ-nitrogen atoms. Notably, ^1H and $^{31}P\{^1H\}$ NMR studies indicate that complex **3-3** is remarkably robust in solution, with no appreciable decomposition or loss of N_2 after 24 hours at 55 °C in benzene-d_6. Such thermal stability lies in stark contrast to $L''UCl_2$ which readily loses 1 equiv of N_2 at ambient temperature, and a second equivalent upon heating.[11]

Addition of 3 equiv of $LiCH_2SiMe_3$ to thorium trichloride **3-3** gave rise to a new resonance (δ 59.4) in the $^{31}P\{^1H\}$ NMR spectrum, along with concomitant disappearance of the resonance attributed to **3-3** (δ 63.0). The ^1H NMR spectrum exhibited a sharp singlet (δ 0.34, 27H) and a broad resonance (δ 0.15, 6H), consistent with chemical shifts for known organothorium complexes (δ –0.58 to 0.51, Si*Me*$_3$; δ –0.43 to 0.50, Th–C*H*$_2$;),[19,27] and

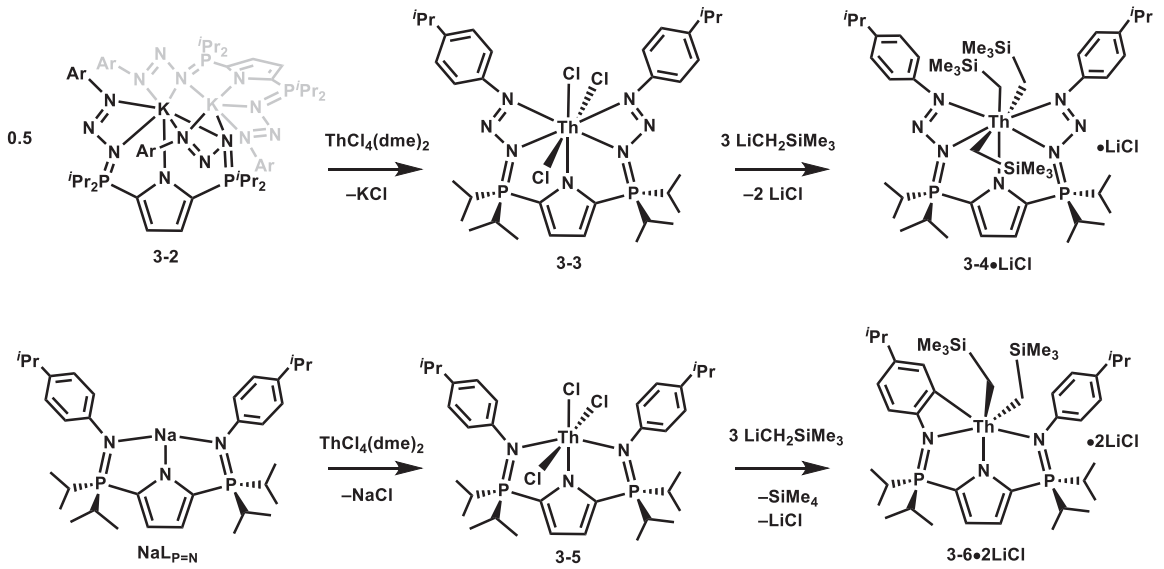

Scheme 3.3. Synthesis of compounds **3-3** to **3-6**.

hence, indicative of three Th–CH_2SiMe_3 alkyl groups that are chemically equivalent on the NMR timescale. In addition, the observed *C*H_2SiMe_3 $^{13}C\{^1H\}$ NMR resonance (δ 85.4) falls within the range reported (δ 70.7–102.7) for published thorium complexes that bear at least one CH_2SiMe_3 substituent.[19,27]

The X-ray crystal structure of $L_{P=N3}Th(CH_2SiMe_3)_3$ (**3-4**) (Figure 3.1, left) confirms that both phosphazide groups remain intact with slightly strained N–N–N angles of 108.9(3)° and 109.4(3)°, when compared to the average N–N–N angle of metal-free and uncoordinated phosphazides (112.2°). The geometry at thorium is best described as distorted hexagonal bipyramidal with the five coordinated nitrogen atoms and C35 comprising the meridional plane (N7 lies 1.031(4) Å out of the N4–N2–N1–N5–C35 plane) and C36 and C37 occupying the axial sites (C36–Th–C37: 157.5(1)°). Notably, one of the Th–C bonds (Th1–C37: 2.581(4) Å) is substantially longer than the other two (Th1–C35: 2.519(4) Å, Th1–C36: 2.513(4) Å). Although these distances are amongst the more elongated of reported Th–CH_2SiMe_3 lengths, they still fall within the range of thorium–

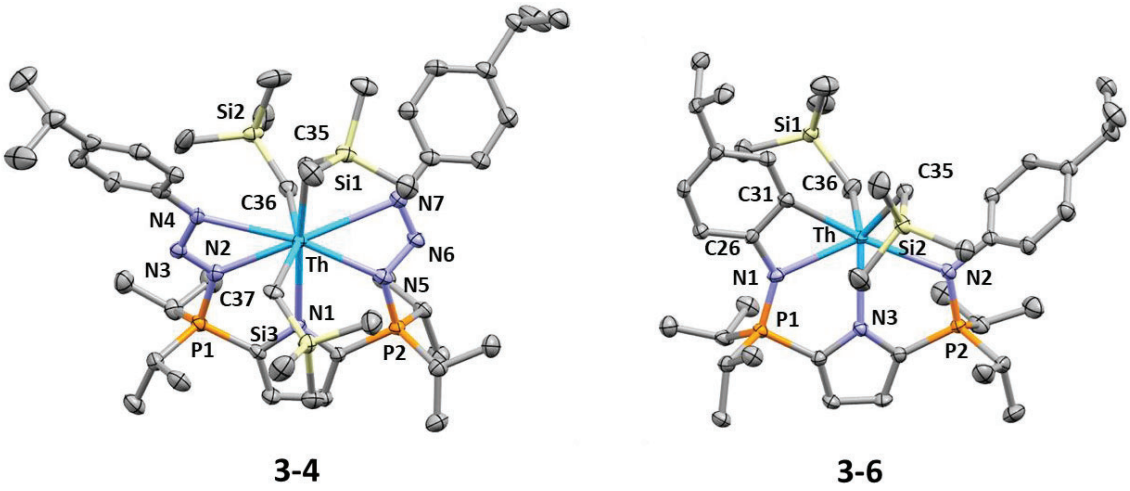

Figure 3.1. Left: X-Ray crystal structure of complex **3-4**. Thermal ellipsoids are represented at 50% probability. Hydrogen atoms have been omitted for clarity. Selected bond distances (Å) and angles (º): Th1–N1 = 2.709(3), Th1–N2 = 2.570(3), Th1–N4 = 2.888(3), Th1–N5 = 2.551(3), Th1–N7 = 2.910(3), Th–C35 = 2.519(4), Th1–C36 = 2.513(4), Th1–C37 = 2.581(4), N2–N3 = 1.350(5), N3–N4 = 1.277(4), N5–N6 = 1.363(4), N6–N7 = 1.268(4), P1–N2 = 1.648(3), P2–N5 = 1.658(3), N2–N3–N4 = 108.9(3), N5–N6–N7 = 109.4(3). Right: X-ray crystal structure of **3-6**. Thermal ellipsoids are represented at 50% probability. Hydrogen atoms have been omitted for clarity. Selected bond distances (Å) and angles (º): Th1–N1 = 2.483(4), Th1–N2 = 2.577(3), Th1–N3 = 2.508(3), Th1–C31 = 2.531(4), Th–C35 = 2.509(4), Th1–C36 = 2.477(5), P1–N1 = 1.601(3), P2–N2 = 1.619(3).

alkyl distances in the chemical literature (2.433(4)–2.598(3) Å).[19,27] The anionic pyrrole nitrogen–thorium distance (Th–N1 = 2.708(3) Å) is long, which we attribute to the propensity for thorium to sit in the centre of the pentadentate ligand binding pocket. The N3–N4 (1.277(4) Å), N6–N7 (1.268(4) Å), P1–N2 (1.648(3) Å) and P2–N5 (1.658(3) Å) distances are more consistent with somewhat localized double bonds, thus supporting the motif of alternating double (P=N), single (N–N) and double (N=N) bonds in the phosphazide unit. Surprisingly, complex **3-4** displays significant stability at ambient temperature in solution, with no change observed after 24 hours in benzene-d_6. At 55 °C, however, decomposition into an intractable mixture occurs in 2 hours.

Given the relative dearth of chemistry featuring metal-coordinated phosphazides, we aimed to compare the chemistry of related phosphazide and phosphinimine complexes. Since pincer ligands have been previously employed to support actinide complexes,[28] and the pyrrole-based bisphosphinimine analogue ($L_{P=N}$) of $L_{P=N3}$ has been used in conjunction with metals across the periodic table (*e.g.* Sc, Lu, and Rh),[25,29] we thereby endeavoured to prepare thorium complexes thereof.

Reaction of $NaL_{P=N}$ with $ThCl_4(dme)_2$ in dme afforded $L_{P=N}ThCl_3$ (**3-5**) as an off-white solid in 89.4% yield (Scheme 3.3, bottom). The formation of complex **3-5** was supported by the emergence of a new resonance (δ 56.1), along with simultaneous disappearance of the signal attributed to $NaL_{P=N}$ (δ 28.0), in the $^{31}P\{^1H\}$ NMR spectrum.[25] Notably, the ^{31}P NMR chemical shift for bisphosphinimine **3-5** appears 7.1 ppm upfield of complex **3-3** (δ 63.0), which matches the empirical trend that phosphazides generally resonate between 7 and 20 ppm downfield of their phosphinimine congeners.[11] An X-ray crystal structure of complex **3-5•C$_7$H$_8$** revealed the geometry at thorium to be pseudo-octahedral, with a Cl–Th–Cl angle of 174.34(3)°. However, thorium sits slightly outside the typical bonding pocket of the ligand causing the small $N_{phosphinimine}$–Th–$N_{phosphinimine}$ angle (135.2(1)°) and long Th–$N_{pyrrole}$ distance (2.474(4) Å; *c.f.* 2.394(4) Å and 2.378(3) Å for Th–$N_{phosphinimine}$). The P=N lengths (1.634(4) Å) are on the long end for coordinated phosphinimines in this ligand system. For example, the P=N bonds in the rhodium complexes $L_{P=N}Rh(CO)$ and $L_{P=N}Rh(CO)_2$ are 1.629(3) and 1.612(2) Å, respectively.[25]

Upon addition of 3 equiv of $LiCH_2SiMe_3$ to a toluene solution of complex **3-5**, two new ^{31}P NMR resonances (δ 47.7, δ 49.5) of equal intensity, as well as two P^{i}Pr methine ^1H NMR signals, were observed, suggesting the formation of a C_s-symmetric product.

Furthermore, 1 equiv of $SiMe_4$ (^{1}H NMR: δ 0.00) was generated and only two Th–CH_2SiMe_3 groups were present. The Th–CH_2 methylene protons appear as two doublets ($^2J_{HH}$ = 11.5 Hz) due to geminal coupling, (confirmed by a 2D ^{1}H-^{1}H COSY experiment) though both CH_2–*SiMe*$_3$ groups are chemically equivalent on the NMR timescale, giving rise to one singlet at δ 0.33 which integrates as 18H. Examples in the literature which also exhibit geminal Th–C*H*$_2$SiMe$_3$ coupling have $^2J_{HH}$ values (10.2 Hz, 12 Hz) that agree well with these findings.[27d, 27j] In the ^{13}C{^{1}H} NMR spectrum, the Th–*C*H_2SiMe$_3$ resonance was located at δ 87.3, similar to complex **3-4** (δ 85.4). A diagnostic signal indicative of a cyclometalated Th–C_{aryl} was found at δ 203.5. Altogether, these data strongly imply that the putative organothorium product, $L_{P=N}Th(CH_2SiMe_3)_3$, readily decomposed *via* cyclometalation of an N-aryl substituent.

The solid-state structure of $L^*_{P=N}Th(CH_2SiMe_3)_2$ (**3-6**, $L^*_{P=N}$ = 2-[(4-^{i}PrC_6H_3)N=P^{i}Pr$_2$]-5-[(4-^{i}PrC_6H_4)N=P^{i}Pr$_2$]N$(C_4H_2)^{2-}$) was confirmed by X-ray diffraction studies (Figure 3.1, right). The 6-coordinate thorium(IV) center exhibits pentagonal pyramidal geometry; the two phosphinimine nitrogen donors, the anionic pyrrole nitrogen, the cyclometalated aryl substituent (C31) and one CH_2SiMe_3 group (C35) comprise the pyramid base, while the remaining CH_2SiMe_3 (C36) occupies the apical site. Thorium sits 0.581(2) Å above the N1–N2–N3–C31–C35 plane. Notably, the Th–C distances in complex **3-6** (Th1–C35: 2.509(4) Å, Th1–C36: 2.477(5) Å, Th1–C31: 2.531(4) Å) are similar to those in 8-coordinate trialkyl **3-4** (2.513(4)-2.581(4) Å).

Although intramolecular C–H activation of $L_{P=N}$ is not common, it appears to be more prevalent for large metals, such as samarium.[30] The enhanced thermal stability of diphosphazide **3-4** relative to complex **3-6** is likely a consequence of the pentadentate

bonding mode of $L_{P=N3}$, which more completely coordinatively and electronically saturates the metal center, thereby mitigating the propensity for cyclometalation. In addition, the phosphazide groups necessarily enforce a larger distance between the N-aryl *ortho*-CHs and the metal center.

3.4. Conclusions

By a straightforward modification to the synthetic protocol for $L_{P=N}$, a versatile and robust diphosphazide ancillary ligand, $L_{P=N3}$, was prepared. Actinide complexes thereof, which can be generated *via* standard salt metathesis routes, are resistant to N_2 loss at ambient temperature and display different chemistry than their bisphosphinimine analogues. As the chemistry of this oft overlooked functionality continues to be developed, its incorporation into new ligand designs will continue to reveal its under-realized value to the fields of coordination and organometallic chemistry.

3.5. Experimental Details for Chapter 3

3.5.1. Laboratory Equipment and Apparatus

An argon filled MBraun glove box was employed for manipulation and storage of all oxygen and moisture sensitive compounds. All thermally unstable compounds were stored in a –35 °C freezer within the glove box. All reactions were performed on a double manifold high vacuum line using standard techniques or in a glove box under an atmosphere of argon.[31] Commonly utilized specialty glassware includes the swivel frit assembly, needle valves, and thick walled (5 mm) glass bombs equipped with Kontes Teflon stopcocks.[31] All glassware was stored in a 110 °C oven for a minimum of 12 hours,

or flame-dried before immediate transfer to the glove box antechamber or assembled on the vacuum line and evacuated while hot.

3.5.2. Solvents

Toluene, pentane, and tetrahydrofuran (THF) solvents were dried and purified using the Grubbs/Dow purification system and stored in evacuated 500 mL bombs over titanocene[32] (toluene and hexanes) or sodium/benzophenone ketal (THF).[33] Diethyl ether, pentane, heptane, benzene, benzene-d_6, toluene-d_8, and THF-d_8 were dried and stored over sodium/benzophenone ketal in glass bombs under vacuum. Unless otherwise noted, solvents were introduced *via* vacuum transfer with condensation at –78 °C. Liquid nitrogen (–196 °C), liquid nitrogen/pentane (–130 °C), dry ice/acetone (–78 °C), dry ice/acetonitrile (–45 °C) and water/ice (0 °C) baths were used for cooling receiving flasks and to maintain low temperature conditions.

3.5.3. Instrumentation and Details for NMR Experiments

All NMR spectra were recorded at ambient temperature, except where noted, with a Bruker Avance II NMR spectrometer (300.13 MHz for ^{1}H, 75.47 MHz for ^{13}C and 121.48 MHz for ^{31}P) or Avance III NMR spectrometer (700.13 MHz for ^{1}H, 176.05 MHz for ^{13}C, and 283.54 MHz for ^{31}P) NMR spectrometer. All ^{1}H NMR spectra were referenced to $SiMe_4$ through the residual ^{1}H resonance(s) of the employed solvent; benzene-d_6 (7.16 ppm), toluene-d_8 (2.09, 6.98, 7.02 and 7.09 ppm), chloroform-d_1 (7.26 ppm) or THF-d_8 (1.73 and 3.58 ppm). ^{13}C NMR spectra were referenced relative to $SiMe_4$ through the resonance(s) of the employed solvent; benzene-d_6 (128.0 ppm), toluene-d_8 (20.4, 125.2, 128.0, 128.9, 137.5 ppm), chloroform-d_1 (77.16 ppm) or THF-d_8 (25.4, 67.6 ppm). ^{1}H

NMR data for diamagnetic compounds are reported as follows: chemical shift, multiplicity (s = singlet, d = doublet, t = triplet, q = quartet, quint = quintet, sp = septet, br = broad, m = multiplet, app = apparent, obsc = obscured, ov = overlapping), coupling constants (Hz), integration, assignment. ^{13}C NMR data for diamagnetic compounds are reported as follows: chemical shift, assignment. Assignment of resonances were supported by ^{1}H–^{1}H COSY, $^{13}C\{^{1}H\}$ APT, ^{1}H–$^{13}C\{^{1}H\}$ and HSQC/HMBC experiments.

3.5.4. Additional Instrumentation

Elemental analyses (%CHN) were conducted at the University of Lethbridge by Dylan Webb on an Elementar Americas Vario MicroCube Analyzer (C, H, N, O, S capabilities).

3.5.5. Additional Safety Considerations

Organic azides are both toxic and explosive. Care should be taken while handling azides, particularly if they are solvent free and/or at elevated temperatures. Phosphines are toxic and care should be taken while handling. Natural thorium (primary isotope ^{232}Th) is a weak α-emitter (4.012 MeV) with a half-life of 1.41×10^{10} years; manipulations and reactions should be carried out in a fume hood or in an inert atmosphere glove box.

3.5.6. Synthetic Methods

Synthesis of 2,5-bis(diisopropylphosphino)-*N*-K-pyrrole, (3-1).

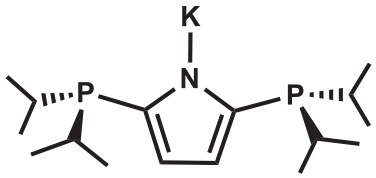

In an inert atmosphere glove box, 2,5-(P^iPr_2)$_2$NH(C_4H_2) (49.8 mg, 0.167 mmol)[3] and potassium hydride (9.7 mg, 0.24 mmol, 1.4 equiv) were added to a 100 mL RBF with a Teflon® coated stir bar. The reaction vessel was attached to a double manifold vacuum line and 10 mL of THF was transferred to the flask at –78 °C. Evolution of H_2 gas was observed upon gradual warming to ambient temperature. The reaction mixture was then heated while stirring under argon at 45 ºC for 2 hours. The solvent was removed *in vacuo* leaving an off-white solid. The product was extracted into benzene (1 × 1.5 mL) and the solution was filtered through Celite® to remove excess KH. After filtration, benzene was removed *in vacuo*, affording a white solid. Yield: 42.1 mg, 74.6%. ^{1}H NMR (C_6D_6, 300.13 MHz): δ 1.16 (m, 24H, CH(C*H*$_3$)$_2$), 2.06 (sp, $^3J_{HH}$ = 6.7 Hz, 4H, C*H*(CH$_3$)$_2$), 6.70 (s, 2H, pyrrole-C*H*). ^{13}C{^{1}H} NMR (C_6D_6, 75.47 MHz): δ 20.2 (d, $^2J_{CP}$ = 6.7 Hz, CH(*C*H$_3$)$_2$), 21.4 (d, $^1J_{CP}$ = 19.0 Hz, *C*H(CH$_3$)$_2$), 24.6 (d, $^2J_{CP}$ = 9.1 Hz, CH(*C*H$_3$)$_2$), 115.5 (s, 3,4-pyrrole *C*H), 135.02 (dd,$^1J_{CP}$ = 15.9 Hz, $^3J_{CP}$ = 12.6, 2,5-pyrrole *C*). ^{31}P{^{1}H} NMR (C_6D_6, 121.49 MHz): δ –4.9 (s). Anal. Calcd. (%) for $C_{16}H_{30}KNP_2$: C: 56.95; H: 8.96; N: 4.15. Found: C: 56.98; H: 8.97; N: 4.30.

Synthesis of $KL_{P=N3}$, (3-2).

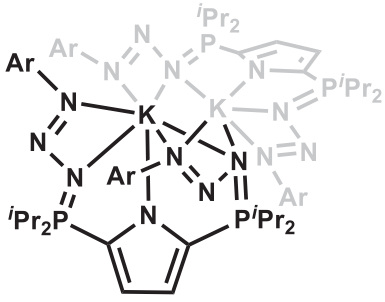

In an inert atmosphere glove box, compound **3-1** (175.3 mg, 0.5195 mmol) was added into a 20 mL scintillation vial and dissolved in toluene (3 mL). Pipp azide (167.0 mg, 1.036 mmol, 2 equiv), diluted in toluene (1 mL) was added dropwise to the vial containing **3-1**, resulting in a clear

dark yellow solution. The solution was stirred for two minutes with a Teflon® coated stir bar and the solvent was removed *in vacuo.* The product was washed with pentane (3 × 2 mL) and dried *in vacuo* resulting in a pale yellow solid. Yield: 0.1753 g, 61.25%. ^{1}H NMR (C_6D_6, 300.13 MHz): δ 1.02 (dd, $^{3}J_{HP}$ = 14.9 Hz, $^{3}J_{HH}$ = 6.9 Hz, 24H, P–CH(C*H*$_3$)$_2$), 1.23 (d, $^{3}J_{HH}$ = 6.9 Hz, 12H, Ar–CH(C*H*$_3$)$_2$), 2.44 (dsp, $^{3}J_{HH}$ = 6.9 Hz, $^{2}J_{HP}$ = 2.4 Hz, 4H, P–C*H*(CH$_3$)$_2$), 2.81 (sp, $^{3}J_{HH}$ = 6.9 Hz, 2H, Ar–C*H*(CH$_3$)$_2$), 6.88 (d, $^{3}J_{HP}$ = 2.2 Hz, 2H, pyrrole-C*H*), 7.19 (d, $^{3}J_{HH}$ = 8.4 Hz, 4H, *meta*-aromatic C*H*), 7.59 (d, $^{3}J_{HH}$ = 8.4 Hz 4H, *ortho*-aromatic C*H*). ^{13}C{^{1}H} NMR (C_6D_6, 75.47 MHz): δ 16.0 (d, $^{2}J_{CP}$ = 2.8 Hz, P–CH(*C*H$_3$)$_2$), 16.8 (d, $^{2}J_{CP}$ = 1.9 Hz, P–CH(*C*H$_3$)$_2$), 24.2 (d, $^{1}J_{CP}$ = 54.8 Hz, P–*C*H(CH$_3$)$_2$), 24.8 (s, Ar–CH(*C*H$_3$)$_2$), 34.5 (s, Ar–*C*H(CH$_3$)$_2$), 118.0 (dd,$^{2}J_{CP}$ = 27.5 Hz, $^{3}J_{CP}$ = 10.5 Hz, 3,4-pyrrole *C*H), 121.5 (s, aromatic *C*H), 127.3 (s, aromatic *C*H), 125.0 (dd, $^{1}J_{CP}$ = 134.1 Hz, $^{3}J_{CP}$ = 20.8 Hz, 2,5-pyrrole *C*), 145.7 (s, aromatic *ipso*-*C*), 152.04 (s, aromatic *ipso*-*C*). ^{31}P{^{1}H} NMR (C_6D_6, 121.49 MHz): δ 44.7 (s). Anal. Calcd. (%) for $C_{34}H_{52}KN_7P_2$: C: 61.89; H: 7.94; N: 14.86. Found: C: 61.85; H: 7.98; N: 14.76.

Synthesis of $L_{P=N3}ThCl_3$ (3-3).

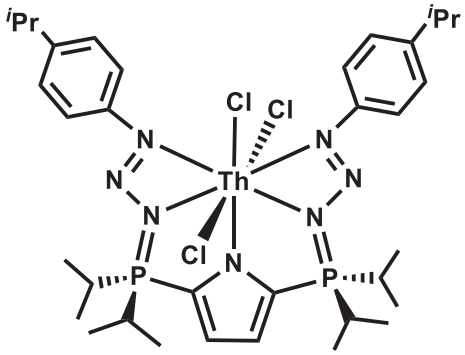

In an inert atmosphere glove box, compound **3-2** (31.2 mg, 0.0455 mmol) and $ThCl_4(dme)_2$ (26.1 mg, 0.0455 mmol) were weighed into a 20 mL scintillation vial with a Teflon® coated stir bar. THF cooled to –35 °C was added (3 mL) to the vial and the cloudy solution was kept cold (–35 °C) and stirred with a Teflon® coated stir bar for 5 minutes. The solution was then quickly filtered through Celite® to remove salts and the

THF was removed *in vacuo*. The product was washed with pentane (3 × 3 mL) and dried *in vacuo*. The resulting product was an off-white solid. Yield: 38.6 mg, 85.1%. ^{1}H NMR (THF-d_8, 300.13 MHz): δ 1.27 (d, $^{3}J_{HH}$ = 6.9 Hz, 12H, Ar–CH(CH_3)$_2$), 1.34 (m, 24H, P–CH(CH_3)$_2$), 2.97 (ov sp and dsp, 6H, P–CH(CH$_3$)$_2$ and Ar–CH(CH$_3$)$_2$), 7.0 (dd, $^{2}J_{HP}$ = 2.4 Hz, $^{3}J_{HP}$ = 1.2 Hz, 2H, pyrrole-CH), 7.27 (d, $^{3}J_{HH}$ = 8.4 Hz, 4H, *meta*-aromatic CH), 7.93 (d, $^{3}J_{HH}$ = 8.4 Hz, 4H, *ortho*-aromatic CH). ^{13}C{^{1}H} NMR (C$_6$D$_6$, 75.47 MHz): δ 15.9 (s, P–CH(*C*H$_3$)$_2$), 16.2 (s, P–CH(*C*H$_3$)$_2$), 24.4 (s, Ar–CH(*C*H$_3$)$_2$), 26.0 (d,$^{1}J_{CP}$ = 50.7 Hz, P–*C*H(CH$_3$)$_2$), 34.6 (s, Ar–*C*H(CH$_3$)$_2$), 118.8 (s, 3,4-pyrrole *C*H), 123.0 (s, aromatic *C*H), 126.6 (d, $^{1}J_{CP}$ = 15.7 Hz, 2,5-pyrrole *C*), 127.5 (s, aromatic *C*H), 147.4 (s, aromatic *ipso-C*), 149.8 (s, aromatic *ipso-C*). ^{31}P{^{1}H} NMR (C$_6$D$_6$, 121.49 MHz): δ 63.0(s). Anal. Calcd. (%) for $C_{34}H_{52}Cl_3N_7P_2Th$: C: 42.58; H: 5.46; N: 10.22. Found: C: 41.81; H: 5.04; N: 10.02.

Synthesis of $L_{P=N3}Th(CH_2SiMe_3)_3$•LiCl, (3-4•LiCl).

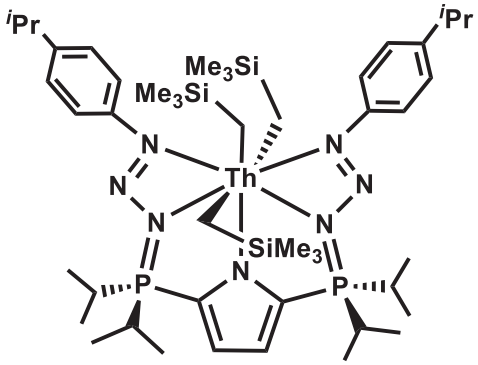

In an inert atmosphere glove box, complex **3-3** (34.8 mg, 0.0363 mmol) and LiCH$_2$SiMe$_3$ (11.3 mg, 0.120 mmol, 3.3 equiv) were weighed into a 20 mL scintillation vial and dissolved in 2 mL of toluene. The solution was agitated for 2 minutes and the cloudy solution was filtered through Celite® yielding a clear dark orange solution. The toluene was removed *in vacuo*, resulting in an orange oil. Pentane (2 mL) was added to the oil, and the solution was cooled to –35 ºC for 15 minutes resulting in the formation of X-ray quality crystals. Yield: 30.2 mg, 71.9%. ^{1}H NMR (C$_6$D$_6$, 300.13 MHz): δ 0.15 (br s, 6H, Th–CH_2), 0.34 (s, 27H, Si(CH_3)$_3$), 1.01 (m,

24H, P–CH(CH_3)$_2$), 1.12 (d, $^3J_{HH}$ = 6.9 Hz, 12H, Ar–CH(CH_3)$_2$), 2.31 (dsp, $^3J_{HH}$ = 7.0 Hz, $^2J_{HP}$ = 3.6 Hz, 4H, P–CH(CH$_3$)$_2$), 2.71 (sp, $^3J_{HH}$ = 6.9 Hz, 2H, Ar–CH(CH$_3$)$_2$), 2.44 (d, $^3J_{HP}$ = 6.6 Hz, 2H, pyrrole-CH), 7.30 (d, $^3J_{HH}$ = 8.4 Hz, 4H, *meta*-aromatic CH), 8.13 (d, $^3J_{HH}$ = 8.4 Hz, 4H, *ortho*-aromatic CH). ^{13}C{^{1}H} NMR (C$_6$D$_6$, 75.47 MHz): δ 5.6 (s, Si(*C*H$_3$)$_3$), 16.7 (s, P–CH(*C*H$_3$)$_2$), 16.8 (s, P–CH(*C*H$_3$)$_2$), 24.4 (s, Ar–CH(*C*H$_3$)$_2$), 27.0 (d, $^1J_{CP}$ = 49.9 Hz, P–*C*H(CH$_3$)$_2$), 34.51 (s, Ar–*C*H(CH$_3$)$_2$), 85.4 (br s, Th–*C*H$_2$), 119.2 (dd,$^2J_{CP}$ = 25.9 Hz, $^3J_{CP}$ = 10.4 Hz, 3,4-pyrrole *C*H), 122.60 (s, aromatic *C*H), 126.0 (dd, $^1J_{CP}$ = 133.3 Hz, $^3J_{CP}$ = 16.3 Hz, 2,5-pyrrole *C*), 127.6 (s, aromatic *C*H), 148.6 (s, aromatic *ipso-C*), 149.3 (s, aromatic *ipso-C*). ^{31}P{^{1}H} NMR (C$_6$D$_6$, 121.49 MHz): δ 59.4 (s). Anal. Calcd. (%) for C$_{46}$H$_{85}$N$_7$P$_2$Si$_3$Th•LiCl: C:47.76; H: 7.41; N: 8.48. Found: C: 47.74; H: 7.46; N: 8.48. The presence of LiCl was confirmed by ^{7}Li{^{1}H} NMR: ^{7}Li{^{1}H} NMR (D$_2$O, 272.22 MHz): δ 0.1 (s).

Synthesis of $L_{P=N}ThCl_3$, (3-5).

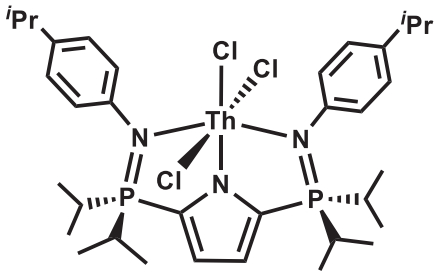

In an inert atmosphere glove box, NaL$_{P=N}$ (111.2 mg, 0.1892 mmol)[3] and ThCl$_4$(dme)$_2$ (104.8 mg, 0.1891 mmol) were added to a 20 mL scintillation vial with a Teflon® coated stir bar. To this mixture, 5 mL of dme was added and the solution was stirred for one hour. The solution was filtered through Celite® to remove salts, and the solvent was removed *in vacuo*. The product was washed with pentane (2 × 2 mL) and dried *in vacuo* resulting in an off-white solid. Yield: 151.7 mg, 89.4%. ^{1}H{^{31}P} NMR (C$_6$D$_6$, 300.13 MHz): δ 1.01 (m, 24H, P–CH(CH_3)$_2$), 1.09 (d, $^3J_{HH}$ = 7.0 Hz, 12H, Ar–CH(CH_3)$_2$), 1.97 (m, 4H, P–CH(CH$_3$)$_2$), 2.64 (sp, $^3J_{HH}$ = 7.0 Hz,

2H, Ar–C*H*(CH_3)$_2$), 6.54 (s, 2H, pyrrole-C*H*), 7.11 (d, $^3J_{HH}$ = 8.4 Hz, 4H, *meta*-aromatic C*H*), 7.75 (d, $^3J_{HH}$ = 8.4 Hz, 4H, *orth*-aromatic C*H*). $^{13}C\{^1H\}$ NMR (C_6D_6, 75.47 MHz): δ 16.4 (d, $^2J_{CP}$ = 45.4 Hz, P–CH(*C*H_3)$_2$), 24.4 (s, Ar–CH(*C*H_3)$_2$), 27.7 (d, $^1J_{CP}$ = 53.4 Hz, P–*C*H(CH_3)$_2$), 34.2 (s, Ar–*C*H(CH_3)$_2$), 116.6 (dd, $^2J_{CP}$ = 25.8 Hz, $^3J_{CP}$ = 9.9 Hz, 3,4-pyrrole *C*H), 129.7 (s, aromatic *C*H), 130.0 (d,$^3J_{CP}$ = 5.2 Hz aromatic *C*H), 135.6 (s, aromatic *ipso*-*C*), 148.2 (s, aromatic *ipso*-*C*). The 2,5-pyrrole *C* resonance overlapped with the benzene-d_6 solvent, but was observed using d_8-THF: 130.2 (dd, $^1J_{CP}$ = 132.1 Hz, $^3J_{CP}$ = 14.3 Hz, 2,5-pyrrole *C*). $^{31}P\{^1H\}$ NMR (C_6D_6, 121.49 MHz): δ 56.1(s). Anal. Calcd. (%) for $C_{34}H_{52}N_3P_2Th$: C: 45.22; H: 5.80; N: 4.65. Found: C: 45.16; H: 5.89; N: 4.42.

Synthesis of $L_{P=N}$*Th(CH_2SiMe_3)$_2$•2LiCl, (3-6•2LiCl).

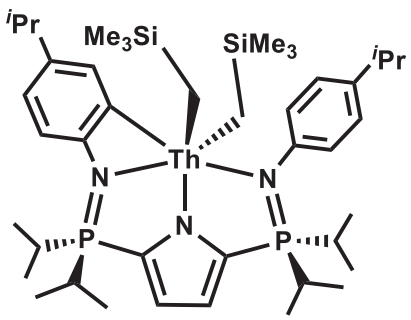

In an inert atmosphere glove box, complex **3-5** (29.8 mg, 0.0330 mmol) and $LiCH_2SiMe_3$ (9.3 mg, 0.099 mmol, 3 equiv) were weighed into a 20 mL scintillation vial and dissolved in toluene (2 mL). The vial was agitated for 2 minutes and the cloudy solution was quickly filtered through Celite® to remove salts. The toluene was removed *in vacuo* yielding an off-white sticky solid. The product was washed with pentane (3 × 1 mL), cooled to –35 °C and dried *in vacuo* to yield a crystalline white solid. X-ray quality crystals were grown from pentane at –35 °C in 15 minutes. Yield: 18.8 mg, 54.0%. $^1H\{^{31}P\}$ NMR (C_6D_6, 700.44 MHz): δ 0.02 (d, $^2J_{HH}$ = 11.5 Hz, 2H, Th–C*H*$_2$), 0.29 (d, $^2J_{HH}$ = 11.5 Hz, 2H, Th–C*H*$_2$), 0.33 (s, 18H, Si(C*H*$_3$)$_3$), 0.90 (ov m, 24H, P–CH(C*H*$_3$)$_2$), 1.22 (d, $^3J_{HH}$ = 6.9 Hz, 6H, Ar–CH(C*H*$_3$)$_2$), 1.44 (d, $^3J_{HH}$ = 6.9 Hz, 6H, Ar–CH(C*H*$_3$)$_2$), 1.99 (sp, $^3J_{HH}$ = 7.1 Hz, 2H, P–C*H*(CH_3)$_2$), 2.20 (sp,

$^{3}J_{HH}$ = 7.1 Hz, 2H, P–C*H*$(CH_3)_2$), 2.79 (sp, $^{3}J_{HH}$ = 6.9 Hz, 1H, Ar–C*H*$(CH_3)_2$), 3.00 (sp, $^{3}J_{HH}$ = 6.9 Hz, 1H, Ar–C*H*$(CH_3)_2$), 6.42 (d, $^{3}J_{HH}$ = 3.3 Hz, 1H, pyrrole-C*H*), 6.49 (d, $^{3}J_{HH}$ = 3.3 Hz, 1H, pyrrole-C*H*), 6.54 (d, $^{3}J_{HH}$ = 7.8 Hz, 1H, *ortho*-cyclometallated Ar–C*H*), 7.13 (dd, $^{3}J_{HH}$ = 7.8 Hz, $^{4}J_{HH}$ = 2.0 Hz, 1H, *meta*-cyclometallated Ar–C*H*), 7.28 (d, $^{3}J_{HH}$ = 8.2 Hz, 2H, *meta*-aromatic C*H*), 7.46 (d, $^{3}J_{HH}$ = 8.2 Hz, 2H, *ortho*-aromatic C*H*), 8.30 (d, $^{4}J_{HH}$ = 2.1 Hz, 1H, *meta*-cyclometallated Ar–C*H*). $^{13}C\{^{1}H\}$ NMR (C_6D_6, 176.13 MHz): δ 4.4 (s, Si(CH_3)$_3$), 15.9 (d, $^{2}J_{CP}$ = 2.3 Hz P–CH(CH_3)$_2$), 16.3 (d, $^{2}J_{CP}$ = 1.8 Hz, P–CH(CH_3)$_2$), 16.4 (d, $^{2}J_{CP}$ = 2.0 Hz, P–CH(CH_3)$_2$), 16.8 (d, $^{2}J_{CP}$ = 2.3 Hz, P–CH(CH_3)$_2$), 24.7 (s, Ar–CH(CH_3)$_2$), 25.5 (s, Ar–CH(CH_3)$_2$), 26.8 (d, $^{1}J_{CP}$ = 53.3 Hz, P–*C*H$(CH_3)_2$), 26.9 (d, $^{1}J_{CP}$ = 53.3 Hz, P–*C*H$(CH_3)_2$), 34.2 (s, Ar–*C*H$(CH_3)_2$), 35.3 (s, Ar–*C*H$(CH_3)_2$), 87.3 (s, Th–*C*H_2), 116.9 (s, aromatic *C*H), 117.4 (dd, $^{2}J_{CP}$ = 25.6 Hz, $^{3}J_{CP}$ = 10.4 Hz, 3,4-pyrrole *C*H), 119.2 (dd, $^{2}J_{CP}$ = 24.4 Hz, $^{3}J_{CP}$ = 10.4 Hz, 3,4-pyrrole *C*H), 125.0 (s, aromatic *C*H), 128.7 (s, aromatic *C*H), 128.8 (d, $^{3}J_{CP}$ = 6.4 Hz, aromatic *C*H), 130.3 (dd, $^{1}J_{CP}$ = 136.4 Hz, $^{3}J_{CP}$ = 14.4 Hz, 2,5-pyrrole *C*), 132.3 (dd, $^{1}J_{CP}$ = 139.4 Hz, $^{3}J_{CP}$ = 13.5 Hz, 2,5-pyrrole *C*), 135.8 (d, $^{4}J_{CP}$ = 5.0 Hz, aromatic *C*H), 140.8 (s, aromatic *ipso*-*C*), 143.8 (d, $^{2}J_{CP}$ = 4.7 Hz, aromatic *ipso*-*C*), 145.0 (d, $^{5}J_{CP}$ = 3.6 Hz, aromatic *ipso*-*C*), 150.8 (d, $^{2}J_{CP}$ = 3.7 Hz, aromatic *ipso*-*C*), 203.5 (br s, cyclometallated Th-C). $^{31}P\{^{1}H\}$ NMR (C_6D_6, 283.54 MHz): δ 47.7 (s), 49.5 (s). Anal. Calcd. (%) for $C_{42}H_{73}N_3P_2Si_2Th$•2LiCl: C: 47.82; H: 6.97; N: 3.98. Found: C: 47.81; H: 6.97; N: 4.00. The presence of LiCl was confirmed by $^{7}Li\{^{1}H\}$ NMR: $^{7}Li\{^{1}H\}$ NMR (D_2O , 272.22 MHz): δ 0.1 (s).

3.5.7. Crystallographic Details

All structures were collected on a Rigaku SuperNova diffractometer equipped with a Dectris Pilatus 3R 200K-A hybrid-pixel-array detector, a four-circle goniometer, sealed graphite-monochromated Mo Kα (λ = 0.71073 Å) and Cu Kα (λ = 1.54178 Å) X-ray sources, and an Oxford cryostream-cooling device fixed at 100 K. Single crystals suitable for X-ray diffraction studies were mounted on a MiTiGen cryo-loop using desiccated Paratone–*N* oil stored in a glove box. Data reduction was accomplished by the CrysAlis^{Pro} (version 1.171.38.43) software package. Absorption corrections were applied by multi-scan techniques and empirical absorption correction using spherical harmonics, implemented in SCALE3 ABSPACK scaling algorithm. Structures were solved in the Olex2[34] environment using intrinsic phasing and refined by full-matrix least squares method on F^2 using the SHELX software suite.[35,36] All non-hydrogen atoms were refined anisotropically, C–H hydrogens were calculated and refined isotropically as a riding model. All measurements were performed at the University of Lethbridge.

Single crystals of complexes **3-4** and **3-6** were grown from pentane/toluene at –35 °C, and single crystals of **3-5•C$_7$H$_8$** were grown from a saturated solution of toluene at –35 °C. Unfortunately, single crystals of **3-2** grown in toluene, and **3-3** grown in benzene-d_6, succumb to rapid decomposition upon removal from the mother liquor, resulting in the crystals becoming covered with amorphic material. However, inner portions of the crystals remain intact, allowing for modest diffraction of X-ray radiation, despite interference from the polycrystalline material. The data is not ideal, however, and therefore discussions of the metrical parameters are not included in the thesis. The data set does, though, allow for qualitative discussions associated with the connectivity and geometry of complexes **3-2** and

3-3. Therefore, these structures will be referred to within this thesis as “connectivity structures”. Summary of the crystallographic data can be found below in **Table 3.1.**

Table 3.1. X-ray Crystallographic data and structure refinement for complexes **3-2**, **3-3**, **3-4**, **3-5** and **3-6**.

	3-2	**3-3**	**3-4**
CCDC #	N/A	N/A	1973166
Empirical formula	$C_{67}H_{97}K_2N_{14}P_4$	$C_{34}H_{51}Cl_3N_7P_2Th$	$C_{46}H_{85}N_7P_2Si_3Th$
Formula weight/g mol^{-1}	1300.66	1916.29	1114.45
Temperature/K	145(1)	120.01(10)	99.9(4)
Crystal system	monoclinic	orthorhombic	monoclinic
Space group	$P2_1/c$	$Pna2_1$	C2/c
a/Å	25.756(8)	12.3671(2)	38.1800(2)
b/Å	13.402(3)	26.5522(5)	12.01066(7)
c/Å	24.793(8)	26.8457(6)	24.88322(15)
α/°	90	90	90
β/°	106.25(3)	90	101.1728(6)
γ/°	90	90	90
Volume/Å^3	8216(4)	8815.4(3)	11194.37(12)
Z	4	4	8
ρ_{calc}g/cm^3	1.051	13.717	1.323
μ/mm^{-1}	2.085	128.268	10.010
F(000)	2780.0	36100.0	4576.0
Crystal size/mm^3	0.2 × 0.1 × 0.02	0.2 × 0.2 × 0.02	0.35 × 0.31 × 0.25
Radiation (Å)	CuKα (λ = 1.54184)	CuKα (λ = 1.54184)	CuKα (λ = 1.54184)
2Θ range for data collection/°	7.504 to 103.954	8.548 to 160.35	7.242 to 160.772
Index ranges	-25 ≤ h ≤ 26, -7 ≤ k ≤ 10, -25 ≤ l ≤ 21	-15 ≤ h ≤ 15, -33 ≤ k ≤ 24, -34 ≤ l ≤ 34	-48 ≤ h ≤ 48, -14 ≤ k ≤ 14, -31 ≤ l ≤ 24
Reflections collected	14731	23685	65766
Independent reflections	6994 [R_{int} = 0.2942, R_{sigma} = 0.4697]	8689 [R_{int} = 0.1012, R_{sigma} = 0.0667]	12093 [R_{int} = 0.0393, R_{sigma} = 0.0242]
Data/restraints/parameters	6994/0/322	8689/1/81	12093/6/577
Goodness-of-fit on F^2	1.185	6.696	1.177
Final R indexes [I>=2σ (I)]	R_1 = 0.1711 wR_2 = 0.3425	R_1 = 0.4198 wR_2 = 0.7399	R_1 = 0.0300 wR_2 = 0.0805
Final R indexes [all data]	R_1 = 0.3966 wR_2 = 0.4213	R_1 = 0.4403 wR_2 = 0.7622	R_1 = 0.0315 wR_2 = 0.0813
Largest diff. peak/hole / e Å^{-3}	0.82/-0.42	65.17/-14.62	1.14/-1.68

Programs for diffractometer operation, data collection, data reduction, and absorption correction were those supplied by Rigaku.

	3-5 · (C_7H_8)	**3-6**
CCDC #	1973168	1973167
Empirical formula	$C_{41}H_{60}Cl_3N_3P_2Th$	$C_{42}H_{73}N_3P_2Si_2Th$
Formula weight/g mol^{-1}	995.25	970.19
Temperature/K	100.01(17)	100.00(10)
Crystal system	monoclinic	monoclinic
Space group	$P2_1/c$	$P2_1/c$
a/Å	11.44990(10)	12.25321(8)
b/Å	23.70340(10)	19.54444(14)
c/Å	17.73280(10)	20.87594(14)
α/°	90	90
β/°	108.7210(10)	97.9130(6)
γ/°	90	90
Volume/$Å^3$	4558.08(6)	4951.81(6)
Z	4	4
$\rho_{calc}g/cm^3$	1.450	1.301
μ/mm^{-1}	13.051	10.989
F(000)	1992.0	1976.0
Crystal size/mm^3	0.4 × 0.2 × 0.05	0.15 × 0.1 × 0.02
Radiation (Å)	CuKα (λ = 1.54184)	CuKα (λ = 1.54184)
2Θ range for data collection/°	6.45 to 160.4	7.284 to 160.65
Index ranges	$-13 \le h \le 14$, $-28 \le k \le 30$, $-22 \le l \le 22$	$-15 \le h \le 14$, $-22 \le k \le 24$, $-26 \le l \le 26$
Reflections collected	28177	56770
Independent reflections	8728 [R_{int} = 0.0235, R_{sigma} = 0.0214]	10779 [R_{int} = 0.0494, R_{sigma} = 0.0340]
Data/restraints/parameters	8728/0/464	10779/4/477
Goodness-of-fit on F^2	1.072	1.156
Final R indexes [I>=2σ (I)]	R_1 = 0.0248 wR_2 = 0.0655	R_1 = 0.0328 wR_2 = 0.0885
Final R indexes [all data]	R_1 = 0.0259 wR_2 = 0.0679	R_1 = 0.0362 wR_2 = 0.0901
Largest diff. peak/hole / e $Å^{-3}$	0.81/-1.17	1.15/-1.71

Programs for diffractometer operation, data collection, data reduction, and absorption correction were those supplied by Rigaku.

3.6. References for Chapter 3

1. Staudinger, H.; Meyer, J. Über neue organische Phosphorverbindungen III. Phosphinmethylenderivate und Phosphinimine. *Helv. Chim. Acta* **1919**, *2*, 635–645.

2. a) Cariou, R.; Dahcheh, F.; Graham, T. W.; Stephan, D. W. Mononuclear and dinuclear palladium and nickel complexes of phosphinimine-based tridentate ligands. *Dalton Trans.* **2011**, *40*, 4918–4925. b) Gololobov, Y. G.; Kasukhin, L. F. Recent advances in the staudinger reaction. *Tetrahedron* **1992**, *48*, 1353–1406. c) Zamora, M. T.; Zahir, S. M.; Johnson, K. R. D.; Barnson, C. J.; Wheaton, C. A.; Hänninen, M. M.; Hayes, P. G. Synthesis of Sterically Demanding Bis(phosphinimine) Dibenzofuran Ligands and Subsequent Zinc Metalation. *Aust. J. Chem.* **2015**, *68*, 373–384.

3. a) Chan, K. T. K.; Spencer, L. P.; Masuda, J. D.; McCahill, J. S. J.; Wei, P.; Stephan, D. W. Anionic Phosphinimine-Chelate Complexes of Rh and Ir: Steric and Electronic Influences on Oxidative Addition of CH_2Cl_2. *Organometallics* **2004**, *23*, 381–390. b) Liddle, S. T.; Mills, D. P.; Wooles, A. Early metal bis(phosphorus-stabilised)carbene chemistry. *J. Chem. Soc. Rev.* **2011**, *40*, 2164–2176. c) Sun, R.; Wang, H.; Hu, J.; Zhao, J.; Zhang, H. Pyridine-phosphinimine ligand-accelerated Cu(I)-catalyzed azide–alkyne cycloaddition for preparation of 1-(pyridin-2-yl)-1,2,3-triazole derivatives. *Org. Biomol. Chem.* **2014**, *12*, 5954–5963. d) Wheaton, C. A.; Hayes, P. G. Exploring the versatility of a bis(phosphinimine) pincer ligand: effect of sterics on structure and lactide polymerization activity of cationic zinc complexes. *Catal. Sci. Technol.* **2012**, *2*, 125–138.

4. Stephan, D. W. The Road to Early-Transition-Metal Phosphinimide Olefin Polymerization Catalysts. *Organometallics* **2005**, *24*, 2548–2560.

5. Gamer, M. T.; Roesky, P. W.; Palard, I.; Le Hellaye, M.; Guillaume, S. M. In Situ Formation of Bis(phosphinimino)methanide Rare Earth Alkoxide Initiators for the Ring-Opening Polymerization of ε-Caprolactone. *Organometallics* **2007**, *26*, 651–657.

6. Bebbington, M. W. P.; Bourissou, D. Stabilised phosphazides. *Coord. Chem. Rev.* **2009**, *253*, 1248–1261.

7. a) Goerlich, J. R.; Farkens, M.; Fischer, A.; Jones, P. G.; Schmutzler, R. Über die Umsetzung von Tris(dimethylamino)phosphin, Triisopropylphosphin und tButyldifluorphosphin mit tertiären Alkylaziden: Phosphazidbildung versus Phosphinimidbildung. Röntgenstrukturen von Triphenylmethylazid und Tris(dimethylamino)-N-triphenylmethylphosphazid. *Z. Anorg. Allg. Chem.* **1994**, *620*, 707–717. b) Kennedy, R. D. Stabilization of acyclic phosphazides using the ortho-closo-dicarbadodecaboranyl residue. *Chem. Commun.* **2010**, *46*, 4782–4784.

8. a) Chidester, C. G.; Szmuszkovicz, J.; Duchamp, D. J.; Laurian, L. G.; Freeman, J. P. Reaction of 3-azidopropanol with tris(dimethylamido)phosphorus and structure of the phosphazide reaction product. *Acta Crystallogr.*, *Sect. C: Struct. Chem.* **1988**, *44*, 1080–1083; b) Velasco, M. D.; Molina, P.; Fresneda, P. M.; Sanz, M.A. Isolation, Reactivity and Intramolecular Trapping of Phosphazide Intermediates in the Staudinger Reaction of Tertiary Phosphines with Azides. *Tetrahedron* **2000**, *56*, 4079–4084.

9. a) Liu, B.; Cui, D. Rare-earth metal complexes stabilized by amino-phosphine ligand. Reaction with mesityl azide and catalysis of the cycloaddition of organic azides and aromatic alkynes. *Dalton Trans.* **2009**, 3, 550–556. b) Hillhouse, G. L.; Goeden, G. V.; Haymore, B. L. Stabilization of RN:NN:PR_3. Preparation and structural characterization of stable tetraarylphosphazide complexes containing molybdenum and tungsten. *Inorg. Chem.* **1982**, *21*, 2064–2071. c) LePichon, L.; Stephan, D. W. Contrasting Formation of a (Phenylthio)phosphinimine and (Phenylthio)phosphazide. Synthesis of Metal Complexes. *Inorg. Chem.* **2001**, *40*, 3827–3829.

10. Ogawa, T.; Suzuki, T.; Hein, N. M.; Pick, F. S.; Fryzuk, M. D. Cleavage of an aryl carbon–nitrogen bond of a phosphazido iron(II) complex promoted by hydride metathesis. *Dalton Trans.* **2015**, *44*, 54–57.

11. Dickie, T. K. K. MacNeil, C. S.; Hayes, P. G. Consecutive N_2 loss from a uranium diphosphazide complex. *Dalton Trans*. **2020**, *49*, 578–582.

12. Behrle, A. C.; Walensky, J. R. Actinides: Organometallic Chemistry. In *Encyclopedia of Inorganic and Bioinorganic Chemistry*; Scott, R. A., Ed.; John Wiley & Sons, Ltd: Chichester, UK, 2014; pp 1–41.

13. Du, J.; King, D. M.; Chatelain, L.; Lu, E.; Tuna, F.; McInnes, E. J. L.; Wooles, A. J.; Maron, L.; Liddle, S. T. Thorium- and uranium-azide reductions: a transient dithorium-nitride versus isolable diuranium-nitrides. *Chem. Sci.* **2019**, *10*, 3738–3745.

14. Gregson, M.; Lu, E.; Mills, D. P.; Tuna, F.; McInnes, E. J. K.; Hennig, C.; Scheinost, A. C.; McMaster, J.; Lewis, W.; Blake, A. J.; Kerridge, A.; Liddle, S. T. The inverse-trans-influence in tetravalent lanthanide and actinide bis(carbene) complexes. *Nat. Commun.* **2016**, *8*, 14137–14147.

15. Cruz, C. A.; Emslie, D. J. H.; Robertson, C. M.; Harrington, L. E.; Jenkins, H. A.; Britten, J. F. Cationic Thorium Alkyl Complexes of Rigid NON- and NNN-Donor Ligands: Arene Coordination as a Persistent Structural Motif. *Organometallics* **2009**, *28*, 1891–1899.

16. Jantunen, K. C.; Haftbaradaran, F.; Katz, M. J.; Batchelor, R. J.; Schatte, G.; Leznoff, D. B. Synthesis and structure of diamido ether uranium(IV) and thorium(IV) halide "ate" complexes and their conversion to salt-free bis-alkyl complexes. *Dalton Trans.* **2005**, 3083–3091.

17. Mintz, E. A.; Moloy, K. G.; Marks, T. J.; Day, V. W. Actinide tris(hydrocarbyls). Synthesis, properties, structure, and molecular dynamics of thorium and uranium pentamethylcyclopentadienyltris (eta n-benzyls). *J. Am. Chem. Soc.* **1982**, *104*, 4692–4695.

18. Chen, R.; Qin, G.; Li, S.; Edwards, A. J.; Piltz, R. O.; Del Rosal, I.; Maron, L.; Cui, D.; Cheng, J. Molecular Thorium Trihydrido Clusters Stabilized by Cyclopentadienyl Ligands. *Angew. Chem. Int. Ed.* **2020**, *59*, 11250–11255.

19. Qin, G; Cheng, J. Thorium(IV) trialkyl complexes of non-carbocyclic ligands as highly active isoprene polymerisation catalysts. *Dalton Trans.* **2019**, *48*, 11706–11714.

20. Casellato, U.; Sitran, S.; Tamburini, S.; Vigato, P. A.; Graziani, R. Lanthanide and actinide complexes with bidentate ligands. Crystal structure of

dimethylformamidetetrakis(1-oxo-2-thiopyridinato) thorium(IV). *Inorg. Chim. Acta* **1984**, *94*, 69–70.

21. Monreal, M. J.; Wright, R. J.; Morris, D. E.; Scott, B. L.; Golden, J. T.; Power, P. P.; Kiplinger, J. L. Thorium(IV) and Uranium(IV) Halide Complexes Supported by Bulky β-Diketiminate Ligands. *Organometallics* **2013**, *32*, 1423–1434.

22. Karmel, I. S. R.; Elkin, T.; Fridman, N.; Eisen, M. S. Dimethylsilyl bis(amidinate)actinide complexes: synthesis and reactivity towards oxygen containing substrates. *Dalton Trans.* **2014**, *43*, 11376–11387.

23. Camp, C.; Settineri, N.; Lefèvre, J.; Jupp, A. R.; Goicoechea, J. M; Maron, L.; Arnold, J. Uranium and thorium complexes of the phosphaethynolate ion. *Chem. Sci.* **2015**, *6*, 6379–6384.

24. Garner, M. E.; Hohloch, S.; Maron, L.; Arnold, J. A New Supporting Ligand in Actinide Chemistry Leads to Reactive Bis(NHC)borate Supported Thorium Complexes. *Organometallics* **2016**, *35*, 2915–2922.

25. MacNeil, C. S.; Glynn, K. E.; Hayes, P. G. Facile Activation and Deoxygenative Metathesis of CO. *Organometallics* **2018**, *37*, 3248–3252.

26. Shannon, R. D. Revised effective ionic radii and systematic studies of interatomic distances in halides and chalcogenides. *Acta Cryst.* **1976**, *A32*, 751–767.

27. a) Fagan, P. J.; Manriquez, J. M.; Maatta, E. A.; Seyam, A. M.; Marks, T. J. Synthesis and properties of bis(pentamethylcyclopentadienyl) actinide hydrocarbyls and hydrides. A new class of highly reactive *f*-element organometallic compounds. *J. Am. Chem. Soc*. **1981**, *103*, 6650–6667. b) Bruno, J.W.; Marks, T.J.; Day, V.W. Actinide-centered cyclometalation chemistry. An unusually distorted thorium bishydrocarbyl: $Thp[\eta^5\text{-}(CH_3)_5C_5]_2CH_2Si(CH_3)_3]_2$. *J. Organomet. Chem.* **1983**, *250*, 237–246. c) Fendrick, C. M.; Mintz, E. A.; Schertz, L. D.; Marks, T. J. Manipulation of organoactinide coordinative unsaturation and stereochemistry. Properties of chelating bis(polymethylcyclopentadienyl) hydrocarbyls and hydrides. *Organometallics* **1984**, *3*, 819–821. d) Butcher, R. J.; Clark, D. L.; Grumbine, S. K.; Scott, B. L.; Watkin, J. G. Mono(pentamethylcyclopentadienyl)thorium Chemistry: Synthesis, Structural Characterization, and Reactivity of Aryloxide and Alkyl Derivatives. *Organometallics* **1996**, *15*, 1488–1496. e) Clark, D. L.; Grumbine, S. K.; Scott, B. L.; Watkin, J. G. Sterically Demanding Aryloxides as Supporting Ligands in Organoactinide Chemistry. Synthesis, Structural Characterization, and Reactivity of $Th(O\text{-}2,6\text{-}t\text{-}Bu_2C_6H_3)_2(CH_2SiMe_3)_2$ and Formation of the Trimeric Thorium Hydride $Th_3H_6(O\text{-}2,6\text{-}t\text{-}Bu_2C_6H_3)_6$ *Organometallics* **1996**, *15,* 949–957. f) Jantunen, K. C.; Batchelor, R. J.; Leznoff, D. B. Synthesis, Characterization, and Organometallic Derivatives of Diamidosilyl Ether Thorium(IV) and Uranium(IV) Halide Complexes. *Organometallics* **2004**, *23*, 2186–2193. g) Cruz, C. A.; Emslie, D. J. H.; Harrington, L. E.; Britten, J. F.; Robertson, C. M. Extremely Stable Thorium(IV) Dialkyl Complexes Supported by Rigid Tridentate 4,5-Bis(anilido)xanthene and 2,6-Bis(anilidomethyl)pyridine Ligands. *Organometallics* **2007**, *26*, 692–701. h) Hayes, C. E.; Platel, R. H.; Schafer, L. L.; Leznoff, D. B. Diamido-Ether Actinide Complexes as Catalysts for the Intramolecular Hydroamination of Aminoalkenes. *Organometallics* **2012**, *31*, 6732–6740. i) Hayes, C. E.; Sarazin, Y.; Katz, M. J.;

Carpentier, J.-F.; Leznoff, D. B. Diamido-Ether Actinide Complexes as Initiators for Lactide Ring-Opening Polymerization. *Organometallics* **2013**, *32*, 1183–1192. j) Mora, E.; Maria, L.; Biswas, B.; Camp, C.; Santos, I. C.; Pecaut, J.; Cruz, A.; Carretas, J. M.; Marcalo, J.; Mazzanti, M. Diamine Bis(phenolate) as Supporting Ligands in Organoactinide(IV) Chemistry. Synthesis, Structural Characterization, and Reactivity of Stable Dialkyl Derivatives. *Organometallics* **2013**, *32*, 1409–1422. k) Settineri, N. S.; Garner, M. E.; Arnold, J. A Thorium Chalcogenolate Series Generated by Atom Insertion into Thorium-Carbon Bonds. *J. Am. Chem. Soc.* **2017**, *139*, 6261–6269. l) Suvova, M.; O'Brien, K. T. P.; Farnaby, J. H.; Love, J. B.; Kaltsoyannis, N.; Arnold, P. L. Thorium(IV) and Uranium(IV) *trans*-Calix[2]benzene[2]pyrrolide Alkyl and Alkynyl Complexes: Synthesis, Reactivity, and Electronic Structure. *Organometallics* **2017**, *36*, 4669–4681. m) Hohloch, S.; Garner, M. E.; Parker, B. F.; Arnold, J. New supporting ligands in actinide chemistry: tetramethyltetraazaannulene complexes with thorium and uranium. *Dalton Trans.* **2017**, *46*, 13768–13782. n) Andreychuk, N. R.; Dickie, T.; Emslie, D. J. H.; Jenkins, H. A. Thorium(IV) alkyl and allyl complexes of a rigid NON-donor pincer ligand with flanking 1-adamantyl substituents. *Dalton Trans.* **2018**, *47*, 4866–4876. o) Settineri, N. S.; Shiaua, A. A.; Arnold, J. Dioxygen reacts with metal–carbon bonds in thorium dialkyls to produce bis(alkoxides). *Dalton Trans.* **2019**, *48*, 5569–5573.

28. MacNeil, C. S.; Dickie, T. K. K.; Hayes, P. G. Actinide Pincer Chemistry: A New Frontier. In *Pincer Compounds* 1st edition; Morales Morales, D. Eds.; Elsevier: Amsterdam, 2018; Vol. 1, pp 133–172.

29. Knott, J. P.; Hayes, P. G. University of Lethbridge, Lethbridge, Canada. Unpublished work, 2019.

30. a) Johnson, K. R. D.; Kamenz, B. L.; Hayes, P. G. Ligand influence on intramolecular cyclometalation in bis(phosphinimine) rare earth alkyl complexes. *Can. J. Chem.* **2016**, *94*, 330–341. b) Zamora, M. T.; Johnson, K. R.; Hänninen, M. M.; Hayes, P. G. Differences in the cyclometalation reactivity of bisphosphinimine-supported organo-rare earth complexes. *Dalton Trans.* **2014**, *43*, 10739–10750.

31. Burger, B. J.; Bercaw, J. E. *Experimental Organometallic Chemistry*; American Chemical Society: Washington, D.C., 1987.

32. Marvich, R. H.; Brintzinger, H. H. A Metastable Form of Titanocene. Formation from a Hydride Complex and Reactions with Hydrogen, Nitrogen, and Carbon Monoxide. *J. Am. Chem. Soc.* **1971**, *93*, 2046–2048.

33. Pangborn, A. B.; Giardello, M. A.; Grubbs, R. H.; Rosen, R. K.; Timmers, F. J. Safe and Convenient Procedure for Solvent Purification. *Organometallics* **1996**, *15*, 1518–1520.

34. Dolomanov, O. V.; Bourhis, L. J.; Gildea, R. J.; Howard, J. A. K.; Puschmann, H. *OLEX2*: a complete structure solution, refinement and analysis program. *J. Appl. Crystallogr.* **2009**, *42*, 339–341.

35. Sheldrick, G. M. *SHELXT* – Integrated space-group and crystal-structure determination. *Acta Crystallogr. Sect. A* **2015**, *71*, 3–8.

36. Sheldrick, G. M. Crystal structure refinement with *SHELXL*. *Acta Crystallogr. Sect. C* **2015**, *71*, 3–8.

4. Thorium(IV) Diphosphazide Complexes: CO_2 Insertion Into Th–C and Th–N Bonds[i,j]

4.1. Abstract

A thorium(IV) trialkyl complex, $L_{PN3}Th(CH_2SiMe_3)_3$ (L_{PN3} = κ^5-2,5-[(4-^{i}PrC$_6$H$_4$)N$_3$=P^{i}Pr$_2$]$_2$N(C$_4$H$_2$)$^-$), readily inserts carbon dioxide into the three Th–C bonds to afford $L_{PN3}Th(\kappa^2$-$O_2CCH_2SiMe_3)_3$ (**4-1**). A new thorium triamido complex, $L_{PN3}Th(NHAd)_3$ (**4-2**) was synthesized and inserts CO_2 into the Th–N bonds to form the tricarbamate species $L_{PN3}Th(\kappa^2$-$O_2CNHAd)_3$ (**4-3**). *In situ* heating experiments revealed that the supporting diphosphazide ligands in complexes **4-1** and **4-3** liberate two equivalents of N_2 to form the corresponding diphosphinimine-supported complexes $L_{P=N}Th(\kappa^2$-$O_2CCH_2SiMe_3)_3$ (**4-4**, $L_{P=N}$ = κ^3-2,5-[(4-^{i}PrC$_6$H$_4$)N=P^{i}Pr$_2$]$_2$N(C$_4$H$_2$)$^-$) and $L_{P=N}Th(\kappa^2$-$O_2CNHAd)_3$ (**4-5**), respectively. Conversely, only one unit of N_2 was released from **4-2**, affording the asymmetric phosphazide/phosphinimine $L_{P=N/PN3}Th(NHAd)_3$ (**4-6**, $L_{P=N/PN3}$ = κ^3-2-[(4-^{i}PrC$_6$H$_4$)N=P^{i}Pr$_2$]-5-[(4-^{i}PrC$_6$H$_4$)N$_3$=P^{i}Pr$_2$]N(C$_4$H$_2$)$^-$). Addition of three equivalents of either $ClSiMe_3$ or LiI to complex **4-1** generated $L_{PN3}ThX_3$ (X = Cl, I) and the carboxylate by-products $Me_3SiO_2CCH_2SiMe_3$ and $LiO_2CCHSiMe_3$, respectively. Addition of $LiCH_2SiMe_3$ completed the stepwise synthetic cycle of thorium-mediated CO_2 functionalization.

---

[i] *Organometallics* reference style used throughout this chapter

[j] Reprinted with permission from Dickie, T. K. K.; Hayes, P. G. Thorium(IV) Diphosphazide Complexes: CO_2 Insertion Into Th–C and Th–N Bonds. *Organometallics* **2022**, *41*, 278–283.

4.2. Introduction

Actinides have many properties that provide unique reactivity among the periodic table, including large ionic radii, high coordination numbers and involvement of *f*-orbitals in bonding. These properties have inspired the quest for new actinide-mediated stoichiometric and catalytic reactions.[1] While small molecule actinide chemistry is not as well developed as that of the transition metals, the field is growing rapidly, especially with respect to the activation of carbon oxygenates (CO and CO_2).[2]

When exposed to CO_2, An(III) (An = Th and U) complexes can facilitate reductive coupling to form valuable C–C bond-containing products, such as oxalates.[3-6] While An(III) allows for intriguing small molecule reactivity,[7-9] strong reducing agents, such as KC_8, are generally required for An(III) generation, and the desired reactivity may arrest upon metal oxidation, which tends to be highly facile. Conversely, An(IV) compounds primarily undergo CO_2 insertion into An–E bonds to produce carboxylates (E = C)[10,11] and carbamates (E = N).[12] A recent example of CO_2 insertion into hard-soft mismatched An–P bonds was reported by Walensky and co-workers.[13] While stoichiometric functionalizations of CO_2 by Th and U species have been reported,[14-17] to our knowledge, catalytic conversion of CO_2 using an actinide complex has not yet been achieved.

The few reported examples of organoactinide mediated CO_2 transformation have been achieved by utilizing $XSiMe_3$ (X = Cl, I) to regenerate an An–X bond, along with concomitant formation of a silyl ester. The synthetic cycle can then be completed using a salt metathesis reaction to install an alkyl group at the metal centre.[16,17] Recently, the Meyer group reported the anionic U(IV) oxo complex $[(2,6\text{-}Ad_2\text{-}4\text{-}Me\text{-}C_6H_2O)_3U(O)]^-$ (Ad = 1-adamantyl) which inserts CO_2 into U–O bonds to form carbonates.[16] The corresponding carbonates can be removed upon reaction with $ISiMe_3$. Reduction to U(III) using KC_8,

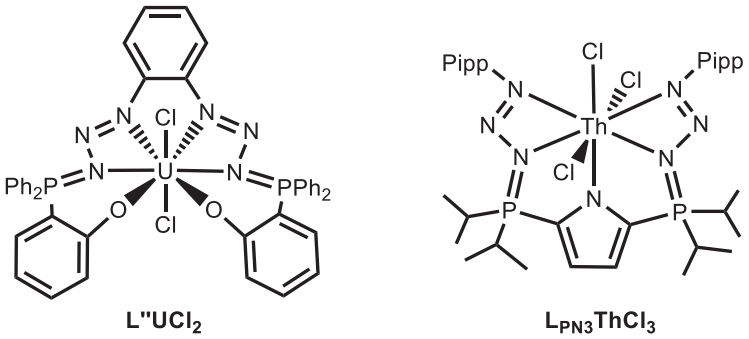

Figure 4.1. Ligand systems that support actinide-stabilized phosphazides.

subsequent oxidation to U(V) with N_2O, and a final KC_8 reduction back to the anionic U(IV) complex are required to complete the synthetic cycle. Additionally, Mazzanti and co-workers observed the formation of $[Th_2Cl(^{tBu}L_{salan})_2(\mu\text{-}\eta^1\text{:}\eta^1\text{-}O_2CCH_2SiMe_3)_2(\mu\text{-}\eta^1\text{:}\eta^2\text{-}O_2CCH_2SiMe_3)]$ ($^{tBu}L_{salan}$ = N,N′-bis(2-hydroxybenzyl-3,5-di-tert-butyl)-1,2-dimethylaminomethane) from the dicarboxylate dimer in the presence of trace amounts of LiCl, cementing the theory that the driving force for removal of the carboxylate group from the metal centre is the resultant Th−halide bond.[17]

We previously reported actinide complexes supported by two ligand systems that contain the unusual phosphazide ($R_3P{=}N{-}N{=}N{-}R$) functionality (Figure 4.1). The 'phosphazidosalen' U(IV) diphosphazide complex $L_{PN3salen}UCl_2$ ($L_{PN3salen}$ = κ^6–1,2-$[N_3{=}PPh_2(2\text{-}O\text{-}C_6H_4)]_2C_6H_4$) features the first example of an actinide-stabilized phosphazide.[18] The monoanionic, pyrrole-based diphosphazide scaffold made it possible to isolate a rare trialkyl thorium complex, $L_{PN3}Th(CH_2SiMe_3)_3$ (L_{PN3} = κ^5-2,5-$[(4\text{-}^i PrC_6H_4)N_3{=}P^i Pr_2]_2N(C_4H_2)^-$).[19] Notably, only a handful of other trialkyl thorium species are known,[20-22] several of which are active isoprene polymerization catalysts when combined with $[Ph_3C][B(C_6F_5)_4]$.[20] A trialkyl complex such as $L_{PN3}Th(CH_2SiMe_3)_3$ could potentially demonstrate high catalytic functionalization of CO_2 because it has three sites where insertion can occur. Herein we describe the reactivity of

$L_{PN3}Th(CH_2SiMe_3)_3$ towards CO_2, as well as the related reaction chemistry of the new triamide complex $L_{PN3}Th(NHAd)_3$ (**4-2**).

4.3. CO_2 Insertion into Th–C and Th–N Bonds

A solution of the trialkyl complex $L_{PN3}Th(CH_2SiMe_3)_3$ in benzene-d_6, when placed under an atmosphere of CO_2, rapidly turns from bright orange to pale-yellow upon vigorous mixing for a period of 5 minutes (Scheme 4.1). The $^{31}P\{^1H\}$ NMR spectrum exhibits a change from a single resonance at δ 59.4 to two peaks at δ 54.7 and δ 55.4. The signal at δ 55.4 subsequently converts slowly to δ 54.7, and after 24 hours, the pale yellow colour gives way to a colourless solution with only the peak at δ 54.7 remaining. The identity of $L_{PN3}Th(\kappa^2\text{-}O_2CCH_2SiMe_3)_3$ (**4-1**), the product of CO_2 insertion into all three Th–C bonds, is supported by ^1H and $^{13}C\{^1H\}$ NMR data. Complete supplantation of the broad Th–CH_2SiMe_3 resonance at δ 0.15 in the ^1H NMR spectrum by a sharp signal at δ 1.77 integrating as 6H is consistent with three chemically equivalent Th–$O_2CCH_2SiMe_3$ groups. Furthermore, a peak in the $^{13}C\{^1H\}$ NMR spectrum at δ 188.3 indicates the presence of a new carbonyl functionality. The complex giving rise to the $^{31}P\{^1H\}$ NMR chemical shift of δ 55.4 is proposed to be the intermediate $L_{PN3}Th(CH_2SiMe_3)(\kappa^2\text{-}O_2CCH_2SiMe_3)_2$, the product of only two CO_2 insertions.

Colourless X-ray quality crystals of complex **4-1** (Figure 4.2, left) were grown from a concentrated pentane solution at –35 °C. Notably, the structure appears to be an average of two different coordination isomers in the lattice, with one of the phosphazide groups

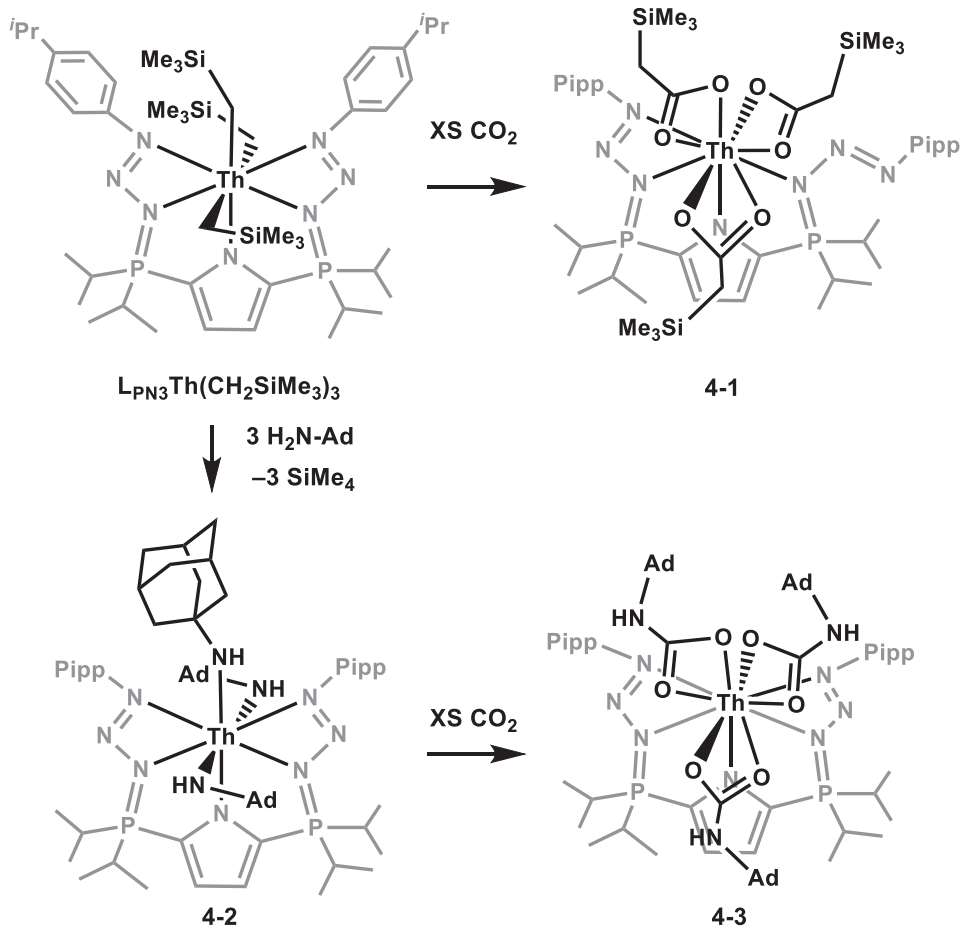

Scheme 4.1. Synthesis of complexes **4-1**, **4-2** and **4-3**.

positionally disordered. One isomer contains both phosphazide groups coordinated to thorium in a κ^2 fashion, and the other has one phosphazide bound only by the α-nitrogen, resulting in an unusual *cis*-phosphazide. The κ^1-*cis* coordination mode is the major component in the structure and refines to an occupancy ratio of 71.9/28.1, suggesting a possible Z' = 4 with one *trans*-component to every three *cis*-molecules. *Cis*-coordinated phosphazides are far less common than their *trans*-counterparts.[23] In fact, this is the first example of a structurally characterized *cis*-phosphazide within this ligand framework—it features alternating N–N distances consistent with single and double bond character (N4–N5 = 1.365(18) Å, N5–N6 = 1.298(18) Å). In addition, the three $O_2CCH_2SiMe_3$ moieties are bound to thorium *via* a κ^2 interaction involving both oxygen atoms (Th–O_{ave} = 2.50 Å).

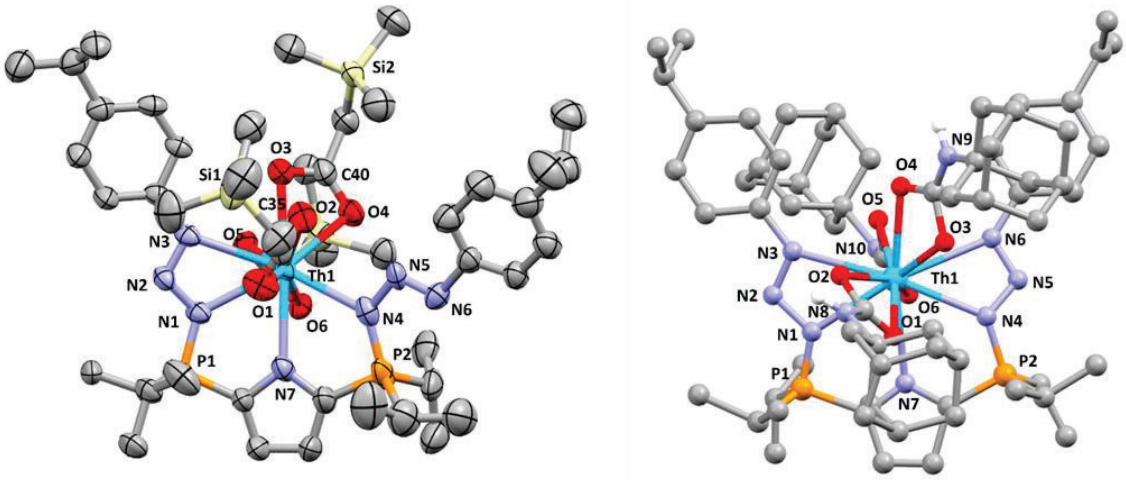

Figure 4.2. Left: X-ray crystal structure of complex **4-1** with thermal ellipsoids drawn at 30% probability. Hydrogens have been removed for clarity. Only the major component of the disorder model is shown. Selected bond distances (Å) and angles (°): P1–N1 = 1.627(9), N1–N2 = 1.344(12), N2–N3 = 1.296(12), N7–Th1 = 2.652(10), Th1–N3 = 2.728(10), P2–N4 = 1.687(12), N4–N5 = 1.365(18), N4–N5B = 1.29(4), N5–N6 = 1.298(18), N5B–N6B = 1.26(7), Th1–O2 = 2.469(10), Th1–O1 = 2.445(10), Th1–O3 = 2.582(10), Th1–O4 = 2.518(8), O5–Th1 = 2.512(9), Th1–O6 = 2.504(7), C45–O6 = 1.273(13), C45–O5 = 1.238(13), O3–C40 = 1.239(16), C40–O4 = 1.294(17), C35–O2 = 1.277(19), C35–O1 = 1.202(18), N1–N2–N3 = 106.8(8), N4–N5–N6 = 105.9(13), O1–C35–O2 = 116.9(14), O3–C40–O4 = 123.3(14), O5–C45–O6 = 121.8(11), N7–Th1–O3 = 171.2(3). Right: Connectivity structure of complex **4-3**. Non-NH hydrogen atoms have been omitted for clarity.

As expected, delocalized C–O bonding is observed, giving rise to an average length of 1.25 Å.

Unlike the solid-state, in benzene-d_6 solution complex **4-1** exhibits C_{2v} symmetry on the NMR timescale (*vide supra*). Hence, the two different phosphazide coordination modes observed by X-ray crystallography are either a solid-state phenomenon or are rapidly exchanging at ambient temperature in solution. Although the κ^1-bonding mode may not dominate in solution, it is important to recognize that the system possesses coordinative isomerism which could prove valuable for accessing reactive intermediates.

Since Th–N bonds are prone to CO_2 insertion in the same manner as thorium alkyls, a thorium triamido complex was targeted for comparison purposes. When

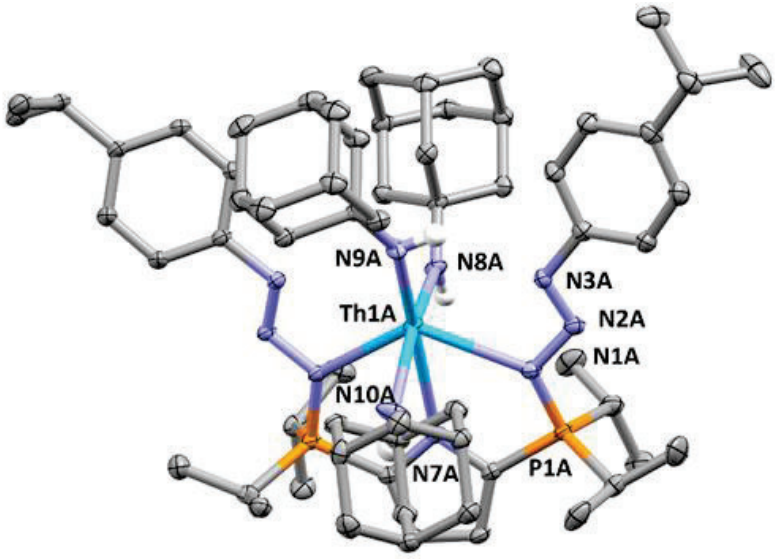

Figure 4.3. X-ray crystal structure of complex **4-2** with thermal ellipsoids drawn at 30% probability. Non-NH hydrogens have been removed for clarity. Only the major component of the disorder model is shown. Only one of the two independent molecules in the asymmetric unit is depicted. Selected bond distances (Å) and angles (°): N1A–P1A = 1.642(3), N1A–N2A = 1.354(4), N2A–N3A = 1.268(4), P2A–N4A = 1.646(3), N4A–N5A = 1.352(4), N5A–N6A = 1.270(4), Th1A–N7A = 2.770(3), Th1A–N8A = 2.332(3), Th1A–N9A = 2.289(3), Th1A–N10A = 2.327(4), N1A–Th1A = 2.596(3), Th1A–N3A = 2.944(3), Th1A–N4A = 2.583(3), Th1A–N6A = 3.080(3), N1A–N2A–N3A = 108.8(3), N4A–N5A–N6A = 110.1(3), Th1A–N8A–C35A = 143.5(2), Th1A–N9A–C45A = 152.7(3), Th1A–N10A–C55A = 148.0(3), N9A–Th1A–N7A = 168.6(1), N10A–Th1A–N8A = 160.1(1).

$L_{PN3}Th(CH_2SiMe_3)_3$ was mixed with three equivalents of 1-adamantylamine in toluene, the orange solution immediately turned bright yellow. Upon washing the residue with pentane, small crystalline yellow needles were obtained. The ^{1}H NMR spectrum of the crystals in benzene-d_6 revealed multiple broad adamantyl signals between δ 1.50 and δ 2.50. Additionally, two broad N–H peaks at δ 3.58 and δ 2.87, integrating to 1H and 2H respectively, suggested the presence of 3 NH–adamantyl groups, two of which are equivalent on the NMR timescale. A lone singlet was observed in the $^{31}P\{^1H\}$ spectrum at δ 53.0.

X-ray diffraction experiments confirmed the identity of $L_{PN3}Th(NHAd)_3$ (**4-2**) indicated spectroscopically (Figure 4.3). Notably, both phosphazides are in the *trans*-

orientation, unlike that observed in complex **4-1**. Furthermore, the phosphazide γ-nitrogens reside quite far from the thorium centre (Th1A–N3A = 2.944(3) Å, Th1A–N6A = 3.080(3) Å c.f. Th1–N3 = 2.73(1) Å in complex **4-1**), and accordingly, the nature of the Th–N_γ interaction, if significant, is unclear. The N–N–N angles (N1A–N2A–N3A = 108.8(3)°, N4A–N5A–N6A = 110.1(3)°) within the *trans*-phosphazide moieties are comparable to those in both complex **4-1**, (N1–N2–N3 = 106.8(8)°) and $L_{PN3}Th(CH_2SiMe_3)_3$ (N2−N3−N4 = 108.9(3)°).[19] The Th–$N_{adamantyl}$ distances range from 2.289(3) Å to 2.332(3) Å.

Upon addition of an atmosphere of CO_2 to a solution of bright yellow **4-2**, the colour lightened immediately, implying the formation of $L_{PN3}Th(\kappa^2\text{-}O_2CNHAd)_3$ (**4-3**). A change in the $^{31}P\{^1H\}$ NMR spectrum (benzene-d_6) from δ 53.0 to δ 54.4 was observed. The broad ^1H NMR NH signals in **4-2** (δ 3.58 and δ 2.87) collapsed into a single sharp peak at δ 3.99 that integrates to 3H. Additionally, the number of adamantyl environments was reduced from five in **4-2** to three in complex **4-3**.

A low-quality connectivity X-ray structure of tricarbamate **4-3** revealed an exceedingly rare 11-coordinate thorium(IV) centre,[24] with three κ^2-bound O_2CNHAd ligands (Figure 4.2, right). In contrast to complex **4-1**, both phosphazide groups are clearly coordinated to thorium *via* the α- and γ-nitrogen atoms. While thorium can access coordination numbers as high as 15, the most common for thorium(IV) is 8[24,25] and the vast majority of complexes that feature coordination numbers in excess of 10 are comprised of very small ligands, such as nitrates and oxides.[24] The geometry about thorium is best described as a distorted edge-coalesced icosahedron, with N1, N4, O1 and O6 forming the 4 vertices of the square plane, O2, N6, N3, O5, and O3 comprising the pentagonal plane and O4 and N7 serving as capping atoms.

4.4. N_2 Loss from Phosphazide Ligands

Phosphazide groups stabilized by metal-coordination, H-bonding and sterically demanding groups are often heat sensitive and will decompose with the loss of N_2 gas, forming the corresponding phosphinimine (P=N). For example, the previously reported phosphazidosalen ligand releases N_2 from the two ligand phosphazides. Specifically, $L_{PN3salen}UCl_2$ readily loses one equivalent of N_2 at ambient temperature, but loss of the second N_2, to form the diphosphinimine complex $L_{P=NSalen}UCl_2$ ($L_{P=NSalen}$ = κ^4-1,2-[N=PPh$_2$(2-O-C$_6$H$_4$)]$_2$C$_6$H$_4$), requires extensive heating at 155 °C.[18] The related pyrrole-based diphosphazide-supported complex $L_{PN3}Th(CH_2SiMe_3)_3$ decomposes into an intractable mixture after heating at 55 °C in hydrocarbon solvents for 24 hours.[19] This decomposition is likely due to the highly reactive Th–C bonds, as well as the potential for cyclometallation of a *para*-isopropylphenyl (Pipp) C–H.

When a solution of **4-1** in benzene-d_6 was heated at 65 °C, a new dominant peak appeared in the $^{31}P\{^1H\}$ NMR spectrum at δ 48.7. In addition, signals at δ 57.0 and δ 48.3, due to low concentration intermediates, were also observed. After heating for 4 days, full conversion to $L_{P=N}Th(\kappa^2\text{-}O_2CCH_2SiMe_3)_3$ (**4-4**), the expected product of sequential loss of two molecules of N_2, was complete (Scheme 4.2). The resonances in the ^1H NMR spectrum attributed to complex **4-4** are shifted upfield from those in **4-1**, and the methylene peak is substantially broadened. Furthermore, the *ortho*-CH Pipp protons appear as a doublet of doublets ($^3J_{HH}$ = 8.4 Hz, $^4J_{HP}$ = 2.1 Hz), as the six bond separation between these atoms and the phosphazide phosphorus in **4-1** has been reduced to four.

Notably, complex **4-4** is inaccessible from the addition of CO_2 to a diphosphinimine complex. As previously established, the diphosphinimine trialkyl $L_{P=N}Th(CH_2SiMe_3)_3$ cannot be isolated as it rapidly undergoes cyclometallative decomposition to afford

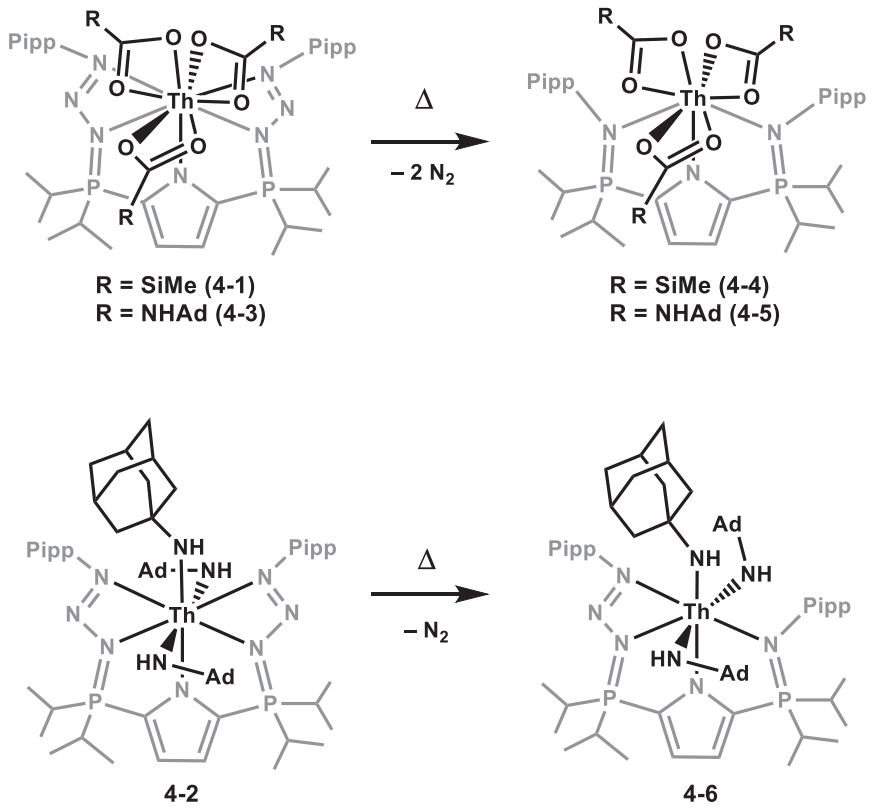

Scheme 4.2. Synthesis of complexes **4-4**, **4-5** and **4-6**.

$L_{P=N}$*Th(CH_2SiMe_3)$_2$ ($L_{P=N}$* = κ^4-2-[(4-^{i}PrC_6H_3)N=P^{i}Pr$_2$]-5-[(4-^{i}PrC_6H_4)N=P^{i}Pr$_2$]N(C_4H_2)$^{2-}$).[19] When the cyclometallated dialkyl complex $L_{P=N}$*Th(CH_2SiMe_3)$_2$ was exposed to an atmosphere of CO_2 in benzene-d_6 solution, immediate decomposition into an intractable mixture occurred. Intriguingly, cyclometallation of the diphosphinimine ligand in complex **4-4** appears to be wholly disfavoured, presumably because such a process would generate the acid $HO_2CCH_2SiMe_3$. Heating complex **4-3** in the same manner as that described above produces the diphosphinimine complex $L_{P=N}$Th(κ^2-O_2CNHAd)$_3$ (**4-5**), which exhibits a $^{31}P\{^1H\}$ NMR resonance at δ 47.2 (Figure 4.4). Prior to complete conversion to complex **4-5**, signals attributed to an asymmetric intermediate were observed at δ 56.3 and δ 47.3. As in complex

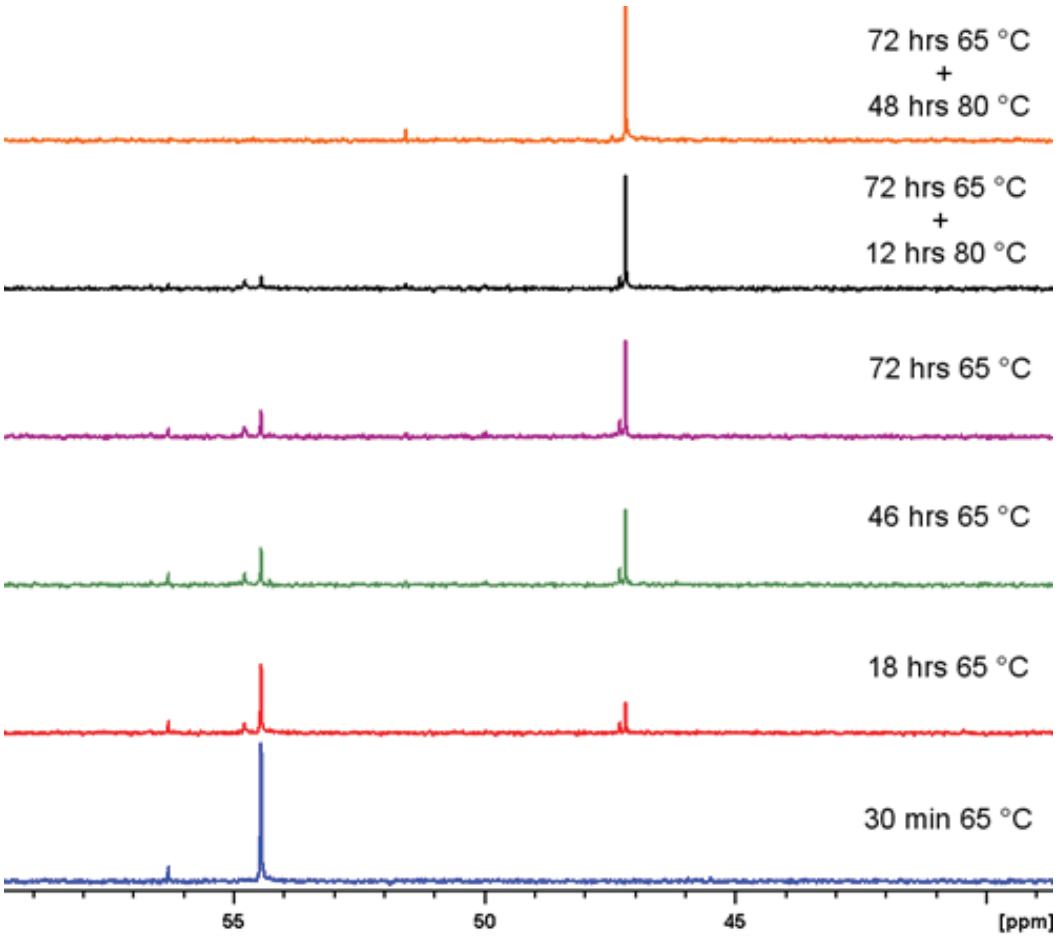

Figure 4.4. Stacked $^{31}P\{^{1}H\}$ NMR spectra of a sample of complex **4-3** in benzene-d_6 heated in a J. Young NMR tube.

4-4, $^{4}J_{HP}$ coupling between the *ortho*-CH Pipp protons and the phosphinimine phosphorus atom was observed ($^{3}J_{HH}$ = 8.4 Hz, $^{4}J_{HP}$ = 2.0 Hz). Unfortunately, exhaustive attempts to isolate pure samples of complexes **4-4** and **4-5** were unsuccessful. Nonetheless, *in situ* NMR experiments unambiguously established liberation of N_2 gas afforded the expected phosphinimine-containing products.

Surprisingly, heating triamide **4-2** at 65 °C in benzene-d_6 for 72 hours permitted isolation of the asymmetric phosphazide/phosphinimine complex $L_{P=N/PN3}Th(NHAd)_3$ (**4-6**, $L_{P=N/PN3}$ = κ^3-2-[(4-^{i}PrC$_6$H$_4$)N=P^{i}Pr$_2$]-5-[(4-^{i}PrC$_6$H$_4$)N$_3$=P^{i}Pr$_2$]N(C$_4$H$_2$)$^{-}$). The $^{31}P\{^{1}H\}$ NMR spectrum of complex **4-6** contains two resonances of equal intensity at δ 49.7 and δ

46.1 ($^4J_{PP}$ = 2.1 Hz). The number of ^{1}H environments has doubled relative to the triamide starting material, and the Pipp group bound to the phosphinimine nitrogen exhibits the familiar doublet of doublets common to complexes **4-4** and **4-5** ($^3J_{HH}$ = 8.3 Hz, $^4J_{HP}$ = 2.1 Hz). As in the ^{1}H NMR spectrum of **4-2**, one of the NH–adamantyl groups is distinct; two sharp NH signals integrate in a 1:2 ratio. It is not known why this asymmetric species is stable in solution at 65 °C while the intermediates *en route* to complexes **4-4** and **4-5** are not. Presumably the difference in stability is due to steric protection exerted by the bulky adamantyl groups which raise the energy barrier for accessing the γ-nitrogen dechelated intermediate necessary for isomerization to the *cis*-phosphazide, and ultimately, loss of N_2. X-ray diffraction experiments on complex **4-6** revealed a 7-coordinate distorted pentagonal bipyramidal thorium centre (Figure 4.5). The intact *cis*-phosphazide is coordinated through both α- and γ-nitrogen atoms. The phosphinimine and pyrrole nitrogens, as well as one of the NH–Ad groups (N7), comprise the pentagonal plane. The N6–Th–N8 angle is nearly linear (171.3(3)°) and the N7 adamantyl group is positionally disordered across two sites. The three Th–N amide distances (Th1–N6 = 2.337(6), Th1–N7B = 2.29(3), Th1–N8 = 2.338(7) Å) are similar to those found in complex **4-2**. The phosphinimine P1=N1 length of 1.610(9) Å is comparable to the coordinated phosphinimine in $L_{P=N}$*Th(CH_2SiMe_3)$_2$ (1.601(3) Å) and slightly shorter than that in $L_{P=N}ThCl_3$ (1.634(4) Å).[19]

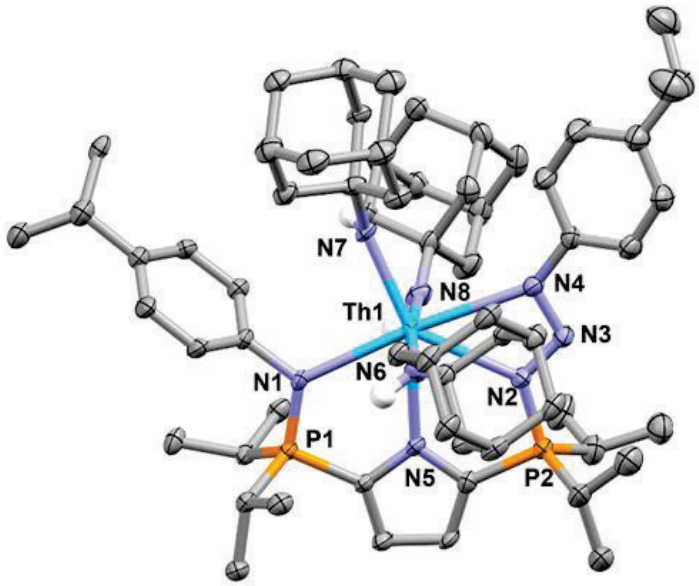

Figure 4.5. X-ray crystal structure of **4-6** with thermal ellipsoids drawn at 30% probability. Non-NH hydrogens have been removed for clarity. Only the major component of the disorder model is shown. Selected bond distances (Å) and angles (°): P1–N1 = 1.610(9), P2–N2 = 1.64(1), N5–Th1 = 2.633(9), Th1–N6 = 2.337(6), Th1–N7B = 2.29(3), Th1–N8 = 2.338(7), Th1–N4 = 2.775(7), Th1–N2 = 2.59(1), Th1–N6–C33 = 152.7(6), Th1–N7B–C43B = 142(2), Th1–N8–C53 = 148.5(7), N2–N3–N4 = 108.0(8), N1–Th1–N4 = 174.6(2), N8–Th1–N6 = 171.3(3).

4.5. Reaction Chemistry of Complex 1

Preliminary experiments indicate that combination of **4-1** with excess H_2, $HSiEt_3$, $ZnMe_2$ or $B[N(SiMe_3)_2]_3$ in benzene-d_6 affords no reaction at ambient temperature. Meanwhile, addition of $AlMe_3$ resulted in rapid decomposition of the thorium complex.

Reaction of $ClSiMe_3$ with **4-1** produced the previously characterized compounds $L_{PN3}ThCl_3$ and $Me_3SiOCOCH_2SiMe_3$. When combined with the stepwise addition of alkyllithium, a closed synthetic cycle that transforms CO_2 and LiR into silyl esters is possible. Unfortunately, since $ClSiMe_3$ and $LiCH_2SiMe_3$ are incompatible reagents, this cycle requires stepwise stoichometric addition for each transformation, making it impossible to complete the process catalytically.

When excess LiI was added to a solution of **4-1** in benzene-d_6 at ambient temperature, immediate yellow colouration occurred and a $^{31}P\{^1H\}$ signal at δ 57.0 dominated the spectrum. This data, as well as that obtained from ^1H NMR spectroscopy, are consistent with $L_{PN3}ThI_3$. For example, the Th-κ^2-$O_2CCH_2SiMe_3$ methylene peak disappeared, and an extremely broad resonance (δ 0.00 to 0.70) attributed to $LiO_2CCH_2SiMe_3$ was observed. The success of this reaction implies that a catalytic transformation of $LiCH_2SiMe_3$ to $LiO_2CCH_2SiMe_3$ using LiI, CO_2 and $L_{PN3}ThCH_2SiMe_3$ is possible. However, $LiCH_2SiMe_3$ reacts with CO_2 under these conditions to form $LiO_2CCH_2SiMe_3$, rendering this actinide-catalyzed CO_2 conversion impractical.

4.6. Conclusions

The monoanionic diphosphazide ligand L_{PN3} stabilizes both trialkyl and triamido thorium(IV) complexes that undergo rapid and clean insertion of CO_2 into Th–C and Th−N bonds. The resulting tricarboxylate and tricarbamate species are a result of the pentadentate diphosphazide ligand framework, as these types of complexes are not accessible using their P=N ligand counterparts. The phosphazide moieties in this unique ligand system exhibit coordinative versatility (i.e., *cis*-, *trans*-, κ^1- and κ^2-bonding modes), providing further evidence that phosphazides are underutilized functional groups in organometallic chemistry. Combination of $L_{PN3}Th(\kappa^2\text{-}O_2CCH_2SiMe_3)_3$ with $ClSiMe_3$ or LiI removes the carboxylate groups completing a synthetic CO_2 conversion cycle; however, further work is needed to achieve catalysis with an actinide complex.

4.7. Experimental Details for Chapter 4

4.7.1. Laboratory Equipment and Apparatus

An argon filled MBraun glove box was employed for manipulation and storage of all oxygen and moisture sensitive compounds. All thermally unstable compounds were stored in a –35 °C freezer within a glove box. All reactions were performed on a double manifold high vacuum line using standard techniques or in a glove box under an atmosphere of argon.[26] Commonly utilized specialty glassware included the swivel frit assembly, needle valves, and thick walled (5 mm) glass bombs equipped with Kontes Teflon stopcocks.[26] All glassware was stored in a 110 °C oven for a minimum of 12 hours, or flame-dried before immediate transfer to the glove box antechamber or assembled on the vacuum line and evacuated while hot.

4.7.2. Solvents

Toluene, pentane, and tetrahydrofuran (THF) solvents were dried and purified using the Grubbs/Dow purification system and stored in evacuated 500 mL bombs over titanocene[27] (toluene and hexanes) or sodium/benzophenone ketal (THF).[28] Diethyl ether, pentane, heptane, benzene, benzene-d_6, toluene-d_8, and THF-d_8 were dried and stored over sodium/benzophenone ketal in glass bombs under vacuum. Unless otherwise noted, solvents were introduced *via* vacuum transfer with condensation at –78 °C. Liquid nitrogen (–196 °C), liquid nitrogen/pentane (–130 °C), dry ice/acetone (–78 °C), dry ice/acetonitrile (–45 °C) and water/ice (0 °C) baths were used for cooling receiving flasks and to maintain low temperature conditions.

4.7.3. Instrumentation and Details for NMR Experiments

All NMR spectra were recorded at ambient temperature, except where noted, with a Bruker Avance II NMR spectrometer (300.13 MHz for ^{1}H, 75.47 MHz for ^{13}C and 121.48 MHz for ^{31}P) or Avance III NMR spectrometer (700.13 MHz for ^{1}H, 176.05 MHz for ^{13}C, and 283.54 MHz for ^{31}P). All ^{1}H NMR spectra were referenced to $SiMe_4$ through the residual ^{1}H resonance(s) of the employed solvent; benzene-d_6 (7.16 ppm), toluene-d_8 (2.09, 6.98, 7.02 and 7.09 ppm), chloroform-d_1 (7.26 ppm) or THF-d_8 (1.73 and 3.58 ppm). ^{13}C NMR spectra were referenced relative to $SiMe_4$ through the resonance(s) of the employed solvent; benzene-d_6 (128.0 ppm), toluene-d_8 (20.4, 125.2, 128.0, 128.9, 137.5 ppm), chloroform-d_1 (77.16 ppm) or THF-d_8 (25.4, 67.6 ppm). ^{1}H NMR data for diamagnetic compounds are reported as follows: chemical shift, multiplicity (s = singlet, d = doublet, t = triplet, q = quartet, quint = quintet, sp = septet, br = broad, m = multiplet, app = apparent, obsc = obscured, ov = overlapping), coupling constants (Hz), integration, assignment. ^{13}C NMR data for diamagnetic compounds are reported as follows: chemical shift, assignment. Assignment of resonances were supported by ^{1}H–^{1}H COSY, ^{13}C{^{1}H} APT, ^{1}H–^{13}C{^{1}H} and HSQC/HMBC experiments.

4.7.4. Additional Instrumentation

Elemental analyses (%CHN) were conducted at the University of Lethbridge by Dylan Webb on an Elementar Americas Vario MicroCube Analyzer (C, H, N, O, S capabilities). Infrared spectroscopy was conducted on a Thermo-Nicolet iS10 FT-IR spectrometer using bulk recrystallized compounds; s = strong, m = medium, w = weak, br = broad.

4.7.5. Additional Safety Considerations

Organic azides are both toxic and explosive. Care should be taken while handling azides, particularly if they are solvent free and/or at elevated temperatures. Phosphines are toxic and care should be taken while handling. Natural thorium (primary isotope ^{232}Th) is a weak α-emitter (4.012 MeV) with a half-life of 1.41×10^{10} years; manipulations and reactions should be carried out in a fume hood or in an inert atmosphere glove box.

4.7.6. Synthetic Methods

Synthesis of $L_{PN3}Th(\kappa^2\text{-}O_2CCH_2SiMe_3)_3$ (4-1)

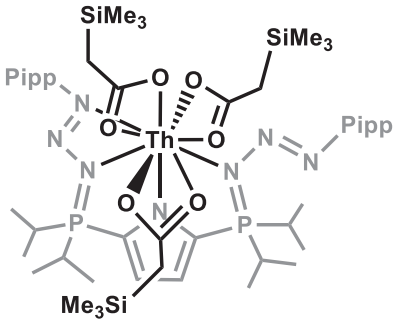

In an inert atmosphere glove box, $L_{PN3}Th(CH_2SiMe_3)_3$ (31.4 mg, 0.0282 mmol) was added to a J. Young NMR tube and dissolved in 0.5 mL of benzene-d_6. The J. Young NMR tube was attached to a double manifold vacuum line and the solution was degassed by one freeze–pump–thaw cycle. A CO_2 atmosphere (1 atm) was applied to the tube. The bright orange colour of the starting material solution immediately lightened and changed to colourless upon agitation. The progress of reaction was monitored by multinuclear NMR spectroscopy. When the reaction was complete, the vessel was degassed and brought into a glove box. The solution was transferred into a vial and the solvent was removed *in vacuo* leaving an off-white solid. Yield: 27.8 mg, 79.2%. IR: (ν_{CO}, cm^{-1}) 2959 (m), 2985 (w), 2875 (w), 1527 (m), 1506 (m), 1433 (s), 1394 (m), 1373 (s), 1280 (w), 1246 (s), 1138 (s), 1099 (m), 1041 (s), 952 (m), 840 (s). ^{1}H NMR (C_6D_6, 300.13 MHz): δ 8.26 (d, $^3J_{HH}$ = 8.1 Hz, 4H, *meta*–aromatic C*H*), 7.28 (d, $^3J_{HH}$ = 8.1 Hz, 4H, *ortho*–aromatic C*H*), 6.72 (d, $^3J_{HP}$ = 2.1 Hz, 2H, pyrrole–C*H*),

2.75 (sp, $^{3}J_{HH}$ = 6.8 Hz, 2H, Ar–C*H*(CH$_3$)$_2$), 2.32 (spd, $^{3}J_{HH}$ = 7.6 Hz, $^{2}J_{HP}$ = 2.0 Hz, 4H, P–C*H*(CH$_3$)$_2$), 1.76 (s, 6H, OCOC*H*$_2$SiMe$_3$), 1.15 (ov dd, dd and d, 36H, P–CH(C*H*$_3$)$_2$ and Ar–CH(C*H*$_3$)$_2$), 0.16 (s, 27H, Si(C*H*$_3$)$_3$). ^{13}C{^{1}H} NMR (C$_6$D$_6$, 75.47 MHz): δ 188.6 (s, Th–O*C*O), 147.9 (s, aromatic *ipso*-*C*), 147.8 (s, aromatic *ipso*-*C*), 126.9 (s, aromatic *C*H), 124.2 (dd, $^{1}J_{CP}$ = 136.3 Hz, $^{4}J_{CP}$ = 16.7 Hz, 2,5-pyrrole *C*), 122.1 (s, aromatic *C*H), 117.3 (dd,$^{2}J_{CP}$ = 26.2 Hz, $^{3}J_{CP}$ = 10.6 Hz, 3,4-pyrrole *C*H), 34.3 (s, Ar–*C*H(CH$_3$)$_2$), 31.5 (s, OCO*C*H$_2$SiMe$_3$), 25.7 (d, $^{1}J_{CP}$ = 50.6 Hz, P–*C*H(CH$_3$)$_2$), 24.3 (s, Ar–CH(*C*H$_3$)$_2$), 16.2 (s, P–CH(*C*H$_3$)$_2$), –0.63 (s, Si(*C*H$_3$)$_3$). ^{31}P{^{1}H} NMR (C$_6$D$_6$, 121.49 MHz): δ 54.7 (s). Anal. Calcd. (%) for C$_{49}$H$_{85}$N$_7$P$_2$O$_6$Si$_3$Th: C: 47.22; H: 6.87; N: 7.87. Found: C: 48.18; H: 6.88; N: 7.88.

Synthesis of L$_{PN3}$Th(NHAd)$_3$ (4-2)

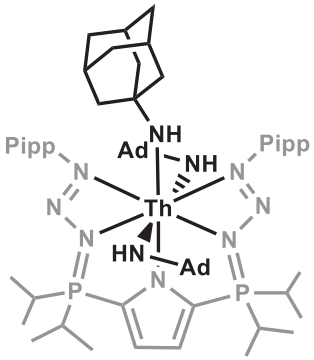

In an inert atmosphere glove box, L$_{PN3}$Th(CH$_2$SiMe$_3$)$_3$ (28.8 mg, 0.0258 mmol) and 1-adamantylamine (11.7 mg, 0.0773 mmol, 3 equiv) were weighed into a 20 mL scintillation vial and dissolved in 2 mL of pentane and 0.5 mL of toluene. The solution was agitated for 2 minutes and the solvent removed *in vacuo* to leave a yellow oil. The yellow oil was dissolved in 1 mL of pentane and the solution cooled to –35 ºC for 15 minutes resulting in the formation of yellow needles. The supernatant was removed and the yellow solid dried *in vacuo*. Yield: 23.1 mg, 68.5%. IR: (ν_{CO}, cm^{-1}) 2959 (w), 2923 (m), 2895 (s), 2841 (m), 1605 (w), 1448 (w), 1434 (w), 1390 (w), 1301 (w), 1259 (w), 1244 (s), 1131 (s), 1093 (m), 1052 (s), 1033 (m), 1021 (w), 939 (m), 834 (s). ^{1}H NMR (C$_6$D$_6$, 300.13 MHz): δ 8.09 (d, $^{3}J_{HH}$ = 8.3 Hz, 4H, *meta*-aromatic C*H*), 7.31 (d, $^{3}J_{HH}$ = 8.3

Hz, 4H, *ortho*-aromatic C*H*), 6.75 (d, $^{3}J_{HP}$ = 2.3 Hz, 2H, pyrrole–C*H*), 3.58 (br s, 1H, Ad–N*H*), 2.87 (br s, 2H, Ad–N*H*), 2.74 (sp, $^{3}J_{HH}$ = 6.9 Hz, 2H, Ar–C*H*(CH_3)$_2$), 2.46 (ov m, 10H, P–C*H*(CH_3)$_2$ and Ad–C*H*), 2.27 (br s, 3H, Ad–C*H*), 2.12 (br s, 6H, Ad–CH_2), 1.77 (br ov m, 30H, Ad–CH_2), 1.13 (ov dd, dd and d, 36H, P–CH(CH_3)$_2$ and Ar–CH(CH_3)$_2$). $^{13}C\{^{1}H\}$ NMR (C_6D_6, 75.47 MHz): δ 149.1 (s, aromatic *ipso*-*C*), 147.3 (s, aromatic *ipso*-*C*), 126.7 (s, aromatic *C*H), 125.2 (dd, $^{1}J_{CP}$ = 134.3 Hz, $^{3}J_{CP}$ = 16.4 Hz, 2,5-pyrrole *C*), 121.8 (s, aromatic *C*H), 117.9 (dd, $^{2}J_{CP}$ = 26.5 Hz, $^{3}J_{CP}$ = 10.3 Hz, 3,4-pyrrole *C*H), 55.5 (s, Ad–*C*), 50.0 (s, Ad–*C*H_2), 37.3 (s, Ad–*C*H_2), 33.9 (s, Ar–*C*H(CH_3)$_2$), 31.0 (s, Ad–*C*H), 26.5 (d, $^{1}J_{CP}$ = 49.5 Hz, P–*C*H(CH_3)$_2$), 23.7 (s, Ar–CH(*C*H_3)$_2$), 16.5 (d, $^{2}J_{CP}$ = 24.3 Hz, P–CH(*C*H_3)$_2$). $^{31}P\{^{1}H\}$ NMR (C_6D_6, 121.49 MHz): δ 53.0 (s). Anal. Calcd. (%) for $C_{64}H_{100}N_{10}P_2Th$: C: 58.97; H: 7.73; N: 10.75. Found: C: 58.80; H: 7.82; N: 10.80.

Synthesis of $L_{PN3}Th(\kappa^2\text{-}O_2CNHAd)_3$ (4-3)

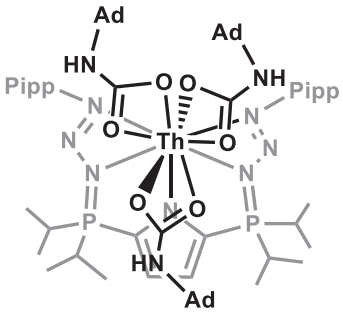

In an inert atmosphere glove box, $L_{PN3}Th(NHAd)_3$ (37.1 mg, 0.0285 mmol) was added to a J. Young NMR tube and dissolved in 0.5 mL of benzene-d_6. The J. Young NMR tube was attached to a double manifold vacuum line and the solution was degassed by one freeze–pump–thaw cycle. A CO_2 atmosphere (1 atm) was applied to the tube. The bright yellow colour immediately lightened and changed to colourless upon agitation. The progress of reaction was monitored by multinuclear NMR spectroscopy. When the reaction was complete, the vessel was degassed and brought into a glove box. The solution was transferred into a vial and the solvent was removed *in vacuo* leaving an off-white solid. Yield: 30.1 mg, 73.4%. IR: (ν_{CO},

cm^{-1}) 3437 (br), 2959 (w), 2904 (s), 2847 (m), 2141 (w), 2111 (w), 1655 (w), 1557 (m), 1486 (s), 1376 (m), 1356 (m), 1306 (m), 1275 (w), 1144 (s), 1098 (m), 1041 (s), 954 (w), 881 (w), 839 (m). ^{1}H NMR (C_6D_6, 300.13 MHz): δ 8.30 (d, $^{3}J_{HH}$ = 8.4 Hz, 4H, *meta*-aromatic C*H*), 7.31 (d, $^{3}J_{HH}$ = 8.4 Hz, 4H, *ortho*-aromatic C*H*), 6.76 (d, $^{3}J_{HP}$ = 2.0 Hz, 2H, pyrrole–C*H*), 3.99 (s, 3H, OCON*H*Ad), 2.78 (sp, $^{3}J_{HH}$ = 6.5 Hz, 2H, Ar–C*H*(CH_3)$_2$), 2.43 (spd, $^{3}J_{HH}$ = 6.9 Hz, $^{2}J_{HP}$ = 3.7 Hz, 4H, P–C*H*(CH_3)$_2$), 1.88 (br s, 9H, Ad–C*H*), 1.81 (br s, 18H, Ad–CH_2), 1.52 (br s, 18H, Ad–CH_2), 1.22 (ov dd, dd and d, 36H, P–CH(CH_3)$_2$ and Ar–CH(CH_3)$_2$). ^{13}C{^{1}H} NMR (C_6D_6, 75.47 MHz): δ 167.9 (s, Th–O*C*O), 148.3 (s, aromatic *ipso*-*C*), 147.3 (s, aromatic *ipso*-*C*), 126.6 (s, aromatic *C*H), 124.3 (dd, $^{1}J_{CP}$ = 138.1 Hz, $^{3}J_{CP}$ = 17.4 Hz, 2,5-pyrrole *C*), 122.2 (s, aromatic *C*H), 116.7 (dd, $^{2}J_{CP}$ = 27.7 Hz, $^{3}J_{CP}$ = 11.5 Hz, 3,4-pyrrole *C*H), 49.3 (s, Ad–*C*), 42.6 (s, Ad–*C*H_2), 36.9 (s, Ad–*C*H_2), 34.3 (s, Ar–*C*H(CH_3)$_2$), 30.1 (s, Ad–*C*H), 25.7 (d, $^{1}J_{CP}$ = 49.7 Hz, P–*C*H(CH_3)$_2$), 24.4 (s, Ar–CH(*C*H_3)$_2$), 16.3 (s, P–CH(*C*H_3)$_2$). ^{31}P{^{1}H} NMR (C_6D_6, 121.49 MHz): δ 54.5 (s). Anal. Calcd. (%) for $C_{67}H_{100}N_{10}O_6P_2Th$: C: 56.06; H: 7.02; N: 9.76. Found: C: 56.07; H: 6.97; N: 9.76.

In Situ Synthesis of $L_{P=N}Th(\kappa^2\text{-}O_2CCH_2SiMe_3)_3$ (4-4)

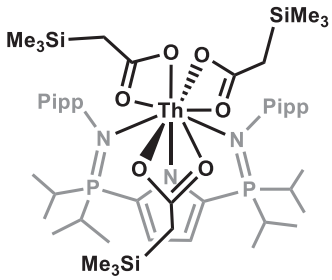

In an inert atmosphere glove box, $L_{PN3}Th(\kappa^2\text{-}O_2CCH_2SiMe_3)_3$ (5.0 mg, 0.0042 mmol) was added to a J. Young NMR tube and dissolved in 0.5 mL of benzene-d_6. The J. Young NMR tube was heated in an oil bath at 65 °C for 4 days. The progress of reaction was monitored by multinuclear NMR spectroscopy. ^{1}H NMR (C_6D_6, 300.13 MHz): δ 7.58 (dd, $^{3}J_{HH}$ = 8.2 Hz, $^{4}J_{HP}$= 2.1 Hz, 4H, *ortho*-aromatic C*H*), 7.21 (d, $^{3}J_{HH}$ = 8.2

Hz, 4H, *meta*-aromatic C*H*), 6.52 (d, $^{3}J_{HP}$ = 1.7 Hz, 2H, pyrrole–C*H*), 2.80 (sp, $^{3}J_{HH}$ = 6.9 Hz, 2H, Ar–C*H*(CH_3)$_2$), 2.15 (dsp, $^{3}J_{HH}$ = 7.0 Hz, $^{2}J_{HP}$ = 2.5 Hz, 4H, P–C*H*(CH_3)$_2$), 1.78 (br s, 6H, OCOC*H*$_2$SiMe$_3$), 1.22 (d, $^{3}J_{HH}$ = 6.9 Hz, 12H, Ar–CH(C*H*$_3$)$_2$), 1.14 (dd, $^{3}J_{HP}$ = 15.8 Hz, $^{3}J_{HH}$ = 7.0 Hz, 12H, P–CH(C*H*$_3$)$_2$), 1.03 (dd, $^{3}J_{HP}$ = 15.2 Hz, $^{3}J_{HH}$ = 7.0 Hz, 12H, P–CH(C*H*$_3$)$_2$). $^{31}P\{^{1}H\}$ NMR (C_6D_6, 121.49 MHz): δ 48.7 (s). Multiple attempts at purification to obtain isolated material of sufficient quality for ^{13}C NMR spectroscopy and combustion analysis were unsuccessful.

In Situ Synthesis of $L_{P=N}Th(\kappa^2\text{-}O_2CNHAd)_3$ (4-5)

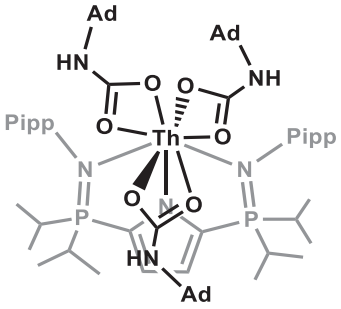

In an inert atmosphere glove box, $L_{PN3}Th(\kappa^2\text{-}O_2CNHAd)_3$ (6.7 mg, 0.0046 mmol) was added to a J. Young NMR tube and dissolved in 0.5 mL of benzene-d_6. The J. Young NMR tube was heated in an oil bath at 65 °C for 3 days, followed by an additional 2 days at 80 °C (required for complete conversion). The progress of reaction was monitored by multinuclear NMR spectroscopy. ^{1}H NMR (C_6D_6, 300.13 MHz): δ 7.77 (dd, $^{3}J_{HH}$ = 8.2 Hz, $^{4}J_{HP}$= 2.0 Hz, 4H, *ortho*-aromatic C*H*), 7.29 (d, $^{3}J_{HH}$ = 8.2 Hz, 4H, *meta*-aromatic C*H*), 6.57 (d, $^{3}J_{HP}$ = 1.8 Hz, 2H, pyrrole–C*H*), 4.00 (s, 3H, OCON*H*Ad), 2.85 (sp, $^{3}J_{HH}$ = 6.5 Hz, 2H, Ar–C*H*(CH_3)$_2$), 2.22 (dsp, $^{3}J_{HH}$ = 6.9 Hz, $^{2}J_{HP}$ = 2.6 Hz, 4H, P–C*H*(CH_3)$_2$), 1.98 (br s, 9H, Ad–C*H*), 1.85 (br s, 18H, Ad–C*H*$_2$), 1.60 (br s, 18H, Ad–C*H*$_2$), 1.16 (ov dd, d and d, 36H, P–CH(C*H*$_3$)$_2$ and Ar–CH(C*H*$_3$)$_2$). $^{31}P\{^{1}H\}$ NMR (C_6D_6, 121.49 MHz): δ 47.2 (s). Multiple attempts at purification to obtain isolated material of sufficient quality for ^{13}C NMR spectroscopy and combustion analysis were unsuccessful.

Synthesis of $L_{P=N/PN3}Th(NHAd)_3$ (4-6)

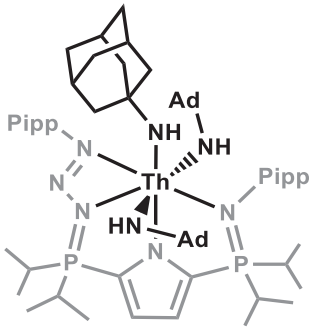

In an inert atmosphere glove box, $L_{PN3}Th(NHAd)_3$ (9.7 mg, 0.0074 mmol) was added to a J. Young NMR tube and dissolved in 0.5 mL of benzene-d_6. The J. Young NMR tube was heated in an oil bath at 65 °C for 4 days. The progress of reaction was monitored by multinuclear NMR spectroscopy. When the reaction was complete, the tube was brought into a glove box. The solution was transferred into a vial and the solvent was removed *in vacuo* leaving a yellow/orange solid. The solid was washed with 0.5 mL of cold $Me_3SiOSiMe_3$. The orange solid was dissolved in 0.5 mL of pentane and cooled to –35 ºC for 24 hours resulting in the formation of yellow/orange needles. The supernatant was removed and the yellow/orange solid dried *in vacuo*. Yield: 8.4 mg, 88%. ^{1}H NMR (C_6D_6, 300.13 MHz): δ 8.27 (d, $^3J_{HH}$ = 8.2 Hz, 2H, Ar–C*H*), 7.49 (dd, $^3J_{HH}$ = 8.2 Hz, $^4J_{HP}$= 2.1 Hz, 2H, Ar–C*H*), 7.32 (d, $^3J_{HH}$ = 8.2 Hz, 2H, Ar–C*H*), 7.21 (d, $^3J_{HH}$ = 8.2 Hz, 2H, Ar–C*H*), 6.73 (t, $^3J_{HH}$ = $^3J_{HP}$ = 3.5 Hz, 1H, pyrrole–C*H*), 6.58 (t, $^3J_{HH}$ = $^3J_{HP}$ = 3.5 Hz, 1H, pyrrole–C*H*), 3.03 (br s, 1H, Ad–N*H*), 2.86 (sp, $^3J_{HH}$ = 6.8 Hz, 1H, Ar–C*H*(CH_3)$_2$), 2.70 (sp, $^3J_{HH}$ = 6.9 Hz, 1H, Ar–C*H*(CH_3)$_2$), 2.56 (br s, 2H, Ad–N*H*), 2.38 (spd, $^3J_{HH}$ = 7.2 Hz, $^2J_{HP}$ = 3.2 Hz, 2H, P–C*H*(CH_3)$_2$), 2.23 (br s, 3H, Ad–C*H*), 2.11 (ov sp and s, 8H, P–C*H*(CH_3)$_2$ and Ad–C*H*), 1.86 (br s, 18H, Ad–CH_2), 1.68 (br ov m, 18H, Ad–CH_2), 1.15 (ov dd, dd and d, 36H, P–CH(CH_3)$_2$ and Ar–CH(CH_3)$_2$). ^{13}C{^{1}H} NMR (C_6D_6, 75.47 MHz): δ 149.1 (d, $^5J_{CP}$ = 1.95 Hz, aromatic *ipso*-*C*), 147.7 (s, aromatic *ipso*-*C*), 146.7 (d, $^2J_{CP}$ = 5.2 Hz, aromatic *ipso*-*C*), 143.6 (d, $^2J_{CP}$ = 3.8 Hz, aromatic *ipso*-*C*), 131.2 (dd, $^1J_{CP}$ = 135.0 Hz, $^3J_{CP}$ = 15.1 Hz, 2,5-pyrrole *C*), 129.7 (d, $^3J_{CP}$ = 6.0 Hz, aromatic *C*H), 127.0 (d, $^4J_{CP}$ = 2.5 Hz, aromatic *C*H), 126.8 (s, aromatic *C*H), 123.3 (dd, $^1J_{CP}$ = 140.4

Hz, $^{3}J_{CP}$ = 17.1 Hz, 2,5-pyrrole *C*), 122.2 (s, aromatic *C*H), 117.6 (dd, $^{2}J_{CP}$ = 27.0 Hz, $^{3}J_{CP}$ = 10.2 Hz, 3,4-pyrrole *C*H), 116.5 (dd, $^{2}J_{CP}$ = 26.2 Hz, $^{3}J_{CP}$ = 11.3 Hz, 3,4-pyrrole *C*H), 56.6 (s, Ad–*C*), 57.4 (s, Ad–*C*), 50.5 (s, Ad–*C*H_2), 49.6 (s, Ad–*C*H_2), 37.7 (s, Ad–*C*H_2), 37.6 (s, Ad–*C*H_2), 34.2 (s, Ar–*C*H(CH_3)$_2$), 33.9 (s, Ar–*C*H(CH_3)$_2$), 31.4 (s, Ad–*C*H), 31.3 (s, Ad–*C*H), 27.7 (d, $^{1}J_{CP}$ = 54.4 Hz, P–*C*H(CH_3)$_2$), 27.0 (d, $^{1}J_{CP}$ = 48.9 Hz, P–*C*H(CH_3)$_2$), 24.5 (s, Ar–CH(*C*H_3)$_2$), 24.1 (s, Ar–CH(*C*H_3)$_2$), 17.0 (d, $^{2}J_{CP}$ = 2.4 Hz, P–CH(*C*H_3)$_2$), 16.9 (d, $^{2}J_{CP}$ = 2.6 Hz, P–CH(*C*H_3)$_2$), 16.5 (d, $^{2}J_{CP}$ = 1.4 Hz, P–CH(*C*H_3)$_2$), 16.4 (d, $^{2}J_{CP}$ = 2.6 Hz, P–CH(*C*H_3)$_2$). $^{31}P\{^{1}H\}$ NMR (C_6D_6, 121.49 MHz): δ 49.7 (br s), 46.1 (d, $^{4}J_{PP}$ = 2.1 hz). Anal. Calcd. (%) for $C_{64}H_{100}N_8P_2Th$: C: 60.26; H: 7.90; N: 8.78. Found: C: 58.05; H: 7.90; N: 8.58.

4.7.7. Crystallographic Details

All structures were collected on a Rigaku SuperNova diffractometer equipped with a Dectris Pilatus 3R 200K-A hybrid-pixel-array detector, a four-circle goniometer, sealed graphite-monochromated Mo Kα (λ = 0.71073 Å) and Cu Kα (λ = 1.54178 Å) X-ray sources, and an Oxford cryostream-cooling device fixed at 100 K. Single crystals suitable for X-ray diffraction studies were mounted on a MiTiGen cryo-loop using desiccated Paratone–*N* oil stored in a glove box. Data reduction was accomplished by the CrysAlis^{Pro} (version 1.171.38.43) software package. Absorption corrections were applied by multi-scan techniques and empirical absorption correction using spherical harmonics, implemented in SCALE3 ABSPACK scaling algorithm. Structures were solved in the Olex2[29] environment using intrinsic phasing and refined by full-matrix least squares method on F^2 using the SHELX software suite.[30,31] All non-hydrogen atoms were refined anisotropically, C–H

hydrogens were calculated and refined isotropically as a riding model. All measurements were performed at the University of Lethbridge.

Single crystals of complexes **4-1**, **4-2** and **4-6** were grown from pentane/toluene at –35 °C. Single crystals were coated in dry Paratone® oil under an inert argon atmosphere. Unfortunately, single crystals of **4-3** grown from pentane succumb to rapid decomposition upon removal from the mother liquor, resulting in the crystals becoming covered with amorphic material. However, inner portions of the crystals remain intact, allowing for modest diffraction of X-ray radiation, despite interference from the polycrystalline material. The data is low quality, and therefore, metrical parameters are not included, or discussed, in the body of the manuscript. The data set does, though, allow for qualitative discussion associated with atom connectivity and geometry. Therefore, these structures will be referred to within this thesis as "connectivity structures". Summary of the crystallographic data can be found below in **Table 4.1**

Table 4.1. X-ray crystallographic data and structure refinement for complexes **4-1**, **4-2**, **4-3** and **4-6**.

	4-1	**4-2**
CCDC #	2108094	2108093
Empirical formula	$C_{49}H_{85}N_7O_6P_2Si_3Th$	$C_{64}H_{100}N_{10}P_2Th$
Formula weight/g mol^{-1}	1246.48	1303.51
Temperature/K	100.1(5)	103(8)
Crystal system	monoclinic	monoclinic
Space group	$P2_1/n$	$P2_1/c$
a/Å	18.3001(3)	13.00230(10)
b/Å	13.2301(2)	22.2683(2)
c/Å	26.1455(3)	43.6139(4)
α/°	90	90
β/°	106.0010(10)	91.0650(10)
γ/°	90	90
Volume/Å^3	6084.89(16)	12625.75(19)
Z	4	8
ρ_{calc}g/cm^3	1.361	1.372
μ/mm^{-1}	9.345	8.447
F(000)	2552.0	5392.0
Crystal size/mm^3	0.2 × 0.096 × 0.081	0.174 × 0.119 × 0.085
Radiation (Å)	Cu Kα (λ = 1.54184)	Cu Kα (λ = 1.54184)
2Θ range for data collection/°	5.278 to 150.164	4.052 to 150.302
Index ranges	-18 ≤ h ≤ 22, -16 ≤ k ≤ 15, -32 ≤ l ≤ 32	-16 ≤ h ≤ 14, -27 ≤ k ≤ 27, -54 ≤ l ≤ 54
Reflections collected	36694	121073
Independent reflections	12187 [R_{int} = 0.0308, R_{sigma} = 0.0321]	25395 [R_{int} = 0.0484, R_{sigma} = 0.0409]
Data/restraints/parameters	12187/1073/776	25395/1642/1510
Goodness-of-fit on F^2	1.061	1.048
Final R indexes [I>=2σ (I)]	R_1 = 0.0880, wR_2 = 0.2289	R_1 = 0.0322, wR_2 = 0.0701
Final R indexes [all data]	R_1 = 0.1001, wR_2 = 0.2404	R_1 = 0.0435, wR_2 = 0.0753
Largest diff. peak/hole / e Å^{-3}	5.48/-3.40	1.21/-1.34

Programs for diffractometer operation, data collection, data reduction, and absorption correction were those supplied by Rigaku.

	4-3	4-6
CCDC #	N/A	2108092
Empirical formula	$C_{67}H_{100}N_{10}O_6P_2Th$	$C_{64}H_{99}N_8P_2Th$
Formula weight/g mol^{-1}	1435.54	1274.49
Temperature/K	179(110)	99.9(4)
Crystal system	monoclinic	triclinic
Space group	$P2_1/c$	P-1
a/Å	15.7123(13)	12.5298(4)
b/Å	14.2863(5)	12.7021(3)
c/Å	34.165(3)	22.4177(4)
α/°	90	104.163(2)
β/°	98.595(7)	94.301(2)
γ/°	90	114.430(3)
Volume/Å^3	7582.9(9)	3086.33(15)
Z	4	2
ρ_{calc}g/cm^3	1.257	1.371
μ/mm^{-1}	7.143	8.616
F(000)	2960.0	1318.0
Crystal size/mm^3	0.174 × 0.119 × 0.085	0.133 × 0.119 × 0.026
Radiation (Å)	Cu Kα (λ = 1.54184)	Cu Kα (λ = 1.54184)
2Θ range for data collection/°	5.232 to 155.754	4.148 to 151.526
Index ranges	-19 ≤ h ≤ 15, -14 ≤ k ≤ 17, -39 ≤ l ≤ 42	-15 ≤ h ≤ 15, -14 ≤ k ≤ 15, -27 ≤ l ≤ 28
Reflections collected	21352	28184
Independent reflections	11563 [R_{int} = 0.1103, R_{sigma} = 0.1370]	11220 [R_{int} = 0.0580, R_{sigma} = 0.0517]
Data/restraints/parameters	11563/206/357	11220/1103/845
Goodness-of-fit on F^2	2.398	1.028
Final R indexes [I>=2σ (I)]	R_1 = 0.2834, wR_2 = 0.6266	R_1 = 0.0573, wR_2 = 0.1406
Final R indexes [all data]	R_1 = 0.3258, wR_2 = 0.6388	R_1 = 0.0634, wR_2 = 0.1436
Largest diff. peak/hole / e Å^{-3}	15.67/-11.44	3.34/-1.83

Programs for diffractometer operation, data collection, data reduction, and absorption correction were those supplied by Rigaku.

4.8. References for Chapter 4

(1) Liu, H.; Ghatak, T.; Eisen, M. S. Organoactinides in catalytic transformations: scope, mechanisms and Quo Vadis. *Chem. Commun.* **2017**, *53*, 11278–11297.

(2) Arnold, P.; Turner, Z. R. Carbon oxygenate transformations by actinide compounds and catalysts. *Nat. Rev. Chem.* **2017**, 1, 0002.

(3) Button, Z. E.; Higgins, J. A.; Suvova, M.; Cloke, F. G. N.; Roe, S. M. Mixed sandwich thorium complexes incorporating bis(tri-isopropylsilyl)cyclooctatetraenyl and pentamethylcyclopentadienyl ligands: synthesis, structure and reactivity. *Dalton Trans*. **2015**, *44*, 2588–2596.

(4) Schmidt, A-C.; Heinemann, F. W.; Kefalidis, C. E.; Maron, L.; Roesky, P. W.; Meyer, K. Activation of SO_2 and CO_2 by Trivalent Uranium Leading to Sulfite/Dithionite and Carbonate/Oxalate Complexes. *Chem. Eur. J.* **2014**, *20*, 13501–13506.

(5) Tsoureas, N.; Castro, L.; Kilpatrick, A. F. R.; Cloke, F. G. N.; Maron, L. Controlling selectivity in the reductive activation of CO_2 by mixed sandwich uranium (iii) complexes. *Chem. Sci*. **2014**, *5*, 3777–3788.

(6) Formanuik, A.; Ortu, F.; Inman, C. J.; Kerridge, A.; Castro, L.; Maron, L.; Mills, D. P. Concomitant Carboxylate and Oxalate Formation From the Activation of CO_2 by a Thorium(III) Complex. *Chem. Eur. J.* **2016**, *22*, 17976–17979.

(7) Boreen, M. A.; Arnold J. The synthesis and versatile reducing power of low-valent uranium complexes. *Dalton Trans*. **2020**, *49*, 15124–15138.

(8) Odom, A. L.; Arnold, P. L.; Cummins, C. C. Heterodinuclear uranium/molybdenum dinitrogen complexes. *J. Am. Chem. Soc.* **1998**, *120*, 5836–5837.

(9) Summerscales, O. T.; Cloke, F. G. N.; Hitchcock, P. B. ; Green, J. C.; Hazari, N. Reductive cyclotrimerization of carbon monoxide to the deltate dianion by an organometallic uranium complex. *Science* **2006**, *311*, 829–831.

(10) Moloy, K. G.; Marks, T. J. The insertion of carbon dioxide into actinide alkyl and hydride bonds. *Inorg. Chim. Acta* **1985**, *110,* 127–131.

(11) Higgins, J. A.; Cloke, F. G. N.; Roe, S. M. Synthesis and CO_2 Insertion Chemistry of Uranium(IV) Mixed-Sandwich Alkyl and Hydride Complexes. *Organometallics* **2013**, *32*, 5244−5252.

(12) Bagnall, K. W.; Yanir, E. Thorium (IV) and uranium (IV) carbamates. *J. Inorg Nucl. Chem*. **1974**, *36*, 777–779.

(13) Tarlton, M. L.; Del Rosal, I.; Vilanova, S. P.; Kelley, S. P.; Maron, L; Walensky, J. R. Comparative Insertion Reactivity of CO, CO_2, ^{t}BuCN, and ^{t}BuNC into Thorium– and Uranium–Phosphorus Bonds. *Organometallics* **2020**, *39*, 2152–2161.

(14) Matson, E. M.; Forrest, W. P.; Fanwick, P. E.; Bart, S. C. Functionalization of carbon dioxide and carbon disulfide using a stable uranium (III) alkyl complex. *J. Am. Chem. Soc.* **2011***, 133*, 4948–4954.

(15) Webster, C. L.; Ziller, J. W.; Evans, W. J., Synthesis and CO_2 Insertion Reactivity of Allyluranium Metallocene Complexes. *Organometallics* **2012**, *31*, 7191−7197.

(16) Waldschmidt, P.; Hoerger, C. J.; Riedhammer, J.; Heinemann, F. W.; Hauser, C. T.; Meyer, K., CO2 Activation with Formation of Uranium Carbonate Complexes in a Closed Synthetic Cycle. *Organometallics* **2020**, *39*, 1602−1611.

(17) Mora, E.; Maria, L.; Biswas, B.; Camp, C.; Santos, I. C.; Pécaut, J.; Cruz, A.; Carretas, J. M.; Marçalo, J.; Mazzanti, M., Diamine Bis(phenolate) as Supporting Ligands in Organoactinide(IV) Chemistry. Synthesis, Structural Characterization, and Reactivity of Stable Dialkyl Derivatives. *Organometallics* **2013**, *32*, 1409–1422.

(18) Dickie, T. K. K.; MacNeil, C. S.; Hayes, P. G. Consecutive N_2 loss from a uranium diphosphazide complex. *Dalton Trans*. **2020**, *49*, 578–582.

(19) Dickie, T. K. K.; Aborawi, A. A.; Hayes, P. G. Diphosphazide-Supported Trialkyl Thorium(IV) Complex. *Organometallics* **2020**, *39*, 2047–2052.

(20) Qin, G.; Cheng, J. Thorium(IV) trialkyl complexes of non-carbocyclic ligands as highly active isoprene polymerisation catalysts. *Dalton Trans.* **2019**, *48*, 11706−11714.

(21) Qin, G.; Wang, Y.; Del Rosal, I.; Maron, L.; Cheng, J. Monomeric thorium dihydrido complexes: versatile precursors to actinide metallacycles. *Chem. Commun.* **2019**, *55*, 8560−8563.

(22) Chen, R.; Qin, G.; Li, S.; Edwards, A. J.; Piltz, R. O.; Del Rosal, I.; Maron, L.; Cui, D.; Cheng, J. Molecular Thorium Trihydrido Clusters Stabilized by Cyclopentadienyl Ligands. *Angew. Chem. Int. Ed.* **2020**, *59*, 11250−11255.

(23) Bebbington, M. W. P.; Bourissou, D. Stabilised phosphazides. *Coord. Chem. Rev.* **2009**, *253*, 1248−1261.

(24) Tutson, C. D.; Gorden, A. E. V. Thorium coordination: A comprehensive review based on coordination number. *Coord. Chem. Rev*. **2017**, *333*, 27-43.

(25) Daly, S.; Piccoli, P.; Schultz, A.; Todorova, T.; Gagliardi, L.; Girolami, G. Synthesis and Properties of a Fifteen-Coordinate Complex: The Thorium Aminodiboranate $[Th(H_3BNMe_2BH_3)_4]$. *Angew. Chem. Int. Ed.* **2010**, *49*, 3379–3381.

(26) Burger, B. J.; Bercaw, J. E. Experimental Organometallic Chemistry; American Chemical Society: Washington, D.C., 1987.

(27) Marvich, R. H.; Brintzinger, H. H. A Metastable Form of Titanocene. Formation from a Hydride Complex and Reactions with Hydrogen, Nitrogen, and Carbon Monoxide. *J. Am. Chem. Soc.* **1971**, *93*, 2046–2048.

(28) Pangborn, A. B.; Giardello, M. A.; Grubbs, R. H.; Rosen, R. K.; Timmers, F. J. Safe and Convenient Procedure for Solvent Purification. *Organometallics* **1996**, *15*, 1518–1520.

(29) Dolomanov, O. V.; Bourhis, L. J.; Gildea, R. J.; Howard, J. A. K.; Puschmann, H. *OLEX2*: a complete structure solution, refinement and analysis program. *J. Appl. Crystallogr.* **2009**, *42*, 339–341.

(30) Sheldrick, G. M. *SHELXT* – Integrated space-group and crystal-structure determination. *Acta Crystallogr. Sect. A* **2015**, *71*, 3–8.

(31) Sheldrick, G. M. Crystal structure refinement with *SHELXL*. *Acta Crystallogr. Sect. C* **2015**, *71*, 3–8.

5. Preliminary Results and Future Work[k]

5.1. U(VI) Oxo Complexes

5.1.1. Background

The focus of the research in this thesis features primarily thorium and uranium in the 4+ oxidation state. However, as stated in Chapter 1, uranium can access oxidation states ranging from +3 to +6.[2] Uranium(VI) is often accompanied by an "oxo" ligand, and the uranyl functionality (O=U=O) is a common motif in U(VI) chemistry, especially in aqueous environments. The uranyl dication $[UO_2]^{2+}$ is water soluble and is the primary form of uranium in the environment, leading to a search for a method to functionalize the effectively inert U=O bond. Activation of U=O can be achieved through multiple methods, including reductive silylation from U(VI) to U(V) or U(IV).[3] The Arnold group successfully silylated U=O by employing supporting macrocyclic ligands in an anaerobic environment. They observed a single electron reduction of the uranyl to $[O=U–OR]^{+}$ in the presence of other transition metal ions.[4] Additionally, Mazzanti and co-workers have used salen ligands to support reactive pentavalent uranium oxo species, a system which is similar to our phosphasalen and phosphazidosalen ligand systems.[5] Thus, preliminary reactions to synthesize U(VI) uranyl complexes featuring our phosphazidosalen and phosphasalen ligand were attempted and are described below.

5.1.2. U(VI) Oxo Phosphasalen and Phosphazidosalen Complexes

The potassiated phosphasalen ligand K_2L'' was combined with $U(O)_2Cl_2(THF)_3$ in

[k] *Organometallics* reference style used throughout this chapter

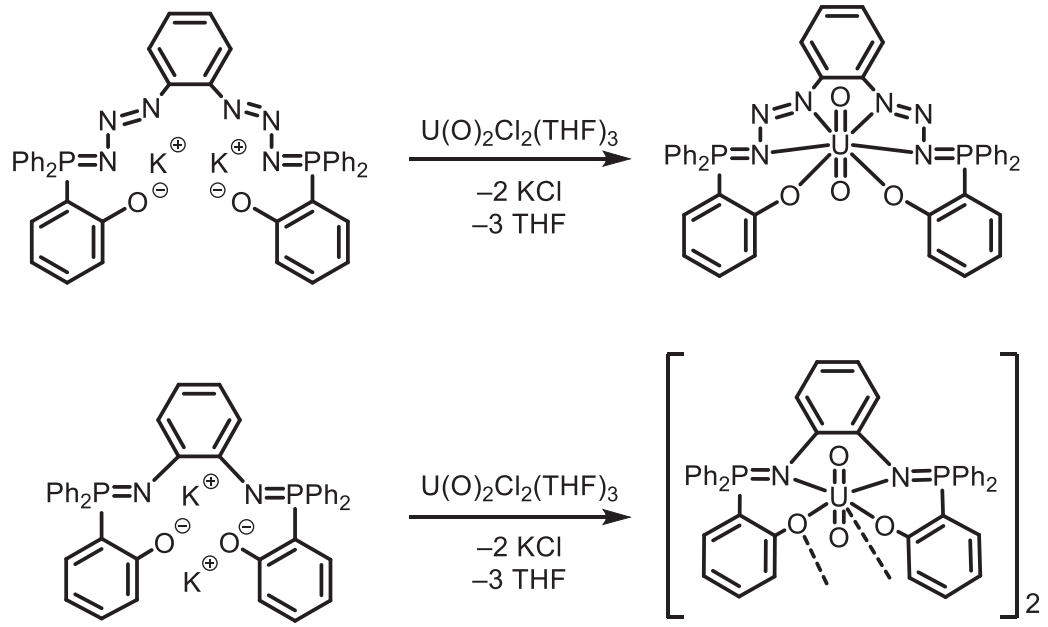

Scheme 5.1. Synthesis of U(VI) phosphazidosalen and phosphasalen complexes.

THF and the bright red solution was monitored by $^{31}P\{^{1}H\}$ NMR spectroscopy (Scheme 5.1, top). Several resonances suggesting formation of a diamagnetic metal complex were observed between δ 24.2 and δ 29.9 in THF-d_8. A small batch of crystals grown in benzene gave rise to an X-ray crystal structure featuring two different U(VI) metal centres (Figure 5.1, Table 5.1). Within the structure, one U(VI) centre is distorted hexagonal bipyramidal and isostructural with L"UCl_2; the oxo ligands occupy the axial sites, mirroring the chloride ligands in L"UCl_2. The other uranium(VI) centre features a distorted pentagonal bipyramidal coordination environment, with the two oxygen atoms of the ligand bridging between the two metal centres. A chloride and a $Ph_2P[(2\text{-}O)C_6H_4]^-$ group are bound to uranium, likely the result of $Ph_2P[(2\text{-}OK)C_6H_4]$ contamination. While this is not the ideal L"$U(O)_2$ structure, the L"$U(O)_2$ fragment can still be compared to L"UCl_2; notably the two systems are essentially isostructural (Figure 5.2). The N1–N2–N3 angles of the phosphazides of "L"U(O)2" and L"UCl2 are comparable with values of 104.6(5)° and 103.7(2)°, respectively. Both axial ligand angles are somewhat similar (Cl1–U1–Cl2 =

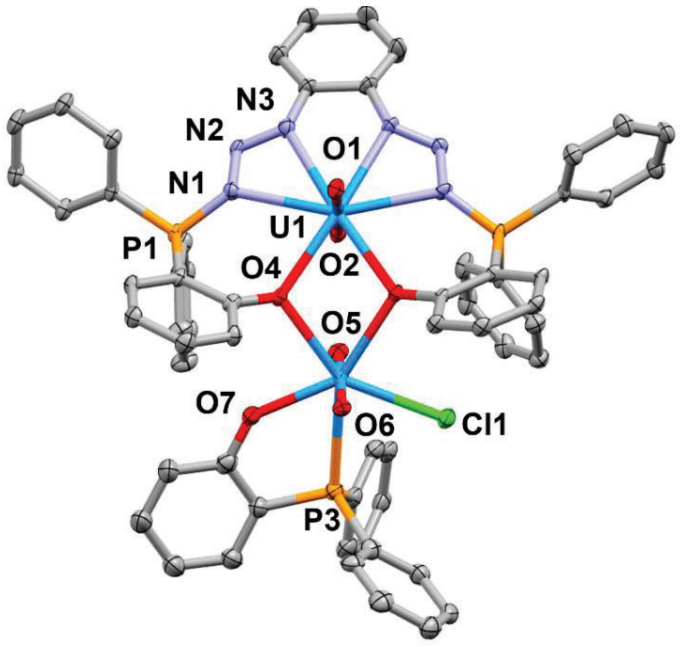

$L''U(O)_2U(O)_2Cl[Ph_2P[(2\text{-}O)C_6H_4]$

Figure 5.1. X-ray crystal structure of L"$U(O)_2U(O)_2Cl[Ph_2P[(2\text{-}O)C_6H_4]$. Thermal ellipsoids are drawn at 30% probability. Hydrogens have been removed for clarity.

Table 5.1. Selected bond distances (Å) and angles (°) for L"$U(O)_2U(O)_2Cl[Ph_2P[(2\text{-}O)C_6H_4]$.

Parameter	$L''U(O)_2U(O)_2Cl[Ph_2P[(2\text{-}O)C_6H_4]$
Bond Distance (Å)	
P1–N1	1.639(5)
U1–O1	1.779(5)
U1–O4	2.418(5)
U2–Cl1	2.685(2)
U2–O7	2.272(5)
U2–P3	2.960(2)
U2–O4	2.487(5)
Bond Angle (°)	
N1–N2–N3	104.6(5)
O3–U1–O4	68.2(2)
O1–U1–O2	178.4(2)
O5–U2–O6	177.4(2)

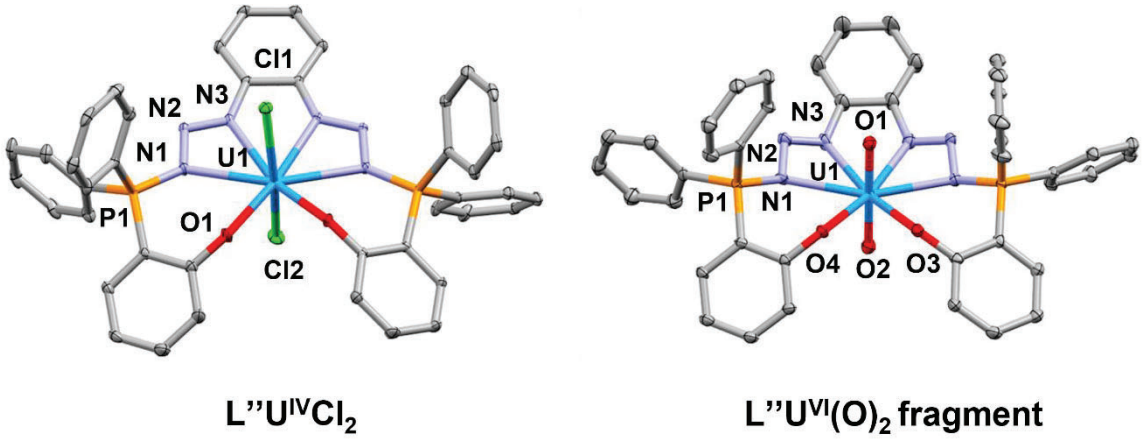

Figure 5.2. X-ray crystal structures of L"UCl_2 (left) and L"$U(O)_2U(O)_2Cl[Ph_2P[(2\text{-}O)C_6H_4]$ fragment (right). Thermal ellipsoids are drawn at 30% probability. Hydrogens have been removed for clarity. Only the L"$U(O)_2$ fragment of L"$U(O)_2U(O)_2Cl[Ph_2P[(2\text{-}O)C_6H_4]$ is shown for comparison purposes.

163.08(3)°; O1−U1−O2 = 178.4(2)°), though the uranyl O=U=O is, unsurprisingly, much closer to the ideal value of 180°. The U–N lengths in the U(VI) fragment are marginally shorter than in the U(IV) complex (U^{VI}–N1 = 2.555(6) Å ; U^{VI}–N3 = 2.557(8) Å; U^{IV}–N1 = 2.589(3) Å ; U^{IV}–N3 = 2.586(2) Å). As expected for a uranium-oxygen double bond, the U–O_{oxo} distances are substantially shorter than the U–O ligand contacts (U^{VI}–O1 = 1.779(5) Å; U^{VI}–O3 = 2.443(5) Å).

Upon close inspection of the signals in the $^{31}P\{^1H\}$ NMR spectrum, 3 distinct complexes can be identified, two symmetric complexes and one asymmetric intermediate. A peak at δ 29.9 in THF-d_8 is postulated to be the U(VI) phosphazidosalen complex L"$U(O)_2$, as it is the most downfield resonance, and the intermediate signals likely correspond to the mixed phosphazide/phosphinimine complex L'$U(O)_2$ at δ 29.5 and δ 25.3 (1:1 ratio).

A final symmetric complex at δ 24.2 is postulated to be the U(VI) phosphasalen complex $LU(O)_2(THF)$, the result of loss of two equivalents of N_2 loss from the

phosphazidosalen ligand and THF solvento adduct. To verify the assignment of δ 24.2, K_2L was combined with $UO_2Cl_2(THF)_3$ in THF-d_8 (Scheme 5.1, bottom). The $^{31}P\{^1H\}$ NMR spectrum indeed showed the expected resonance at δ 24.2, as well as two resonances in a 1:1 ratio (δ 23.0 and δ 25.4) that are presumably due to an asymmetric product. X-ray crystallography performed on crystals grown in acetonitrile confirmed the structure of the U(VI) phosphasalen complex as a dimer wherein one of the oxygen atoms of the ligand bridges the two 7-coordinate metal centres (Figure 5.3). The complex observed in the solid state, if it maintained its structure in solution, would likely exhibit two slightly different ^{31}P resonances due to the asymmetry of the ligand oxygens. Thus, this structure is tentatively assigned to the signals observed at δ 23.0 and δ 25.4. As presented in chapter 2, the uranium(IV) complex can be isolated as the THF adduct $LUCl_2(THF)$. Therefore, the signal at δ 24.2 in THF-d_8 is likely $LU(O)_2(THF)$. A dimeric complex similar to $[LU^{VI}(O)_2]_2$ was obtained upon heating $LU^{IV}Cl_2(THF)$ to reflux in benzene, which afforded $LU^{IV}Cl(\mu–Cl)]_2$, along with concurrent loss of THF (Figure 5.3). The two dimeric phosphasalen complexes $[LU^{VI}(O)_2]_2$ and $[LU^{IV}Cl(\mu–Cl)]_2$ share many similarities (Figure 5.3, Table 5.2). In both complexes, the uranium atoms exhibit distorted pentagonal bipyramidal geometry. The difference between the coordinated phosphinimine P–N distances is not statistically significant ($[LU^{IV}Cl(\mu–Cl)]_2$: P1–N1 = 1.619(6) Å; $[LU^{VI}(O)_2]_2$: P1–N1 = 1.612(5) Å). The uranium–uranium distance in $[LU^{IV}Cl(\mu–Cl)]_2$ is 4.4929(4) Å, compared to 3.9674(5) Å in $[LU^{VI}(O)_2]_2$ and the $U^{IV}–Cl–U^{IV}$ angle of 105.83(4)° is slightly smaller than the $U^{VI}–O–U^{VI}$ angle of 108.4(2)°. Therefore, with both the phosphasalen and phosphazidosalen ligand systems we see direct structural analogies between the U(IV) dichloride species and U(VI) oxo complexes.

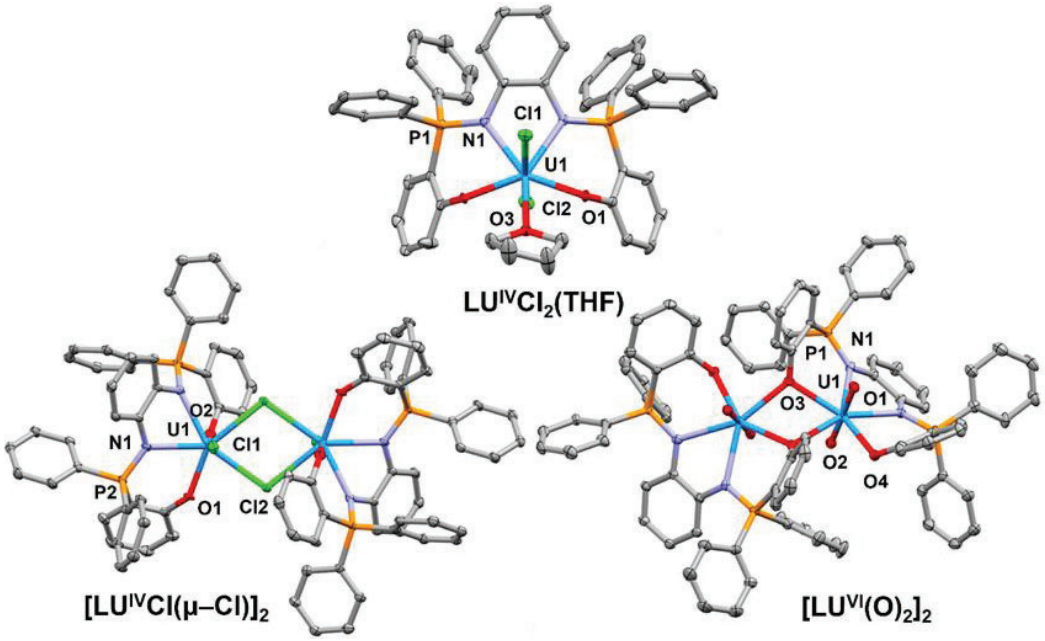

Figure 5.3. X-ray crystal structures of $[LUCl(\mu\text{–}Cl)]_2$, $[LU(O)_2]_2$ and $LUCl_2(THF)$. The $LUCl_2(THF)$ structure is not of sufficient quality to discuss metrical parameters and is only used to determine atom connectivity. Thermal ellipsoids are drawn at 30% probability. Hydrogens have been removed for clarity.

Table 5.2. Selected bond distances (Å) and angles (°) for $[LU^{VI}(O)_2]_2$ and $[LU^{IV}Cl(\mu\text{–}Cl)]_2$

Parameter	$[L^{VI}U(O)_2]$	$[LU^{IV}Cl(\mu\text{–}Cl)]_2$
Bond Distance (Å)		
U1–O1	1.793(4)	2.197(4)
U1–O2	1.780(5)	2.160(4)
U1–Cl1	-	2.630(2)
U1–Cl2	-	2.809(1)
U1–O7	2.457(5)	-
U1–N1	2.486(5)	2.452(5)
P1–N1	1.612(5)	1.619(6)
Bond Angle (°)		
O1–U1–O2	178.1(2)	86.9(1)
U1–O3–U2	108.4(2)	-
O3–U1–O4	145.6(2)	-
C11–U1–Cl2	-	74.17(4)
Cl1–U1–O2	-	166.4(1)

5.1.3. Future Work – Towards U(VI) Oxo Chloride Complexes

Intriguingly, the presence of $LU(O)_2(THF)$ in the THF-d_8 solution of $L''U(O)_2$ suggests that N_2 loss from the U(VI) phosphazidosalen complex is faster than in the $L''UCl_2$ analogue. The difference in ionic radii between the two oxidation states (6-coordinate U(IV) = 0.89 Å; 6-coordinate U(VI) = 0.73 Å)[6], as well as the effect of the oxo vs. chloro ligands, should impact the ability of the phosphazide groups to *cis*-isomerize, which is required for N_2 extrusion. An in-depth study of the stability of the two complexes, with respect to nitrogen evolution, should be pursued in the future with an expert computational collaborator.

The addition of $U(O)_2Cl_2(THF)_3$ to KL_{PN3} would give a U(VI) oxo chloride complex within our pyrrole-based diphosphazide ligand system. A complex such as $L_{PN3}U(O)_2Cl$ would be an interesting candidate to explore for chemical reduction to U(V) species with a reagent such as KC_8, as the chloride ligand would permit facile elimination of KCl and C_8 to provide the 7-coordinate U(V) complex $L_{PN3}U^{V}(O)_2$ (Scheme 5.2).

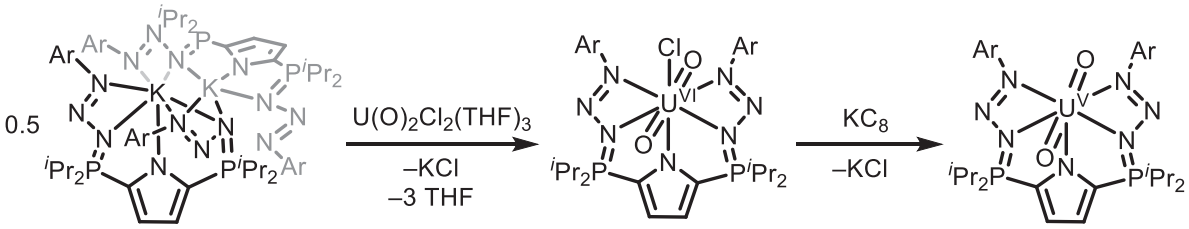

Scheme 5.2. Proposed synthesis of a U(V) diphosphazide complex

5.2. Cationic Thorium Alkyl Complexes

5.2.1. Background

Cationic metal centres have been shown to display greater reactivity than their neutral counterparts, as they are often more electrophilic and contain an open site for a molecule/ion to coordinate.[7] Cationic metal centres can mediate polymerization of alkenes and heterocyclic ethers.[8-9] Alkyl group abstraction, by way of reaction with a Lewis acid, such as $B(C_6F_5)_3$, or by cation exchange with a reagent such as $[CPh_3][B(C_6F_5)_4]$, are common methods for the production of metal cations.[7] While cationic transition metal complexes are common,[10] non-aqueous actinide cations are rare. The Cheng group reported a series of trialkyl thorium species similar to $L_{PN3}Th(CH_2SiMe_3)_3$ that are active isoprene polymerization catalysts upon the addition of 2 equivalents of $[CPh_3][B(C_6F_5)_4]$.[11] The active species were not isolated, but were presumed to be monoalkyl dicationic thorium species. Additionally, the Emslie group has made a series of cationic thorium complexes featuring their dianionic xanthene-based ligand XA_2 [XA_2 = 4,5-bis(2,6-diisopropylanilido)-2,7-di-tert-butyl-9,9-dimethylxanthene].[12-13] Reaction of $(XA_2)Th(R)_2$ (R = CH_2SiMe_3 or CH_2Ph) with $[CPh_3][B(C_6F_5)_4]$ in benzene or toluene allowed for the isolation of arene-coordinated cations, such as $[(XA_2)Th(CH_2SiMe_3)(\eta^6\text{-arene})][B(C_6F_5)_4]$ (arene = C_6H_6 and toluene) and $[(XA_2)Th(\eta^2\text{-}CH_2Ph)(\eta^6\text{-}C_6H_5Me)][B(C_6F_5)_4]$.[12] In contrast, reaction of $[(XA_2)Th(CH_2Ph)_2]$ with 2 equivalents of $B(C_6F_5)_3$ resulted in, to my knowledge, the only example of an isolated non-aqueous thorium dication $[(XA_2)Th][PhCH_2B(C_6F_5)_3]_2$.[13] Unfortunately, these large ion-pairs can be difficult to characterize, as they often tenaciously retain solvent, rendering them oily in nature. In addition, they typically have low solubility in common hydrocarbon and aromatic solvents.

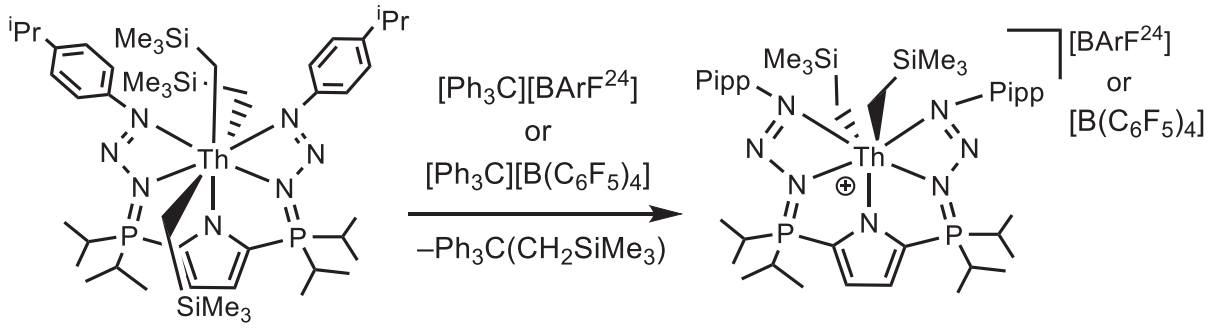

$BArF^{24} = B(C_6H_3(CF_3)_2)_4$

Scheme 5.3. Synthesis of a thorium diphosphazide cation

Furthermore, the open coordination site generated by ligand abstraction can increase fluxionality in solution resulting in broad NMR signals. This open coordination site promotes high catalytic activity by allowing easier coordination of the substrate,[7-8, 14] so the use of Lewis basic solvents (such as THF, dme and acetonitrile) can be deleterious to this chemistry. With this in mind, it was postulated that the numerous nitrogen donors of the L_{PN3} diphosphazide ligand system might render it possible to isolate a soluble, base-free alkylthorium cation, and potentially an alkylthorium dication.

5.2.2. Synthesis of Alkylthorium Cations and Evidence for a Thorium Dication

Addition of $B(C_6F_5)_3$ to $L_{PN3}Th(CH_2SiMe_3)_3$ in benzene-d_6 resulted in a shift in the single $^{31}P\{^1H\}$ NMR resonance from δ 49.4 to δ 66.1. Noteably, while the $^{31}P\{^1H\}$ NMR spectrum indicated a single product, the alkyl region had many peaks that do not correlate with the predicted product $[L_{PN3}Th(CH_2SiMe_3)_2][(Me_3SiCH_2)B(C_6F_5)_3]$. It is possible that a single methide group was abstracted instead of the entire CH_2SiMe_3 group. Methide abstraction from a CH_2SiMe_3 group is not unfounded, and usually leads to silyl group migration, creating a $CH_2SiMe_2CH_2SiMe_3$ substituent.[15-17] However, the alkyl region did

not match up predictably with a $CH_2SiMe_2CH_2SiMe_3$ group, so the product cannot be clearly assigned at this stage. However, it appears that reaction of $L_{PN3}Th(CH_2SiMe_3)_3$ with $[CPh_3][B(C_6F_5)_4]$ or $[CPh_3][B(C_6H_3(CF_3)_2)_4]$ allowed for complete abstraction of the entire CH_2SiMe_3 group (Scheme 5.3). The complex $[L_{PN3}Th(CH_2SiMe_3)_2][B(C_6F_5)_4]$ is stable at ambient temperature in benzene-d_6 or toluene for several days and can be isolated as an oily solid when taken into Et_2O and the volatiles removed. The ^{1}H NMR spectrum shows the expected cationic resonances for $[L_{PN3}Th(CH_2SiMe_3)_2]^+$, with the signals at δ –0.17 and δ 0.39 assigned to $Si(CH_3)_3$ and $Th–CH_2$ respectively. There does not appear to be tight coordination of a solvent toluene molecule, as there are no resonances associated with a coordinated arene. Residual peaks assigned to $Me_3SiCH_2CPh_3$ can be seen in the ^{1}H NMR spectrum, which presumably was not fully removed with multiple heptane washes. Unfortunately, neither crystals of $[L_{PN3}Th(CH_2SiMe_3)_2][B(C_6H_3(CF_3)_2)_4]$ nor $[L_{PN3}Th(CH_2SiMe_3)_2][B(C_6F5)_4]$ were obtained.

Upon addition of 2 equivalents of $[CPh_3][B(C_6H_3(CF_3)_2)_4]$ to $L_{PN3}Th(CH_2SiMe_3)_3$ in benzene-d_6, the NMR spectra revealed only $[L_{PN3}Th(CH_2SiMe_3)_2][B(C_6H_3(CF_3)_2)_4]$ in solution after 2 hours. However, after 24 hours, all of the signals in the ^{1}H NMR spectrum had become extremely broad, and a ^{31}P NMR chemical shift could not be found. This suggests that a fluxional thorium dication could exist; however, characterization of this species would likely prove quite difficult. Intruigingly, these broad resonances do not appear when only 1 equivalent of $[CPh_3][B(C_6H_3(CF_3)_2)_4]$ is employed, lending further evidence to a dication.

5.2.3. CO_2 Insertion into a Thorium Alkyl Cation

When a solution of $[L_{PN3}Th(CH_2SiMe_3)_2][B(C_6F_5)_4]$ in benzene-d_6 was exposed to CO_2, the $^{31}P\{^1H\}$ NMR resonance at δ 64.0 was supplanted by a new signal at δ 63.3. The CH_2 resonance moved downfield from δ 0.42 to δ 1.51, as expected upon CO_2 insertion into each of the remaining two Th–CH_2SiMe_3 bonds. Overall, the NMR spectra of $[L_{PN3}Th(\kappa^2\text{-}O_2CCH_2SiMe_3)_2][B(C_6F_5)_4]$ is highly similar to that of $L_{PN3}Th(\kappa^2\text{-}O_2CCH_2SiMe_3)_3$.

5.2.4. Future Work – Towards Cationic Thorium Polymerization Catalysts

The structural characterization of the ion pairs $[L_{PN3}Th(CH_2SiMe_3)_2][B(C_6F_5)_4]$ and $[L_{PN3}Th(CH_2SiMe_3)_2][B(C_6H_3(CF_3)_2)_4]$ is of fundamental interest. Therefore, further attempts to crystallize these complexes is needed, perhaps using different crystallization methods and mixed solvent systems. Additionally, the formation of these cations in Lewis basic solvents (THF or pyridine) could be explored, to see if the phosphazide groups would prevent exogenous base coordination.

When one equivalent of an amine such as H_2NAd is added to the cation, it is hypothesized that one of four things will occur: 1) the neutral amine would coordinate to the cationic centre creating $[L_{PN3}Th(CH_2SiMe_3)_2(NH_2Ad)]^+$; 2) one equivalent of $SiMe_4$ would eliminate, leaving a mixed alkyl amido system, $[L_{PN3}Th(CH_2SiMe_3)(NHAd)]^+$; 3) the mixed alkyl amido system would then spontaneously eliminate a second equivalent of $SiMe_4$, resulting in a thorium imide, $[L_{PN3}Th{=}NAd]^+$; or 4) the alkyl amido cations could comproportionate leading to the diamido cation and dialkyl cations, $[L_{PN3}Th(CH_2SiMe_3)_2]^+$ and $[L_{PN3}Th(NHAd)_2]^+$. Preliminary results indicate that a single product is produced upon

the addition of either 1 or 2 equivalents of H_2NAd to $[L_{PN3}Th(CH_2SiMe_3)_2][B(C_6F_5)_4]$; however, more experiments are required to unambiguously establish the identity of the product in this reaction.

Finally, polymerization experiments using these cations and potential dications should be investigated. It is advised to begin with isoprene polymerization in the same manner that the Cheng group reported, as there is precedent for high activity and their performance can be directly compared to those alkylthorium cations and dications.

5.3. Th(IV) and U(IV) Pincer Complexes with a Bisphosphinimine Pyrrole Ligand

5.3.1. Background

The Hayes group has employed *NNN*-monoanionic pyrrole-based ligands as a supporting scaffold for a number of different metals. Notably, base-stabilized rhodium silylenes $L_{P=N}Rh(SiPh_2)(CO)$ and $L_{P=N}Rh(SiHPh)(CO)$, and borylene $L_{P=N}Rh(BMes)(CO)$, were isolated.[18-19] In each of these species one of the phosphinimine donors stabilized the Lewis acidic silicon or boron atom in excellent examples of metal-ligand cooperation.[18-19] The ligand $L_{P=N}$ contains Pipp groups on nitrogen and isopropyl substituents on phosphorus, but these can be easily fine-tuned to alter the electronic and steric properties of the ligand. For example, a series of aluminum, indium and gallium complexes bearing $L_{P=N}$ ligand variants that feature Mes and Dipp groups on nitrogen were synthesized.[20] Finally, a rhodium(I) complex capable of alkene hydrogenation used a variant of $L_{P=N}$ that contained phenyl units on phosphorus; this proved to be advantageous as a stabilizing interaction exists between one of the phenyl rings and the two rhodium atoms in the dinuclear resting state of the catalyst.[21] Therefore, a series of thorium and uranium

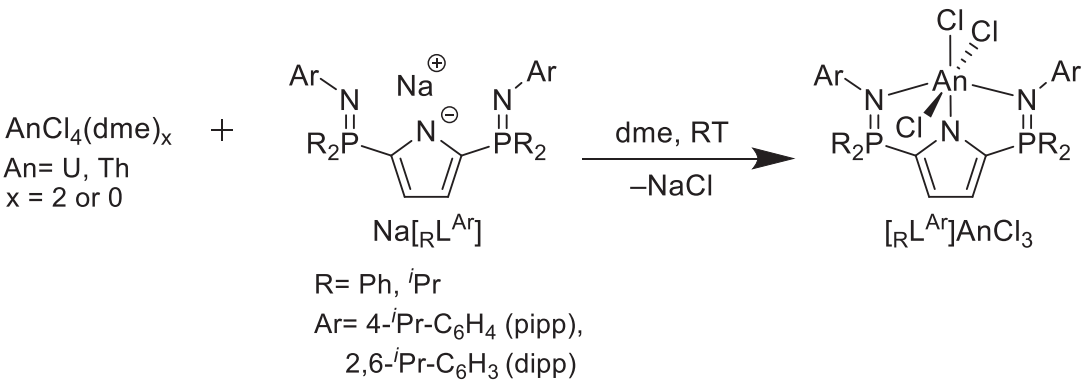

Scheme 5.4 Synthesis of a series of uranium(IV) and thorium (IV) pincer complexes

complexes with variation of the substituents at nitrogen and phosphorus were prepared, and their structural and spectral differences assessed. For clarity, for the remainder of this chapter, the ligands will be referred to as [$_{R}L^{Ar}$], with R indicating the functional groups at phosphorus and Ar representing those on nitrogen.

5.3.2. Synthesis of Th(IV) and U(IV) Pincer Complexes

The ligands $_{R}L^{Ar}$ (R = Ph, ^{i}Pr; Ar = Pipp, Dipp) were used to create five uranium(IV) and thorium(IV) complexes, including [$_{iPr}L^{Pipp}$]$ThCl_3$, as featured in chapter 3 (Scheme 5.4). The sodium salts Na[$_{R}L^{Ar}$] were utilized to transfer the ligand to an actinide metal *via* a salt metathesis reaction with either $ThCl_4(dme)_2$ or $UCl_4(dme)_x$ (x = 0 or 2). This process afforded five different 6-coordinate uranium and thorium trichloride pincer complexes. The complexes are all thermally stable for days at ambient temperature in solution. The uranium(IV) complexes [$_{iPr}L^{Pipp}$]UCl_3, [$_{Ph}L^{Pipp}$]UCl_3 and [$_{iPr}L^{Dipp}$]UCl_3 cannot be reasonably assigned a trend in ^{31}P NMR chemical shift, as the three paramagnetically shifted $^{31}P\{^{1}H\}$ NMR resonances are expectedly varied (δ –81.0, δ –127.4, δ –83.2, respectively in THF-d_8). The $^{31}P\{^{1}H\}$ and ^{1}H resonances for [$_{iPr}L^{Dipp}$]UCl_3 are extremely broad in comparison to the other uranium complexes. Such broadness may be due to

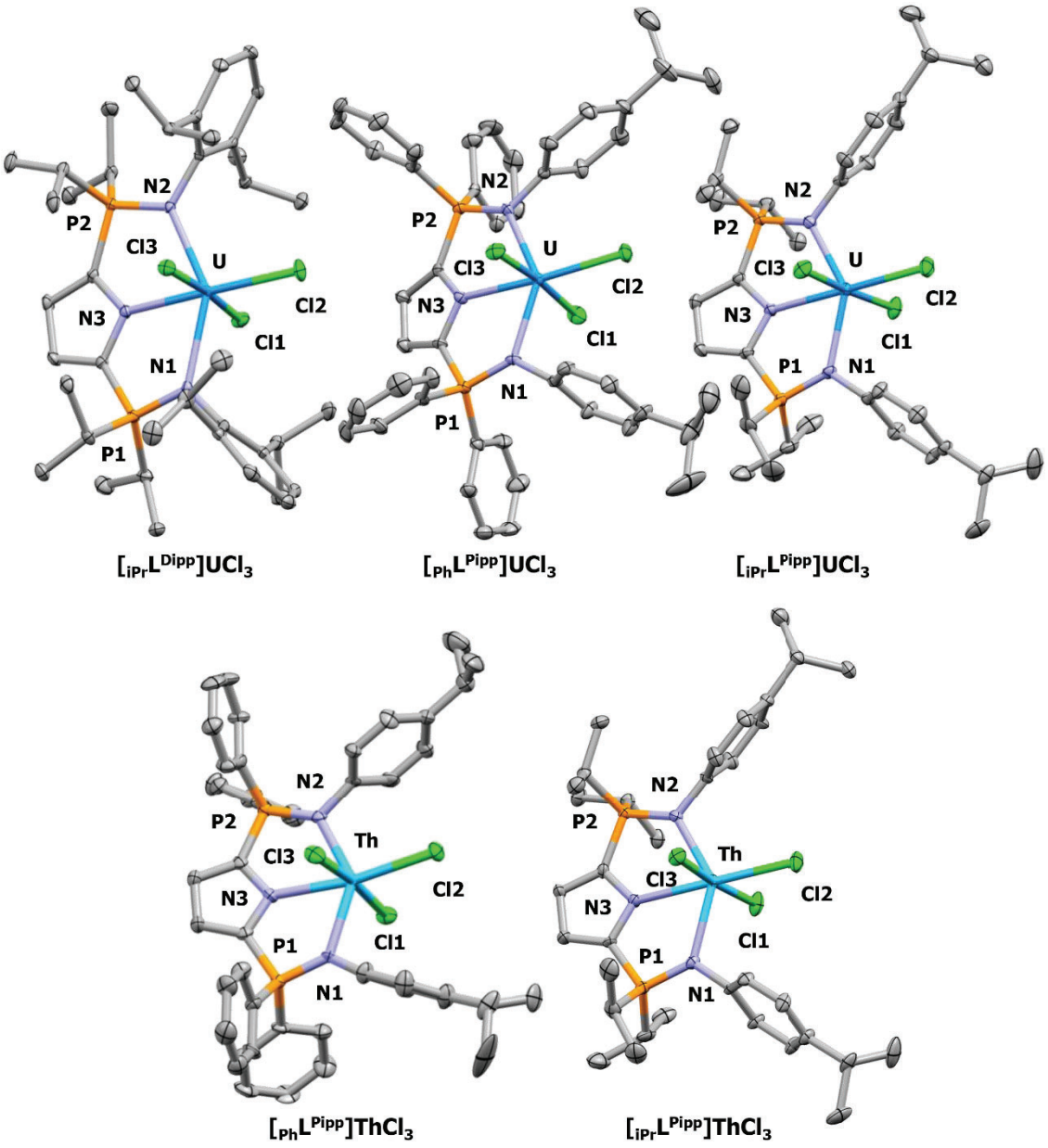

Figure 5.4 X-ray crystal structures of uranium(IV) and thorium(IV) pincer complexes. Thermal ellipsoids are drawn at 50% probability. Hydrogens have been removed for clarity.

dechelation of the phosphinimine nitrogens in solution. The $^{31}P\{^{1}H\}$ chemical shift for $[_{Ph}L^{Pipp}]ThCl_3$ is δ 35.8 which is upfield of that found for $[_{iPr}L^{Pipp}]ThCl_3$ (δ 54.3 in THF-d_8), and consistent with the trend observed for PPh_2 vs. P^iPr_2 groups in ^{31}P NMR spectroscopy.

5.3.3. X-Ray Crystal Structure Comparisons

Table 5.3 Selected bond distances (Å) and angles (°) for $[^{iPr}L^{Pipp}]UCl_3$, $[^{Ph}L^{Pipp}]UCl_3$, $[^{iPr}L^{Dipp}]UCl_3$, $[^{Ph}L^{Pipp}]ThCl_3$ and $[^{iPr}L^{Pipp}]ThCl_3$

Parameter	$[^{iPr}L^{Pipp}]UCl_3$	$[^{Ph}L^{Pipp}]UCl_3$	$[^{iPr}L^{Dipp}]UCl_3$	$[^{Ph}L^{Pipp}]ThCl_3$	$[^{iPr}L^{Pipp}]ThCl_3$
Space Group	$P2_1/c$	$Pca2_1$	$P2_1/n$	$Pca2_1$	$P2_1/c$
Bond Distance (Å)					
M–Cl1 (Å)	2.6172(9)	2.623(2)	2.6117(7)	2.685(3)	2.687(1)
M–Cl2 (Å)	2.632(1)	2.623(2)	2.6263(8)	2.688(2)	2.699(1)
M–Cl3 (Å)	2.6286(9)	2.611(2)	2.5969(7)	2.673(2)	2.689(1)
M–N1 (Å)	2.344(3)	2.327(5)	2.441(2)	2.364(5)	2.378(3)
M–N3 (Å)	2.415(3)	2.404(6)	2.365(2)	2.481(9)	2.474(4)
P1–N1 (Å)	1.626(3)	1.627(5)	1.649(2)	1.623(6)	1.635(4)
Bond Angle (°)					
Cl1–M–Cl3 (°)	175.72(3)	175.00(6)	175.42(3)	173.89(7)	174.34(4)
N1–M–N2 (°)	138.32(9)	138.5(2)	142.82(7)	135.5(2)	135.2(1)

X-ray crystal structures were collected for $[^{iPr}L^{Pipp}]UCl_3$, $[^{Ph}L^{Pipp}]UCl_3$, $[^{iPr}L^{Dipp}]UCl_3$ and $[^{Ph}L^{Pipp}]ThCl_3$ and compared to the previously reported $[^{iPr}L^{Pipp}]ThCl_3$ (Figure 5.4). The complexes are isostructural, but they crystallized in different space groups, depending on the ligand that was present (Table 5.3). The complexes all feature pseudo-octahedral geometry, with the N3–M–Cl2 and Cl1–M–Cl3 angles close to 180°. The Th–N and Th–Cl bond lengths are consistently longer than the U–N and U–Cl bonds, in accordance with the difference in ionic radii of the two metals (6-coordinate Th(IV) = 0.94 Å; 6-coordinate U(IV) = 0.89 Å).[6] Notably, $[^{iPr}L^{Dipp}]UCl_3$ is the only complex in which the M–N1 and M–N2 bonds are longer than the distance between uranium and the central pyrrole nitrogen (M–N3). Additionally, the phosphinimine P–N bonds in $[^{iPr}L^{Dipp}]UCl_3$ are longer than in the other complexes by about 0.2 Å. The ligands all provide a planar coordination environment, with the metal, pyrrole ring, P1, P2, N1, N2 and Cl2 forming a plane.

5.3.4. Cationic Pincer Complexes

As mentioned in section 5.2, cationic complexes contain an open coordination site that is often filled when the cation is exposed to a Lewis-basic solvent. When Na[BArF^{24}] or [CPh$_3$][BArF^{24}] was added to [$_{iPr}$L^{Pipp}]ThCl$_3$ in dme or [$_{iPr}$L^{Pipp}]UCl$_3$ in THF, the cationic complexes [($_{iPr}$L^{Pipp})ThCl$_2$(dme)][BArF^{24}] and [($_{iPr}$L^{Pipp})UCl$_2$(THF)][BArF^{24}], respectively, were produced, as confirmed by X-ray crystallography (Scheme 5.5, Figure 5.5). The structure of [($_{iPr}$L^{Pipp})UCl$_2$(THF)][BArF^{24}] is of too poor quality to discuss metrical parameters; however, [($_{iPr}$L^{Pipp})ThCl$_2$(dme)][BArF^{24}] is similar to [$_{iPr}$L^{Pipp}]ThCl$_3$. The solid-state structure reveals [($_{iPr}$L^{Pipp})ThCl$_2$(dme)][BArF^{24}] has a 7-coordinate thorium centre with a dme molecule coordinated to thorium through both oxygens (Figure 5.5, right). The Th–N1 distance in [($_{iPr}$L^{Pipp})ThCl$_2$(dme)][BArF^{24}] (Th–N1 = 2.421(8) Å) is longer than that in [$_{iPr}$L^{Pipp}]ThCl$_3$ (Th–N1 = 2.378(3)Å); however, the Th–N3 distance is shorter (2.433(6) vs. 2.474(4) Å). The Th–Cl bond lengths are similar between [($_{iPr}$L^{Pipp})ThCl$_2$(dme)][BArF^{24}] and [$_{iPr}$L^{Pipp}]ThCl$_3$ (Table 5.4).

When either [($_{iPr}$L^{Pipp})ThCl$_2$(dme)][BArF^{24}] or [($_{iPr}$L^{Pipp})UCl$_2$(THF)][BArF^{24}] is left in THF-d_8 at ambient temperature for more than 12 hours, the solvent in the NMR tube polymerizes. Unsurprisingly, the solubility of these complexes in non-Lewis basic solvents

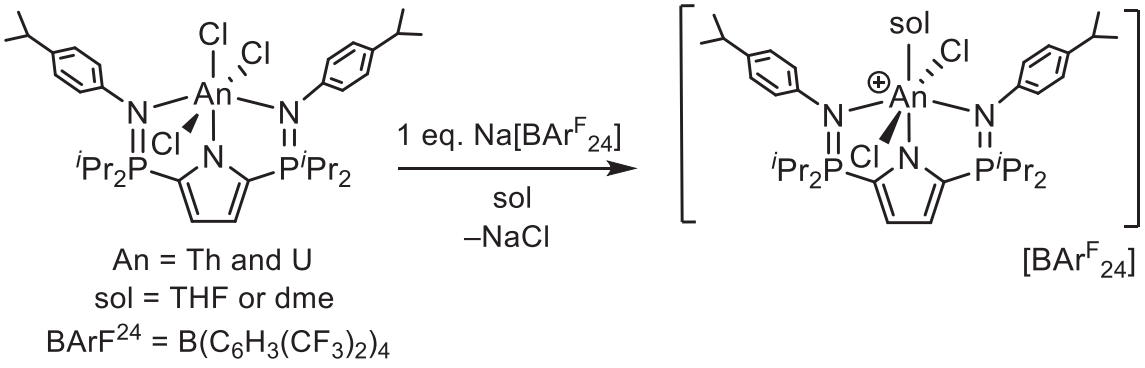

Scheme 5.5 Synthesis of a uranium(IV) and thorium(IV) pincer cation

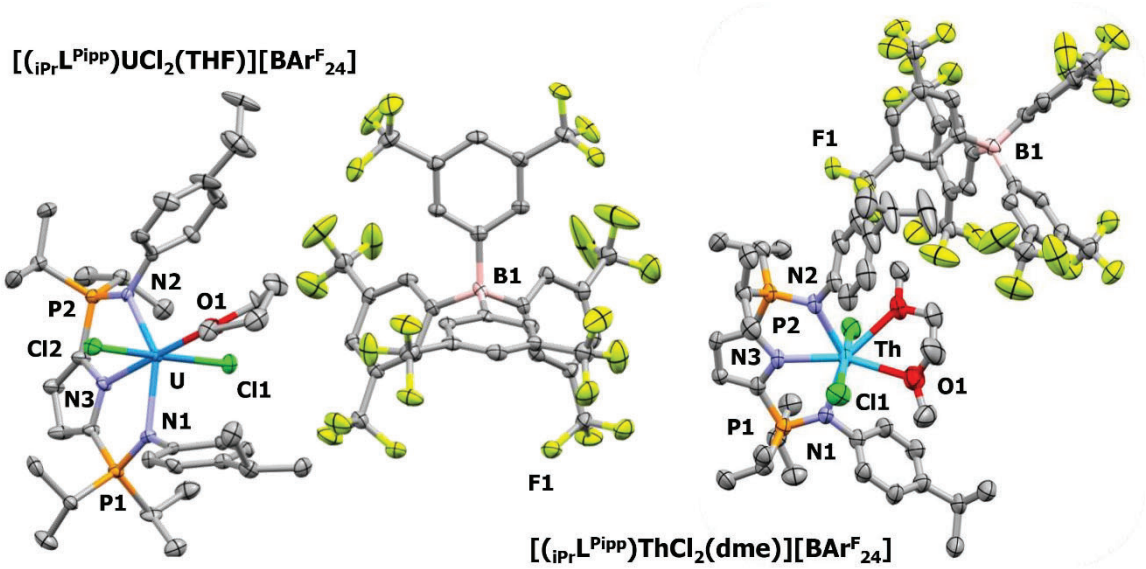

Figure 5.5 X-ray crystal structures of $[(_{iPr}L^{Pipp})UCl_2(THF)][BArF^{24}]$ and $[(_{iPr}L^{Pipp})ThCl_2(dme)][BArF^{24}]$. Thermal ellipsoids are drawn at 50% probability. Hydrogens have been removed for clarity.

Table 5.4 Selected bond distances (Å) and angles (°) for $[(_{iPr}L^{Pipp})ThCl_2(dme)][BArF^{24}]$ and $[_{iPr}L^{Pipp}]ThCl_3$

Parameter	$[(_{iPr}L^{Pipp})ThCl_2(dme)][BArF^{24}]$	$[_{iPr}L^{Pipp}]ThCl_3$
Space Group	P-1	$P2_1/c$
Bond Distance (Å)		
Th–Cl1 (Å)	2.680(2)	2.687(1)
Th–Cl2 (Å)	2.679(2)	2.699(1)
Th–Cl3 (Å)	-	2.689(1)
Th–N1 (Å)	2.421(8)	2.378(3)
Th–N3 (Å)	2.433(6)	2.474(4)
P1–N1 (Å)	1.624(7)	1.635(4)
Th–O1 (Å)	2.639(8)	-
Th–O2 (Å)	2.599(6)	-
Bond Angle (°)		
Cl1–Th–Cl3 (°)	-	174.34(4)
Cl1–Th–Cl2 (°)	173.19(9)	87.02(4)
N1–Th–N2 (°)	136.6(2)	135.2(1)

is minimal and they are oils in aromatic hydrocarbon solvents. Unfortunately, attempts to crystallize these complexes in bromobenzene, benzene or toluene were unsuccessful. The

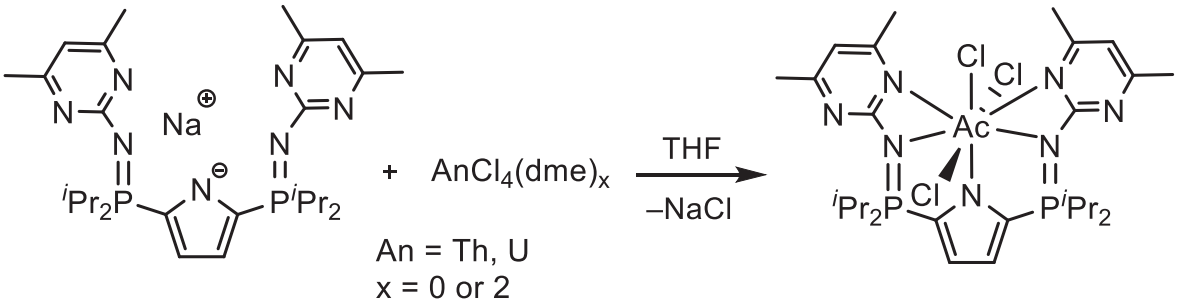

Scheme 5.6 Synthesis of a uranium(IV) and thorium(IV) complex with internal lewis-bases

solution state NMR spectra exhibit extremely broad peaks when $[CPh_3][B(C_6F_5)_4]$ is added to $[_{iPr}L^{Pipp}]ThCl_3$ or $[_{iPr}L^{Pipp}]UCl_3$ in benzene-d_6 or bromobenzene-d_5. Future investigations are needed to determine if there is solvent arene coordination.

5.3.5. Future Work – Towards Base-free Cationic Actinide Complexes

It was theorized that internal Lewis bases incorporated into the ligand could allow for solvent-free cation formation, even when such cations are formed in Lewis basic solvents, such as THF or dme. Therefore, a ligand previously synthesized in the Hayes lab that features 2,5-dimethylpyrimidine groups at nitrogen[22] was considered for complexation with uranium and thorium. The complexes $[_{iPr}L^{Pyr}]UCl_3$ and $[_{iPr}L^{Pyr}]ThCl_3$ were made in the same manner as the previously described pincer complexes (Scheme 5.6). X-ray crystallography revealed 8-coordinate actinide complexes with the two pyrimidine groups coordinated to the metal through one nitrogens from each pyrimidine (Figure 5.6). The M–Cl bonds in $[_{iPr}L^{Pyr}]MCl_3$ are longer than those in $[_{iPr}L^{Pipp}]MCl_3$ and $[_{Ph}L^{Pipp}]MCl_3$ (M = Th and U) (*c.f.* Table 5.3 and Table 5.5). Structurally, the pyrimidine ligand $[_{iPr}L^{Pyr}]$ is comparable to L_{PN3} as they are both pentadentate ligands with all nitrogen donors. Intriguingly, the N1–C17–N5 angle in $[_{iPr}L^{Pyr}]UCl_3$ of 110.7(3)° is similar to the

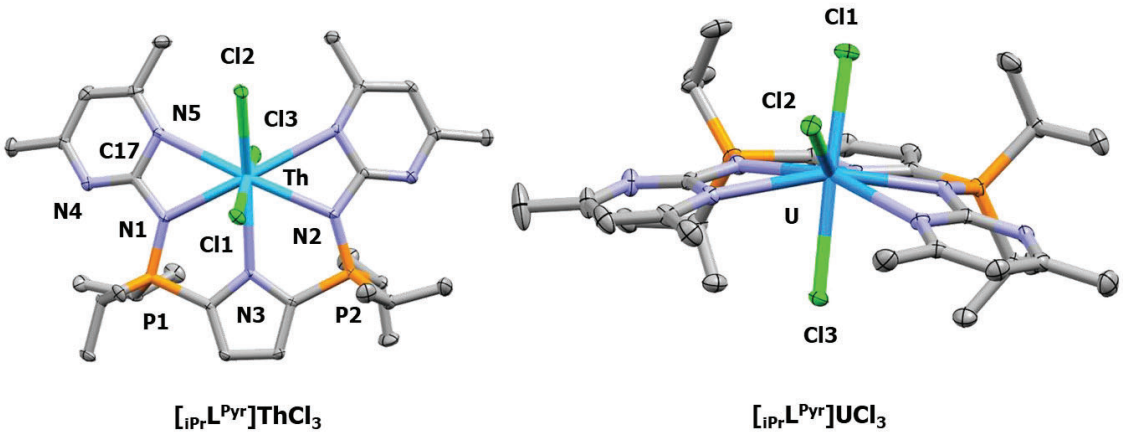

$[_{iPr}L^{Pyr}]ThCl_3$ $[_{iPr}L^{Pyr}]UCl_3$

Figure 5.6 X-ray crystal structures of $[_{iPr}L^{Pyr}]ThCl_3$ and $[_{iPr}L^{Pyr}]UCl_3$. Thermal ellipsoids are drawn at 50% probability. Hydrogens have been removed for clarity.

Table 5.5 Selected bond distances (Å) and angles (º) for $[_{iPr}L^{Pyr}]ThCl_3$ and $[_{iPr}L^{Pyr}]UCl_3$.

Parameter	$[_{iPr}L^{Pyr}]ThCl_3$	$[_{iPr}L^{Pyr}]UCl_3$
Space Group	P-1	$P2_1/c$
Bond Distance (Å)		
M–Cl1 (Å)	2.7277(7)	2.6399(9)
M–Cl2 (Å)	2.7073(9)	2.6993(8)
M–Cl3 (Å)	2.7148(8)	2.6766(9)
M–N1 (Å)	2.519(2)	2.463(3)
M–N3 (Å)	2.578(3)	2.515(3)
P1–N1 (Å)	1.626(3)	1.632(3)
M–N5 (Å)	2.707(3)	2.629(2)
Bond Angle (°)		
Cl1–M–Cl3 (°)	169.68(3)	165.82(3)
N1–M–N2 (°)	128.02(9)	131.57(9)
N1–C17–N5 (°)	111.1(3)	110.7(3)

phosphazide N1–N2–N3 angle of 107.1(3)° in $L_{PN3}UCl_3$. An ambient temperature solution state ^{1}H NMR spectum of $[_{iPr}L^{Pyr}]ThCl_3$ exhibited two distinct broad pyrimidine methyl resonances at δ 2.74 and δ 2.34, confirming that the pyrimidine nitrogens remain coordinated in solution. The reaction chemistry of these complexes should be studied in the

future by adding Na[BArF^{24}] to them in THF or dme to see if the coordinated pyrimidine nitrogens preclude the coordination of a solvent molecule.

5.4. Titanium(III) Coordination Complexes with Phosphazide Ligands

5.4.1. Background

Titanium as an element has many things in common with thorium. Both metals are earth abundant and are most commonly found in the +4 oxidation state.[23] Low valent titanium(III), however, behaves quite differently than either Th(IV) or Ti(IV). Titanium (III) is paramagnetic and readily undergoes 1-electron oxidation to return to Ti(IV). Nevertheless, the increased reactivity of the low-valent metal allows for diverse reaction chemistry. Homogeneous titanium catalysts have been shown to reduce N_2 to ammonia, usually by way of a Ti(III)-N_2 or *in situ* prepared Ti(II)-N_2 intermediate.[24] Titanium(III) complexes often bridge N_2 end-on when exposed to an atmosphere of dinitrogen.[25] When metal-coordinated phosphazides lose N_2, the nitrogen must necessarily do so within the coordination sphere of the metal. To date, there have been no examples of N_2 capture by a metal from the decomposition of a phosphazide complex. A stable Ti(III) phosphazide might provide an avenue for this unprecedented process, or at least a starting material for further reduction to Ti(II), if necessary.

5.4.2. Titanium(III) and U(IV) Diphosphazide Complexes

When $TiCl_3(THF)_3$ was combined with K_{LPN3} in dme, a dark green/blue solution was visible (Scheme 5.7). When left to crystallize from dme at –35 °C, X-ray quality crystals were obtained; diffraction experiments confirmed the identity of $L_{PN3}TiCl_2$ (Figure

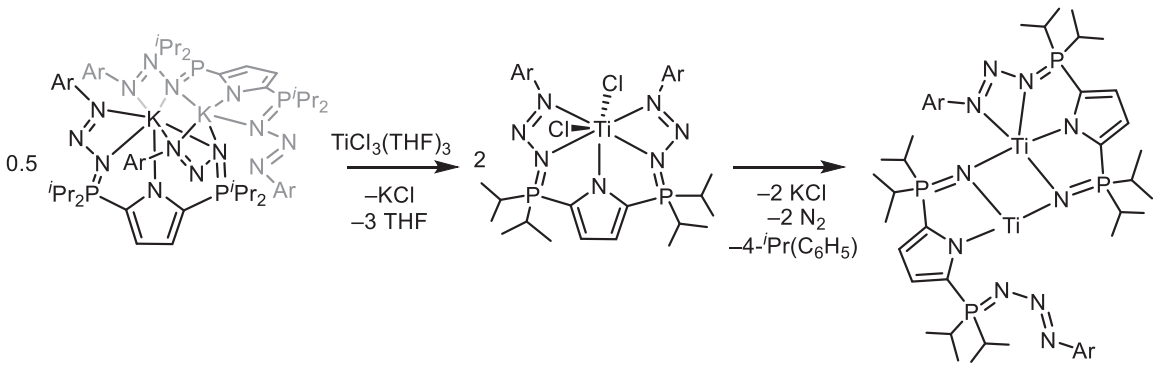

Scheme 5.7. Synthesis of a titanium(III) diphosphazide complex and its decomposition

5.7). Additionally, $L_{PN3}UCl_3$ crystals were also obtained in the same manner, and can be compared to $L_{PN3}TiCl_2$, as well as previously characterized $L_{PN3}ThCl_3$ (see chapter 3) (Figure 5.7). All three complexes, $L_{PN3}TiCl_2$, $L_{PN3}UCl_3$ and $L_{PN3}ThCl_3$, contain two phosphazide units coordinated to the metal centre *via* both the α- and γ-nitrogens. While the isostructural $L_{PN3}UCl_3$ and $L_{PN3}ThCl_3$ contain three chloride ligands which yields pseudo-hexagonal bipyramidal geometry at the metal centre, the seven-coordinate $L_{PN3}TiCl_2$ possesses a distorted pentagonal bipyramidal titanium. The N1–N2–N3 angles in $L_{PN3}TiCl_2$ (105.1(4)°) and $L_{PN3}UCl_3$ (107.1(3)°) are similar, but the N1–Ti–N6 angle of 104.3(2)° is significantly smaller than N1–U1–N6 (129.0(1)°), as there is one less chloride ligand, allowing the phosphazide γ-nitrogens to sit closer together (Table 5.6). The shorter metal–N1 and metal–N7 distances in $L_{PN3}TiCl_2$ (N1–Ti1 = 2.114(5) Å, N7–Ti1 = 2.168(5) Å; N1–U1 = 2.452(3) Å, N7–U1 = 2.562(3) Å) are likely a result of the smaller ionic radius of titanium compared to uranium (6-coordinate Ti(III) = 0.67 Å; 6-coordinate U(IV) = 0.89 Å; 8-coordinate U(IV) = 1.00 Å)[6]. The metal–N3 distance of 2.737(5) Å in $L_{PN3}TiCl_2$, however, is quite long and might not represent a meaningful interaction.

Notably, the titanium(III) centre does not have a coordinated dme or THF molecule, despite an excess of both in solution. This implies that the 7-coordinate environment around

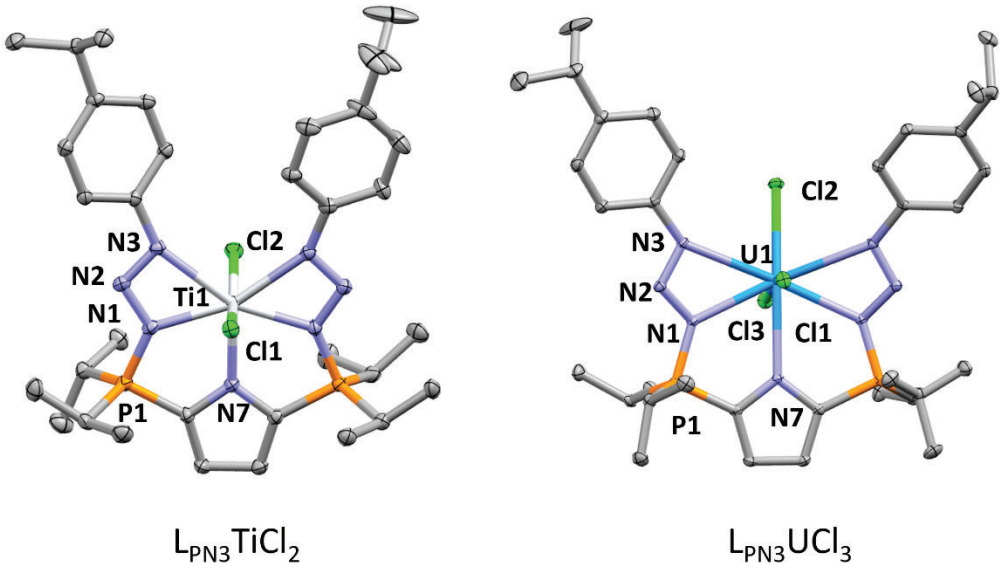

$L_{PN3}TiCl_2$ $L_{PN3}UCl_3$

Figure 5.7 X-ray crystal structures of $L_{PN3}TiCl_2$ and $L_{PN3}UCl_3$. Thermal ellipsoids are drawn at 50% probability. Hydrogens have been removed for clarity.

Table 5.6 Selected bond distances (Å) and angles (º) for $L_{PN3}TiCl_2$ and $L_{PN3}UCl_3$.

Parameter	$L_{PN3}TiCl_2$	$L_{PN3}UCl_3$
Bond Distance (Å)		
N1–M	2.114(5)	2.452(3)
N3–M	2.737(5)	2.760(3)
N7–M	2.168(5)	2.562(3)
Bond Angle (°)		
N1–N2–N3	105.1(4)	107.1(3)
N3–M–N6	104.3(2)	129.0(1)

titanium might only allow for ligands that are smaller than THF to fit in the binding pocket of the complex, such as N_2 or acetonitrile. An initial experiment in which an atmosphere of N_2 was added to a degassed solution of $L_{PN3}TiCl_2$ in dme caused an immediate colour change from blue/green to orange. Additional experiments (such as X-ray or IR analysis) are needed to confirm that this was due to N_2 complex formation and not accidental introduction of air or moisture. Unfortunately, NMR analysis of these titanium(III)

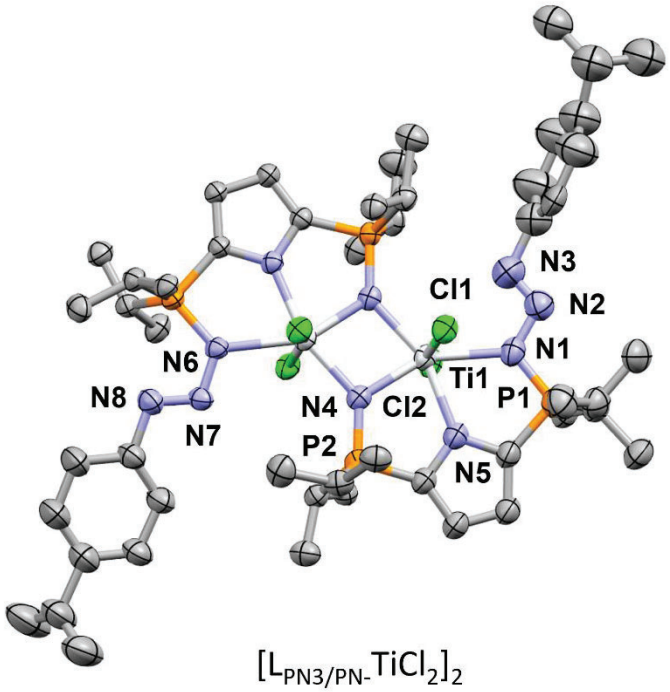

Figure 5.8 X-ray crystal structure of [$L_{PN3/PN-}TiCl_2$]$_2$. Thermal ellipsoids are drawn at 50% probability. Hydrogens have been removed for clarity.

complexes is exceedingly difficult due to their paramagnetism, and the spectra obtained were broad and uninformative. However, if multiple spectra of confirmed products were collected, a database of the paramagnetic spectra could be created to monitor changes in the composition of products in solution.

5.4.3. N_2 loss from Titanium(III) Diphosphazide Complex

A solution of $L_{PN3}TiCl_2$ in dme was heated at 80 °C for 10 minutes with stirring. The solution was then placed in a –35 °C freezer. X-ray diffraction studies on the resulting yellow/orange crystals revealed the structure as the Ti(IV) dimer [$L_{PN3/PN-}TiCl_2$]$_2$ ($L_{PN3/PN-}$ = 2-[(4-^{i}PrC$_6$H$_4$)N$_3$=P^{i}Pr$_2$]-5-(N=P^{i}Pr$_2$)N(C$_4$H$_2$)$_2^{2-}$) (Figure 5.8). Unfortunately, the X-ray data was not of sufficient quality to permit a detailed discussion of metrical parameters; however, atom connectivity can still be assessed. One of the aromatic groups on each ligand

has been lost, leaving an anionic phosphinimide. Hence, $1e^-$ oxidation from Ti(III) to Ti(IV) has occurred (Scheme 5.7). This conversion from phosphazide to phosphinimide is the first example of such a transformation by our group, and to our knowledge, has only been reported in one other instance.[26] Fryzuk and co-workers introduced $KBEt_3H$ to their Fe(II) phosphazide [$FeBr(EpN_3^{iPr,Me})(THF)$] ($EpN_3^{iPr,Me}$ = (2,6-$^i Pr_2C_6H_3$)N=C_5H_6[2-P$^i Pr_2N_3$(2,6-$Me_2C_6H_3$)]) in an attempt to make an iron(II) hydride, but instead isolated a dinuclear complex with bridging phosphinimido units [$Fe_2(EpN')_2$] (EpN' = (2,6-$^i Pr_2C_6H_3$)N=C_5H_6[2-P$^i Pr_2N^-$]).[26] Deuterium labelling experiments performed by Fryzuk *et al.* revealed that the elimination of N_2 and xylene (1,3-$Me_2C_6H_4$) likely proceeded *via* a radical pathway. It is currently unknown how the decomposition process that created [$L_{PN3/PN}$-$TiCl_2$]$_2$ occurred as there are no obvious hydride sources present. Accordingly, investigation into this mechanism is warranted for future studies, as this will provide valuable information on N_2 loss from phosphazides in these systems. The two remaining intact phosphazide groups in the structure are coordinated in a κ^1 fashion to titanium; one is in the *cis* conformation and the other is *trans* in the solid state.

5.4.4. Future Work – Towards N_2 Capture from a Coordinated Phosphazide

Unwanted oxidation of Ti(III) to Ti(IV) is an obstacle in the goal of N_2 capture from a coordinated phosphazide. Therefore, a milder method of inducing N_2 loss might be required, such as lower temperatures or UV irradiation. Additionally, reduction of $L_{PN3}TiCl_2$ with KC_8 might provide a better path to an N_2 complex *via* transient Ti(II). The ideal conditions for this unprecedented reactivity will likely require highly precise investigations (i.e. low temperature, mixed-solvent systems etc.).

5.5. Group 1 Phosphazide Complexes and Other Phosphazides

5.5.1. Background

Though metal-coordinated phosphazides are heavily featured in this thesis, they are only one of the many known effective phosphazide isolation strategies. Sterics, electronic effects, hydrogen bonding and cyclization have also been demonstrated to produce stable phosphazides, although it can be difficult to determine whether it is one or several of these factors that contribute to the overall stability of a given phosphazide.[27] Therefore, a systematic study of simple phosphazides, in which each of these variables can be independently assessed, is warranted. Notably, the phosphazide ligands in this thesis use potassium ions to stabilize the phosphazide. The large group 1 ion appears to be well-suited to stabilizing multiple phosphazides (*vide supra*). It is my hypothesis that the large ionic radius of the potassium ion (4-coordinate K^+ = 1.37 Å)[6] is a contributing factor to the stability of the group 1 phosphazide; therefore, a comparative study of isostructural K^+, Na^+ (4-coordinate Na^+ = 0.99 Å) and Li^+ (4-coordinate Li^+ = 0.59 Å) phosphazides, and their corresponding relative thermal stabilities, is of interest.[6]

5.5.2. *Cis* and *Trans* Aryl Phosphazides

In order to ascertain whether nearby hydrogen bonding would aid the isolation of a phosphazide in a simple system, a solution of $Ph_2P[(2\text{-}OH)C_6H_4]$ in toluene was added to a separate solution of Pipp–N_3. The $^{31}P\{^1H\}$ NMR spectrum of the reaction contained 3 resonances: one that corresponded to a small quantity of residual phosphine, a large signal at δ 18.59 (P=N) and a small peak at δ 28.88 ($P=N_3$). The integration of the resonances indicate a 3:1 ratio of phosphinimine to phosphazide. This large initial quantity of

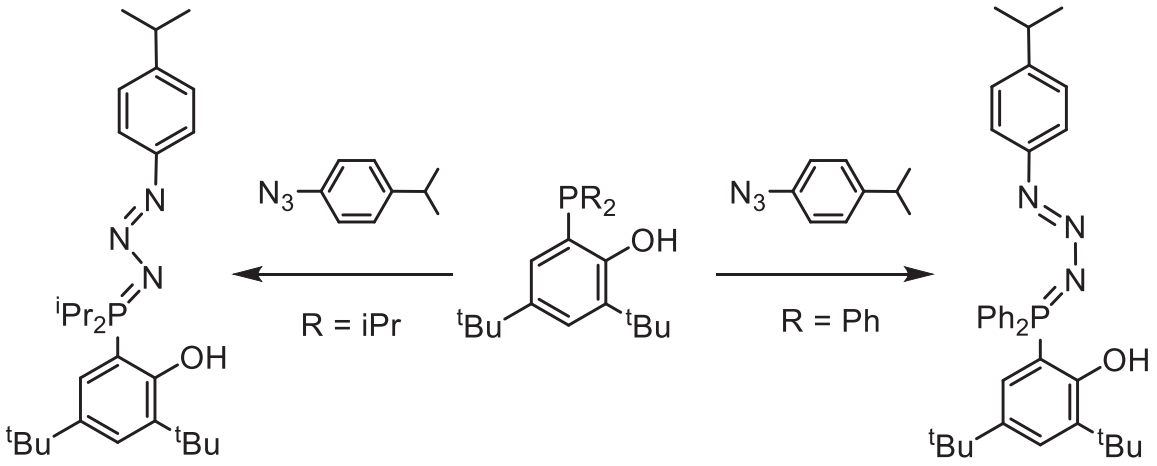

Scheme 5.8 Synthesis of *cis* and *trans* aryl phosphazides

phosphinimine implies that N_2 loss is facile in this system. Moreover, $Ph_2P[(2\text{-}NH_2)C_6H_4]$ and Pipp–N_3 afforded similar results. The isolation of phosphazides in this system is likely to be difficult and would require low temperature, if it is indeed possible at all. These results imply that hydrogen bonding alone may be insufficient to produce a stable phosphazide.

In order to determine if increased steric bulk allows for phosphazide isolation, a phosphine containing ^{t}Bu groups in the *meta*-positions of an aromatic substituent, $Ph_2P[(2\text{-}OH)(3,5\text{-}^t Bu)C_6H_2]$, was added to Pipp–$N_3$ (Scheme 5.8, right). Colourless crystals grew within 16 hours from pentane at –35 °C. The $^{31}P\{^1H\}$ NMR spectrum exhibited one major peak at δ 30.7, along with a few minor by-products. A broad OH resonance was observed at δ 15.00 in the ^1H NMR spectrum, which is far downfield for an alcohol, suggesting the existence of contact with the phosphazide moiety. X-ray data was collected on a poor-quality crystal, which established atom connectivity of this *cis*-phosphazide (Figure 5.9, left). For comparison purposes, $^i Pr_2P[(2\text{-}OH)(3,5\text{-}^t Bu)C_6H_2]$ was reacted with Pipp–N_3 in order to see if the steric bulk at phosphorus would affect the formation of the phosphazide (Scheme 5.8, left). Crystals grown from this reaction showed 95% purity by NMR spectroscopy: a $^{31}P\{^1H\}$ NMR resonance was observed at δ 59.8. The OH proton appears

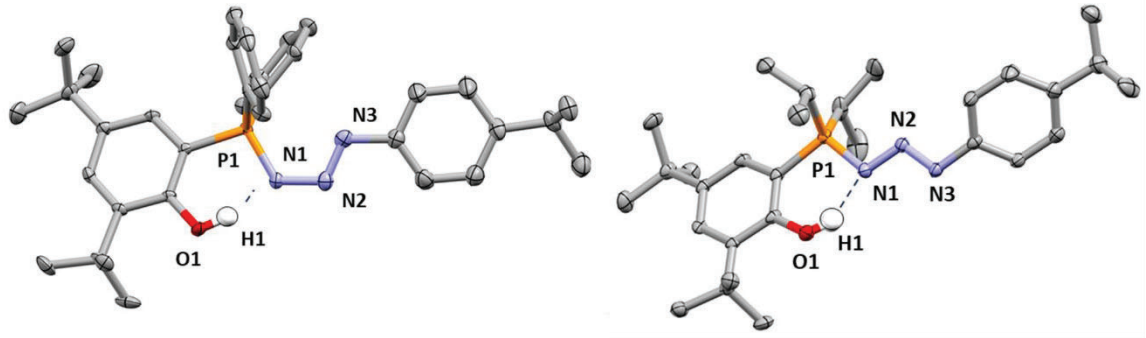

Figure 5.9 X-ray crystal structures of $Ph_2P[(2\text{-}OH)(3,5\text{-}^tBu)C_6H_2]$ and $^iPr_2P[(2\text{-}OH)(3,5\text{-}^tBu)C_6H_2]$. Thermal ellipsoids are drawn at 50% probability. Hydrogens, except for H1, have been removed for clarity.

Table 5.7 Selected bond distances (Å) and angles (º) for $^iPr_2P[(2\text{-}OH)(3,5\text{-}^tBu)C_6H_2]$ and cyclopyrrolazide.

Parameter	$^iPr_2P[(2\text{-}OH)(3,5\text{-}^tBu)C_6H_2]$	Cyclopyrrolazide
Bond Distance (Å)		
N1–N2	1.362(2)	1.327(4)
N2–N3	1.271(2)	1.281(3)
P1–N1	1.648(2)	1.657(3)
Bond Angle (°)		
N1–N2–N3	113.4(2)	117.4(2)

as a broad singlet in the ^1H NMR spectrum at δ 14.81 (Figure 5.9). The X-ray structure revealed a *trans*-phosphazide with an N1–N2–N3 angle of 113.4(2)° (Table 5.7). The intriguing change from a *cis*-phosphazide in $[(2\text{-}OH)(3,5\text{-}Bu)C_6H_2]Ph_2P{=}N_3(Pipp)$ to a *trans*-phosphazide in $[(2\text{-}OH)(3,5\text{-}^tBu)C_6H_2]^iPr_2P{=}N_3(Pipp)$ is likely a consequence of either an electronic effect or steric effect imposed by the phenyl vs. the isopropyl groups on phosphorus.

5.5.3. Group 1 Phosphazides

Addition of $LiCH_2SiMe_3$, NaH or KH to $^iPr_2P[(2\text{-}OH)(3,5\text{-}^tBu)C_6H_2]$ in THF resulted in deprotonation of the OH group and production of a series of group 1 metal salts.

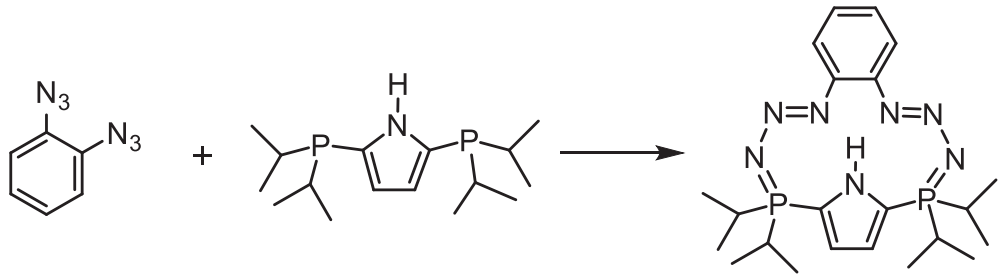

Scheme 5.9 Synthesis of a cyclic *cis*-diphosphazide

When $^{i}Pr_2P[(2\text{-}OK)(3,5\text{-}^{t}Bu)C_6H_2]$ was added to N_3–Pipp in pentane, crystals grew from the cold (–35 °C) yellow solution over the course of 16 hours. The $^{31}P\{^{1}H\}$ NMR spectrum contained a single peak at δ 51.8. While an X-ray crystallography study has yet to be conducted, the similar ^{31}P NMR resonance to that of $[(2\text{-}OH)(3,5\text{-}^{t}Bu)C_6H_2]^{i}Pr_2P{=}N_3$(Pipp) suggests that the product is indeed a stabilized phosphazide. Combination of one equivalent of 18-crown-6 with $[(2\text{-}OK)(3,5\text{-}^{t}Bu)C_6H_2]^{i}Pr_2P{=}N_3$(Pipp) resulted in immediate effervescence. The $^{31}P\{^{1}H\}$ NMR spectrum broadened dramatically and shifted to δ 52.7. The ^{i}Pr methine resonance shifted downfield from δ 2.84 to δ 3.67 in the ^{1}H NMR spectrum. Intriguingly, despite the confidence with which this $^{31}P\{^{1}H\}$ resonance has been assigned to the phosphinimine (due to the vigorous bubbling observed) this is the only example in which the phosphinimine resonance has been observed at a frequency that is downfield of the analogous phosphazide. If the series of group 1 phosphazides can be isolated, a study of their solution-state stability is warranted.

5.5.4. Cyclopyrrolazide Ligand

In order to make a cyclic phosphazide, 1,2-diazidobenzene was coupled with diphosphine $2,5\text{-}(^{i}Pr_2P)_2NH(C_4H_2)$ in toluene (Scheme 5.9). No bubbling was observed and small yellow needles immediately precipitated from solution. The NH ^{1}H NMR resonance

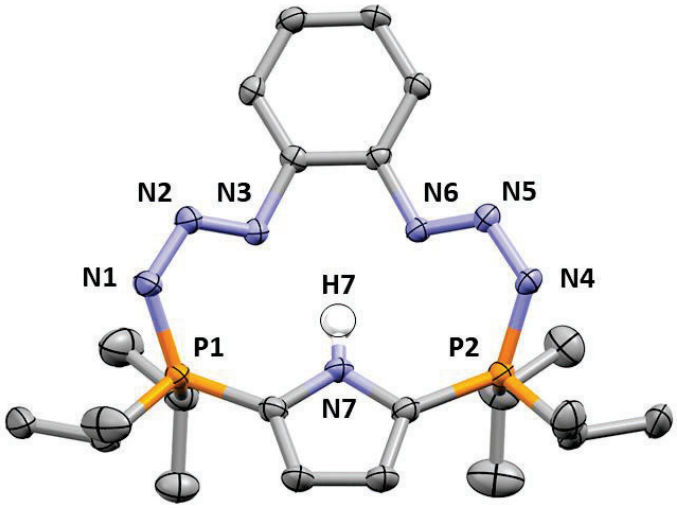

Figure 5.10 X-ray crystal structure of cyclopyrrolazide. Thermal ellipsoids are drawn at 50% probability. Hydrogens, except for H7, have been removed for clarity.

was remarkably downfield at δ 14.90 and the $^{31}P\{^{1}H\}$ NMR spectrum exhibited a signal at δ 25.0, which is downfield shifted from δ –11.1 in 2,5-($^{i}Pr_2P)_2NH(C_4H_2)$. X-ray crystallography revealed a 13-atom macrocycle with two *cis*-phosphazides (Figure 5.10, Table 5.7). The N1–N2–N3 angle is 117.4(2)°, which is larger than the average metal-coordinated phosphazide angle of 111.3°[l], but smaller than that of the cyclic metal-free phosphazide $(^{i}Pr_2N)_2PN_3[CH(CO_2Me)]_2$ isolated by Bertrand and colleagues (124.0(3)°).[28] The N1, N2, N4 and N5 atoms lie outside of the plane defined by P1–P2–N3–N6–N7 by 0.693 Å (N1–plane), 0.677 Å (N4–plane), 0.587 Å (N2–plane), and 0.576 Å (N5–plane). Heating this 'cyclopyrrolazide' compound in benzene-d_6 caused decomposition to multiple unidentified products.

[l] The N_α–N_β–N_γ angle for all metal- and boron-phosphazides with reported X-ray crystal structures from 1978-2022 was collected and the mean was calculated (52 in total).

5.5.5. Future Work – Towards A Systematic Comparison of Stabilized Phosphazides

The next stage of this study would be to assess the stability differences between these phosphazides in solution, by heating them and monitoring their decomposition *via* ^{31}P NMR spectroscopy. In addition, further studies regarding steric and electronic effects should be investigated. By using NMe_2 groups on phosphorus, instead of ^{i}Pr groups, the electronic effect of enhanced electron donation could be determined without a large change to the steric environment.

The 'cyclopyrrolazide' compound could be used as a planar macrocyclic ligand to support a small metal in the centre. For example, addition of $AlMe_3$ could allow for elimination of methane and formation of a dimethyl aluminum complex. Furthermore, the use of furan-based 2,5-$(^{i}Pr_2P)_2NH(C_4H_2)$ could determine if the NH bond is necessary for stabilizing the cyclic diphosphazide, as well as creating a neutral planar ligand similar to 'cyclopyrrolazide'.

5.6. Experimental Details for Chapter 5

5.6.1. Laboratory Equipment and Apparatus

An argon filled MBraun glove box was employed for manipulation and storage of all oxygen and moisture sensitive compounds. All thermally unstable compounds were stored in a –35 °C freezer within the glove box. All reactions were performed on a double manifold high vacuum line using standard techniques or in a glove box under an atmosphere of argon.[29] Commonly utilized specialty glassware includes the swivel frit assembly, needle valves, and thick walled (5 mm) glass bombs equipped with Kontes Teflon stopcocks.[29] All glassware was stored in a 110 °C oven for a minimum of 12 hours, or flame-dried before immediate transfer to the glove box antechamber or assembled on the vacuum line and evacuated while hot.

5.6.2. Solvents

Toluene, pentane, and tetrahydrofuran (THF) solvents were dried and purified using the Grubbs/Dow purification system and stored in evacuated 500 mL bombs over titanocene[30] (toluene and hexanes) or sodium/benzophenone ketal (THF).[31] Diethyl ether, pentane, heptane, benzene, benzene-d_6, toluene-d_8, and THF-d_8 were dried and stored over sodium/benzophenone ketal in glass bombs under vacuum. Unless otherwise noted, solvents were introduced *via* vacuum transfer with condensation at –78 °C. Liquid nitrogen (–196 °C), liquid nitrogen/pentane (–130 °C), dry ice/acetone (–78 °C), dry ice/acetonitrile (–45 °C) and water/ice (0 °C) baths were used for cooling receiving flasks and to maintain low temperature conditions.

5.6.3. Instrumentation and Details for NMR Experiments

All NMR spectra were recorded at ambient temperature, except where noted, with a Bruker Avance II NMR spectrometer (300.13 MHz for ^{1}H, 75.47 MHz for ^{13}C and 121.48 MHz for ^{31}P) or Avance III NMR spectrometer (700.13 MHz for ^{1}H, 176.05 MHz for ^{13}C, and 283.54 MHz for ^{31}P) NMR spectrometer. All ^{1}H NMR spectra were referenced to $SiMe_4$ through the residual ^{1}H resonance(s) of the employed solvent; benzene-d_6 (7.16 ppm), toluene-d_8 (2.09, 6.98, 7.02 and 7.09 ppm), chloroform-d_1 (7.26 ppm) or THF-d_8 (1.73 and 3.58 ppm). ^{13}C NMR spectra were referenced relative to $SiMe_4$ through the resonance(s) of the employed solvent; benzene-d_6 (128.0 ppm), toluene-d_8 (20.4, 125.2, 128.0, 128.9, 137.5 ppm), chloroform-d_1 (77.16 ppm) or THF-d_8 (25.4, 67.6 ppm). ^{1}H NMR data for diamagnetic compounds are reported as follows: chemical shift, multiplicity (s = singlet, d = doublet, t = triplet, q = quartet, quint = quintet, sp = septet, br = broad, m = multiplet, app = apparent, obsc = obscured, ov = overlapping), coupling constants (Hz), integration, assignment. ^{13}C NMR data for diamagnetic compounds are reported as follows: chemical shift, assignment. Assignment of resonances were supported by ^{1}H–^{1}H COSY, ^{13}C{^{1}H} APT, ^{1}H–^{13}C{^{1}H} and HSQC/HMBC experiments. All uranium compounds in this paper are paramagnetic. For paramagnetic compounds, $w_{1/2}$ denotes width at half height in hertz.

5.6.4. Additional Instrumentation

Elemental analyses (%CHN) were conducted at the University of Lethbridge by Jackson Knott or Dylan Webb on an Elementar Americas Vario MicroCube Analyzer (C, H, N, O, S capabilities).

5.6.5. Additional Safety Considerations

Organic azides are both toxic and explosive. Care should be taken while handling azides, particularly if they are solvent free and/or at elevated temperatures. Phosphines are toxic and care should be taken while handling. ^{238}U is a weak α-emitter with a half-life of 4.47 x 10^9 years. Natural thorium (primary isotope ^{232}Th) is a weak α-emitter (4.012 MeV) with a half-life of 1.41 × 10^{10} years; manipulations and reactions should be carried out in a fume hood or in an inert atmosphere glove box.

5.6.6. Synthetic Procedures

Synthesis of L''U(O)$_2$U(O)$_2$Cl[Ph$_2$P[(2-O)C$_6$H$_4$]:

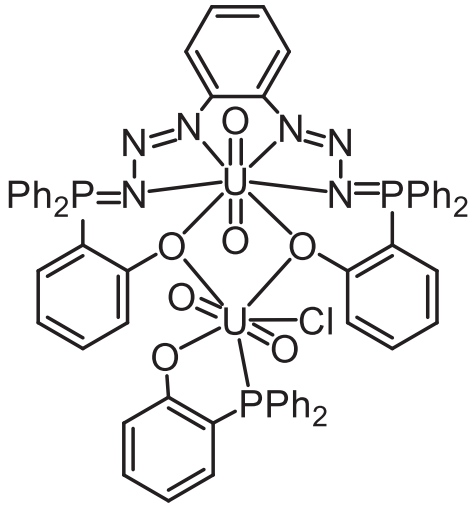

In an argon-filled glove box, a 5 mL shell vial was charged with K_2L" (8.6 mg, 0.011 mmol) and $UO_2Cl_2(THF)_3$ (6.0 mg, 0.011 mmol). To this mixture 2 mL of THF was added. The solution turned red immediately. The solution was agitated for 2 minutes and the THF was removed *in vacuo*. The product was extracted into C_6D_6 and filtered through Celite® (to remove salts) into an NMR tube. Red crystals grew over 16 hours in the NMR tube at ambient temperature. ^1H NMR (C_6D_6, 300.13 MHz): Multiple overlapping signals from δ 6.3 to 8.6, resulting from several products, were observed. $^{31}P\{^1H\}$ NMR (C_6D_6, 121.49 MHz): δ 75.48 (s), 38.48 (s, signal for L"U(O)$_2$), 37.07 (s),.

Synthesis of $[LU(O)_2]_2$:

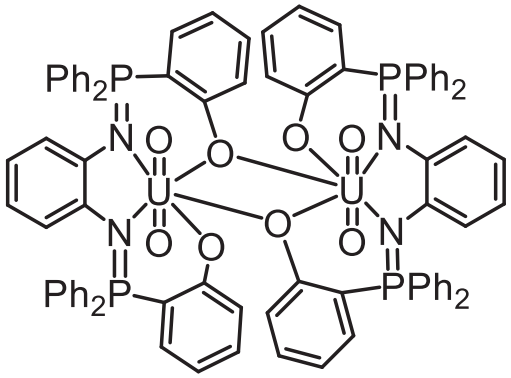

In an argon-filled glove box, an NMR tube was charged with K_2L (4.1 mg, 0.0056 mmol) and $UO_2Cl_2(THF)_3$ (3.1 mg, 0.0056 mmol) and dissolved in THF-d_8. The solution turned red immediately and red crystals crashed out of solution after 10 minutes at ambient temperature. ^1H NMR (C_6D_6, 300.13 MHz): Multiple overlapping signals were observed between δ 5.8 and δ 8.2, arising from two different products. $^{31}P\{^1H\}$ NMR (C_6D_6, 121.49 MHz): δ 25.48 (s), 24.23 (s, $LU(O)_2(THF)$), 23.06 (s).

Synthesis of $[LUCl(\mu–Cl)]_2$:

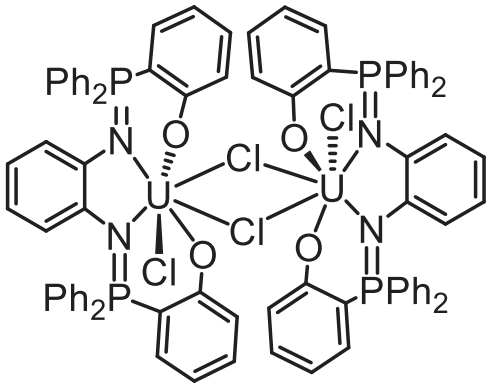

In an inert atmosphere glove box, a solution of $LUCl_2$ in 5 mL of benzene (16.4 mg, 0.0169 mmol) and heated to reflux in a sealed 2 mL screw cap vial for 10 minutes. The solution was left at ambient temperature for 16 hours. Bright green crystals formed on the surface of the solvent. The solvent was decanted and the crystals dried *in vacuo*.

***In situ* synthesis of [$L_{PN3}Th(CH_2SiMe_3)_2$][$BArF^{24}$]:**

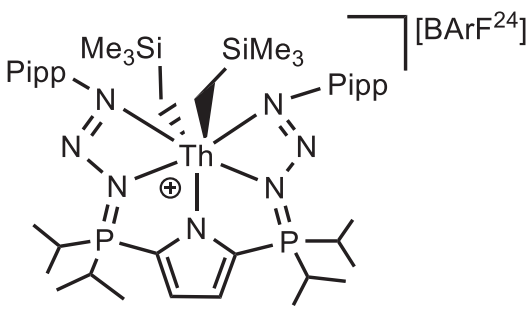

In an inert atmosphere glove box, an NMR tube was charged with $L_{PN3}Th(CH_2SiMe_3)_3$ (10.3 mg, 0.0092 mmol) and [CPh_3][$BArF^{24}$] (9.2 mg, 0.0092 mmol). To the solids, 2 mL of C_6D_6 was added and a yellow oil formed. ^{1}H NMR (C_6D_6, 300.13 MHz): δ 8.41 (s, 8H, anion *ortho*-CH), 7.82 (d, $^3J_{HH}$ = 8.4 Hz, 4H, aromatic C*H*), 7.70 (s, 4H, anion *para*-CH), 7.19 (d, $^3J_{HH}$ = 8.4 Hz, 4H, aromatic C*H*), 6.50 (s, 2H, pyrrole-C*H*), 2.64 (sp, $^3J_{HH}$ = 6.8 Hz, 2H, Ar–C*H*(CH_3)$_2$), 2.06 (m, 4H, P–C*H*(CH_3)$_2$), 1.06 (d, $^3J_{HH}$ = 6.9 Hz, 12H, Ar–CH(C*H*$_3$)$_2$), 0.81 (m, 24H, P–CH(C*H*$_3$)$_2$), 0.39 (br s, 4H, Th–C*H*$_2$), –0.17 (s, 12H, Si(C*H*$_3$)$_3$). ^{11}B{^{1}H} NMR (C_6D_6, 96.29 MHz): δ –5.88 (s). ^{19}F{^{1}H} NMR (C_6D_6, 282.40): δ –62.1 (s). ^{31}P{^{1}H} NMR (C_6D_6, 121.49 MHz): δ 63.6 (s).

***In situ* synthesis of $_{Ph}L^{Pipp}ThCl_3$:**

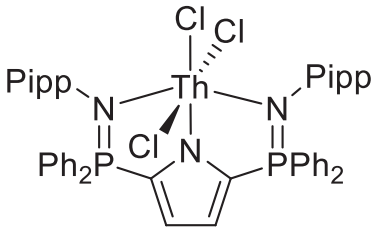

In an inert atmosphere glove box an NMR tube was charged with $Na_{iPr}L^{Pipp}$ (3.9 mg, 0.0054 mmol) and $ThCl_4(dme)_2$ (3.0 mg, 0.0054 mmol). To this mixture, THF-d_8 was added. Colourless crystals grew in the NMR tube over 16 hours at ambient temperature. ^{1}H NMR (THF-d_8, 300.13 MHz): δ 7.72 (m, 8H, aromatic CH), 7.55 (m, 4H, aromatic CH), 7.43 (m, 8H, aromatic CH), 6.96 (m, 4H, aromatic CH), 6.85 (m, 4H, aromatic C*H*), 6.51 (ov dd, 2H, pyrrole-C*H*), 2.74 (sp, $^3J_{HH}$ = 7.0 Hz, 2H, Ar–C*H*(CH_3)$_2$), 1.14 (d, $^3J_{HH}$ = 6.9 Hz, 12H, Ar–CH(C*H*$_3$)$_2$). ^{31}P{^{1}H} NMR (THF-d_8, 121.49 MHz): δ 35.8 (s).

Synthesis of $_{iPr}L^{Pipp}UCl_3$:

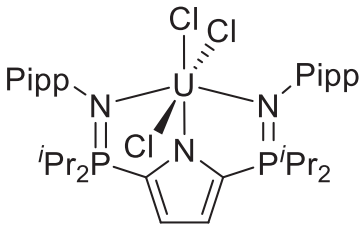

In an inert atmosphere glove box, $Na_{iPr}L^{Pipp}$ (120.0 mg, 0.203 mmol) and $UCl_4(dme)_2$ (114.0 mg, 0.204 mmol) were added to a 20 mL scintillation vial with a Teflon® coated stir bar. To this mixture, 5 mL of dme was added and the solution was stirred for one hour. The solution was filtered through Celite® to remove salts, and the solvent was removed *in vacuo*. The product was washed with pentane (2 × 2 mL) and dried *in vacuo* resulting in a light green solid. Yield: 153 mg, 82.7%. ^{1}H NMR (C_6D_6, 300.13 MHz): δ 0.21 (s, 2H, pyrrole-C*H*), –0.68 (dd, $^3J_{HP}$ = 16.8 Hz, $^3J_{HH}$ = 7.0 Hz, 12H, P–CH(C*H*$_3$)$_2$), –2.14 (dd, $^3J_{HP}$ = 16.0 Hz, $^3J_{HH}$ = 7.0 Hz, 12H, P–CH(C*H*$_3$)$_2$), –4.24 (d, $^3J_{HH}$ = 6.6 Hz, 12H, Ar–CH(C*H*$_3$)$_2$), –4.79 (d, $^3J_{HH}$ = 7.5 Hz, 4H, aromatic C*H*), –5.11 (sp, $^3J_{HH}$ = 6.8 Hz, 2H, Ar–C*H*(CH$_3$)$_2$), –11.89 (m, 4H, P–C*H*(CH$_3$)$_2$), –12.38 (d, $^3J_{HH}$ = 7.5 Hz, 4H, aromatic C*H*). ^{13}C{^{1}H} NMR (C_6D_6, 75.47 MHz): δ 130.5, 126.0, 107.1, 73.2, 28.6, 15.6, 13.7, 9.2, 8.3, –149.4. ^{31}P{^{1}H} NMR (C_6D_6, 121.49 MHz): δ –64.8 (s)

Synthesis of $_{Ph}L^{Pipp}UCl_3$:

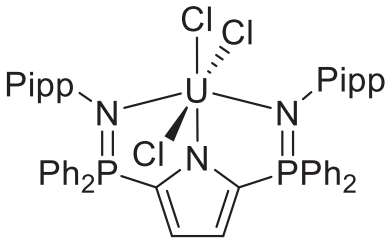

In an inert atmosphere glove box, $Na_{Ph}L^{Pipp}$ (64.0 mg, 0.089 mmol) and $UCl_4(dme)_2$ (50.0 mg, 0.089 mmol) were added to a 20 mL scintillation vial with a Teflon® coated stir bar. To this mixture, 5 mL of dme was added and the solution was stirred for one hour. The solution was filtered through Celite® to remove salts, and the solvent was removed *in vacuo*. The product was washed with pentane (2 × 2 mL) and dried *in vacuo* resulting in a light green solid. Yield: 98.0 mg, 104.7% (the product

contained residual dme). ^{1}H NMR (THF-d_8, 300.13 MHz): δ 7.33 (m, 4H, aromatic CH), 7.49 (m, 8H, aromatic C*H*), 4.04 (m, 8H, aromatic CH), –0.50 (d, $^{3}J_{HH}$ = 6.5 Hz, 4H, Aromatic–CH), –1.83 (s, 2H, pyrrole-C*H*), –2.21 (sp, $^{3}J_{HH}$ = 6.9 Hz, 2H, Ar–C*H*(CH$_3$)$_2$), –2.87 (d, $^{3}J_{HH}$ = 6.9 Hz, 12H, Ar–CH(C*H$_3$*)$_2$), –4.18 (d, $^{3}J_{HH}$ = 6.5 Hz, 4H, Aromatic–CH). ^{31}P{^{1}H} NMR (THF-d_8, 121.49 MHz): δ –127.4 (s).

Synthesis of $_{iPr}$L^{Dipp}UCl$_3$:

In an inert atmosphere glove box, Na$_{iPr}$L^{Dipp} (112.6 mg, 0.167 mmol) and UCl$_4$(dme)$_2$ (93.8 mg, 0.168 mmol) were added to a 20 mL scintillation vial with a Teflon® coated stir bar. To this mixture, 5 mL of toluene was added and the solution was stirred for 16 hours. The solution was filtered through Celite® to remove salts, and the solvent was removed *in vacuo*. The product was washed with pentane (2 × 2 mL) and dried *in vacuo* resulting in a light green solid. Yield: 94.3 mg, 55.9 %. ^{1}H NMR (THF-d_8, 300.13 MHz): δ 10.24, –1.18, –1.47, –2.15, –4.47, –7.26, –11.99. ^{31}P{^{1}H} NMR (THF-d_8, 121.49 MHz): δ –83.7 (s).

Synthesis of $_{iPr}$L^{Pyr}UCl$_3$:

In an inert atmosphere glove box, Na$_{iPr}$L^{Pyr} (96.8 mg, 0.171 mmol) and UCl$_4$ (65.2 mg, 0.172 mmol) were added to a 250 mL round-bottom flask with a Teflon® coated stir bar, connected to a swivel frit and attached to a double manifold vacuum line. THF (20 mL) was condensed into the flask at –78 °C and warmed to ambient

temperature while stirring. The purple solution turned orange over 10 minutes and the solution was left to stir at ambient temperature for one hour. The THF was removed *in vacuo* and $CHCl_3$ (20 mL) was condensed into the flask at –78 °C. The solution was filtered to remove salts. The $CHCl_3$ was removed *in vacuo*. The orange solid was washed with pentane (2 × 5 mL). To this residue, 5 mL of dme was added and the solution was stirred for one hour. The solution was filtered through Celite® to remove salts, and the solvent was removed *in vacuo*. The product was washed with pentane (2 × 2 mL) and dried *in vacuo* resulting in an orange solid. Yield: 131.0 mg, 86.4%. ^{1}H NMR (THF-d_8, 300.13 MHz): δ 10.75, 1.28, 0.86, –0.23, –0.66, –4.70, –6.59. ^{31}P{^{1}H} NMR (THF-d_8, 121.49 MHz): δ –54.6 (s).

***In situ* synthesis of $_{iPr}L^{Pyr}ThCl_3$:**

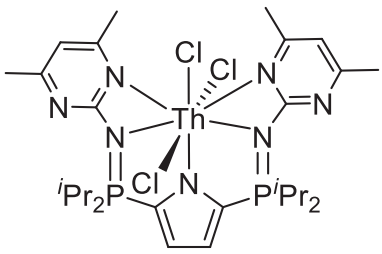

In an inert atmosphere glove box an NMR tube was charged with $Na_{iPr}L^{Pyr}$ (5.0 mg, 0.009 mmol) and $ThCl_4(dme)_2$ (4.9 mg, 0.009 mmol). To this mixture, THF-d_8 was added and the solution turned orange. Orange crystals grew in the NMR tube over 16 hours at ambient temperature. ^{1}H{^{31}P} NMR (THF-d_8, 300.13 MHz): δ 6.77 (m, 2H, pyrimidine-aromatic C*H*), 6.74 (s, 2H, pyrrole-C*H*), 3.06 (dsp, $^3J_{HH}$ = 7.0 Hz, $^2J_{HP}$ = 2.5 Hz, 4H, P–C*H*(CH_3)$_2$), 2.74 (br s, 6H, pyrimidine-CH_3), 2.34 (br s, 6H, pyrimidine-CH_3), 1.31 (ov m, 24H, P–CH(C*H*$_3$)$_2$). ^{31}P{^{1}H} NMR (THF-d_8, 121.49 MHz): δ 58.3 (s).

Synthesis of $L_{PN3}UCl_3$:

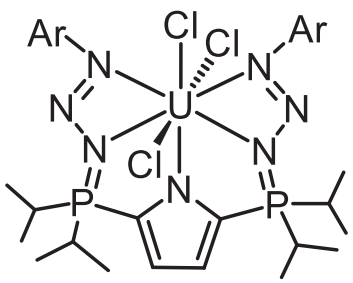

Method 1: In an inert atmosphere glove box, KL_{PN3} (20.0 mg, 0.030 mmol) and $UCl_3(THF)_{3.5}$ (contaminated with UCl_4) (23.8 mg, 0.0399 mmol) were added to a 20 mL scintillation vial. To this mixture, 7 mL of THF was added and the solution turned orange. The mixture was agitated for 2 minutes and then filtered through Celite® to remove salts. The THF was removed *in vacuo.* A small amount of crystals were grown from a concentrated solution in toluene at –35 °C. Method 2: In an argon-filled glove box, an NMR tube was charged with KL_{PN3} (3.2 mg, 0.030 mmol) and UCl_4 (3.1 mg, 0.0081 mmol) and dissolved in pyridine-d_5. The solution turned reddish-brown. ^{1}H NMR (pyridine-d_5, 300.13 MHz): δ 11.40, 4.15, 2.25, 0.26, –0.10, –1.71, –2.65, –6.13. ^{31}P{^{1}H} NMR (pyridine-d_5, 121.49 MHz): δ 14.1 (s).

Synthesis of $L_{PN3}TiCl_2$:

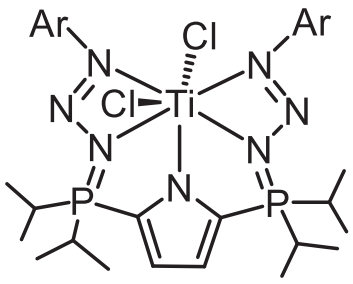

In an inert atmosphere glove box, KL_{PN3} (21.3 mg, 0.0323 mmol) and $TiCl_3(THF)_3$ (12.0 mg, 0.032 mmol) were added to a 20 mL scintillation vial with a Teflon® coated stir bar. To this mixture, 2 mL of dme was added and the solution was stirred for 5 minutes. The solution was filtered through Celite® to remove salts, and the solvent removed *in vacuo*. The product was washed with pentane (2 × 2 mL) to fully remove dme. Yield: 18.4 mg, 77.0%. X-ray quality green/blue crystals grew from a concentrated dme solution at –35 °C. NMR spectroscopy was attempted in pyridine-d_5;

however, only 3 extremely broad peaks were visible in the ^{1}H NMR spectrum (δ 9.2, 4.9 and 2.4)

Synthesis of [$L_{PN3/PN}$-$TiCl_2$]$_2$:

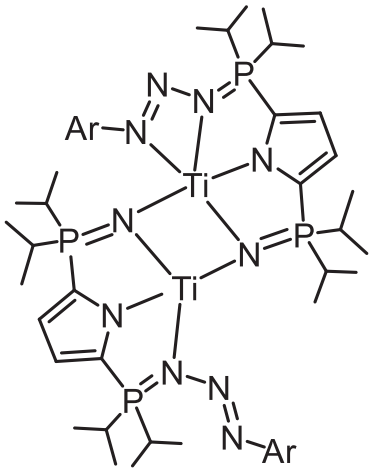

In an inert atmosphere glove box, crystals of $L_{PN3}TiCl_2$ in 5 mL of dme (10.2 mg, 0.0144 mmol) were heated in a sealed 2 mL screw cap vial at 80 °C for 10 minutes. The green/blue mixture turned brown. A small amount of orange crystals grew in solution after 8 months at –35 °C.

Synthesis of [(2-OH)(3,5-^{t}Bu)C_6H_2]Ph_2P=N_3(Pipp):

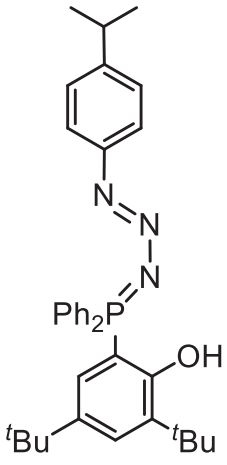

In an inert atmosphere glove box, a solution of N_3–Pipp (8.3 mg, 0.051 mmol) in 1 mL of pentane was added dropwise to a solution of Ph_2P[(2-OH)(3,5-^{t}Bu)C_6H_2] in 2 mL of pentane (20.0 mg, 0.051 mmol). The bright yellow mixture was agitated for 5 minutes and placed in a –35 °C freezer for 16 hours. Colourless block crystals grew in 1 hour. ^{1}H NMR (C_6D_6, 700.44 MHz): δ 15.00 (br s, 1H, OH), 7.76 (m, 4H, *ortho*-aromatic phenyl-CH), 7.69 (d, $^{4}J_{HH}$ = 2.2 Hz, 1H, *para*-aromatic CH), 7.59 (d, $^{3}J_{HH}$ = 8.3 Hz, 2H, aromatic Pipp-CH), 7.08 (dd, $^{4}J_{HH}$ = 2.2, $^{3}J_{HP}$ = 15.4 Hz, 1H, *ortho*-aromatic CH), 7.00 (d, $^{3}J_{HH}$ = 8.3 Hz, 2H, aromatic Pipp-CH), 6.95 (m, 2H, *para*-

aromatic phenyl-CH), 6.88 (m, 4H, *meta*-aromatic phenyl-CH), 2.63 (sp, $^{3}J_{HH}$ = 6.9 Hz, 2H, Ar–C*H*$(CH_3)_2$), 1.67 (s, 9H, ^{t}Bu), 1.10 (s, 9H, ^{t}Bu), 1.07 (d, 6H, $^{3}J_{HH}$ = 6.9 Hz, Ar–CH(C*H*$_3)_2$). $^{31}P\{^{1}H\}$ NMR (C_6D_6, 283.54 MHz): δ 30.7 (s).

Synthesis of [(2-OH)(3,5-^{t}Bu)C_6H_2]^{i}Pr$_2$P=N$_3$(Pipp):

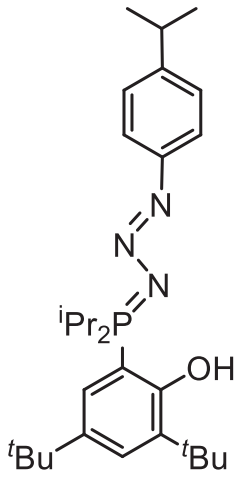

In an inert atmosphere glove box, a solution of N_3–Pipp (10.0 mg, 0.062 mmol) in 1 mL of pentane was added dropwise to a solution of $^{i}Pr_2P$[(2-OH)(3,5-^{t}Bu)C_6H_2] in 2 mL of pentane (20.0 mg, 0.062 mmol). The bright yellow mixture was agitated for 5 minutes and placed in a –35 °C freezer for 16 hours. Colourless crystals grew during this period. ^{1}H NMR (C_6D_6, 700.44 MHz): δ 14.82 (br s, 1H, OH), 7.81 (d, $^{3}J_{HH}$ = 8.3 Hz, 2H, aromatic Pipp-CH), 7.69 (d, $^{4}J_{HH}$ = 2.2 Hz, 1H, *para*-aromatic CH), 7.21 (d, $^{3}J_{HH}$ = 8.3 Hz, 2H, aromatic Pipp-CH), 6.88 (dd, 1H, $^{4}J_{HH}$ = 2.3, $^{3}J_{HP}$ = 12.7 Hz, *ortho*-aromatic CH), 2.76 (sp, $^{3}J_{HH}$ = 7.1 Hz, 1H, Ar-C*H*$(CH_3)_2$), 2.46 (dsp, $^{3}J_{HH}$ = 7.2 Hz, $^{2}J_{HP}$ = 2.5 Hz, 2H, P–C*H*$(CH_3)_2$), 1.60 (s, 9H, ^{t}Bu), 1.25 (s, 9H, ^{t}Bu), 1.18 (d, $^{3}J_{HH}$ = 6.9 Hz, 6H, Ar–CH(C*H*$_3)_2$), 1.03 (dd, $^{3}J_{HP}$ = 15.8 Hz, $^{3}J_{HH}$ = 7.1 Hz, 6H, P–CH(C*H*$_3)_2$), 0.84 (dd, $^{3}J_{HP}$ = 15.8 Hz, $^{3}J_{HH}$ = 7.1 Hz, 6H, P–CH(C*H*$_3)_2$). $^{31}P\{^{1}H\}$ NMR (C_6D_6, 283.54 MHz): δ 59.8 (s).

Synthesis of Ph$_2$P[(2-OLi)(3,5-^{t}Bu)C_6H_2]:

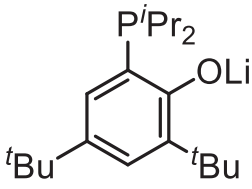

In an inert atmosphere glove box, Ph$_2$P[(2-OH)(3,5-^{t}Bu)C_6H_2] (47.8 mg, 0.148 mmol) and $LiCH_2SiMe_3$ (14.0 mg, 148 mmol) were added to a 20 mL scintillation vial with a Teflon® coated stir bar. To this

mixture, 5 mL of toluene was added and the solution was stirred for 3 hours. The solvent was removed *in vacuo* leaving a white solid. Yield: 50.9 mg, 104.5% (the final product contained residual $SiMe_4$). ^1H NMR (C_6D_6, 300.13 MHz): δ 7.61 (br s, 1H, aromatic C*H*), 7.21 (br s, 1H, aromatic C*H*), 2.01 (br sp, $^3J_{HH}$ = 5.2 Hz, 2H, PC*H*$(CH_3)_2$), 1.65 (s, 9H, ^{t}Bu), 1.47 (s, 9H, ^{t}Bu), 1.03 (m, 12H, P–CH(C*H*$_3)_2$). $^{31}P\{^1H\}$ NMR (C_6D_6, 121.49 MHz): δ –6.7 (s).

Synthesis of $Ph_2P[(2\text{-}ONa)(3,5\text{-}^t Bu)C_6H_2]$:

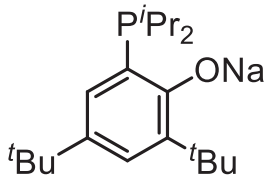

In an inert atmosphere glove box, $Ph_2P[(2\text{-}OH)(3,5\text{-}^t Bu)C_6H_2]$ (63.0 mg, 0.20 mmol) and excess NaH (5.1 mg, 0.21 mmol) were added to a 20 mL scintillation vial equipped with a Teflon® coated stir bar. To this mixture, 5 mL of THF was added after which the solution bubbled vigorously and the solution was stirred for 3 hours. The solution was filtered through Celite® to remove excess NaH. The solvent was removed *in vacuo* and the white solid washed with cold pentane (2 × 1 mL). Yield: 72.3 mg, 110.9% (the final product contained residual NaH). ^1H NMR (C_6D_6, 300.13 MHz): δ 7.58 (s, 1H, aromatic C*H*), 7.20 (s, 1H, aromatic C*H*), 2.10 (br m, 2H, P–C*H*$(CH_3)_2$), 1.66 (s, 9H, ^{t}Bu), 1.49 (s, 9H, ^{t}Bu), 1.12 (m, 12H, P–CH(C*H*$_3)_2$). $^{31}P\{^1H\}$ NMR (C_6D_6, 121.49 MHz): δ –7.9 (s).

Synthesis of $Ph_2P[(2\text{-}OK)(3,5\text{-}^t Bu)C_6H_2]$:

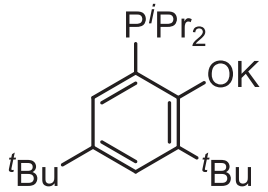

In an inert atmosphere glove box, $Ph_2P[(2\text{-}OH)(3,5\text{-}^t Bu)C_6H_2]$ (86.0 mg, 0.27 mmol) and excess KH (11.0 mg, 0.27 mmol) were added to a 20 mL scintillation vial with a Teflon® coated stir bar. To this

mixture, 5 mL of THF was added after which the solution bubbled vigorously and the solution was stirred for 3 hours. The solution was filtered through Celite® to remove excess KH. The solvent was removed *in vacuo* and the white solid washed with cold pentane (2 × 1 mL). Yield: 115.1 mg, 119.7% (the final product contained residual KH). ^{1}H NMR (C_6D_6, 300.13 MHz): δ 7.56 (br s, 1H, aromatic C*H*), 7.19 (br s, 1H, aromatic C*H*), 2.09 (br sp, $^{3}J_{HH}$ = 6.7 Hz, 2H, P–C*H*(CH_3)$_2$), 1.64 (s, 9H, ^{t}Bu), 1.53 (s, 9H, ^{t}Bu), 1.15 (m, 12H, P–CH(C*H*$_3$)$_2$). ^{31}P{^{1}H} NMR (C_6D_6, 121.49 MHz): δ –3.8 (s).

Synthesis of [(2-OK)(3,5-^{t}Bu)C_6H_2]^{i}Pr$_2$P=N$_3$(Pipp):

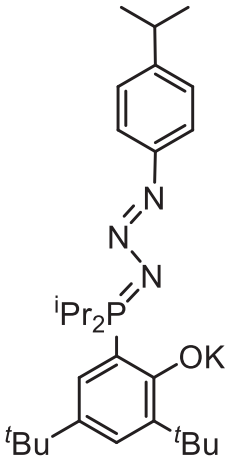

In an inert atmosphere glove box, a solution of N_3–Pipp (10.7 mg, 0.066 mmol) in 1 mL of pentane was added dropwise to a solution of ^{i}Pr$_2$P[(2-OK)(3,5-^{t}Bu)C_6H_2] in 1 mL of pentane (24.0 mg, 0.066 mmol). The bright yellow mixture was agitated for 5 minutes and placed in a –35 °C freezer for 16 hours. Colourless crystals grew over 30 minutes. The supernatant was removed and the remaining solvent was removed *in vacuo*. Yield: 23.1 mg, 66.6%. ^{1}H NMR (C_6D_6, 700.44 MHz): δ 7.67 (d, $^{4}J_{HH}$ = 2.2 Hz, 1H, *para*-aromatic CH), 7.44 (d, $^{3}J_{HH}$ = 8.1 Hz, 2H, aromatic Pipp-CH), 7.21 (d, $^{3}J_{HH}$ = 8.1 Hz, 2H, aromatic Pipp-CH), 7.14 (dd, 1H, $^{3}J_{HP}$ = 12.6 Hz, *ortho*-aromatic CH), 2.84 (ov dsp and sp, 3H, P–C*H*(CH_3)$_2$ and Ar–C*H*(CH_3)$_2$), 1.55 (s, 9H, ^{t}Bu), 1.48 (s, 9H, ^{t}Bu), 1.27 (d, $^{3}J_{HH}$ = 6.8 Hz, 6H, Ar–CH(C*H*$_3$)$_2$), 1.16 (dd, $^{3}J_{HP}$ = 15.2 Hz, $^{3}J_{HH}$ = 7.3 Hz, 6H, P–CH(C*H*$_3$)$_2$), 1.10 (dd, $^{3}J_{HP}$ = 14.3 Hz, $^{3}J_{HH}$ = 7.3 Hz, 6H, P–CH(C*H*$_3$)$_2$). ^{31}P{^{1}H} NMR (C_6D_6, 283.54 MHz): δ 51.8 (s).

***In situ* synthesis of [(2-OK)(3,5-^{t}Bu)C$_6$H$_2$]^{i}Pr$_2$P=N(Pipp)[18-crown-6]:**

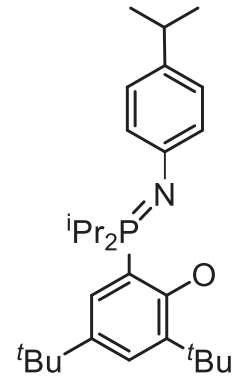

K[18-crown-6]

In an inert atmosphere glove box, an NMR tube was charged with [(2-OK)(3,5-^{t}Bu)C$_6$H$_2$]^{i}Pr$_2$P=N$_3$(Pipp) (2.3 mg, 0.0044 mmol) and excess 18-crown-6. To the solids 2 mL of C_6D_6 was added and the solution bubbled vigorously. ^{1}H NMR (C_6D_6, 700.44 MHz): δ 7.72 (ov doublet and singlet, 3H, aromatic Pipp-CH and *para*-aromatic CH), 7.50 (dd, 1H, $^3J_{HP}$ = 12.2 Hz, $^4J_{HH}$ = 2.6 Hz, *ortho*-aromatic CH), 7.24 (d, $^3J_{HH}$ = 8.3 Hz, 2H, aromatic Pipp-CH), 3.67 (m, 2H, P–C*H*(CH$_3$)$_2$), 2.82 (sp, $^3J_{HH}$ = 6.9 Hz, 1H, Ar-C*H*(CH$_3$)$_2$), 1.99 (s, 9H, ^{t}Bu), 1.63 (dd, $^3J_{HP}$ = 15.5 Hz, $^3J_{HH}$ = 7.1 Hz, 12H, P–CH(C*H$_3$*)$_2$), 1.48 (s, 9H, ^{t}Bu), 1.42 (dd, $^3J_{HP}$ = 14.6 Hz, $^3J_{HH}$ = 7.1 Hz, 12H, P–CH(C*H$_3$*)$_2$), 1.23 (d, $^3J_{HH}$ = 6.9 Hz, 6H, Ar–CH(C*H$_3$*)$_2$). ^{31}P{^{1}H} NMR (C_6D_6, 283.54 MHz): δ 52.7 (s).

Synthesis of cyclopyrrolazide:

In an inert atmosphere glove box, a solution of 1,2-diazidobenzene (37.1 mg, 0.231 mmol) in 1 mL of toluene was added immmediately to a solution of 2,5-(^{i}Pr$_2$P)$_2$NH(C$_4$H$_2$) in 2 mL of toluene (69.3 mg, 0.231 mmol). The bright yellow mixture was agitated until small yellow needles precipitated (~30 seconds). The slurry was placed in a –35 °C freezer for 2 minutes and then the supernatant was removed. The crystals were washed with 0.5 mL of cold toluene and the solvent was removed *in vacuo*. Yield: 87.7 mg, 82.5%. ^{1}H NMR (THF-d_8, 700.44 MHz): δ 14.90 (s, 1H, N-*H*), 7.38 (m, 2H,

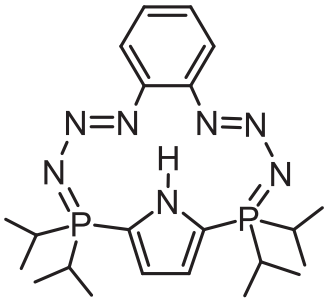

aromatic C*H*), 6.92 (m, 2H, aromatic C*H*), 6.66 (s, 2H, pyrrole-C*H*), 2.53 (dsp, $^{3}J_{HH}$ = 7.0 Hz, $^{2}J_{HP}$ = 3.3 Hz, 4H, P–C*H*(CH_3)$_2$), 1.16 (dd, $^{3}J_{HP}$ = 15.8 Hz, $^{3}J_{HH}$ = 7.1 Hz, 12H, P–CH(C*H*$_3$)$_2$), 1.10 (dd, $^{3}J_{HP}$ = 16.1 Hz, $^{3}J_{HH}$ = 7.1 Hz, 12H, P–CH(C*H*$_3$)$_2$). $^{13}C\{^{1}H\}$ NMR (THF-d_8, 176.13 MHz): δ 148.5 (s, aromatic ipso-*C*), 128.2 (d, $^{1}J_{CP}$ = 135.6 Hz, 2,5-pyrrole *C*), 125.1 (s, aromatic-*C*H), 118.0 (s, aromatic-*C*H), 117.3 (d, $^{2}J_{CP}$ = 7.1 Hz, 3,4-pyrrole *C*H), 16.8 (d, $^{2}J_{CP}$ = 3.2 Hz, P–CH(*C*H$_3$)$_2$), 15.5 (d, $^{2}J_{CP}$ = 3.5 Hz, P–CH(*C*H$_3$)$_2$). The resonance for P–*C*H(CH_3)$_2$ could not be found and is likely coincident with the THF-d_8 solvent. $^{31}P\{^{1}H\}$ NMR (THF-d_8, 283.54 MHz): δ 25.0 (s).

5.6.7. Crystallographic Details

All structures were collected on a Rigaku SuperNova diffractometer equipped with a Dectris Pilatus 3R 200K-A hybrid-pixel-array detector, a four-circle goniometer, sealed graphite-monochromated Mo Kα (λ = 0.71073 Å) and Cu Kα (λ = 1.54178 Å) X-ray sources, and an Oxford cryostream-cooling device fixed at 100 K. Single crystals suitable for X-ray diffraction studies were mounted on a MiTiGen cryo-loop using desiccated Paratone–*N* oil stored in a glove box. Data reduction was accomplished by the CrysAlis^{Pro} (version 1.171.38.43) software package. Absorption corrections were applied by multi-scan techniques and empirical absorption correction using spherical harmonics, implemented in SCALE3 ABSPACK scaling algorithm. Structures were solved in the Olex2[32] environment using intrinsic phasing and refined by full-matrix least squares method on F^2 using the SHELX software suite.[33,34] All non-hydrogen (except N–H) atoms were refined anisotropically, C–H hydrogens were calculated and refined isotropically as a riding model.

The N–H hydrogen in cyclopyrrolazide was located by the Fourier difference maps and refined isotropically. All measurements were performed at the University of Lethbridge.

Single crystals of $LU(O)_2]_2$ were grown from acetonitrile at –35 °C. Single crystals of $L"U(O)_2U(O)_2Cl[Ph_2P[(2\text{-}O)C_6H_4]$, $[LUCl(\mu\text{–}Cl)]_2$ and $_{iPr}L^{Dipp}UCl_3$ were grown from benzene at ambient temperature. Single crystals of $_{Pr}L^{Pipp}UCl_3$, $_{Ph}L^{Pipp}UCl_3$, $_{Ph}L^{Pipp}ThCl_3$, $L_{PN3}UCl_3$, and cyclopyrrolazide were grown from toluene at –35 °C. Single crystals of $_{iPr}L^{Pyr}UCl_3$ and $_{iPr}L^{Pyr}ThCl_3$ were grown from THF at ambient temperature. Single crystals of $[(_{iPr}L^{Pipp})UCl_2(THF)][BArF^{24}]$ and $[(_{iPr}L^{Pipp})ThCl_2(dme)][BArF^{24}]$ were grown from toluene/pentane at –35 °C. Single crystals of $L_{PN3}TiCl_2$ and $[L_{PN3/PN\text{-}}TiCl_2]_2$ were grown from dme at –35 °C. Single crystals of $^tPr_2P[(2\text{-}OH)(3,5\text{-}^tBu)C_6H_2]$ and $Ph_2P[(2\text{-}OH)(3,5\text{-}^tBu)C_6H_2]$ were grown from pentane at –35 °C

A solvent mask for $_{Pr}L^{Pyr}UCl_3$ was calculated and 288 electrons were found in a volume of 1418/Å^3 in 1 void per unit cell. This is consistent with the presence of 1 $[C_4H_8O]$ per unit cell which accounts for 320 electrons per unit cell.

A summary of the crystallographic data can be found below in **Table 5.8.**

Table 5.8. X-ray crystallographic data and structure refinement for the structurally characterized complexes in Chapter 5.

	$[LU(O)_2]_2 \cdot 2(C_2H_3N)$	**$L''U(O)_2U(O)_2Cl[Ph_2P[(2\text{-}O)C_6H_4] \cdot 3(C_6H_6)$**	**$[LUCl(\mu\text{–}Cl)]_2 \cdot 2(C_6H_6)$**
Empirical formula	$C_{88}H_{70}N_6O_8P_4U_2$	$C_{78}H_{64}ClN_6O_7P_3U_2$	$C_{96}H_{76}Cl_4N_4O_4P_4U_2$
Formula weight/g mol^{-1}	1939.44	1801.77	2091.34
Temperature/K	152(70)	99.97(16)	100.00(10)
Crystal system	triclinic	monoclinic	triclinic
Space group	P-1	$P2_1/c$	P-1
a/Å	9.95200(10)	15.6035(2)	12.3118(4)
b/Å	17.5338(2)	29.8749(3)	12.5650(3)
c/Å	24.8207(3)	15.15470(10)	14.4556(4)
α/°	92.6390(10)	90	82.9507(19)
β/°	90.8130(10)	92.2630(10)	74.380(3)
γ/°	92.1660(10)	90	79.476(2)
Volume/$Å^3$	4322.89(8)	7058.90(12)	2111.03(10)
Z	2	4	1
$\rho_{calc}g/cm^3$	1.490	1.695	1.645
μ/mm^{-1}	11.610	14.286	13.030
F(000)	1896.0	3504.0	1024.0
Crystal size/mm^3	0.334 × 0.161 × 0.069	0.161 × 0.06 × 0.038	0.15 × 0.1 × 0.05
Radiation (Å)	Cu Kα (λ = 1.54184)	Cu Kα (λ = 1.54184)	CuKα (λ = 1.54184)
2Θ range for data collection/°	7.132 to 160.31	6.394 to 160.782	7.178 to 159.76
Index ranges	$-12 \le h \le 9$, $-22 \le k \le 22$, $-31 \le l \le 31$	$-19 \le h \le 19$, $-38 \le k \le 32$, $-19 \le l \le 14$	$-15 \le h \le 15$, $-15 \le k \le 16$, $-18 \le l \le 18$
Reflections collected	95740	79422	46159
Independent reflections	18715 [R_{int} = 0.0661, R_{sigma} = 0.0376]	15351 [R_{int} = 0.0682, R_{sigma} = 0.0448]	9112 [R_{int} = 0.0566, R_{sigma} = 0.0381]
Data/restraints/parameters	18715/0/975	15351/0/874	9112/2/515
Goodness-of-fit on F^2	1.051	1.050	1.089
Final R indexes [I>=2σ (I)]	R_1 = 0.0527, wR_2 = 0.1395	R_1 = 0.0440, wR_2 = 0.1076	R_1 = 0.0445, wR_2 = 0.1164
Final R indexes [all data]	R_1 = 0.0571, wR_2 = 0.1431	R_1 = 0.0520, wR_2 = 0.1120	R_1 = 0.0472, wR_2 = 0.1184
Largest diff. peak/hole / e $Å^{-3}$	4.62/-2.77	3.71/-2.39	4.45/-2.73

Programs for diffractometer operation, data collection, data reduction, and absorption correction were those supplied by Rigaku.

	$_{iPr}L^{Dipp}UCl_3 \cdot (C_6H_6)$	$_{iPr}L^{Pipp}UCl_3 \cdot (C_7H_8)$	$_{Ph}L^{Pipp}UCl_3 \cdot 2(C_7H_8)$
Empirical formula	$C_{46}H_{70}Cl_3N_3P_2U$	$C_{41}H_{60}Cl_3N_3P_2U$	$C_{60}H_{60}Cl_3N_3P_2U$
Formula weight/g mol^{-1}	1071.37	1001.24	1229.43
Temperature/K	293.41(10)	100.00(10)	293.41(10)
Crystal system	monoclinic	monoclinic	orthorhombic
Space group	$P2_1/n$	$P2_1/c$	$Pca2_1$
a/Å	10.3664(4)	11.4866(4)	20.6834(7)
b/Å	21.5583(7)	23.6401(9)	13.3750(5)
c/Å	21.8793(8)	17.6170(6)	19.8329(7)
α/°	90	90	90
β/°	97.444(4)	108.258(4)	90
γ/°	90	90	90
Volume/Å^3	4848.4(3)	4543.0(3)	5486.6(3)
Z	4	4	4
ρ_{calc}g/cm^3	1.468	1.464	1.488
μ/mm^{-1}	3.612	3.850	3.203
F(000)	2160.0	2000.0	2456.0
Crystal size/mm^3	0.2 × 0.15 × 0.05	0.254 × 0.143 × 0.109	0.194 × 0.049 × 0.041
Radiation (Å)	Mo Kα (λ = 0.71073)	Mo Kα (λ = 0.71073)	Mo Kα (λ = 0.71073)
2Θ range for data collection/°	6.726 to 61.11	6.894 to 52.744	6.648 to 61.198
Index ranges	-13 ≤ h ≤ 12, -27 ≤ k ≤ 28, -27 ≤ l ≤ 29	-13 ≤ h ≤ 14, -25 ≤ k ≤ 29, -22 ≤ l ≤ 22	-24 ≤ h ≤ 29, -16 ≤ k ≤ 16, -24 ≤ l ≤ 22
Reflections collected	56564	38479	33688
Independent reflections	12157 [R_{int} = 0.0491, R_{sigma} = 0.0447]	9228 [R_{int} = 0.0484, R_{sigma} = 0.0436]	12220 [R_{int} = 0.0493, R_{sigma} = 0.0604]
Data/restraints/parameters	12157/0/515	9228/12/455	12220/16/623
Goodness-of-fit on F^2	1.039	1.056	1.032
Final R indexes [I>=2σ (I)]	R_1 = 0.0271, wR_2 = 0.0470	R_1 = 0.0276, wR_2 = 0.0555	R_1 = 0.0352, wR_2 = 0.0608
Final R indexes [all data]	R_1 = 0.0402, wR_2 = 0.0492	R_1 = 0.0380, wR_2 = 0.0578	R_1 = 0.0479, wR_2 = 0.0635
Largest diff. peak/hole / e Å^{-3}	0.57/-0.55	0.89/-0.48	0.94/-0.67

Programs for diffractometer operation, data collection, data reduction, and absorption correction were those supplied by Rigaku.

	$_{Ph}L^{Pipp}ThCl_3 \cdot (C_7H_8)$	$_{iPr}L^{Pyr}UCl_3 \cdot (C_4H_8O)$	$_{iPr}L^{Pyr}ThCl_3$
Empirical formula	$C_{53}H_{52}Cl_3N_3P_2Th$	$C_{32}Cl_3H_{52}N_7OP_2U$	$C_{28}H_{44}N_7P_2Cl_3Th$
Formula weight/g mol^{-1}	1131.30	885.02	879.03
Temperature/K	100.01(11)	99.9(4)	100.0(5)
Crystal system	orthorhombic	monoclinic	triclinic
Space group	$Pca2_1$	$P2_1/c$	P-1
a/Å	20.7213(2)	17.6473(5)	10.2844(4)
b/Å	13.35470(10)	24.8122(7)	10.5437(4)
c/Å	20.0055(2)	18.0144(5)	17.9141(7)
α/°	90	90	81.323(3)
β/°	90	91.653(3)	77.394(3)
γ/°	90	90	63.696(4)
Volume/$Å^3$	5536.06(9)	7884.7(4)	1696.15(13)
Z	4	8	2
$\rho_{calc}g/cm^3$	1.357	1.491	1.721
μ/mm^{-1}	10.823	4.428	4.757
F(000)	2248.0	3472.0	864.0
Crystal size/mm^3	0.1 × 0.05 × 0.01	0.172 × 0.131 × 0.08	0.149 × 0.055 × 0.034
Radiation (Å)	Cu Kα (λ = 1.54184)	Mo Kα (λ = 0.71073)	Mo Kα (λ = 0.71073)
2Θ range for data collection/°	6.618 to 159.36	6.69 to 61.85	6.554 to 63.08
Index ranges	-26 ≤ h ≤ 25, -17 ≤ k ≤ 15, -17 ≤ l ≤ 25	-23 ≤ h ≤ 25, -33 ≤ k ≤ 35, -25 ≤ l ≤ 22	-14 ≤ h ≤ 14, -15 ≤ k ≤ 14, -26 ≤ l ≤ 25
Reflections collected	32443	94577	43226
Independent reflections	8930 [R_{int} = 0.0382, R_{sigma} = 0.0379]	20311 [R_{int} = 0.0481, R_{sigma} = 0.0430]	9378 [R_{int} = 0.0549, R_{sigma} = 0.0472]
Data/restraints/parameters	8930/1/564	20311/771/763	9378/0/382
Goodness-of-fit on F^2	1.107	1.062	1.028
Final R indexes [I>=2σ (I)]	R_1 = 0.0279, wR_2 = 0.0692	R_1 = 0.0317, wR_2 = 0.0683	R_1 = 0.0284, wR_2 = 0.0559
Final R indexes [all data][b]	R_1 = 0.0309, wR_2 = 0.0761	R_1 = 0.0437, wR_2 = 0.0711	R_1 = 0.0363, wR_2 = 0.0577
Largest diff. peak/hole / e $Å^{-3}$	0.65/-0.92	3.82/-1.15	1.46/-1.11

Programs for diffractometer operation, data collection, data reduction, and absorption correction were those supplied by Rigaku.

	[($_{iPr}$L^{Pipp})UCl$_2$(THF)][BArF^{24}]	**[($_{iPr}$L^{Pipp})ThCl$_2$(dme)][BArF^{24}] · (C$_7$H$_8$)**	**L$_{PN3}$UCl$_3$ · (C$_7$H$_8$)**
Empirical formula	$C_{70}H_{72}BCl_2F_{24}N_3OP_2U$	$C_{78}H_{82}BCl_2F_{24}N_3O_2P_2Th$	$C_{48}H_{68}Cl_3N_7P_2U$
Formula weight/g mol^{-1}	1808.98	1943.39	1149.41
Temperature/K	99.97(16)	100.0(2)	100.00(10)
Crystal system	triclinic	triclinic	monoclinic
Space group	P-1	P-1	$P2_1$
a/Å	16.1350(4)	15.7379(3)	12.5456(2)
b/Å	16.4818(5)	16.8307(3)	14.7341(2)
c/Å	17.7430(3)	19.3082(3)	14.8122(2)
α/°	112.104(2)	114.8830(10)	90
β/°	98.3884(17)	113.958(2)	109.432(2)
γ/°	113.978(3)	90.0890(10)	90
Volume/Å^3	3737.29(18)	4147.14(14)	2582.04(7)
Z	2	2	2
ρ_{calc}g/cm^3	1.608	1.556	1.478
μ/mm^{-1}	2.390	7.663	3.399
F(000)	1796.0	1941.0	1156.0
Crystal size/mm^3	0.2 × 0.03 × 0.025	0.02 × 0.02 × 0.02	0.401 × 0.312 × 0.303
Radiation (Å)	MoKα (λ = 0.71073)	Cu Kα (λ = 1.54184)	Mo Kα (λ = 0.71073)
2Θ range for data collection/°	6.764 to 61.048	6.282 to 155.398	5.2 to 61.542
Index ranges	-21 ≤ h ≤ 23, -20 ≤ k ≤ 21, -25 ≤ l ≤ 24	-19 ≤ h ≤ 19, -20 ≤ k ≤ 21, -24 ≤ l ≤ 24	-17 ≤ h ≤ 16, -21 ≤ k ≤ 20, -19 ≤ l ≤ 19
Reflections collected	86612	81213	113979
Independent reflections	18447 [R_{int} = 0.0698, R_{sigma} = 0.0639]	17308 [R_{int} = 0.0637, R_{sigma} = 0.0471]	13489 [R_{int} = 0.0533, R_{sigma} = 0.0351]
Data/restraints/parameters	18447/0/949	17308/6/1021	13489/494/565
Goodness-of-fit on F^2	1.150	1.038	1.087
Final R indexes [I>=2σ (I)]	R_1 = 0.0819, wR_2 = 0.2107	R_1 = 0.0688, wR_2 = 0.1799	R_1 = 0.0244, wR_2 = 0.0498
Final R indexes [all data][b]	R_1 = 0.0975, wR_2 = 0.2164	R_1 = 0.0798, wR_2 = 0.1885	R_1 = 0.0293, wR_2 = 0.0507
Largest diff. peak/hole / e Å^{-3}	8.96/-3.30	2.21/-3.46	1.27/-0.57

Programs for diffractometer operation, data collection, data reduction, and absorption correction were those supplied by Rigaku.

	$L_{PN3}TiCl_2 \cdot (C_4H_{10}O_2)$	$[L_{PN3/PN}\text{-}TiCl_2]_2$	Cyclopyrrolazide
Empirical formula	$C_{38}H_{62}Cl_2N_7O_2P_2Ti$	$C_{50}H_{82}Cl_4N_{10}P_4Ti_2$	$C_{22}H_{35}N_7P_2$
Formula weight/g mol^{-1}	829.68	1184.73	457.51
Temperature/K	100.00(10)	99.9(4)	117.4(4)
Crystal system	monoclinic	trigonal	orthorhombic
Space group	$P2_1/c$	R-3	$P2_12_12_1$
a/Å	12.3009(4)	49.527(2)	12.5646(2)
b/Å	22.1110(6)	49.527(2)	13.6404(2)
c/Å	16.0546(5)	15.4636(9)	14.6243(2)
α/°	90	90	90
β/°	97.647(3)	90	90
γ/°	90	120	90
Volume/$Å^3$	4327.8(2)	32849(4)	2506.40(6)
Z	4	18	4
$\rho_{calc}g/cm^3$	1.273	1.078	1.212
μ/mm^{-1}	3.828	4.305	1.738
F(000)	1764.0	11232.0	980.0
Crystal size/mm^3	0.2 × 0.1 × 0.05	0.149 × 0.105 × 0.05	0.14 × 0.067 × 0.056
Radiation (Å)	Cu Kα (λ = 1.54184)	Cu Kα (λ = 1.54184)	Cu Kα (λ = 1.54184)
2Θ range for data collection/°	6.844 to 150.734	6.182 to 98.31	8.866 to 160.512
Index ranges	$-9 \le h \le 15$, $-27 \le k \le 26$, $-20 \le l \le 16$	$-44 \le h \le 37$, $-45 \le k \le 31$, $-13 \le l \le 12$	$-15 \le h \le 16$, $-17 \le k \le 17$, $-16 \le l \le 18$
Reflections collected	17397	5120	16170
Independent reflections	8453 [R_{int} = 0.0678, R_{sigma} = 0.0647]	4159 [R_{int} = 0.0286, R_{sigma} = 0.0416]	5286 [R_{int} = 0.0368, R_{sigma} = 0.0389]
Data/restraints/parameters	8453/7/480	4159/656/639	5286/0/289
Goodness-of-fit on F^2	1.097	1.621	0.982
Final R indexes [I>=2σ (I)]	R_1 = 0.0803, wR_2 = 0.2613	R_1 = 0.1213, wR_2 = 0.3584	R_1 = 0.0391, wR_2 = 0.1038
Final R indexes [all data]	R_1 = 0.1082, wR_2 = 0.2874	R_1 = 0.1365, wR_2 = 0.3685	R_1 = 0.0422, wR_2 = 0.1058
Largest diff. peak/hole / e $Å^{-3}$	1.13/-0.65	1.70/-0.56	0.67/-0.37

Programs for diffractometer operation, data collection, data reduction, and absorption correction were those supplied by Rigaku.

	$^{i}Pr_2P[(2\text{-}OH)(3,5\text{-}^{t}Bu)C_6H_2]$	$Ph_2P[(2\text{-}OH)(3,5\text{-}^{t}Bu)C_6H_2]$
Empirical formula	$C_{29}H_{46}N_3OP$	$C_{35}H_{42}N_3OP$
Formula weight/g mol^{-1}	483.66	551.68
Temperature/K	100.01(10)	169(90)
Crystal system	triclinic	monoclinic
Space group	P-1	$P2_1/c$
a/Å	13.4421(2)	15.9233(4)
b/Å	15.9926(2)	11.1467(3)
c/Å	18.7379(3)	18.5935(4)
α/°	66.8990(10)	90
β/°	86.2840(10	108.429(2)
γ/°	72.2040(10)	90
Volume/$Å^3$	3520.89(9)	3130.95(14)
Z	4	4
$\rho_{calc}g/cm^3$	0.912	1.170
μ/mm^{-1}	0.834	1.006
F(000)	1056.0	1184.0
Crystal size/mm^3	0.32 × 0.153 × 0.125	0.21 × 0.19 × 0.15
Radiation (Å)	Cu Kα (λ = 1.54184)	Cu Kα (λ = 1.54184)
2Θ range for data collection/°	6.92 to 160.72	9.386 to 162.578
Index ranges	$-16 \le h \le 14$, $-20 \le k \le 20$, $-23 \le l \le 23$	$-20 \le h \le 20$, $-13 \le k \le 14$, $-23 \le l \le 17$
Reflections collected	61893	34506
Independent reflections	12565 [R_{int} = 0.0526, R_{sigma} = 0.0318]	6768 [R_{int} = 0.4919, R_{sigma} = 0.2217]
Data/restraints/parameters	12565/0/647	6768/0/370
Goodness-of-fit on F^2	1.056	1.535
Final R indexes [I>=2σ (I)]	R_1 = 0.0504, wR_2 = 0.1406	R_1 = 0.1142, wR_2 = 0.2853
Final R indexes [all data]	R_1 = 0.0564, wR_2 = 0.1449	R_1 = 0.1466, wR_2 = 0.3587
Largest diff. peak/hole / e $Å^{-3}$	0.51/-0.30	1.21/-1.68

Programs for diffractometer operation, data collection, data reduction, and absorption correction were those supplied by Rigaku.

5.7. References for Chapter 5

1. Staudinger, H.; Meyer, J. Über neue organische Phosphorverbindungen III. Phosphinmethylenderivate und Phosphinimine. *Helv. Chim. Acta*. **1919**, *2*, 635–646.
2. Cotton, S. A. The actinides. *Annu. Rep. Prog. Chem., Sect. A* **2010**, *106*, 286–294.
3. Cowie, B. E.; Purkis, J. M.; Austin, J.; Love, J. B.; Arnold, P. L. Thermal and Photochemical Reduction and Functionalization Chemistry of the Uranyl Dication, [U(VI)O2](2+). *Chem. Rev.* **2019**, *119*, 10595–10637.
4. Arnold, P. L.; Jones, G. M.; Odoh, S. O.; Schreckenbach, G.; Magnani, N.; Love, J. B. Strongly coupled binuclear uranium-oxo complexes from uranyl oxo rearrangement and reductive silylation. *Nat. Chem*. **2012**, *4*, 221–227.
5. Mougel, V.; Horeglad, P.; Nocton, G.; Pecaut, J.; Mazzanti, M. Cation-cation complexes of pentavalent uranyl: from disproportionation intermediates to stable clusters. *Chem. Eur J*. **2010**, *16*, 14365–14377.
6. Shannon, R. D. Revised effective ionic radii and systematic studies of interatomic distances in halides and chalcogenides. *Acta Cryst*. **1976**, *A32*, 751–767.
7. Chen, C. Designing catalysts for olefin polymerization and copolymerization: beyond electronic and steric tuning. *Nat. Chem. Rev.* **2018**, *2*, 6–14.
8. Köhn, R. Oligo- and Polymerization of Olefins. In *Comprehensive Inorganic Chemistry II*, **2013**; pp 127–154.
9. Wheaton, C. A.; Hayes, P. G. Cationic zinc complexes: a new class of catalyst for living lactide polymerization at ambient temperature. *Chem. Commun*. **2010**, *46*, 8404–8406.
10. Green, M.; Kuc, T. A.; Taylor, S. H. Cationic transition-metal complexes. Part I. Synthesis and reactions of bis(diene)-rhodium and -iridium tetrafluoroborates. *J. Chem. Soc. A* **1971**, 2334–2237.
11. Qin, G.; Cheng, J. Thorium(IV) trialkyl complexes of non-carbocyclic ligands as highly active isoprene polymerisation catalysts. *Dalton Trans*. **2019**, *48*, 11706–11714.
12. Cruz, C. A.; Emslie, D. J. H.; Robertson, C. M.; Harrington, L. E.; Jenkins, H. A.; Britten, J. F. Cationic Thorium Alkyl Complexes of Rigid NON- and NNN-Donor Ligands: π-Arene Coordination as a Persistent Structural Motif. *Organometallics* **2009**, *28*, 1891–1899.
13. Cruz, C. A.; Emslie, D. J. H.; Harrington, L. E.; Britten, J. F. Single and Double Alkyl Abstraction from a Bis(anilido)xanthene Thorium(IV) Dibenzyl Complex: Isolation of an Organothorium Cation and a Thorium Dication. *Organometallics* **2007**, *27*, 15–17.
14. Motolko, K. S. A.; Price, J. S.; Emslie, D. J. H.; Jenkins, H. A.; Britten, J. F. Zirconium Complexes of a Rigid, Dianionic Pincer Ligand: Alkyl Cations, Arene Coordination, and Ethylene Polymerization. *Organometallics* **2017**, *36*, 3084–3093.

15. Fischer, M.; Barbul, D.; Schmidtmann, M.; Beckhaus, R. Unexpected Selective Methyl Group Abstractions from SiMe3 Moieties of CH2SiMe3 Ligands To Give New Cationic Titanium Complexes. *Chem. Eur J.* **2019**, *25*, 7119–7130.

16. Cameron, T. M.; Gordon, J. C.; Michalczyk, R.; Scott, B. L. Unusual alkyl group activation and cationic complex formation from a novel lutetium dialkyl complex supported by a tridentate monoanionic ligand. *Chem. Commun*. **2003**, *18*, 2282–2283.

17. Hayes, P. G.; Piers, W. E.; Parvez, M. Synthesis, Structure, and Ion Pair Dynamics of β-Diketiminato-Supported Organoscandium Contact Ion Pairs. *Organometallics* **2005**, *24*, 1173–1183.

18. MacNeil, C. S.; Hsiang, S. J.; Hayes, P. G. Reversible dehydrogenation of a primary aryl borane. *Chem. Commun.* **2020**, *56*, 12323–12326.

19. MacNeil, C. S.; Hayes, P. G. An H-Substituted Rhodium Silylene. *Chem. Eur J.* **2019**, *25*, 8203–8207.

20. Chisholm, D. T.; Hayes, P. G. Synthesis and characterization of group 13 dichloride (M = Ga, In), dimethyl (M = Al) and cationic methyl aluminum complexes supported by monoanionic NNN-pincer ligands. *New J. Chem*. **2021**, *45*, 15043–15052.

21. Hänninen, M. M.; Zamora, M. T.; MacNeil, C. S.; Knott, J. P.; Hayes, P. G. Elucidation of the Resting State of a Rhodium NNN-Pincer Hydrogenation Catalyst that Features A Remarkably Upfield Hydride 1H NMR Chemical Shift. *Chem. Commun.* **2016**, *52*, 586–589.

22. Knott, J. P. Towards Terminal Rare Earth Imido Complexes. M.Sc. Thesis. University of Lethbridge, Lethbridge, AB, 2016.

23. Valentine, A. M. Titanium: Inorganic & Coordination Chemistry. In Encyclopedia of Inorganic and Bioinorganic Chemistry, John Wiley & Sons, Ltd.: 2011.

24. Burford, R. J.; Yeo, A.; Fryzuk, M. D. Dinitrogen activation by group 4 and group 5 metal complexes supported by phosphine-amido containing ligand manifolds. *Coord. Chem. Rev*. **2017**, *334*, 84–99.

25. Doyle, L. R.; Wooles, A. J.; Jenkins, L. C.; Tuna, F.; McInnes, E. J. L.; Liddle, S. T. Catalytic Dinitrogen Reduction to Ammonia at a Triamidoamine-Titanium Complex. *Angew. Chem. Int. Ed*. **2018**, *57*, 6314–6318.

26. Ogawa, T.; Suzuki, T.; Hein, N. M.; Pick, F. S.; Fryzuk, M. D. Cleavage of an aryl carbon-nitrogen bond of a phosphazido iron(II) complex promoted by hydride metathesis. *Dalton Trans*. **2015**, *44*, 54–57.

27. Bebbington, M. W. P.; Bourissou, D. Stabilised phosphazides. *Coord. Chem. Rev.* **2009**, *253*, 1248–1261.

28. Bieger, K.; Tejeda, J.; Reau, R.; Dahan, F.; Bertrand, G. Synthesis and Reactivity of Cyclic 6-Membered Six-π- and Four-Membered Four-π- Electron Ylides. *J. Am. Chem. Soc.* **2002**, *116*, 8087–8094.

29. Burger, B. J.; Bercaw, J. E. Experimental Organometallic Chemistry; American Chemical Society: Washington, D.C., 1987.

30. Marvich, R. H.; Brintzinger, H. H. A Metastable Form of Titanocene. Formation from a Hydride Complex and Reactions with Hydrogen, Nitrogen, and Carbon Monoxide. *J. Am. Chem. Soc.* **1971**, *93*, 2046–2048.

31. Pangborn, A. B.; Giardello, M. A.; Grubbs, R. H.; Rosen, R. K.; Timmers, F. J. Safe and Convenient Procedure for Solvent Purification. *Organometallics* **1996,** *15*, 1518–1520.

32. Dolomanov, O. V.; Bourhis, L. J.; Gildea, R. J.; Howard, J. A. K.; Puschmann, H. OLEX2: a complete structure solution, refinement and analysis program. *J. Appl. Crystallogr.* **2009**, *42*, 339–341.

33. Sheldrick, G. M. SHELXT – Integrated space-group and crystal-structure determination. *Acta Crystallogr. Sect. A* **2015**, *71*, 3–8.

34. Sheldrick, G. M. Crystal structure refinement with SHELXL. *Acta Crystallogr. Sect. C* **2015**, *71*, 3–8.